

SCIENTIFIC & TECHNICAL REPORT 2023

IMPRINT

Full report title CSEM Scientific and Technical Report 2023

Editor and publisher CSEM SA
info@csem.ch
T +41 32 720 5111

Publication Yearly frequency
Printed and digital editions



Cover page design Contreforme
www.contreforme.ch

Printing Imprimerie Baillod SA, Bevaix (Switzerland)

PREFACE

Dear Reader,

In 2023, CSEM continued to excel in inspiring, sustainable innovation and continues to do so. As a driving force in technological progress, we have achieved cutting-edge advances in addressing critical societal and environmental challenges. Our collaborative ventures across a spectrum including start-ups and established industry leaders have yielded exciting benefits whilst consolidating our role as leader in positive change.

In this report, we provide an overview of our achievements, featuring in-depth case studies and detailed project analyses. They demonstrate our passionate commitment to integrating sustainability, data security, privacy and energy efficiency into our operations. A single goal drives our cross-sector initiatives, which encompass digital health, precision diagnostics, smart mobility, advanced manufacturing, industrial automation, and clean energy: to transform innovative ideas into practical technologies that are beneficial to both our clients and society at large.

As we move forward, our dedication to progress is as strong and heartfelt as ever, whilst cultivating a supportive and diverse work environment. We don't just push boundaries in innovation and efficiency; we make our success long-lasting. We are forging ahead to face even more "challenges of our time" and build a brighter, more sustainable future for all.

Alexandre Pauchard
CEO, CSEM SA

CONTENTS

PREFACE

MULTIDISCIPLINARY INTEGRATED PROJECTS – MIPS

- EFORE – Environmental Footprint Reduction of Electronics
PRIMAFLEX – Connecting Mobility and Electricity Networks for Grid-friendly Charging of Electric Vehicles
FLORES – an Optimized and Ruggedized Design for the SILOSCAPE Escapement
MIRA2 – Miniaturized Multi-Sensing Arrays
ORCA – Semi-automated Workflow for Organoid Selection, Dissociation, and Single-cell Analysis
SUMON – Disposable System for Sensors Monitoring
PRECIZE – Predictive Quality Towards Zero-defect Manufacturing in 3D Printing
COSIMA – Cooperative Sensors for Electrographic Imaging

DIGITALIZATION TECHNOLOGIES

- Approximating Sizeable Combinatorial Optimization Problems with Tree Search Algorithms
MultiOmix – a Multi-modal Framework to Analyze and Interpret Multi-omics Data
Data Acquisition Framework for Smart Weather Station Aurora
AI-enabled Defect Detection and Classification in the Sewers of Lausanne
Securing Embedded Firmware Update over the Air with Distributed Encryption
Fibonacci – a Scalable Approach to Embedded Machine-learning
Integrating Cryptographic Accelerators with the icyflex-V Core
BirdGuard – Protecting Birds from Window Collisions
Software Defined Radio Approach for Bluetooth Dual Mode Digital Baseband
A Dual-mode Bluetooth Transceiver with Two Concurrent RX Paths, Offset-LO, +20 dBm Output Power, and -98 dBm Sensitivity in GF22 FDSOI
A Low-jitter Reference-less Clock and Data Recovery (CDR) with Low Phase-noise Multi-clock Generation
A CMOS Image Sensor with a Stacked Quantum Dot Photon Absorber for Wide-spectral Imaging
Performance Comparison of Radio Frequency-based Angle-of-arrival and Ranging Solutions
Development of an Embedded Bluetooth Low Energy Based Angle-of-arrival Algorithm
Discovering Vulnerabilities in Embedded Firmware with Fuzzing Techniques

1	Enhancing Memory Safety by Integrating Rust in the μ111 Real-time Operating System	33
7	Enabling VGA Graphic Applications with μ111 OS on Cortex-M7 integrated GPU	34
8	Threshold Signatures for Embedded Platforms	35
9	An Autonomous Stereo-imaging System for the Monitoring of Mountain Streams Discharge	36
10	Contactless Distance Measurement using Talbot-diffracted spaceCoder Technology	37
11	Virtual Reality-based Eye Gaze Calibration for Early Diagnosis of Neurological Disorders	38
12	VIVALDI – Steel Billet Tracking with Advanced Computer Vision	39
13	RF Wireless Powering: Enabling Extended Autonomy in Wireless Devices	40
14	Custom Antenna Design for Vehicles: Additive Manufacturing on Flexible Transparent Substrates	41
15	Robust Aircraft Part Identification	42
17	Expectant – Acoustic Localization of Rare Events	43
18	Smart Systems and Connectivity in the Mining Industry	44
19	Real-time Spore Measurement to Reduce Fungicide Usage in Vineyards	45
20	Gemtelligence – Accelerating Gemstone Classification with Deep Learning	46
21	Abnormal Rhythm Detection from Single-lead ECG	47
22	Highly Accurate Step Detection from a Wrist-worn 3D Accelerometer	48
23	Hearing Instrument Fall Detection	49
24	Blood Pressure Monitoring in People with Spinal Cord Injury	50
25	ULTEEMNite – Ultra-long-term EEG Monitoring during Sleep	51
26	Non-invasive Continuous Measurement of Intra-abdominal Pressure	52
27	EXPERIENCE Physiological Integrated System: a Smart Wearable System for Mid-term 32-channel EEG, 1-lead ECG, and Motion Recording using Dry Electrodes	53
32	PRECISION MANUFACTURING	55
	Ultra-sensitive Photonics-MEMS Accelerometers for Next-generation Seismic Sensor Networks	56
	Lifetime Evaluation and Reliability Assessment Methodology for NEM Switches	57
	In-cavity Marking for Plastic Part Traceability	58
	A Precision Gradient Magnetometer	59
	A MEMS Gas Chromatograph and its Fluidic Connections	60
	Additive Manufacturing for Integrated Active Fluid Control in Life Science Applications	61
	Development of Metal Ultra-thin Cold Plates by L-PBF Technology: Limits and Benefits	62
	MANUELA – Additive Manufacturing using Metal Pilot Line Design Center	63

Chemical Treatment of Aluminum Current Collector in Li-Ion Batteries to Enhance Pitting Corrosion Resistance	64	Recent Developments of the Plastics Compounding Platform	94
Carbon Nanotubes Field-effect Transistors for Biosensing Application	65	Progress of Copper Metallization at CSEM	95
Sol-gel Chemistry for Resistant Bactericidal Coatings	66	New In-house Tool for Rapid and Automated Life Cycle Assessment of Photovoltaic Systems	96
Chemical Sensors for Water Quality Monitoring	67	Ultralight Weight Amorphous Silicon Solar Modules for Solar Power Satellites	97
Integration of Sensors for Monitoring of Multiple Parameters for Newborns	68	Perovskite Semiconductors for Light Emitting Diodes and Energy Harvesting	98
Molecular Imprinted Polymers-based Sensors for Nicotine Monitoring in Aerosol	69	Lightweight PV Modules for Mobility Applications	99
Large Area UV Imprinting of Optical Microstructures	70	I-V Curve Simulation of Curved PV Modules for Vehicle Integration	100
Mastering of Multi-sag Microlens Arrays at Wafer Scale	71	Glass-free PV Module for Automotive Application	101
Phase-shifting Metasurfaces for Flexible and Foldable Displays	72	Microservices for Robust Estimation and Activation of Demand-side Flexibility	102
Thin-film Lithium Niobate on Insulator Photonic Integrated Circuits (LNOI PICs) Platform	73	Probabilistic Forecasting of Irradiance and PV Power Production on a Variable Set of Locations with Graph Machine Learning	103
Statistical Measurements of LNOI PICs for Quality Assurance of the Process Design Kit	74	A Dataspace for Secure and Collaborative Data Exchange in the PV Industry	104
Acoustofluidic Platform for Controlled Microtissue Manipulation	75	Predicting Advection-Diffusion Phenomena with Physics-informed Graph Machine Learning	105
Automated Multi-axis Bioreactor for Standardized Preclinical Assessment of ex vivo Tissues	76	Optimizing Battery Storage Systems through Behavioral Models in Predictive Energy Management	106
Automated Sorting of Microtissues using Deep Learning for Label-free Characterization	77	DRT-based State of Charge Estimation for Commercial Li-Ion Battery Pack	107
Automated Well Plate Sampling and Integrated Glucose Measurement	78	HYSTIMATOR – EIS-based Method to Physically Model Hysteresis of LFP Battery	108
Droplet Microfluidics – Artificial Compartments for Applications in Life Sciences	79	Internal Temperature Estimation of a Li-Ion Battery Cell by using EIS	109
AML.AI – Deciphering Bone Marrow Remodelling in Acute Myeloid Leukaemia using Single-cell Omics	80	High-energy Density Li-Metal Anode by Physical Vapor Deposition	110
Self-standing Sensor System as in vivo Implant for Smart Bone Regeneration	81	SOLiD Project – Dual-layer Polymer Batteries with Vacuum Deposited Li-Metal Anode	111
Portable Fluorescence Biosensing System for Low-cost, Quantitative, and Multiplexed Allergen Screening	82		
Mid-IR QCL-powered Modular Platform for Contactless, Real-time Metabolite Monitoring	83	ANNEXES	113
CRISPR-Cas Systems	84	Publications	113
LiDAR and End-effector Technologies for In-orbit Servicing Demonstration Mission	85	Proceedings	114
fs-Laser System for the Repair of Defective Pixels and Defective Circuits in µled Displays	86	Conferences and Workshops	116
Nonlinear Photonic Circuits on Lithium Niobate on Insulator for Laser Metrology and Atomic Sensors	87	Research Projects	117
Electro-optic Laser Frequency Comb for the NIRPS Spectrograph Calibration	88	Innosuisse – Swiss Innovation Agency	120
Test and Characterization of Photodiodes for the Earth Observation TRUTHS Mission	89	European Commission Projects	124
WAVEGUIDE – Custom Voice Coil Actuator for Flexure-based Electromechanical RF Switch	90	European Space Agency, Swiss Space Office, and Space Science Projects	128
SUSTAINABLE ENERGY	91	Industrial Property	129
Adding a Perovskite Thin Film on Silicon for the Next Generation of High-efficiency Photovoltaic Modules	92	Collaboration with Research Institutes and Universities	129
PILATUS Project – Highly Reliable Silicon Heterojunction Tunnel Interdigitated Back Contact Solar Cells and Modules	93	Teaching	136
		Theses	137
		Commissions and Committees	138
		Prizes and Awards	141

CSEM SA

CSEM, a non-profit, public-private Swiss technology innovation center, is at the cutting-edge of technology innovation and research. It plays a crucial role in connecting academic research with industrial application. Committed to serving both society and industry, we work tirelessly to meet the challenges of our time. Our mission is to foster innovation, develop and refine cutting-edge technologies, and ensure their transfer to the industrial sector, thereby energizing the Swiss market and extending its global impact. We are particularly focused on supporting and/or developing key technologies in precision manufacturing, digital domains, and sustainable energy. All of these are vital to environmental, economic, and social well-being.

Digital transformation is bringing significant changes to various aspects of our society. Some of the key issues that our **Digital Technologies** initiative addresses are secure and confidential data management, advanced communication, and quantum technologies. These technologies are particularly relevant to the Internet of Things (IoT), as well as to specific sectors such as manufacturing (Industry 4.0) and healthcare (Digital Health), which are of particular interest to Swiss industry. In many of these areas, the development of advanced low-power hardware and embedded algorithms is crucial. By integrating these components, we enable energy-efficient and sustainable data sensing, analysis, and communication.

Another focus area for us is **Precision Manufacturing**, where we aim to support Swiss industry in a rapidly evolving landscape. We recognize the necessity for constant innovation in a high-wage country and adapt to the significant changes in processes and business models brought by Industry 4.0. We leverage advanced microfabrication processes to produce precise, functional components with well-controlled surface properties. For instance, we develop photonic integrated circuits (PICs), offering groundbreaking solutions in advanced instrumentation. These solutions find applications in multiple sectors, ranging from aerospace to life sciences, showcasing our commitment to versatile and forward-thinking innovations.

Our research in **Sustainable Energy** meets growing demand for renewable energy solutions, enhanced by technology and digital innovations. We emphasize the development of, on the one hand, large-scale solar photovoltaic modules for buildings and, on the other, innovative, smaller-scale solar technologies for wearables and IoT applications. Along with our solutions for the decentralization of energy production, enhancement of storage capabilities, and digitalization of operations and services, we pave the way towards a more sustainable future.

MULTIDISCIPLINARY INTEGRATED PROJECTS – MIPS

Harry Heinzelmann

CSEM's Multidisciplinary Integrated Projects (MIPs) are an integral part of its research program. The MIP program fosters synergies between three research priorities: **Precision Manufacturing, Digital Technologies, and Sustainable Energy**. Every year, CSEM dedicates considerable resources to these multidisciplinary projects, thus increasing its potential to generate innovative solutions.

MIPs are initiated regularly to ensure a constant renewal of the program and a quick response to emerging market needs. Each project aims to develop technology demonstrators with a high maturity level and high market potential, well within a typical project lifetime of one year.

A short summary of the MIP 2023 program is given here. For a more detailed description of the projects, please refer to the following pages.

EFORE – Environmental footprint reduction of electronics

The increasing need for sustainable solutions and products requires the development of new materials and fabrication processes. Future research and development activities need to consider sustainability criteria in ever-multiplying ways. The EFORE project aims to extend the Life Cycle Analysis (LCA) methodology, which CSEM has already established in photovoltaics, to other domains such as electronics. The results of this project will enable a better response to customers' increasing demand for sustainable solutions. It is hoped that the LCA framework can be further extended to other R&D fields and that this type of analysis will become an integral part of CSEM's offer to industry.

PRIMAFLEX – Connecting mobility and electricity networks for grid-friendly charging of electric vehicles

Mobility electrification is an important contribution to future sustainable transportation. However, the proliferation of electric vehicles is challenging the stability of existing electricity networks. The PRIMAFLEX project aims to better manage demand for electricity, relying on forecasting methods for numbers of electric vehicles, as well as a model predictive control algorithm. The framework was tested on a simulated dataset of 1000 electric vehicles. These promising results will lead to a more efficient exploitation of the network infrastructure without a need to invest in physical reinforcements.

FLORES – An optimized and ruggedized design for the SILOSCAPE escapement

Novel watch mechanisms based on flexible silicon blades (FlexMEMS) are an important innovation driver in mechanical watchmaking. Traditional bearings and lubrication in watch escapements can be replaced with a frictionless guiding method. CSEM's latest development is the improved SILOSCAPE escapement, which offers remarkable enhancements in robustness and precision. This new design works well with low-amplitude oscillators and ensures consistent isochronism.

MIRA2 – Miniaturized multi-sensing array

The integration of electrochemical sensors for the simultaneous detection of multiple analytes is a key enabler for innovative

applications in medical and environmental monitoring. The MIRA2 project aims to develop miniaturized sensors which utilize a CMOS platform for readout and machine learning algorithms, which in turn support data analysis. The goal is to enable complex electrochemical measurements in challenging media, such as the detection of body fluid dysfunction markers or harmful industrial compounds.

ORCA – Semi-automated workflow for organoid selection, dissociation, and single-cell analysis

Working with complex *in vitro* models is a challenging and time-consuming task. The ORCA project aims to develop a semi-automated workflow to facilitate the handling and analysis of organoids, featuring AI-supported sorting and dissociation into single cells, which can be subsequently analyzed. This development helps bridge the gap between 3D organoid models and single-cell analysis, leading to a better understanding of complex biological systems, e.g., for drug development.

SUMON – Disposable system for sensors monitoring

The growing trend towards personal monitoring of biochemical analytes is generating large numbers of sensors, which typically consist of bulky monitoring devices reading out signals from disposable sensors. The SUMON project aims to simplify the use of such sensors and reduce the overall cost. It achieves this in a stable manner via miniaturization and integration of sensor readouts and connectivity with the sensor substrate. A SUMON sensor stick could be easily disposed of by the user after the measurement. Target applications include analysis of saliva and urine for disease detection and monitoring in sports.

PRECIZE – Predictive quality towards zero-defect manufacturing in 3D printing

Additive manufacturing (AM), also known as 3D printing, is a novel fabrication technique that enables innovative designs and customized fabrication down to lot sizes of one, albeit at fabrication speeds that are often slow compared to traditional fabrication methods. Such speeds do however allow the implementation of process monitoring to assess the quality of the work piece during the fabrication process. This in turn allows fabrication parameters to be adapted and enhances potential for first-time-right fabrication. The PRECIZE project has successfully implemented optical monitoring techniques and machine learning for quality prediction and control.

COSIMA – Cooperative sensors for electrographic imaging

Electrographic imaging is a key technology to improve preventive diagnostics and to support surgery. To this end, CSEM has developed over the years a cooperative sensor solution based on miniaturized electrodes in arrays and with light and flexible interconnects. It is ideally suited to wearable biopotential and bioimpedance imaging in wearable form factors. The latest development of an application-specific integrated circuit (ASIC) has allowed the integration of a 12-lead ECG demonstrator, which delivers signals comparable to those measured with conventional equipment.

EFORE – Environmental Footprint Reduction of Electronics

A. Barrou, A. Zandara, C. Rupf, B. Paviet-Salomon, P. Nussbaum

This project represents a comprehensive environmental assessment of conventional PCBs (Printed Circuit Board) as well as an exploration of various alternative PCB materials and manufacturing methods. By using Life Cycle Assessment (LCA), we identified environmentally friendlier alternatives to standard PCB, like bio-based and disposable substrates, alternative pastes, and printing processes for metallization. These findings could be used firstly to help CSEM customers active in the electronic field to produce more sustainable PCBs, secondly to develop internally new PCB with low-environmental footprint; making CSEM a reference point for electronic companies with sustainable goals.

PCBs are essential to the electronics industry as they form the core platform for interconnecting and integrating electronic components, enabling communication and functionality in devices ranging from consumer electronics to industrial systems. However, standard PCB (see Figure 1) are synonym to a significant environmental impact arising from resource-intensive production processes, energy consumption, use of hazardous chemicals, disposal challenges, and complex supply chains [1]. In this context, CSEM's interdisciplinary teams aims to find solutions, that could be implemented by electronic industries, to limit the impact of PCBs on the environment.



Figure 1: Standard PCB composed of a substrate (FR4) and a metallization (copper) protected by solder stop.

LCA of standard PCB

The main goal of this study is to evaluate, with LCA methodology, the environmental footprint of a standard PCB. A second objective is to compare the potential alternatives to lower the carbon footprint of standard PCB. The system boundary includes the PCB production (raw materials, chemicals, resources, pollution & wastes) as well as PCB end-of-life (disposal or recycling) and excludes PCB use and its components. The Functional Unit is defined as all the fluxes necessary for the production and end-of-life of 1 m² of a 2-layers PCB. Obtaining accurate environmental results requires up-to-date data because of the rapid evolution of materials and processes uses to produce PCB. Such data were collected and assessed by collaborating with CSEM industrial partners (Logitech, Elephantech) and performing a literature review on the subject.

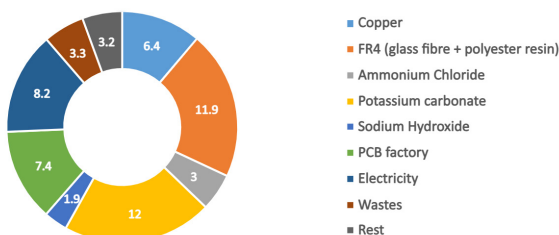


Figure 2: Carbon footprint of 1 m² of a 2-layers standard PCB production.

[1] M. N. Nassajfar, et al., "Alternative materials for printed circuit board production: an environmental perspective" (2021).

[2] <https://www.jivamaterials.com/>

[3] <https://www.4eantenna.com/>

The production (only) of 1 m² standard 2-layers PCB has a carbon footprint of 57.3 kgCO₂-eq/m². Figure 2 shows that 2/3 of the PCB carbon footprint is due to FR4 substrate and copper-etched metallization. On one hand, carbon-intensive processes necessary for glass fiber and polyester resin are mainly responsible for FR4 impact. On the other hand, etching copper employs numerous chemicals and generate important wastes, leading to an elevated carbon footprint. This first overview highlights the need to find alternatives to high impacting materials and to processes using chemicals.

Alternatives to FR4 substrate

As a first step, different alternatives to FR4 substrate are evaluated. The PCB thickness's substrate is set to 1.5 mm (representative of the market). Overall, PET, Soluboard and paper-based substrates have the lowest carbon footprint. Furthermore, Soluboard and paper-based substrates are commercially available [2, 3], easy to recycle and even biodegradable.



Figure 3: Carbon footprint of 1 m² of 1.5 mm thick substrate.

Alternatives for metallization

As a second step, switching from etching process to additive manufacturing reduces aggressively the environmental footprint of metallization, because chemicals are not used anymore. For example, DP-Patterning [4] is an additive manufacturing process depositing Al or Cu interconnect layers on flexible substrate. Such changes are already applied by PCB companies such as Elephantech, reaching a PCB's carbon footprint of 25 kgCO₂-eq/m² by optimizing the metal deposition (using nano-ink and copper electroplating instead of etched-copper) [5].

Conclusion

Overall, this project assesses the environmental impact of standard PCB and identifies pathways to reduce its footprint. The results obtained and discussion with its industrial partners enables CSEM to develop new low-environmental PCBs. The transfer to industry of these innovations will then contribute to more sustainable electronics.

[4] <https://dppatterning.com/>

[5] <https://info.elephantech.co.jp/en/reduction-of-environmental-impact>

PRIMAFLEX – Connecting Mobility and Electricity Networks for Grid-friendly Charging of Electric Vehicles

D. Achi, R. Carrillo, P.-J. Alet, R. Langou, L. Meier, D. Vizár, S. Dasen

The electrification of mobility increases the strain on electricity networks. CSEM developed a solution to exploit the demand-side flexibility of electric vehicles and contribute to their smooth integration into the grid. The solution aggregates electric vehicles into a pool to alleviate grid congestion by limiting the power at the substations and participating in ancillary services through the implementation of forecasting methods for the state of the electric vehicles and a model predictive control approach. This method reduces the need for physical reinforcement of the infrastructure while ensuring the users' comfort.

The electrification of mobility is characterized by a widespread adoption of electric vehicles (EVs). It offers promising opportunities as a sustainable alternative to fuel-powered vehicles. However, it is accompanied by considerable challenges on the electrical grid. The increased demand of electricity creates a strain on the network, especially during peak charging times. In the absence of a different solution, this calls for physical reinforcement of the infrastructure. The exploitation of the demand-side flexibility of EVs would promote their smooth integration in the grid and mitigate grid congestion.

To cope with these upcoming challenges, CSEM has developed a solution for managing the demand-side flexibility of the EVs. The solution aggregates the EVs into a pool (similar to a “virtual power plant”) to alleviate grid congestion, in particular to prevent overloading on a set of grid substations. It implements a model predictive control (MPC) algorithm under constraints to set the charging profile for each EV such that the pool can respond to congestion management requests (or constraints) by limiting the peak power at the substations. A global overview of the solution, with the flow of information, is presented in Figure 1.

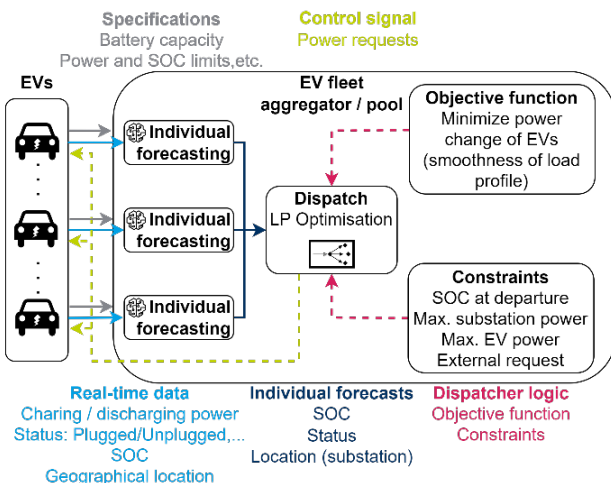


Figure 1: Overview of the developed solution.

The control algorithm requires as inputs forecasted trajectories of selected variables for each EV across a given time horizon to dispatch optimal charging profiles. For each EV, these variables include the state-of-charge (SOC) and whether it is plugged in. The trajectories are forecasted using machine learning methods.

The MPC algorithm is a linear program (LP) optimization that minimizes the power variation of EVs to promote smoothness in the profiles for better control quality and to preserve the health of the EV batteries. It considers a time horizon of 6 hours ahead with 5-minute timesteps. This horizon was selected to adequately

exploit the flexibility of EVs, i.e., to take advantage of EVs staying at a charging station longer than they need to fully charge. Furthermore, the dispatcher incorporates the following constraints to guarantee the functionality of the service in addition to end-users' satisfaction:

- A maximum load can be set for each substation to fulfil the functional purpose of the solution.
- An external request to modulate the power of the pool can be included as an additional feature of the solution.
- The forecasted value for the SoC of each EV at departure is incorporated to ensure the comfort of the end users.
- The maximum charging power for each EV is specified to respect their physical constraints.

The complete solution is coupled with an operator interface displayed in Figure 2. This interface provides the visual support for the service by displaying the load profiles and highlighting its performance in terms of compliance with the set of constraints at the substations and the fulfilment of external requests.

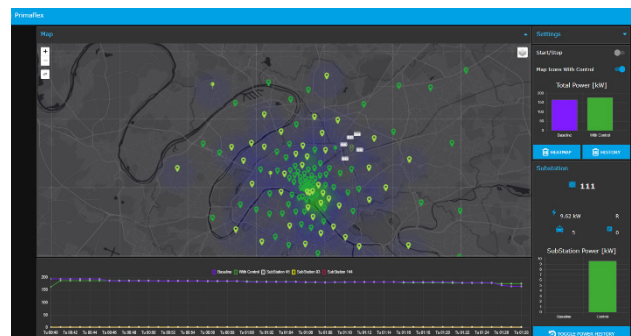


Figure 2: Snapshot of the cloud-based operator interface.

The complete service was tested on simulated data. 1'000 EVs were simulated using simBEV^[1] with a 1-minute resolution. The list of extracted datasets is shown in Figure 1. 150 substations were sampled in the Greater Paris Metropolis using the open data from Agence ORE^[2]. The solution was applied for two weeks in August 2022, with three different set of constraints. During the tests, the constraints on the substations were respected 96% of the time, and the deviation from the total request was 7.4% on average, hence providing a satisfactory success rate for the service of the pool.

CSEM developed a complete framework bridging the growth of electric mobility with grid-friendly EV charging through the exploitation of demand-side flexibility. The whole solution is cloud native to facilitate deployment and scale up.

[1] “simBEV.” Reiner Lemoine Institut, Apr. 15, 2023.

[2] “Postes de distribution publique (postes HTA/BT).” Agence ORE.

FLORES – an Optimized and Ruggedized Design for the SILOSCAPE Escapement

F. Barrot, G. Musy, O. Laesser*, Y. Petremand, R. Winiger*, L. Giriens, E. Dominé

Leveraging its combined expertise in micro-fabrication techniques and in the design of precision mechanisms guided by flexure blades in lieu of classical bearings, a frictionless guiding approach requiring no lubrication, CSEM has been a pioneer in proposing to the Watch Industry the so called "FlexMEMS approach" for the design and production of novel high-end oscillators and escapements. This year, CSEM presents an enhanced implementation of the SILOSCAPE Escapement, resulting in increased robustness and precision.

CSEM designed the SILOSCAPE [1] escapement with low power in mind, targeting a high-power reserve. To remove friction, inherent to conventional ruby bearings, its balance wheel is guided in rotation on a symmetrical crossed flexure pivot arranged in the so called Wittrick configuration which is very compact and has a low intrinsic sensitivity to gravity.

To handle low power on the escapement wheel, the SILOSCAPE escapement is specifically designed to work with low-amplitude oscillators and can operate with a small lift angle thanks to the direct impulse between the escapement wheel and the pallets rigidly connected to the balance wheel.

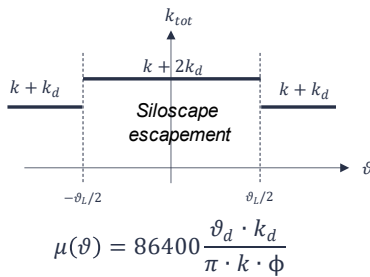


Figure 1: Total stiffness of the oscillator k_{tot} as a function of the angle of the balance wheel θ (stiffness of the flexible pivot k and the detents k_d when supported on the balance wheel).

Two detents are used to achieve a reliable isochronism at low amplitudes; they alternatively stop the escapement wheel beyond the angle of lift, avoiding any contact with the balance wheel during the locking phase. The detents of the SILOSCAPE escapement serve a triple function. Firstly, they prevent friction losses during the resting phase, which would require working with higher-amplitude impulses. Secondly, they counterbalance the isochronism error of the impulse, which is correlated to the intensity of the impulse and predominantly impacts regulators with low amplitudes. Thirdly, they compensate for the inherent isochronism defects of the Wittrick oscillator.

However, using a single correction mean proves very challenging to compensate flawlessly for two distinct defects arising from two different sources. Furthermore, this approach to reduce the overall isochronism defect has practical limitations. This is due to several reasons, including the fact that the minimum thickness achievable in the production of detents blades is a limiting factor in minimizing the defect. Additionally, the different defects do not perfectly compensate over the nominal range of oscillations. Moreover, controlling the shape of the disturbance curves to achieve compensation is highly challenging. To counter these limitations, the isochronism of the system has been optimized by minimizing the isochronism of the escapement and the oscillator separately.

* External key contributors: Olivier Laesser and Winiger Horloger

[1] G. Musy, "Les technologies de micro-fabrication et de l'aérospatiale au service de l'innovation horlogère", JE2021 De nouvelles complications dans le monde horloger?, 2021.

Auxiliary detents have been introduced to minimize the isochronism defect of the escapement. They have the effect of reducing the variation of the oscillator stiffness between the angle of lift and the supplementary arc. To put it simply, the isochronism disturbance of the escapement no longer relies on the stiffness of the main detents, but on the difference in stiffness between the main and auxiliary detents, which is much more manageable in practice. Its minimization is therefore no longer limited by the minimum thickness achievable for flexible blades and it is possible to accurately minimize the isochronism of the impulse with that of the main detents working with the auxiliary detents.

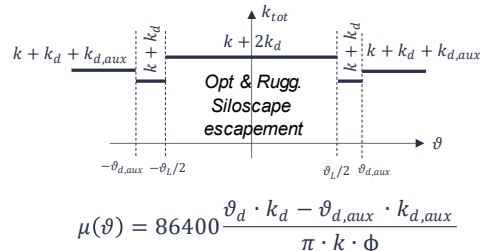


Figure 2: Total stiffness of the oscillator k_{tot} as a function of the angle of the balance wheel θ (stiffness of the flexible pivot k plus the main & auxiliary detents, k_d & $k_{d,aux}$, when supported on the balance wheel).

To minimise the isochronism defect of the balance wheel, the Wittrick pivot was combined in series with an RCC pivot: the stiffness of the Wittrick pivot increases while that of the RCC pivot decreases as the angle of oscillation increases. This principle was already applied in the practical implementation of the Genequand escapement [2] where the anchor, pivoted on an RCC pivot, carried in series an oscillator on a Wittrick pivot. These two techniques combine to produce a regulator with an excellent isochronism.

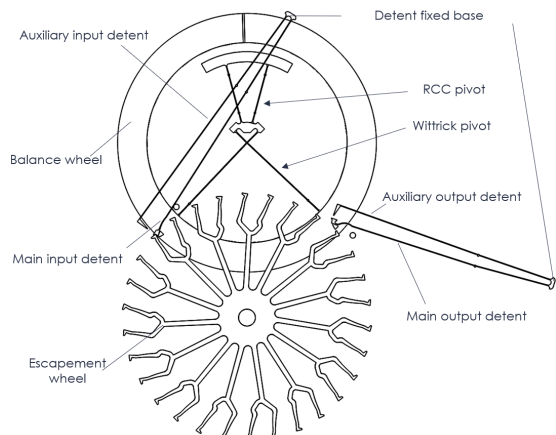


Figure 3: The optimized and ruggedized architecture of the SILOSCAPE escapement.

[2] F. Barrot, T. Hamaguchi, "Un nouveau régulateur pour une réserve de marche exceptionnelle", JE2014 Les vecteurs de l'innovation horlogère - matériaux, conception, calculs, 2014.

MIRA2 – Miniaturized Multi-Sensing Arrays

R. Krähenbühl, X. Lefèvre, J. Disser, B. Petkus, P.-F. Rüedi, M. Dorrestijn, S. Khan, M. Dia, I. Stergiou

The MIRA project aims to miniaturize electrochemical sensors for use in complex media and buffers, with two primary objectives: detecting body fluid dysfunction markers (e.g., albumin, creatinine, glucose, ions) and monitoring harmful industrial compounds (e.g., nicotine). CSEM expanded its electrochemical sensor portfolio with the introduction of a Urine Albumin Protein sensor and enhanced the CMOS platform's process compatibility through techniques such as Aerosol Jet Deposition, Ink Jet, and Screen Printing. An in-house reader with galvanically isolated channels, offering new electrochemical measurement capabilities, including cyclic voltammetry and EIS, was also developed. Finally, an advanced measurement setup, with integrated air traps to remove bubbles, had been fabricated, measurements in complex media were taken, and using specially adapted machine learning models, the generated multi-analyte sensor datasets were analyzed.

Biosensors and chemical sensors receive significant traction from several megatrends: the COVID-19 pandemic accelerated the adoption of point-of-care diagnostic kits, organoids, and organs-on-chips boom with shift to personalized medicine, and food and water quality awareness are quickly following the trend of air quality monitoring. Extending and augmenting the printed electrochemical multi-sensor which can be integrated on various substrates is an advantageous way to address these and future applications. Furthermore, incorporating them on a CMOS chip is an additional promising approach for developing miniaturized environmental and health monitoring sensors, as electronic and sensing parts are embedded in a small area.

On the one hand, a CMOS platform has been fabricated and functionalized with sensors, thereby demonstrating the possibility to functionalize the platform using in-house Aerosol Jet, Ink Jet, and Screen Printing. Although the adhesion of the metallic functionalization was not optimal due to the absence of an intermediate anchoring layer, measurements were performed. We were thus able to deposit our MIP-based sensors and successfully measured interaction with target molecules.

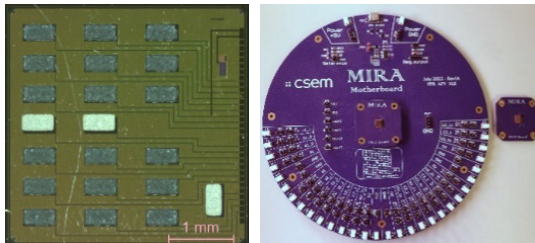


Figure 1: CMOS chip (left) with screen-printed carbon sensors and Ag/AgCl reference electrodes, as well as the motherboard and sensor board (right) for measuring the chips.

To expand our electrochemical sensor portfolio, we successfully realized a proof of concept of a Urine Albumin Protein sensor based on cyclic voltammetry. The figure below demonstrates a successful calibration over the relevant concentration range in buffer, as well as first measurements in urine.

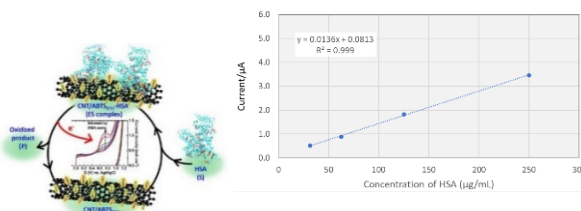


Figure 2: Albumin sensor operating principle and initial results in buffer over relevant albumin range.

To generate data for machine learning, as well as mature our multi-sensor arrays, a "large experiment" testing 6 sensors on flexible polymer foil in parallel across 30 urine samples was

carried out. Thereby, an advanced measurement setup had been fabricated and tested integrating an air trap to remove bubbles.

Furthermore, addressing customer need for a flexible readout system, an in-house modular electrochemical reader is in development, to enable simultaneous execution of various electrochemical methods on all channels thereby offering the user full flexibility during parallel operation.

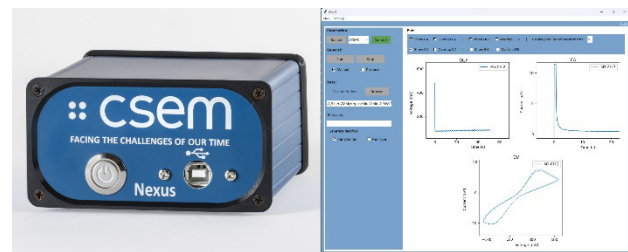


Figure 3: (left) Multichannel electrochemical reader for OCP, CA, CV, and EIS; with dimensions 127x107x57 mm³; (right) Graphical User Interface.

Finally, to enhance the multi-analyte sensors performance in complex media, the generated data is then fed into the data processing pipeline. Exploratory data analysis has been conducted on first data sets to quantify sensor variabilities, detect outliers, and spot interactions between sensors. Furthermore, various ML models, using linear and non-linear ML algorithms for both classification and regression tasks, have been trained to predict the type and concentration of mixtures based on multi-sensor responses. The results show promising directions where the random forest model learnt non-linear interactions between three sensors and classified two mixtures with high accuracy.

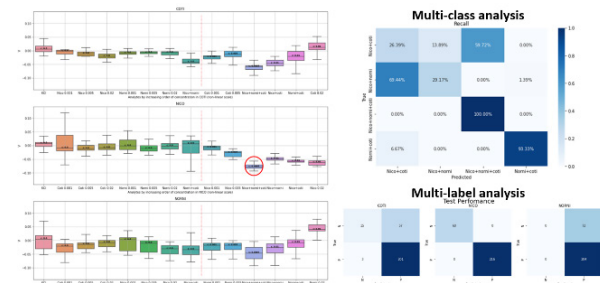


Figure 4: Preliminary machine learning models showing non-linear matrix effect.

Future work will target the wafer-level CMOS integration of sensors and processing, the validation of the albumin sensor, and extend the ML analysis to larger datasets.

ORCA – Semi-automated Workflow for Organoid Selection, Dissociation, and Single-cell Analysis

E. Aeby, S. Boder-Pasche, J. Goldowsky, T. Heinemann, C. Fonta, P. Rottmann, P. Cristofolini, C. Bichsel, S. Heub, T. M. Valentin, F. Kurth, V. Revol, G. Weder

Complex *in vitro* models are gaining in popularity for the development of new drugs. The tools and procedures available for the handling, sorting and analysis of organoids remain quite limited. A workflow named ORganoid Cell Analysis (ORCA) was launched to sort a bulk organoid solution based on an artificial intelligence algorithm into individualized organoids in a multiwell plate. These organoids are subsequently dissociated into single cells, which are encapsulated and analyzed with fluorescence.

Conventional 2D cell models used for the early phases of drug development often fail to reproduce the complexity and environment of the living body. In the last 15 years, organoids were shown to be valuable *in vitro* complex 3D models, bridging the gap between *in vitro* and *in vivo* testing. However, these new models still rely on manual handling as manipulation tools are missing, and their analysis fails to reproduce their complex architecture and heterogeneous cell composition. The goal of ORCA is to automate the workflow from organoid handling to single-cell analysis with three specific aims.

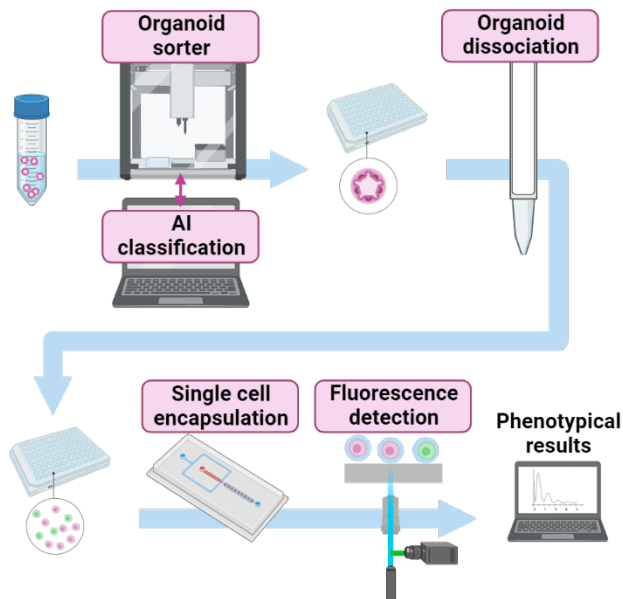


Figure 1: Overview of ORCA workflow starting with organoid individualization, dissociation and finally single-cell analysis through encapsulation and fluorescence detection.

- Aim 1: Sorting a pool of large ($>500 \mu\text{m}$) organoids into a 96-well plate, using a mechanical sorter relying on microfluidics and artificial intelligence. Based on an unsupervised approach, the AI algorithm clusters the images into groups of similar looking organoids, whereas subsequent testing (e.g., viability) can classify the groups among each other.
- Aim 2: Dissociation of each single organoid into single-cell suspension for further analysis at the cell level. The dissociation of individualized organoids combines mechanical and enzymatic actions in a small volume dedicated labware, aiming at facing the challenge of high cell recovery from a single organoid and with low volume.
- Aim 3: Encapsulation of single cells using droplet microfluidics, fluorescence labelling and detection with a versatile fluorescence detection module, while ensuring high cell viability and maximizing the cell recovery rate for further analysis.

The single-cell encapsulation process is summarized in Figure 2. Relying on droplet microfluidics, this process demonstrated high cell recovery rate (no observable cell loss), while maintaining high cell viability. A microfluidic chip is used to mix a single-cell suspension with oil and create droplets of several tens of micrometers. The exact size of the droplets can be finely tuned using different parameters such as flow rate and chip design. In the end of the process, the cells are present in a medium droplet surrounded by oil.

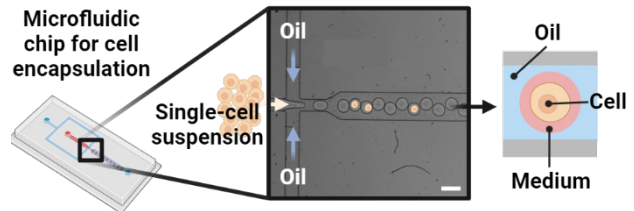


Figure 2: Concept of single-cell encapsulation. Scale bar is 100 μm .

The fluorescent encapsulated cells flowing in the microfluidic chip are analyzed using a fluorescence detection setup compatible with the chip (Figure 3). Excitation relies on a laser line projected onto the microfluidic channel, whereas the emitted light at a different wavelength is detected by a photomultiplier tube. The resulting electrical signal can subsequently be analyzed to retrieve single cell data. This entire setup was built in a modular way: up to 3 different lasers and PMTs can easily be installed or replaced, and different modules can be built on top of the existing setup for increased functionalities.

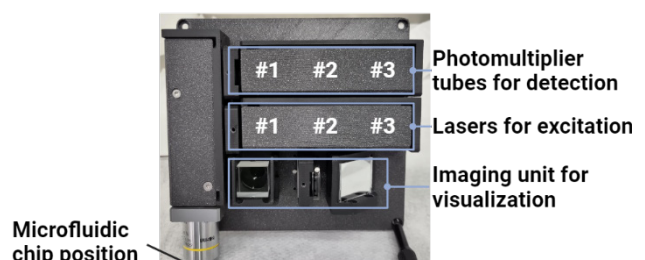


Figure 3: Image of the fluorescence analysis module.

This multidisciplinary workflow involves various approaches from the fields of biology, automation, machine learning, and multi-omics analysis including organoid individualization, organoid dissociation, and single-cell analysis. Bridging the gap between complex 3D models and single-cell analysis is a cutting-edge area of research to advance our understanding of complex biological systems and their role in health and disease. The single cell encapsulation lays the ground for cellomics applications.

SUMON – Disposable System for Sensors Monitoring

A. Sukumaran, H. Chai-Gao, I. Stergiou, F. Caruso, R. Cattenoz, A. Zandara, G. Oravez, S. Sunier, L. Burr, P. Nussbaum

SUMON covers the realization of multiple technology bricks including various types of sensors (ionic, enzymatic and bioassays) having a small sensing area, electro-chemical AFE dedicated to the sensors, a demonstration at the brick-level including the management of data and the related security.

Personal monitoring of biochemical analytes is a growing trend for which many products are already on the market: disease detection, food pathogens detection, body fluids monitoring for sport or health, etc. Most of the sensors involved are and will remain short-lived. The usual scheme of use consists in coupling a disposable sensor to a costly and bulky monitoring device performing analysis management. SUMON addresses this by integrating the sensor management and connectivity in the same miniaturized, expandable, and sustainable sensor substrate. Instead of addressing multiple pieces of miniaturized equipment, the user would just have to take another SUMON stick from the bottle and dispose of it after use. The scenario applies for sensing in saliva, urine, perfusion bags and many others: the device is activated at the start of use and discarded (no maintenance) after operations.

Most of the disposable sensors require a digital readout based on re-usable electronics. The disposable sensor + reusable electronic is indeed a quite attractive business model for many applications (e.g., chronic diseases and therapy monitoring) but not sustainable for applications that don't require repeated monitoring (e.g., pregnancy test, infectious disease, training monitoring) or in extreme remote conditions. For single-point analysis or in extreme remote conditions, the opportunity of offering disposable sensor + disposable sensor management would be a game changer. A first step towards this goal is to make the various components within SUMON independently disposable.

The architecture of the SUMON SoC is shown in Figure 1. A brief description of each component is given below.

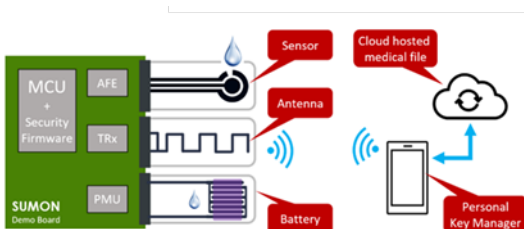


Figure 1: Architecture of SUMON prototype showing the SoC emulation board and the sustainable components (sensor, antenna, battery).

Sensors: Enzymatic sensors like lactate and glucose sensors and ionic sensors like potassium and sodium for saliva testing have been developed internally. The electrodes have been designed according to system constraints and screen-printed on a polymer film (Figure 2). This sensor could be further miniaturized. The sensors were prototyped, characterized and quality controlled for the bare electrode and the sensor. The sensor was tested by means of calibration curve in artificial saliva and subjected to interferences testing and lifetime storage stability testing.

Battery: A glucose fuel-cell activated by water has been selected from BeFC company. All materials used in the construction of the battery are biodegradable. Figure 3 illustrated how the battery



Figure 2: Biochemical sensor.

naturally degrades over 45 days. The battery requires specific power management to avoid premature degradation.



Figure 3: Natural degradation of the battery.

System-on-Chip (SoC): The final solution will consist in a SoC containing an analog front-end (AFE), a wireless transceiver, a power management unit (PMU) and a microcontroller (MCU). In the present iteration, we focused on the chemical sensor analog front-end whose architecture is depicted in Figure 4. The two 20-bit oversampled DACs are biasing the Reference and Working Electrodes (RE and WE).

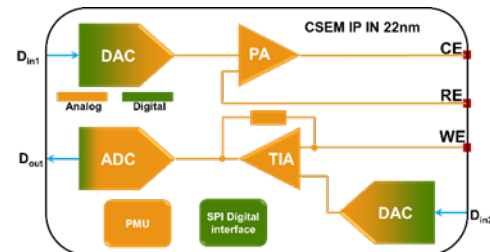


Figure 4: Simplified architecture of the sensing AFE.

The current injected into the WE is measured by the readout path consisting of the Trans-Impedance Amplifier (TIA) and the 18b Analog to Digital Converter (ADC). The AFE contains its own internal PMU and an SPI digital interface for communicating with external MCUs.



Figure 5: Demonstrator PCB.

Demonstrator: A preliminary version emulating the final SoC with COTS components has been designed to prove the concept. An eco-friendly bio-degradable water-soluble board (Figure 5) is used as the substrate to interconnect the functional blocks depicted in Figure 1. The Bluetooth communications with a mobile device will operate through a biodegradable antenna. The PMU regulates and bucks or boosts the biodegradable battery voltage to feed the other blocks. The outer connectors are dedicated to the sustainable components (biosensor, battery, antenna) and a USB port for debugging.

Data management: Sensor activation, powering, operation from a standard terminal like a smartphone and data security during and after transfer will be addressed in the next iteration.

PRECIZE – Predictive Quality Towards Zero-defect Manufacturing in 3D Printing

V. Pejchal, E. C. Poli, F. Crivelli, I. Sideris, N. Cantale, J. Poccard, K. Sharma, O. Vorobyov

The latest industrial revolution, Industry 04, is driven by the emergence of digital manufacturing and, most notably, additive manufacturing (AM) technologies. To achieve the goals set before AM, it is crucial to be able to move closer towards Zero defect manufacturing and to achieve the “first time right” approach, that is, to avoid lengthy and expensive non-destructive testing (NDT), which is often used for assessing quality of complex AM parts. The use of monitoring techniques such as melt pool monitoring and optical tomography, used in combination with machine learning might be the key to quality prediction and control in AM parts, bringing the industry to a more efficient and robust part production.

Within PRECIZE, key technology blocks have been developed towards the predictive quality of 3D-printed objects using the state-of-the-art sensing technologies equipped on EOS/AMCM M290 FDR laser powder bed fusion (LPBF) machine available at CSEM: (i) melt-pool monitoring (MPM) and (ii) optical tomography (OT) shown in Figure 1. The melt-pool monitoring system uses a photodiode, measuring light emissions from the melt pool and providing high resolution and in-depth insights with precise location of process deviations. The optical tomography system uses a sCMOS-based camera measuring the light emitted from the hot laser interaction zone in the near infrared region, permitting the in-situ tracking of defects. The use of these monitoring sensors permit the tracking of process signatures related to quality, layer-by-layer during manufacturing. This is of particular interest in non-destructive quality control of complex parts with hidden features inaccessible from outside, such as interior channels; an example of mm-wave RF antenna as presented in Figure 2.

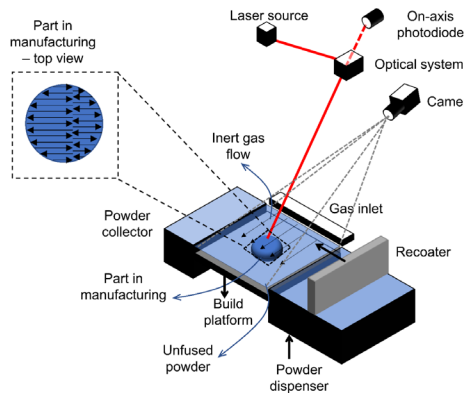


Figure 1: Schematic of the camera set-up within the LPBF machine.



Figure 2: RF antenna with internal corrugation and the corresponding melt-pool monitoring images of hidden corrugation features.

To efficiently process very large amount of data recorded by sensors an algorithm was developed. First, it maps the picture pixels and photodiode values to positions in a physical coordinate frame. Then, a mask is created to isolate the data from one specific area of interest in the part and that data is organized in tables that facilitate querying tasks. This makes it possible to compute metrics indicating the level of stability in the process when printing that area and insights into why potential defects and instabilities arise. Ground truth data provided with the physical measurement of the part surface roughness and

dimensions are then used to develop the metrics that provide insight into the part dimensions, roughness, and internal defects for quality prediction.

The sensor data are then used to obtain the digital twin of a printed object part from OT images (Figure 3). The dataset is meticulously curated through cleaning and filtering and a U-Net-based binary image segmentation model is trained on a target mask generated from MPM data which produces a binary mask representing the object part. The best-trained model is then employed for inference on OT images, generating predicted masks that are stacked and voxelized to create a volumetric representation. The final step involves extracting a surface mesh from the volumetric representation using the marching cube algorithm, completing the pipeline from OT camera images of multiple layers to the 3D reconstructed object part.

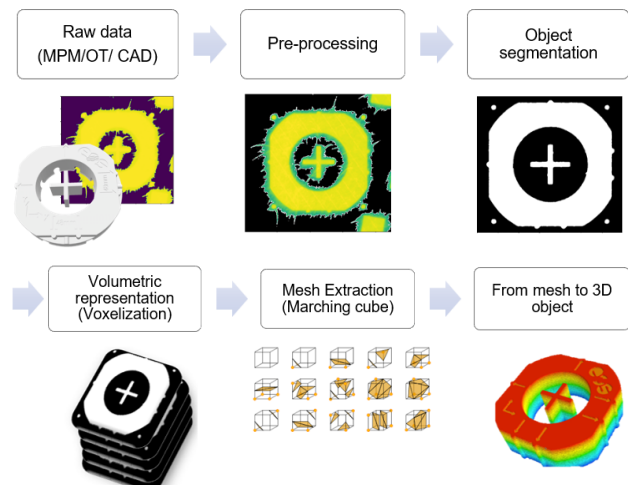


Figure 3: Steps of the 3D reconstruction of LPBF manufactured parts.

Predictive quality algorithms development has been focused on radio frequency components. Radio frequency tools require very precise features in often hidden feature fashion, good surface quality and are thus an ideal use-case scenario for PRECIZE. Figure 2 shows the demonstrator RF antenna with internal corrugation with few hundred microns thickness that is difficult to machine in single piece using conventional manufacturing. The first prototypes have been manufactured and their RF efficiency being tested.

Future work will use the developed data processing and dimensional 3D reconstruction algorithms to establish digital twin model for quality prediction of the RF antenna demonstrator and finally, the component RF properties will be compared with the obtained digital twin of printed RF demonstrator to establish performance prediction.

COSIMA – Cooperative Sensors for Electrographic Imaging

A. Fivaz, O. Chételat, B. Sporrer, S. Emery

Cooperative sensors are CSEM's patented solution for biopotential or bioimpedance imaging wearables. As opposed to the state of the art that individually connects passive or active electrodes in a star arrangement, cooperative sensors are active electrodes connected via a two-wire parallel bus, thus achieving an outstanding level of integration in wearables requiring many electrodes. This paper reports on the latest results obtained in the development of an application-specific integrated circuit (ASIC) for miniature cooperative sensors and its integration in a prototype. The current development status achieved the compliance verification of an ambulatory electrocardiograph with respect to the medical standards (IEC 60601-2-47) and evaluated the approach on one healthy subject.

Electrographic imaging requires applying many electrodes, e.g., on the head for electroencephalography (EEG) or on the chest for electrocardiography (ECG) or electrocardiographic imaging (ECGi). Figure 1 shows on the left the classical approach consisting of many passive gel electrodes, each individually connected by a shielded cable to a central electronic unit (not shown). Such devices are not suited for wearables, i.e., for their integration in (flexible, stretchable, breathable, washable) garments as shown on the right.

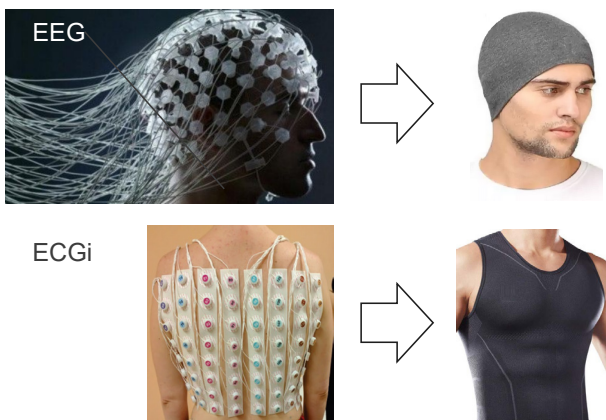


Figure 1: Biopotential imaging (left: classical approach, right: targeted wearable form factors, top: EEG, bottom: ECG/EKG).

CSEM's solution to address the problem is a patented technology called cooperative sensors. Cooperative sensors are active electrodes (i.e., with onsite preamplification) connected by a two-wire parallel bus (which can be, e.g., the two sides of a fabric made conductive). This simple connection scheme drastically reduces the integration complexity of devices requiring the measurement of many biopotentials, i.e., imaging wearables.

This paper reports on the latest results obtained for this technology, designed for up to 250 electrodes and verified so far for a 12-lead ECG, and in particular the miniaturization of the electronics at electrode level. Figure 2 shows the size achieved in the current prototype ($7 \times 7 \text{ mm}^2$).

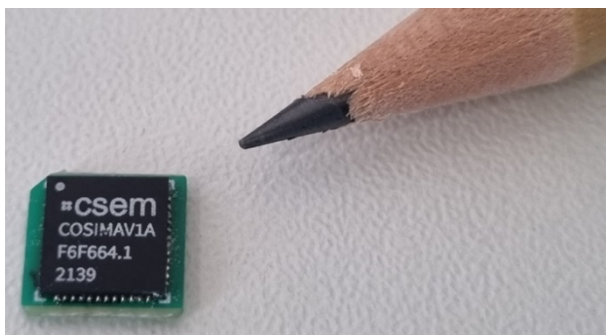


Figure 2: Miniaturized electronics at electrode level.

The device has been evaluated in a healthy subject as shown in Figure 3 (top). The obtained ECG signal (bottom) measured with

stainless steel dry electrodes ($\varnothing 12 \text{ mm}$, i.e., the size of snap buttons) seems reasonably clean and comparable with the records from classical devices.

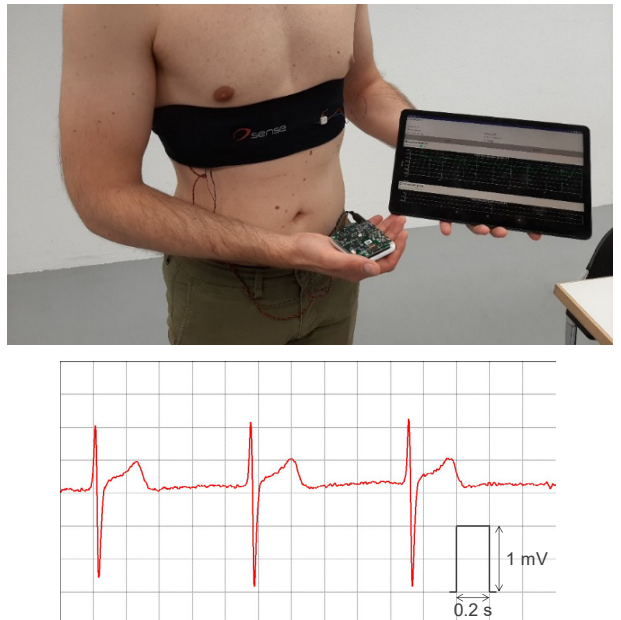


Figure 3: Evaluation of the current device prototype in a healthy subject (top) and acquired ECG signal with unwetted dry electrodes (bottom).

Further validations are foreseen extending to more electrodes, to more subjects, to operation in medical offices and to the different kind of electrographic signals. The main specifications drawn from the current experimentation are summarized in Table 1.

Table 1: Current prototype specifications (as measured).

specification	value
electrode type	dry (stainless steel dia. 12 mm)
number of electrodes	designed for up to 250 (verified so far for 12-lead ECG)
frequency response	0.5–150 Hz
system noise	21–33 μV (pp)
sample rate	2 kHz
sample size	16 bits
input impedance	> 4.5 G Ω @ 10 Hz
electrode impedance monitoring (lead-off)	online (1 nA @ 500 Hz)
power consumption per cooperative sensor	575 μW
electronic size	$7 \times 7 \text{ mm}^2$

DIGITALIZATION TECHNOLOGIES

Alain-Serge Porret

Digital Technologies' priority research at CSEM is to address the pressing challenges and opportunities of the digital era. It leverages digital technologies to provide comprehensive solutions to various problems and needs in the field, ranging from sensing to cloud analytics. These solutions are backed by years of specialized experience in hardware and software development.

Paving the way towards a digital society, the research priority comprises two main initiatives: application-based and technology-focused, which are explained below.

Technology-focused areas

This initiative explores cutting-edge technologies that enable various digital applications. It conducts extensive research and development on data and AI, as well as ASICs for edge and quantum technologies. It also innovates in both high-performance systems for cloud computing and smaller, low-power devices for edge computing.

Data and AI: This focuses on developing data security and privacy, processing and labeling of diverse data sets, and edge AI architectures. It aims to improve system-level integration and customization of advanced algorithms and architectures, emphasizing sustainability. It includes data engineering technologies, algorithm management tools, integration of large language models, edge and hierarchical AI technologies, and AI algorithms and tools for image generation and advanced labeling. It also covers a wide range of security architectures for data protection.

ASICs for the Edge: The aim is to design compact integrated circuits, with a focus on ultra-low power, which process high-level relevant information locally, at the data source. This enables real-time decision-making and feedback with low latency and high privacy. CSEM develops advanced Systems-on-Chip (SoC) that integrate sensor interfaces, imagers, ADCs, MCUs, ML-derived hardware accelerators, timing circuits, and wireless communication.

Quantum Technologies: The focus here is on using quantum phenomena for precise measurements and information processing. Components are first developed for quantum communication and computing, such as miniaturized, low-cost atomic clocks and hot vapor- or NV-based sensors. They are then transferred to industry and advanced up to or beyond the prototype stage.

Application-based areas

This initiative investigates the specific applications that benefit from digital technologies. Its aim is to foster or speed up internet of things (IoT) and machine vision, Industry 4.0, and digital health solutions. It encompasses efforts to improve device performance and lifespan, the integration of digital technologies to optimize production processes, and the development of smart systems that promote positive health outcomes.

IoT and Vision: This topic is about developing tools and technologies for acquiring, processing, and communicating a variety of physical quantities, including complex signals such as multispectral images. Its aim is to create a resilient IoT

infrastructure that improves device lifetime, reduces latency, and enhances service availability.

Industry 4.0: This topic is about facilitating the digital transformation of production processes. It integrates various technologies into a connected digital system for modern manufacturing, enhancing the latter's agility and efficiency, and fostering predictive maintenance and automation.

Digital Health: This topic is about developing solutions in telemonitoring, personalized medicine, and AI-assisted systems. It emphasizes medical innovations with microtechnologies, addressing the needs for portable medical devices.

Approximating Sizeable Combinatorial Optimization Problems with Tree Search Algorithms

I. Sideris, P. A. E. Schmid, F. Crivelli

In the rapidly evolving domain of modern manufacturing, optimizing production processes is crucial. This article delves into the Flexible Job Shop Scheduling (FJSS) problem, highlighting its relevance to process optimization and extends to a practical solution framework leveraging advanced tree-search algorithms. The performance of the framework is validated with experimental results.

Unlike the traditional job shop scenario, where each operation is restricted to a specific machine, the flexible job shop environment allows functions to be processed on any machine from a set of suitable machines. While beneficial in adapting to real-world complexities, this added flexibility introduces more sophistication in finding the optimal schedule.

Similar NP-hard (non-deterministic polynomial-time) problems can be found in the field of operational research, where there has been extensive work in trying to approximate reasonable time solutions to issues what, may seem insurmountable. Among the various problems encountered, the Flexible Job Shop Scheduling (FJSS) problem emerges as a pivotal challenge that encapsulates the essence of operational efficiency and flexibility. It extends the classical Job Shop Scheduling problem by introducing a layer of flexibility in machine assignments, thus mirroring real-world manufacturing scenarios more accurately.

The core of the FJSS problem lies in effectively scheduling a set of jobs across a collection of machines, where each job comprises a sequence of operations, and each operation can be processed on multiple machines. The overarching goal is to optimize a particular objective, such as minimizing the makespan, the total time required to complete all jobs, or reducing the waiting time and job tardiness.

Unlike the traditional job shop scenario, where each operation is restricted to a specific machine, the flexible job shop environment allows functions to be processed on any machine from a set of suitable machines. While beneficial in adapting to real-world complexities, this added flexibility introduces more sophistication in finding the optimal schedule.

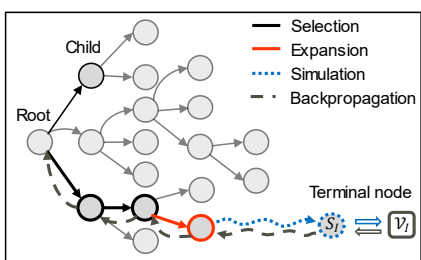


Figure 1: Illustration of the Monte-Carlo tree search algorithm's steps.

The application of FJSS extends significantly in addressing various manufacturing difficulties, particularly those entailing the definition of specific process segments and orchestrating the sequence of available actions within those segments. For instance, in additive manufacturing, determining the sequence in which material layers are deposited is pivotal, and the flexibility

in choosing among multiple deposition paths for each layer mirrors the flexibility in machine assignments inherent in FJSS. Similarly, in assembly line settings, the order in which different components are assembled and the choice among various assembly methods for each component can significantly impact throughput and quality. FJSS provides a structured framework to model and solve these ordering and choice problems by permitting a range of options for each process step while seeking an optimized sequence that minimizes time, cost, or other specified objectives.

Navigating the FJSS problem requires a sophisticated blend of optimization techniques and heuristics. Methods such as Tabu Search^[1] and Genetic Algorithms^[2] are often employed to traverse the expansive search space and converge on optimal or near-optimal solutions. However, these solutions are tied to specific environments or tailored for particular optimization objectives.

In the group for Predictive analytics at CSEM Alpnach, we developed a framework for optimizing scheduling and other similar problems using advanced tree-search algorithms, like the Monte-Carlo tree search (MCTS). These algorithms allow for efficient solutions that can scale in incredibly high dimensional problems, managing to balance between exploration and exploitation, outperforming existing approaches, and generalizing to multiple problem settings.



Figure 2: Process optimization results in better product quality and homogenous properties (right sample).

To demonstrate the capacity and efficacy of the developed algorithms, our framework was applied for the optimization of the deposition paths of additively manufactured parts using Wire Arc additive manufacturing. Our algorithms were able to improve the quality of the manufactured parts, by homogenizing the process-induced temperature fields by a factor of at least 25% allowing for improved dimensional accuracy and optimized material properties (Figure 2, right) compared to reference conditions (Figure 2, left).

[1] Saidi-Mehrabad, Mohammad; Fattahi, Parviz. (2007), "Flexible job shop scheduling with tabu search algorithms", *The International Journal of Advanced Manufacturing Technology*, 32, 563-570, 10.1007/s00170-005-0375-4.

[2] Kexin Sun, Debin Zheng, Haohao Song, Zhiwen Cheng, Xudong Lang, Weidong Yuan, Jiquan Wang, "Hybrid genetic algorithm with variable neighborhood search for flexible job shop scheduling problem in a machining system", *Expert Systems with Applications*, Volume 215, 2023, 119359, ISSN 0957-4174.

MultiOmix – a Multi-modal Framework to Analyze and Interpret Multi-omics Data

J. Meirer, F. Luongo, S. Jagtap, K. Zielinska, T. Heinemann, V. Revol

Multi-omics are the future of personalized medicine. However, multiple challenges present themselves with such data, with one of the main one being their integration. To increase the development speed of tailor-made solutions, CSEM has developed a framework to rapidly integrate multi-modal data in a plug-and-play fashion. Accompanied by a database of ready-to-use models, it enables rapid prototyping and flexible adaptation to novel problems.

In the evolving landscape of life sciences, our capacity to understand complex health conditions is undergoing a transformation with the rise of multi-omics data. Traditional single-modality approaches often fall short in capturing the nuances of diseases like cancer, where patient heterogeneity complicates diagnosis and treatment. Multi-omics – which synergistically combines genomics, transcriptomics, proteomics, and more – can illuminate the intricate mechanisms of health and disease. This comprehensive approach is revolutionizing cancer prognosis, enabling the discovery of biomarkers, and refining predictions for disease onset.

We at CSEM are contributing to this revolution, ensuring that these insights translate into tangible health benefits. Through our innovative framework, we have streamlined the integration of multi-omics data, furnishing researchers with robust, ready-to-deploy tools for their investigations.

The power of modularity in data analysis

Our framework, developed with PyTorch, has been a big leap forward to rapidly and efficiently developing multi-modal algorithms. At its core, the framework hosts a suite of interfaces for combining algorithms in a plug-and-play fashion. This modular structure not only eliminates the need to build from the ground up but also enables the seamless integration of pre-existing models. Imagine connecting a model interpreting bulk RNA with one analyzing histology images, then fusing both data types together to finally model the disease trajectory of a patient. This modularity is where our framework shines, fostering a rapid yet reliable pathway from conceptualization to functional models.

Saving time, reducing errors, and advancing research

Adopting a modular approach allows us to save precious time, especially in the early phases of a project. Instead of reinventing the wheel, we can repurpose our existing, tested models, customizing them as needed for specific tasks. This flexibility has proven essential in accelerating the development of personalized solutions.

Ensuring data protection and regulatory compliance

While our framework serves as a powerful tool for data analysis, we recognize the paramount importance of data protection and regulatory compliance. It is built to be compatible with secure data storage and handling solutions that meet stringent regulatory standards, ensuring that patient data is managed responsibly and ethically.

Interpretability and transparency in machine learning

Interpretability is a cornerstone of trust in machine learning, and our framework acknowledges this by incorporating interpretable models from the onset. Additionally, we maintain a repository of interpretability methods aimed at 'opening the black box' of complex algorithms. For instance, these methods can be used for pinpointing key prognostic genes within aggressive cancer types, allowing for more targeted and effective patient care strategies.

The model store: a repository of ready-made solutions

Our internal model store acts as a repository of both established and newly developed algorithms, housing range of models for different modality types and various fusion approaches. The ability to readily access and deploy these models underscores our commitment to accelerating the pace from prototype to production, exemplifying the agility of our framework. It allows us to quickly generate a baseline by plugging in the best-suited models while being able to quickly adapt and improve where it's needed in a modular way.

Practical applications and future collaborations

Our framework can readily be utilized to serve a diverse array of clients, from startups to established research teams, who benefit from its capacity to predict biological outcomes and identify biomarkers across various cohorts. The applications are as varied as they are impactful, whether it's in refining therapeutic interventions or streamlining the drug discovery process. Imagine the possibilities when multi-omics data is not just available, but also integrated, interpreted, and applied with precision and care. With this, we hope to start the collaborative journey towards a healthier future.

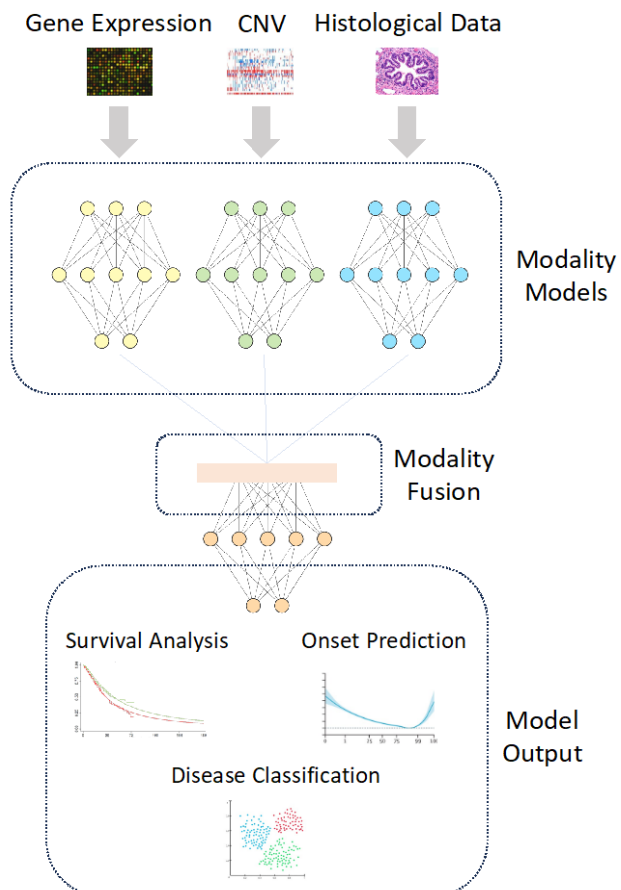


Figure 1: Scheme of "Multi-omix", the unified ML framework for multi-modal data integration developed by CSEM.

Data Acquisition Framework for Smart Weather Station Aurora

J. Beysens, M. Haro, R. Berguerand

After winning the tinyML Challenge 2022, CSEM co-organized in 2023 the follow-up Smart Weather Station challenge, with the aim of building a maintenance-free weather station without moving parts using tinyML technology. We developed a data collection framework with our prototype Aurora to build a large-scale and realistic dataset of acoustic wind and rain intensities from environmental recordings. This dataset will enable the creation of the next-generation tinyML models to efficiently estimate local weather conditions.

Last year, CSEM's team won the tiny Machine Learning (tinyML) Challenge 2022 organized by the tinyML foundation. The goal of the challenge was to develop a smart weather station without mechanical moving parts and to rely on local tiny machine learning to estimate wind and rain conditions. In this challenge, our team successfully developed the prototype Aurora to gather a dataset as well as a tinyML model capable of classifying the intensity of rain and wind intensities using a microphone. This accomplishment motivated the team to pursue the project further.

CSEM co-organized the "Next-Gen tinyML Smart Weather Station 2023" competition to foster collaboration and creativity. 50 participants from diverse backgrounds were challenged to design, build, and deploy a weather station that can accurately measure real-time environmental data (rain and wind), as well as temperature, humidity, pressure, and/or air quality. The competition encourages the use of energy-efficient and cost-effective hardware and software solutions that are capable of processing data locally (no cloud dependence) and can operate autonomously for extended periods.

For this challenge, we improved our prototype Aurora across multiple axes. Figure 1 shows the revised prototype. First, we mitigated synchronization issues due to multiple microcontrollers, by using a single microcontroller for the entire data acquisition framework. Secondly, we added wireless WiFi connectivity which enables to connect the station to an MQTT broker hosted on our server for direct data transmission. Finally, we added a solar panel for fully autonomous operation. The battery gives an autonomy of about two days in case of bad weather conditions.

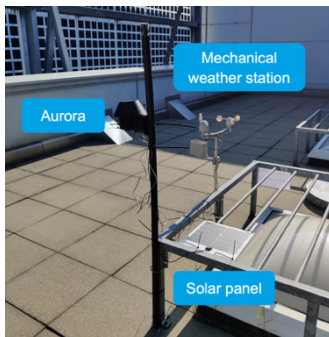


Figure 1: System setup, consisting of Aurora weather station, a mechanical weather station, and a solar panel.

Aurora employs a microphone to capture environmental sounds, a TPH sensor to monitor temperature, pressure and humidity and a mechanical station equipped with a rain gauge and wind sensor tracking both wind intensity and direction. This mechanical station exclusively serves as a ground truth for the ML model in the training phase; it will not be used in the inference phase (the latter is out of the scope of this article). The recorded data is then transmitted to a central server via MQTT which aggregates and processes the data. Subsequently, this data is made available to the participants of the challenge.

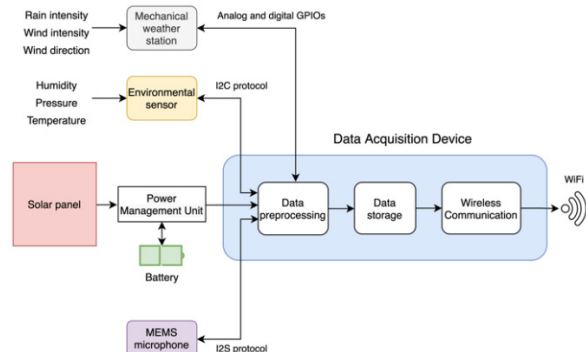


Figure 2: Data acquisition framework of Aurora.

The system is installed at CSEM headquarters and is operational since July 28, 2023. In the first five weeks, a dataset with more than 750 hours of recordings has been acquired, with a total size of 59.3 GB. This dataset is made accessible through the website: <https://aurora.portal.csem.ch/>. Furthermore, the website serves as a repository for sharing essential documentation with participants and showcases real-time weather conditions.

Figure 3 presents a set of preliminary results of the ML models trained on the dataset for binary classification of wind and rain, showing an accuracy of about 90%. Classification of more fine-grained classes and optimization for low-power microcontrollers is subject to further development.

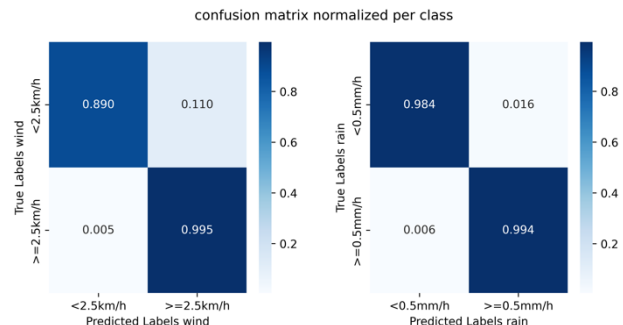


Figure 3: Preliminary ML results for wind (left) and rain (right).

Through this data acquisition framework, we will be able to collect data over a long period of time and in different locations, increasing the diversity of the dataset. Our goal is to deploy around five stations in Switzerland by the end of 2023. This will allow to design next-generation tinyML models that can more accurately estimate local weather conditions with a low memory footprint, low latency and low energy consumption. Furthermore, this platform will serve as the basis for future research, such as secure Firmware Over The Air (FOTA) updates, collaborative ML and online learning techniques. For more information, please check out Aurora's website here:



AI-enabled Defect Detection and Classification in the Sewers of Lausanne

D. Honzátko, S. Blanc, N. Cantale, L. A. Dunbar

This study focuses on using machine learning to automate sewer inspections, overcoming challenges such as low-quality footage, manual camera operation, and subjective defect annotations. By processing and filtering large datasets of inspection videos, the research developed algorithms capable of identifying sewer defects with significant accuracy. The application of machine learning models, including transfer learning for specific defect detection, demonstrates promising advancements towards fully automated sewer inspection systems.

Lausanne is the 4th largest city in Switzerland. Its water service department is responsible for maintaining and developing a vast sewage network system mostly located underneath the city and the neighbouring municipalities. Their maintenance requires frequent checks of sewage pipes, which are currently performed manually using a remote-controlled robot with a single camera.

The water service department is examining the possibilities of automating certain inspection procedures, with the long-term aim of automating the entire inspection process. Given the complex nature of this machine vision task, they asked the Edge AI & Vision Group at CSEM to help them examine the possibilities of automated defect detection in the existing inspection videos.

The task presents several challenges:

- Old CCTV videos have low quality (MPEG-2, 576i).
- The camera is manually controlled, and the operator often stops at defects to inspect them closely, changing the perspective and flow of the videos.
- When the camera is at the position of the labelled defect, the defect is out of the view of the camera as it is looking forward.
- The defects classes have a very uneven distribution, and despite having a common annotation norm, the annotations are subjective and vary from operator to operator.

So far, hundreds of gigabytes of labelled inspection videos, equivalent to 20 km of pipes, have been collected. To prevent the machine-learning-based defect detection algorithms from overfitting to the operator commands (i.e., when the operator stops the robot, there is a high chance of a defect), we first identify *valid sections* of the videos, where the principal axis of the camera and the pipe are parallel, and the robot is moving. We used a classical computer vision technique based on optical flow to make an initial estimate, then manually corrected these estimates and used them to train a neural network that can assess their validity.

A vital step in data processing is to convert the distance-based point and linear annotations into per-frame annotations see Figure 1. One frame may contain many defects. This mapping is possible as each video is accompanied by rough timestamp-to-distance mapping.

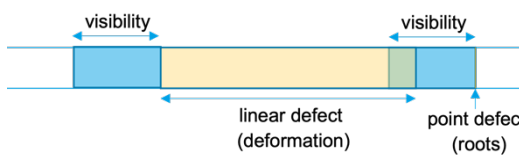


Figure 1: Converting pipe labels into per-frame annotations.

We use the pre-processed data, pruned of invalid sections and with per-frame annotations, for training machine-learning defect detection algorithms. Existing methods for defect detection in sewers either use end-to-end training or two-stage training first identifying defective frames and then classifying them into individual classes. Most of these methods have private training datasets. The only exception is SewerML [1], which provides both the dataset and the pre-trained neural networks but with both valid and invalid regions, and the annotations do not follow the European norm, limiting their direct use.

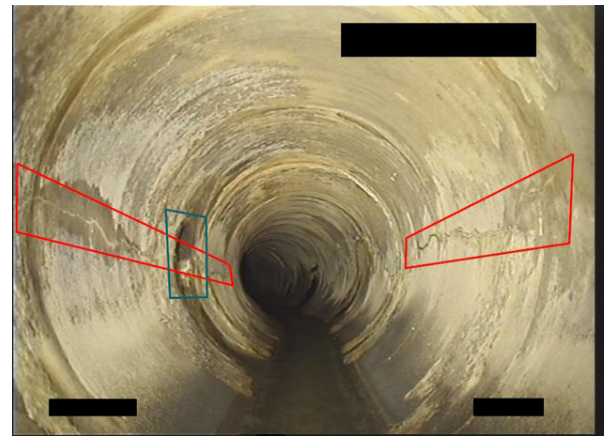


Figure 2: Example frame from an anonymized inspection video showing a defective section with cracks in the concrete wall of the pipe.

We started with binary methods, which only decide whether there is any defect in a frame or not. We fine-tuned existing per-frame SewerML pre-trained networks, and we also designed and trained a multi-frame neural network from scratch. Both methods achieved a similar average precision (AP) of 81% after smoothing the per-frame predictions over time. It should be noted that many of the algorithm failures can be attributed to mislabelled ground-truth annotations rather than algorithm errors.

The experts from the water services selected 14 defect classes of interest. Some classes didn't have sufficient support in the collected dataset; hence we used transfer-learning from the SewerML pre-trained models and fine-tuned them to predict just five classes with reasonable support and two super-classes (one for all obstacle-based defects and one for all structural-based defects). We conclude from this study that detecting obstacles is generally easier, as we were able to detect 88% with an AP of 62%. On the other hand, with the structural defects, we detected only 43% with an AP of 73%. These numbers are neither generalized nor final. Nevertheless, they show the task is generally feasible provided it is possible to acquire more data and, most importantly, provided that they are reliable and annotated in a more objective manner.

[1] J. B. Haurum, B. M. Thomas, "A multi-label sewer defect classification dataset and benchmark", CVPR (2021).

Securing Embedded Firmware Update over the Air with Distributed Encryption

D. Vizár, M. I. Ben Salah, Q. Liang

Secure firmware update over the air (FUOTA) and secure boot are fundamental for every Internet of Things (IoT) device fleet, for ensuring authenticity, integrity and secure remote deployment of firmware used on an embedded device. Also, to protect the IP within, the update packages are routinely encrypted. Using threshold encryption mitigates the risk of an attacker getting a perpetual access to firmware updates after a successful attack.

For applications with many connected embedded devices (a.k.a. IoT applications), the features of secure boot and secure FUOTA are essential. The former ensures that only unmodified firmware intended by the application owner can boot on the devices, which may be subject to remote attacks exploiting vulnerabilities in the communication stack, for example. The latter then enables the firmware in the device to be legitimately and securely changed remotely by the application owner only, e.g., to patch security vulnerabilities, fix bugs or to enable new features. To ensure the integrity and authenticity of the firmware, digital signatures are typically used.

In addition, firmware must routinely remain confidential, to protect sensitive IP contained within, or to mitigate an effective identification of software vulnerabilities by attackers. The typical solution is to encrypt the firmware package in transport, either using the same decryption key for all the devices, or by using a personalized decryption key for every device. The former approach, while simpler to deploy, suffers from a weakness, whereby it suffices for an attacker to successfully extract the decryption key from a single device to ensure a perpetual access to all subsequent firmware updates. Indeed, possessing the universal decryption key makes the attacker equivalent with a genuine device. The approach with personalized keys has the advantage of being able to revoke a compromised device, such that no more updates are encrypted with its keys but at the cost of increased overall complexity, necessitating a secure creation and distribution of personalized update packages. Upon a closer inspection, the security benefits are not always certain, as an intelligent attacker may faithfully simulate the behavior of the attacked device, making it difficult to detect that a device needs to be revoked in the first place.

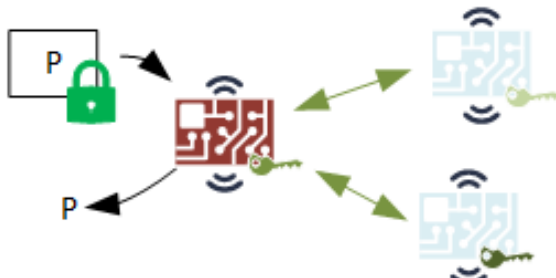


Figure 1: A device (red) performing distributed decryption with help of two other devices, recovering the payload P . Each has a key share, a threshold t (here $t=3$) of key shares is needed for each decryption.

This problem may be alleviated with threshold encryption, which allows a secret key to be split into n shares (n is a parameter), such that each share is given to one device and for every decryption, t devices must interact as depicted in Figure 1. The

threshold t allows for a trade-off between security and efficiency; the higher t , the more shares must an attacker acquire to be able to decrypt but also the more devices are involved in a decryption. CSEM developed an embedded implementation of the threshold encryption scheme DiSE^[1] for the Nordic nRF52840 SoC^[2,3].

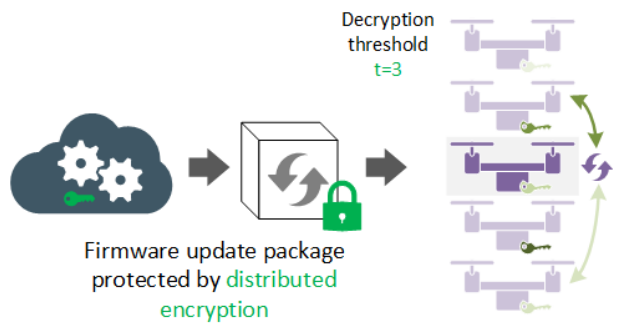


Figure 2: A firmware package secured by threshold encryption is sent from cloud application to an end-device (e.g., a drone), which decrypts the package with help of other nearby devices and updates.

CSEM designed an architecture using the above scheme to mitigate the issues created by leaked device keys. Figure 2 illustrates the process of firmware update, in which the payload of a firmware package is encrypted using threshold encryption prior to distribution, then decrypted by the target device using distributed decryption. In this architecture, a single, well-secured encrypting node may use a master key for efficiency, or a distributed architecture with multiple encryption nodes is possible for extra robustness to attacks on the cloud. It has been implemented by integrating DiSE with the MCUBoot secure boot framework and the CSEM real-time operating system μ111 and demonstrated using AWS cloud as the firmware dispatch backend, sending the update through an AWS-native ESP32 running FreeRTOS as a gateway to an nRF52840 devkit, which successfully updated with help of another nRF52840, performing the distributed decryption over BLE. In addition, the challenge of providing the device bootloader with auxiliary decryption information from other devices without integrating the communication stack into it has been resolved with a dedicated authenticated protocol between the peer devices, where the firmware requests from the peers encrypted auxiliary information on behalf of the bootloader and places the obtained data into a dedicated region of internal flash, such that only the bootloader can decrypt these.

The FUOTA with threshold encryption developed at CSEM can help manage and mitigate risks in many risk-sensitive verticals, such as drone fleets, Industry 4.

[1] S. Agrawal, P. Mohassel, P. Mukherjee, P. Rindal, "DiSE: distributed symmetric-key encryption", ACM CCS (2018) 1993.

[2] D. Vizár "Distributed encryption for robust data confidentiality and integrity for IoT", CSEM Scientific and Technical Report (2021) 48.

[3] R. Müller, "Robust IoT security with threshold cryptography", bachelor's thesis, HEIG VD (2021).

Fibonacci – a Scalable Approach to Embedded Machine-learning

E. Azarkhish, P. Jokic, R. Catteneo, C. Arm, S. Emery

Fibonacci is CSEM's state-of-the-art machine-learning (ML) system-on-chips (SoC) series, designed based on the principle of hierarchical scalability. The SoC can dynamically increase its computational performance by adding accelerator resources based on the application's needs, inspired by the Fibonacci number series. Its heterogenous architecture features a plurality of ML accelerators for temporal and spatial data analysis, energy-optimized on-chip memories, a flexible RISC-V microcontroller core, and a rich set of peripherals. Trained models can be deployed through CSEM's ML compiler, supporting most common formats (e.g., ONNX). Fibonacci targets the power consumption range of 10 uW-100 mW at performance of up to 160 GOPS non-sparse throughput and 2 TOPS/W efficiency.

A conceptual diagram of the Fibonacci SoC is illustrated below.

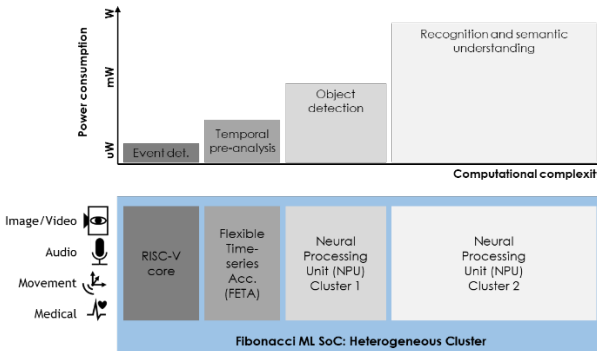


Figure 1: Hierarchical scalability offered by Fibonacci SoC for application-aware energy performance trade-off.

Fibonacci features a multi-cluster architecture with simultaneous support for spatial (e.g., CNN, ResNets) and temporal (RNN) ML network topologies. The Flexible Time-series Accelerator (FETA) cluster focuses on time-series signals, and the Neural Processing Unit (NPU) clusters target spatial models. The two NPU clusters offer similar functionalities at different power and performance targets, allowing the application designer to choose one/both based on the needs.

One key feature of the Fibonacci SoC is the availability of multiple sensing modalities and various data streams to facilitate at-edge data fusion, and multi-modal inference. The embedded transceivers include: I2S (4x), SPI (2x), I2C, OctoSPI, DCMI, UART, JTAG, GPIO, each providing dedicated data streams through various interconnection matrices and DMA engines (2x two channels) to the accelerators. Plus, a complete audio front-end from digital microphones including activity detection and Mel Frequency Cepstral Coefficients (MFCC) is implemented in Smart Front-end (SFE) unit, which can be reprogrammed for other types of time-series signals as well.

The memory hierarchy (illustrated in Figure 2) includes 4 MB of SRAM L2 memory, organized in multiple banks with a wide data bus interface. The accelerators use the same wide-bus interface for higher bandwidth access, but the processor and DMA engines access L2 memory through micro-caches (UC), small write-back caches with software managed coherence, to minimize energy and latency penalties. Each accelerator has small scratchpads (L1) to facilitate intermediate computations.

Power management in Fibonacci follows a hierarchical scheme as well, with a master finite state machine residing in an

always-on domain, controlling, and coordinating power up/down sequences of six other domains.

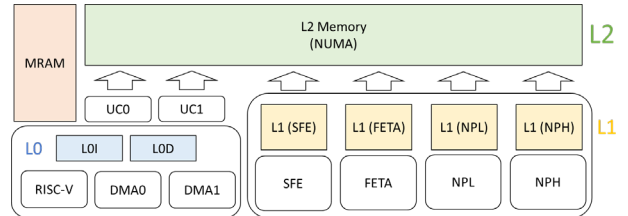


Figure 2: Memory hierarchy of the Fibonacci SoC.

512 kB of MRAM [1] is accessible to the RISC-V [2] cluster to enable zero-leakage weight or program storage for heavily duty-cycled application scenarios.

A mix of different voltages, standard cells and memory flavors are used to further optimize each power domain (a.k.a. cluster) to its range of responsibilities. The always-on cluster is implemented using ultra-low leakage (ULL) transistors, while the other domains use a mix of low VT (LVT) and super-low VT (SLVT) ones. On-chip clock generation and distribution are handled (thanks to existing internal IPs), with frequencies ranging from a few kHz to 400 MHz. To minimize the latency and energy overheads of inter-cluster communications, yet benefit from independent performance settings for individual clusters, a special qualifier-based handshaking mechanism along with a source-synchronous clocking approach are implemented across the chip.

The Fibonacci SoC aims to support multiple classes of applications in the fields of IoT edgeML and smart sensing, such as:

- Multi-modal concurrent data analysis from different sensor types (e.g., audio-visual sensor fusion).
- Multi-stage evaluation, selective/hierarchical execution with increasing complexity, and early exit to reduce energy consumption (e.g., activity tracking and analysis).
- Ultra-low power edge processing, down to μ W power budgets with heavy duty cycling (e.g., condition monitoring).
- Spatial and time-series signal analysis (e.g., audio analysis).

The chip will be implemented in GF22FDX technology. A demonstrator is planned to target different application scenarios from the classes listed above.

[1] <https://gf.com/blog/making-new-memories-22nm-emram-ready-displace-eflash/>

[2] www.csem.ch/en/news/low-power-risc-v-integration-customization-and-soc

Integrating Cryptographic Accelerators with the icyflex-V Core

F. Valencia, J.-L. Nagel, D. Vizár

Modern connected embedded devices need to support secure firmware update over the air, secure wireless communication, device authentication and other security features, requiring the devices to implement cryptographic algorithms. This is often done through dedicated hardware accelerator circuits to optimize energy consumption and satisfy latency or throughput constraints. For the accelerators to yield the desired benefit in constrained systems, an efficient integration with the processor is needed. Here, a system integrating a RISC-V core and cryptographic accelerators is presented. The system is easy to extend and to configure at different levels (core, accelerators, SW) to fit many applications.

Embedded systems often need to optimize latency, throughput, energy consumption, and other metrics of cryptography beyond what is achievable in software, e.g., when verifying a firmware image within a given time limit in the boot sequence or to comply with communication latency limits. These operations are typically computationally heavy, e.g., Elliptic Curve Cryptography (ECC) performs many modular arithmetic operations with 256-bits operands. At the same time, care must be taken to avoid information leakage through side-channels if physical security requirements are applicable. The final challenge is an integration of the dedicated accelerators in a way that preserves the performance benefits and does not disrupt side channel security.

Several cryptographic accelerators were designed at CSEM. A big-integer-arithmetic accelerator was designed to accelerate the most common function, computationally heavy functions of ECC and to facilitate the implementation of the remaining functions in software. A configurable size of internal multiplier modules allows trading-off area and execution time. With 32-bits internal multipliers and a 100 MHz operating frequency, the synthesized module has an area of 25.1 kGE (Global Foundries 22 nm library). For 256-bit integer operands, addition and subtraction each take 14 cycles, modular addition and modular subtraction take 29 cycles, and Montgomery multiplication takes 437 cycles. Another accelerator was designed for Keccak, a cryptographic permutation used in SHA3 hashing standard^[1], recent post-quantum cryptography and other algorithms. Three versions of the accelerator were developed, targeting different levels of side-channel security^[2] overviewed in Figure 1.

Version	Timing [cycles]	Area [kGE] @ 100 [MHz]	SCA defense
Slice-based	1601	24.1	None
Slice-based with masking	1601	67.7	Masking 3 shares
Shuffled	371	43.8	Shuffling

Figure 1: Overview of Keccak HW accelerators designed at CSEM. The reported timings are for a single execution of Keccak permutation.

CSEM maintains an in-house implementation of a lightweight RISC-V core called Icyflex-V, optimized for (ultra) low power and energy consumption to meet requirements for Internet of Things (IoT) systems. An integration framework was designed to allow

^[1] M. Dworkin, "SHA-3 standard: permutation-based hash and extendable-output functions", Federal Inf. Process. Stds. (NIST FIPS), National Institute of Standards and Technology, Gaithersburg, MD (2015), <https://doi.org/10.6028/NIST.FIPS.202>

the IoT processor Icyflex-V execute cryptographic algorithms efficiently. The framework connects hardware accelerators with the processor optimizing the data communication and enabling an easy software accessibility. The accelerators were connected using a register interface as shown in the block diagram of Figure 2. The register interface is connected through the APB (Advance Peripheral Bus) enabling the use of the accelerators with memory operations-like style.

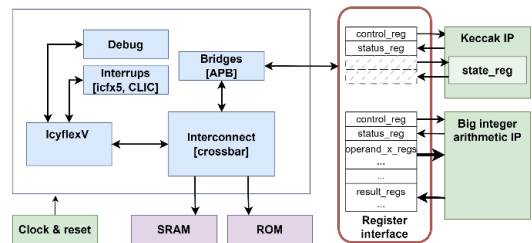


Figure 2: Overview of the system.

ECC accelerator has three inputs of 256-bits corresponding to two operands and a modulus, one 32-bit input for the inverse Montgomery modulus, one 256-bit output for the result, and controls/status signals. Operands and result are saved in the register interface. The operand size and internal representation can be configured in the accelerator at instantiation time.

Keccak accelerator saves the internal state because very often the new inputs are combined with previous state. Therefore, the register interface only saves the control/status parameters and input/output data directed to the accelerator. Adding the register interface to Keccak accelerators has an area overhead around 2%. The accelerator allows to configure the word size, maximum state size and maximum input/output rate at synthesis time. At runtime, the accelerator allows to choose the number of rounds and the actual input/output rate. To fully implement SHA3 algorithms, the padding and prefix addition need to be implemented in software.

The system has been tested in an artix-7 (xc7a100) FPGA with CSEM's u111 operating system. The FPGA resource usage is 17.3k LUTs, 10.3k FF and 10 DPSs. Our system is a perfect baseline for more complex systems because it allows to identify, evaluate and test optimization strategies at different levels (OS, core, accelerator). The architecture allows an easy integration of other modules (i.e., AES) and HW/SW codesigned implementations.

^[2] P. Socha, V. Miškovský, M. Novotný, "A comprehensive survey on the non-invasive passive side-channel analysis", Sensors 2022 (2022). doi: 10.3390/s22218096.

BirdGuard – Protecting Birds from Window Collisions

P. Jokic

Collisions with windows are one of the major causes of death for birds [1], among which are endangered species. In Switzerland alone, more than a million birds are estimated to die from such collisions every year – events that could be avoided. The BirdGuard project develops a solar-powered and computer vision-based patch that is placed on the window to monitor birds and warn them if they are on a collision trajectory with the window, saving their lives. First results from a laboratory demonstrator have shown promising results, successfully detecting and tracking birds, proving the concept.

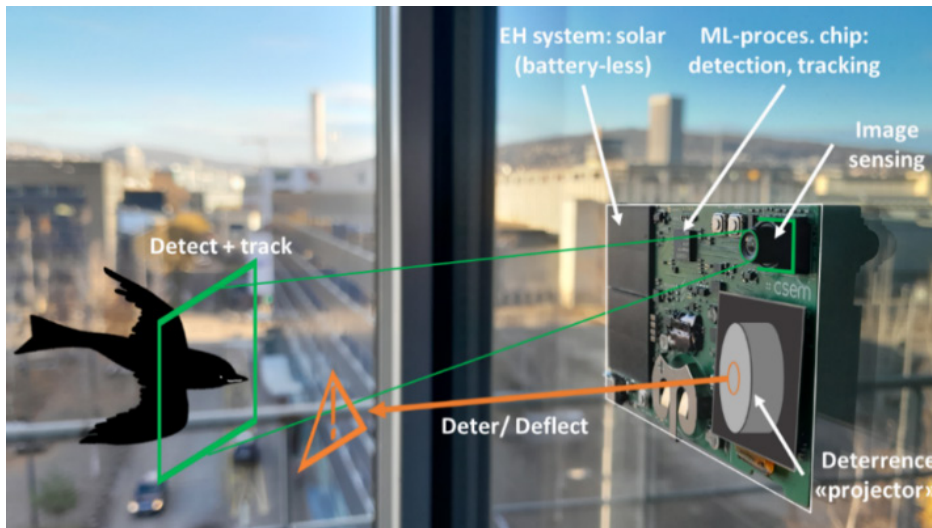


Figure 1: Illustration of the system detecting and deterring an approaching bird.

BirdGuard is an applied research project at CSEM, employing state-of-the-art machine learning (ML) technologies to make houses more bird-friendly and enable a respectful human cohabitation with nature. To cover all bird-specific aspects of the problem, CSEM collaborates with Swiss research institutes that are at the forefront of researching birds and their habitat around humans. This aims to complement existing installations that require pattern stickers covering the entire window, making them unpopular and thus limiting their deployment. BirdGuard provides a small and easy-to-use alternative that enables laymen to retrofit existing windows while being completely self-sustaining through solar power and barely visible due to its small size on the window. The patch is placed on the window and autonomously monitors birds to warn them if they are on a collision trajectory with the window. Aesthetically, this solution does not compromise the window design (as opposed to stickers), providing designers and architects with new opportunities for bird-friendly constructions.

Figure 1 illustrates the business card-sized prototype patch, consisting of a solar energy harvesting subsystem to enable battery-less operation, a CSEM low-power image sensor, and CSEM's ML system-on-chip for processing acquired images and controlling the steerable deterrence mechanism. The high efficiency of the ML chip allows to run complex state-of-the-art detection algorithms onboard the patch while being solely powered by sunlight.

Detecting birds

Robust detection and tracking are essential for monitoring the trajectory of the birds and estimating the collision probability in real time. Machine learning-based detection algorithms, like YOLO, have revolutionized the field and have thus been adopted for this project. Our successfully demonstrated implementation is

trained on a diverse dataset that enables to accurately detect birds of different species (e.g., Figure 2) while avoiding detections of other animals and objects (false positives) to save power and avoid disturbing the environment with false warnings.



Figure 2: Output of the bird detection algorithm on a validation image.

Warning birds

An effective and timely warning of the birds on collision trajectories is essential to make sure the birds understand the obstacle and still have sufficient time to change their course. The warning is directed within a small spatial angle to the bird, reducing power consumption and interference with the environment. For the laboratory demonstration, a servo-driven eye-safe laser has been used, that is being replaced by a miniaturized deterrence subsystem in an ongoing project.

Miniaturized edgeML deployment

In the next phase, the system will be deployed to a miniaturized prototype, based on CSEM's latest machine learning chip Fibonacci SoC [2]. This will enable increased frame rates beyond the currently achieved 10 frames per second and allow to showcase self-sustaining operation using the solar panel.

[1] M. Rössler, et al., "Vogelfreundliches bauen mit glas und licht", Schweizerische Vogelwarte Sempach (2022).

[2] CSEM technical factsheet "Fibonacci ML SoC", <https://hdl.handle.net/20.500.12839/1369> (2023).

Software Defined Radio Approach for Bluetooth Dual Mode Digital Baseband

N. Scolari

The Software Defined Radio is growing in interest because of its flexibility. During the CSEM icyTRX-DM IP (a Bluetooth Dual Mode transceiver) digital baseband design, a similar approach has been chosen to provide maximum flexibility and facilitate the evolution of the IP such as to track new Bluetooth releases or to address other standards.

The advancements and the adoption of CMOS deep submicron technologies causes a shift in the design paradigm: while the analog blocks can not follow the technology shrink for several reasons, the digital blocks easily take advantage of it. This allows to add more functionalities to the digital (Figure 1) and new calibration capabilities of analog blocks done digitally. This new paradigm has been applied to the design of the icyTRX-DM IP, a Bluetooth Dual Mode (DM) – Low Energy and Classic – transceiver in 22 nm technology. While the area of the IP is still dominated by the analog part, the shrink of the digital section opened the doors to new possibilities. The chosen approach is to provide maximum flexibility to the system: the Tx/Rx data-paths are fully reconfigurable as a Software Defined Radio (SDR), and other functionalities such as the packet handler or the Automatic Gain Control (AGC) are implemented as a full software solution.

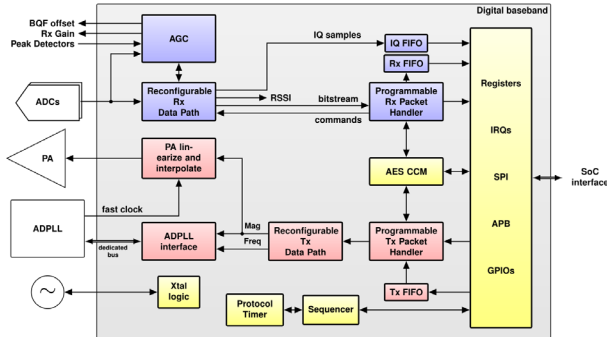


Figure 1: icyTRX-DM digital baseband block diagram.

The Tx/Rx data-path are responsible for the modulation and demodulation of the radio signal, i.e., the conversion from/to a digital bitstream to/from analog signals. These complex operations can be decomposed into simpler ones, such as multiplication, decimation, interpolation, etc. The classic approach is to define the required blocks and connections for the wanted modulation and implement it in a hardware description language (HDL). With a SDR approach, as shown in Figure 2, the basic blocks are not connected in a predetermined configuration, but can be connected dynamically, depending on the use case. This reconfigurability requires that every basic block provides a standard interface, that specifies information such as the data itself, the destination block, or the type of data under process. The resulting datapaths are extremely flexible. The only limitation is the number of integrated blocks and the availability of specific functions, e.g., a very particular coding or filtering. The number and type of blocks that are implemented depends on the complexity required by the desired implementation. On icyTRX-DM, the design choice has been done to support the Bluetooth DM and the IEEE 802.15.4 standards. Hence, as an example of flexibility, it is possible to support both the IEEE 802.15.4 bit to chip encoding with the Bluetooth Enhanced Data Rate (EDR) modulation scheme. Another advantage of the SDR approach is that the insertion of a new block during the design phase is simplified because of the standard interface. The drawback of this approach is that

number of possible connections between blocks can quickly grow and requires to limit the possible connections, in particular between blocks that are not compatible, as for instance bitstream vs integer processing. Since these connection limitations are easily defined, it is also possible to strongly limit the flexibility in order to fallback to a standard version of a digital baseband, such a Bluetooth Low Energy (LE) only version to reduce the footprint.

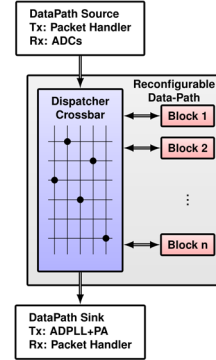


Figure 2: SDR data-path principle.

The packet frames, AGC and power sequences are in general described by Finite State Machines (FSM) that can become quite complex and difficult to maintain. For instance, the Bluetooth LE packets and the associated packet handler FSM are becoming increasingly complex, and the RTL-defined (register transfer level) FSM can quickly be outdated by new Bluetooth releases. Similarly, the AGC strategy is generally difficult to define in advance due to the mixed mode (analog-digital) nature of the controlled signals, and application-dependent trade-offs between different specifications. Finally, the power-up sequences of the transceiver are often subject to change to optimize or mitigate limitations only apparent on physical samples. A software approach for these FSMs with associated micro controllers (uC) seems to be the logical solution: We implemented four uCs in total: 2 for the Tx and Rx packet handlers, one for the AGC and one for the power-up sequences. These uCs have a minimalistic set of instructions and dedicated interfaces, to implement their very specific operations in an efficient way.

The icyTRX-DM digital baseband also includes many interfaces to the analog IP section to perform calibrations required by the analog blocks. For instance, mismatches of the analog baseband filter have to be corrected for and therefore require a dedicated calibration step. This procedure can be coded as an additional procedure of the "AGC" uC.

The programmability added to the icyTRX-DM digital baseband provides great flexibility to the platform in many aspects. On the design side, it facilitates the introduction of new features. On the deployment side, it allows the update the functionalities to comply with a new specification or define a new proprietary mode with a large range of options. Finally, the increased flexibility facilitates both debugging and bug correction as the same function can be implemented in several ways.

A Dual-mode Bluetooth Transceiver with Two Concurrent RX Paths, Offset-LO, +20 dBm Output Power, and -98 dBm Sensitivity in GF22 FDSOI

K. Manetakis, N. Gerber, V. Kopta, F. X. Pengg, E. Pérez Serna, P. Persechini, N. Raemy, C. Salazar, N. Scolari, A. Vouilloz

A Dual-mode Bluetooth transceiver with two concurrent receive (RX) paths for the simultaneous reception of BT and ZigBee is presented. It achieves +20 dBm maximum output transmit power and -98 dBm Sensitivity in BLE 1 Mbps. An offset local oscillator (offset-LO) alleviates pulling.

Compared to the icyTRX-DM, which has a single RX path and delivers +10 dBm maximum output power, this IP offers two RX chains to receive BT (BLE, BR, EDR2, EDR3) and Zigbee simultaneously. The tenfold increase in the output power necessitated 1) the redesign of the digital power amplifier (DPA) to keep the same supply voltage, 2) the rework of the antenna interface to protect the receiver's front end during transmission, and 3) the introduction of an offset-LO scheme to alleviate pulling. Furthermore, the requirement for concurrent reception drove the choice of current-mode RX paths due to their superior linearity. The IP was implemented in the GF22 FDSOI process and occupies two square mm. The block diagram is shown in Figure 1. The layout is depicted in Figure 2.

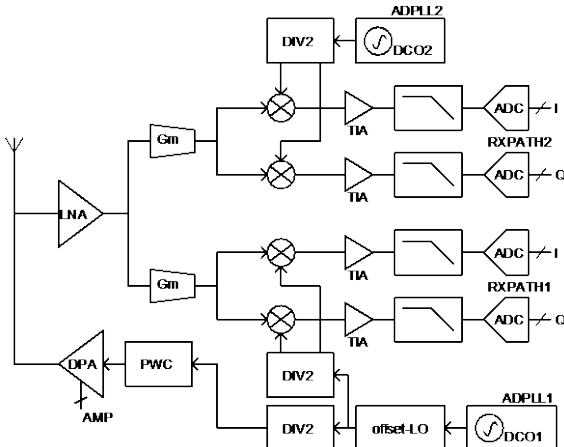


Figure 1: Block diagram.

The first all-digital phase-locked loop (ADPLL1) and the Offset-LO operate when the transmitter is on and ensure that the digitally controlled oscillator DCO1 does not run at an integer multiple of the DPA frequency, thus eliminating pulling. The DCO1 operates in the 3.2-3.3 GHz range and drives the offset-LO, which outputs 4.8-4.96 GHz. The offset-LO consists of an active single-sideband mixer with an inductive load to keep the levels of the generated spurs well below the DPA harmonics. A divide-by-2 (DIV2) generates the required 2.4-2.48 GHz LO signal for the DPA. The phase noise of the offset-LO is designed to be well below the phase noise of the DCO1. The ADPLL1 is also used during the receive operation to generate the LO signals for the first RX path (RXPATH1), while the ADPLL2 generates the LO signals for the second RX path (RXPATH2). The DCO2 operates at twice the LO frequency. The phase noise of the DCOs is -110 dBc/Hz at 1 MHz offset, and each ADPLL dissipates about 1.5 mA. Both DCOs use Fig-8 inductors to minimize magnetic coupling.

A digital inverse class-D power amplifier with an integrated balun provides up to +20 dBm at the antenna. Phase modulation generated within the ADPLL1 feeds directly to the DPA's phase path, which consists of a divide-by-2 (DIV2) and a pulse-width control block (PWC) that offers an additional knob to set the output power and minimize the level of the DPA second harmonic, easing the design of the external harmonic filter. Amplitude

modulation for EDR2 and EDR3 is introduced by dynamically controlling the DPA's 256 slices. Being an RF DAC, it generates aliases in the output spectrum. The amplitude data (AMP) are fed into the DPA at a high rate (400 MHz) to alleviate this effect and meet the out-of-band emission requirements. For constant envelope modulations (BLE, BR, ZigBee), the number of active slices is statically set to control the output power level. AM-AM and AM-PM predistortions are implemented in the digital portion of the IP. Typical maximum output power is +20 dBm with 30 % system efficiency from a 1.8 V external supply.

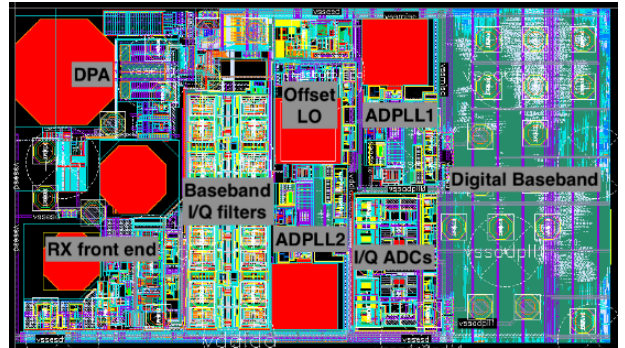


Figure 2: Layout view. The total area is two square mm.

The two low-IF receive paths consist of a common front end connected at the negative side of the DPA balun, shorted to the ground by the integrated TX/RX switch during transmission to protect it from the high swing at the antenna. ESD diodes protect the RX/TX switch. The front end is based on an inductively matched common-gate LNA with an additional inductor in the load tank for good noise performance. The LNA drives two current-mode 25% I/Q passive mixers via transconductance stages (Gm), followed by transimpedance amplifiers (TIA). The TIA outputs feed directly into the baseband analog filters. DC offset calibration is achieved by adjusting the back-gates of the differential pairs at each filter input. The filter cutoff frequency is set to 2 MHz or 4 MHz, depending on the modulation format. Digitization is done with two (per-path) 9-bit SAR ADCs sampled at 48 MHz. Peak detectors along the two RX chains facilitate automatic gain control. The overall gain of each receive path is 72 dB while achieving 5.5 dB NF to meet the -98 dBm sensitivity specification for BLE 1 Mbps. Power dissipation is 2.9 mA for both paths simultaneously and 2.1 mA for single-path operation.

The IP's RF architecture has been reused in the latest versions of the icyTRX-DM in both GF22 FDSOI and TSMC22 bulk processes, albeit at a reduced output power level and with a single RX path and no offset-LO.

A Low-jitter Reference-less Clock and Data Recovery (CDR) with Low Phase-noise Multi-clock Generation

C. Salazar, F. Chicco, A. Dissanayake, A. Vouilloz, D. Ruffieux, S. Stanarevic, R. Ravanilla, N. Gerber, N. Scolari, L. Von Allmen, M. I. Ben Salah, P. A. Dal Fabbro

This paper reports the development of an integrated 2.7 GHz reference-less Clock and Data Recovery (CDR) circuit with an ultra-low phase-noise multi-clock generator for low-jitter and high-speed clocking applications.

Our recent development towards a low-noise Phase-Locked Loop (PLL)^[1] demonstrated 20 dB in-band and 9 dB out-of-band phase noise improvement at a moderate increase of power dissipation compared to CSEM's legacy ULP short range RF-synthesizer expertise. This follow-up work aims at substituting the crystal reference clock with the recovered clock of a Clock and Data Recovery (CDR). This enables cascading multiple devices in a chained configuration, collecting data from individual nodes at the ring's end, while avoiding the need to manage individual crystals and their frequency imprecision. This simplifies network synchronization and reduces costs. Besides guaranteeing wireline communication at 900 Mbps, the focus was obtaining low-noise clocks for medical applications.

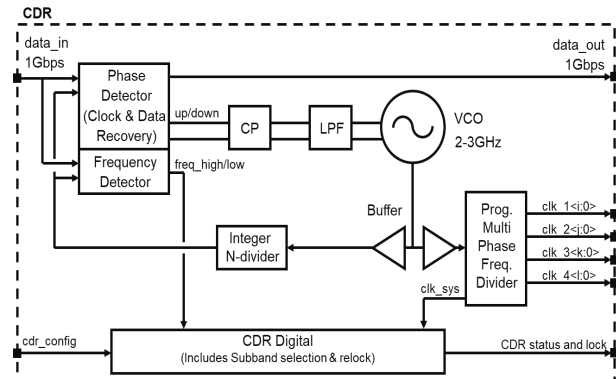


Figure 1: Block diagram of the proposed CDR with ultra-low phase noise multi-clock generation.

This report presents the design of a 900 Mbps low-power reference-less CDR with an ultra-low phase-noise programmable multi-clock generator. The simplified block diagram is illustrated in Figure 1. Contrary to conventional PLL-based CDR's, the proposed architecture does not rely on a crystal oscillator (XO) but rather extracts the timing reference of the system directly from the input data. The loop is composed of a linear Triwave Hogge Phase Detector (PD), a Charge Pump (CP), a 1nF integrated loop Low Pass Filter (LPF), a 2.1 to 3.2 GHz Voltage-Controlled Oscillator (VCO), an integer loop frequency divider and a Frequency Detector (FD). To address a large domain of applications requiring high-performance clocks, the CDR is complemented with versatile ultra-low phase-noise frequency dividers all synchronized by the data recovered clock. It features various division ratios, each with multi-phase clock generation for phase sensitive applications. It also generates the system clock. Automatic sub-band selection during first lock, continuous lock status tracking, and automatic re-lock in case of

unlock detection is performed thanks to a novel digital finite state machine assisted rotational phase FD, capable of operating over a wide frequency range to overcome variable data rates and data-dependent run-lengths. The complete CDR including the programmable frequency divider, at the exception of the bandgap current reference is supplied from a 1.1 V source.

One of the key performance parameters to optimize in CDR's is the data jitter transfer function to guarantee minimal amplification of the jitter, particularly, in applications where multiple chips and thus CDR's are cascaded one after the other. Hence, the proposed CDR is designed for jitter peaking minimization, while providing an excellent phase noise performance both in-band and out-of-band.

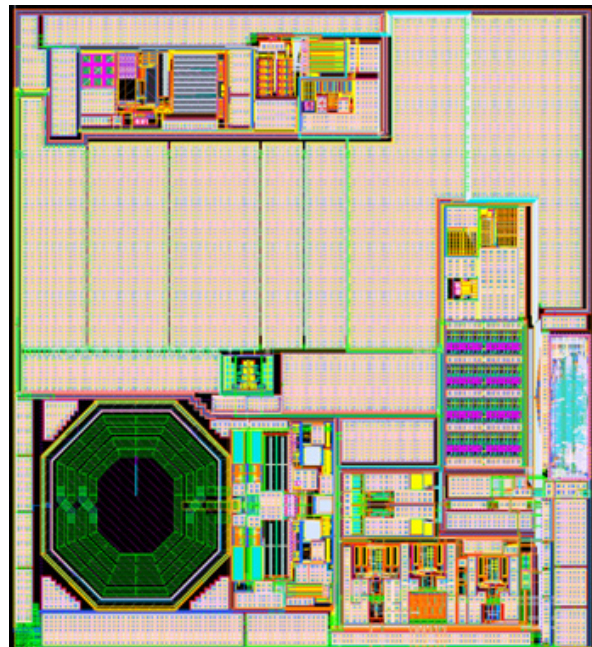


Figure 2: Layout view of the CDR IP.

Figure 2 shows the layout view of the CDR. The circuit, with a footprint of 800×885 μm , was integrated in a low-power RF 40 nm technology. The CDR and the programmable frequency divider consume 20 mA from a 1.1 V supply. Simulation results predict an intrinsic clock-driven RMS absolute jitter of 300 fs with an integrated bandwidth from 1 kHz to 100 MHz at 2.7 GHz. The long-term N-period jitter at 1 ms is 750 fs and the closed loop jitter peaking is <0.5 dB.

[1] C. Salazar, et al., "A frequency synthesizer for ultra-low phase noise multi-clock generation", CSEM Scientific and Technical Report (2019) 111.

A CMOS Image Sensor with a Stacked Quantum Dot Photon Absorber for Wide-spectral Imaging

P.-F. Ruedi, R. Quaglia, A. Paracchino, P. B. Cruz, H.-R. Graf, J.-D. Decoppet, C.-M. Zhang

In the framework of the Clean Sky 2 SWISSMODICS project, a CMOS image sensor made of a readout circuit (ROIC) with a stacked quantum dot photon absorber for wide spectral imaging has been developed. The chip, realized in a 180-nm 1-poly 6-metal CMOS technology, has an area of $12.5 \times 13 \text{ mm}^2$, containing an array of 512×512 pixels with a pixel size of $22.5 \times 22.5 \mu\text{m}^2$.

The requirement of image sensors for applications in which silicon has low quantum efficiency (QE) has resulted in the development of CMOS readout integrated circuits (ROICs) combined with different photon absorber materials. One possible option is to deposit layers of absorption materials directly on top of an ROIC. While exploiting the superior QE of innovative materials, this solution keeps the advantages of modern CMOS technologies such as optimal pixel density and circuitry, low power consumption, and complex readout electronics. Additionally, this offers a much cheaper solution than bump bonded photon absorbers, while offering a fill factor close to 100%.

In recent years, quantum dot materials have gained attention as photon absorbers. Their excellent properties, including a high absorption coefficient, a long carrier diffusion length, and low-temperature compatible deposition, make them suitable candidates for the detection of photons in multiple bands of the spectrum (such as visible, near infrared, and X-ray). This has been exploited to develop a wide spectral range image sensor. Figure 1 shows the concept with a quantum dot layer deposited on top of a CMOS chip. The top metal of the CMOS process is used as the in-pixel bottom electrode to contact the stacked quantum dot photon absorber. The common top electrode is made of a transparent conducting layer.

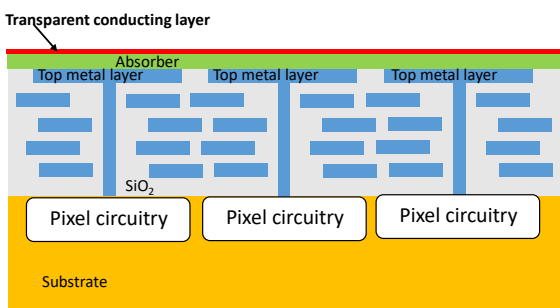


Figure 1: Cross-sectional view of the device with a stacked quantum dot photon absorber.

The chip has been designed in a standard 180-nm 1-poly 6-metal CMOS process. Figure 2 shows a micrograph of the chip. The chip area is $12.5 \times 13 \text{ mm}^2$ including an active imaging region with a resolution of 512×512 pixels and a pixel size of $22.5 \times 22.5 \mu\text{m}^2$. Each pixel can collect electrons or holes and has a programmable integration capacitor, making the chip compatible with different material stacks and photon energies (X-ray versus visible/infrared).

Figure 3 shows the structure of the quantum dot-based photon absorber layer deposited on top of the chip. The absorber is made of a 120 μm thick layer of PbS quantum dots. The absorber has been developed and deposited by QDI, a Dutch start-up. Deposition is done by spray coating. The 120 μm thick layer of quantum dots in addition to being a very good x-ray absorber is also sensitive out of the visible to wavelength up to 1300 nm.



Figure 2: Micrograph of the chip hosted in a dedicated board.

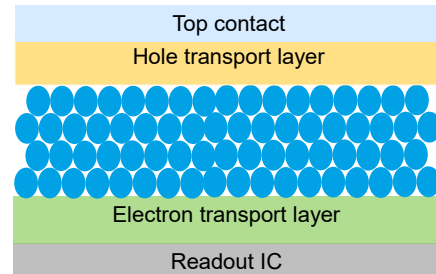


Figure 3: Structure of the photon absorber.

Figure 4 shows an X-ray image of a screw in a plastic tube acquired with the processed chip including a stacked quantum dot absorber.

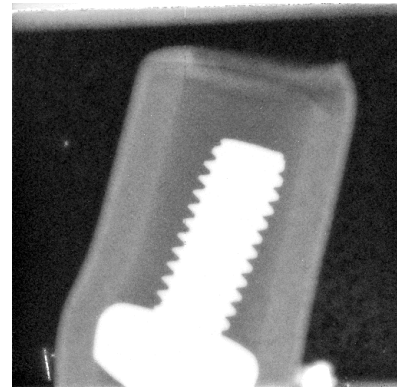


Figure 4: X-ray image acquired with the Swissmodics sensor. Courtesy of QDI.

The present development shows better resolution and sensitivity than scintillator-based X-ray detectors and opens the door to low-cost, wide spectral range and highly efficient image sensors usable for a wide range of applications.

This work, which is led by CSEM, receives the support of the European Union Clean Sky 2 program under grant 887192.

We thank QDI (www.qdisystems.com) for their collaboration.

Performance Comparison of Radio Frequency-based Angle-of-arrival and Ranging Solutions

J. Beysens

This project conducts an extensive indoor analysis to assess the performance of several radio frequency (RF) based technologies that estimate the angle-of-arrival (AoA) and the distance of a tag with respect to an anchor. In addition, these technologies are compared with a vision-based solution using a camera and an ArUco marker. The aim is to benchmark state-of-the art solutions in view of industrial applications such as asset tracking, industrial IoT and robotics.

The received signal strength indicator (RSSI) has been widely used for localization in wireless communication systems. However, RSSI is influenced by various environmental factors such as multipath propagation, interference, and shadowing, which can lead to unpredictable fluctuations in signal strength even within a relatively stable environment. These fluctuations result in inaccurate position estimations. This project investigates state-of-the-art RF-based solutions for AoA and ranging (distance estimation) to achieve robust and accurate localization. We benchmarked them against a vision-based solution because of its reliability. Figure 1 presents the system architecture.

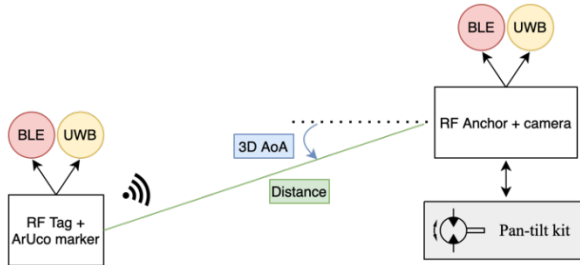


Figure 1: System architecture of RF and vision setup.

The system consists of a RF tag and anchor. While the tag has a single antenna, the anchor has up to 16 antennas to be able to estimate the 3D AoA based on their phase difference. We assess the performance of both an off-the-shelf Bluetooth Low Energy (BLE) and Ultra-wideband (UWB) solution. As opposed to the UWB solution from NXP which provides both AoA and distance, for the BLE we use two different boards: one from Silicon Labs for the AoA (standardized in Bluetooth 5.1) and one from Nordic for distance (not standardized yet). For all solutions, we use the AoA and distance algorithms provided by the supplier.

The anchor is installed on a pan-tilt kit to automatically adapt its orientation during the measurements in both the horizontal direction (azimuth) and vertical direction (elevation). In addition, a reference vision-based solution consisting of an ArUco marker and a camera is used as ground truth. Based on the position of the marker on the camera frame, the AoA and distance is determined. Using this setup in Figure 2, we conducted an indoor measurement campaign at the CSEM headquarters.

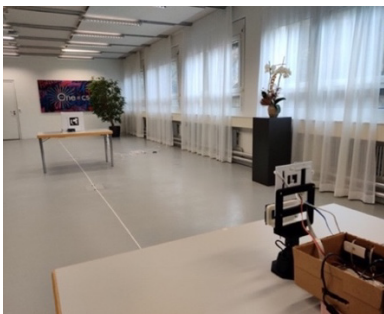


Figure 2: Indoor measurement setup at CSEM headquarters.

We place the RF tag and ArUco marker at different distances in a range of 0.2 m to 12 m with respect to the anchor and camera. The three RF solutions are installed sequentially on the pan-tilt kit. For every distance, we move the pan-tilt kit to a set of predefined orientations, varying its azimuth and elevation angle in a range of -60° to 60°. For every orientation, 50 data points are collected (distance/angle estimates) for the installed RF solution. Once these measurements are finished, the pan-tilt kit moves to the next desired orientation and the process is repeated.

Figure 3 shows the estimated azimuth angle of the UWB solution at 6 m. We observe that overall, the estimations match well with the ground truth provided by the pan-tilt kit. Furthermore, we see an increasing error in the estimation at the extreme angles.

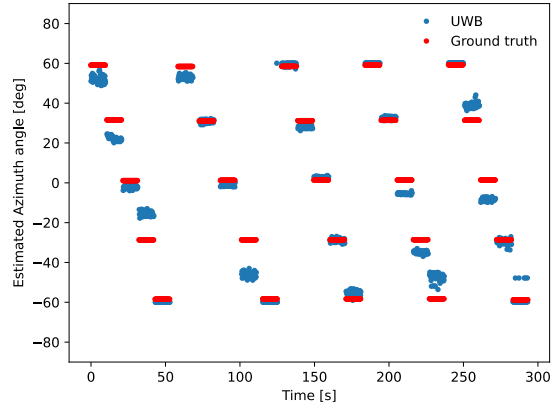


Figure 3: Estimated azimuth angle by UWB solution at 6 m.

Table 1 shows the average error and standard deviation of the estimations for all tested solutions. We conclude that the UWB solution outperforms BLE in both the absolute mean error (measure of trueness) and the standard deviation (measure of precision). Especially the UWB distance estimation shows a low standard deviation, enabling highly repeatable measurements.

Table 1: Performance result for AoA and distance estimation at 6 m.

	BLE azimuth [°]	BLE elevation [°]	BLE distance [m]	UWB azimuth [°]	UWB elevation [°]	UWB distance [m]
Absolute mean error	17.73	14.77	0.71	4.80	7.68	0.36
Standard deviation	6.03	3.43	0.23	1.61	1.84	0.01

As the indoor measurements were performed in a controlled environment, it might not reflect realistic conditions. Therefore, the next step includes performing measurements in real environments (both indoor and outdoor) to further validate the performance of BLE and UWB. We will especially focus on UWB due to its superior performance in the conducted measurements, making it suitable for industrial applications that require robust and accurate localization.

Development of an Embedded Bluetooth Low Energy Based Angle-of-arrival Algorithm

Y. Piguet, J. Beysens

Bluetooth Low Energy (BLE) based indoor localization enables new IoT applications without the cost of additional hardware. Based on an extension of the BLE 5.1 standard, we developed an in-house 3D angle-of-arrival (AoA) algorithm tailored for embedded systems. Its code size, memory footprint and computational efficiency are compatible with low-power microcontrollers such as the Cortex M4.

Indoor people and assets localization enables new applications in a wide range of domains, such as keychain loss prevention, elderly safety at home, or player tracking in sports. Among the different potential techniques, those that can be integrated with Bluetooth Low Energy (BLE) are of particular interest as they incur no or little extra cost, since BLE support is already ubiquitous in existing connected devices. Moreover, the addition of this feature does not increase cost or degrade power consumption in normal operation. Support for measuring the angle-of-arrival (AoA) has been defined in the BLE standard since version 5.1. The AoA represents the relative angle of an emitting BLE tag as perceived by a BLE anchor.

Figure 1 shows the proposed system architecture. The BLE tag sends out a periodic Constant Tone Extension (CTE), which is appended to BLE advertising packets. The BLE anchor, consisting of multiple antennas, samples the quadrature (IQ) signal at each of its antennas in a consecutive manner. After correcting the phase shift to emulate simultaneous sampling of all antennas, the IQ samples are fed to the MUSIC algorithm (Multiple Signal Classification). This algorithm is a popular and effective way to compute the 3D AoA (i.e., both the azimuth and elevation angle) by discriminating between the signal power and the noise power, using eigenvalue decomposition. Spatial smoothing helps to decorrelate the reception of delayed copies of the same signal caused by reflections (multipath propagation).

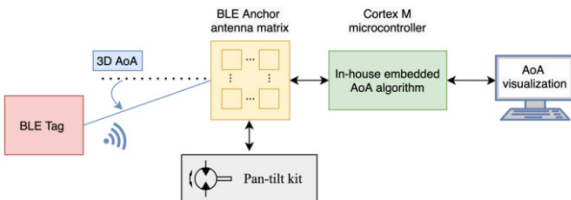


Figure 1: System architecture of real-time AoA demonstrator.

Angles corresponding to successive BLE packets are filtered to provide a better estimate: outliers are rejected, and an infinite impulse response filter is applied to reduce the detrimental effect of noise. The choice of the cut-off frequency is a trade-off between the latency and accuracy suitable to the application.

The algorithm was first implemented in Python and validated with synthetic data, then written in C. To the best of the authors' knowledge, the developed AoA algorithm is the first solution suitable for low-power microcontrollers. Validation with experimental data is achieved in two different configurations: 1) acquisition of sample sequences for batch analysis on a desktop computer, and 2) real-time AoA calculation on a microcontroller.

The purpose of the desktop-based batch analysis is to obtain a large dataset of experimental data for different angles in a controlled, interference-free environment (an anechoic chamber). This dataset is used to evaluate the performance of the AoA estimations. As shown in Figure 1, the antenna matrix of the anchor is installed on a pan-tilt kit, to automatically adapt the

orientation of the anchor during the measurements. The information from the pan-tilt kit serves as a ground truth of the anchor's orientation in the analysis.

Figure 2 presents a selection of the results obtained in the anechoic chamber. The distance between the tag and anchor is set to 3.5 m. The shown standard deviation is calculated on 100 BLE packets for an elevation angle of -10°, 0° and 10° and an azimuth angle between -50° and 50° in steps of 2°. Despite the presence of some outliers, the standard deviation of the azimuth and elevation angles for separate BLE packets is limited to 1.7° on average. The mean absolute error equals 0.8°. This allows applications to perform accurate and repeatable AoA estimations.

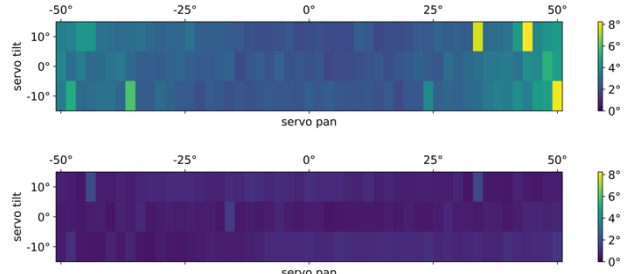


Figure 2: Standard deviation of calculated azimuth (top) and elevation (bottom) for different angles.

Next, the algorithm was implemented on a microcontroller to analyze performance in real-time. Figure 3 shows the setup. The antenna matrix board from Silicon Labs is directly connected to an STM32L4R5 (Cortex-M4) running at 120 MHz. The computation time of the developed algorithm is about 100 ms per BLE packet. The AoA code footprint is about 17 KB, while the RAM usage is about 5 KB.

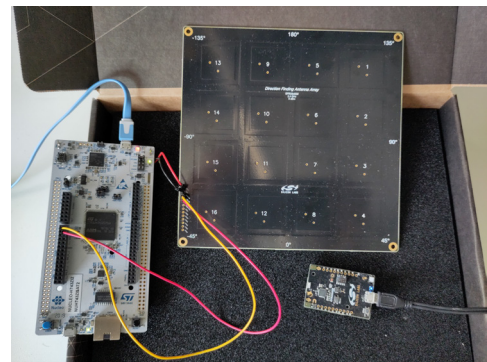


Figure 3: Receiving antenna matrix with on-board BLE (top right) connected to a Cortex-M4 microcontroller (left) via a serial connection; emitting BLE tag (bottom right).

Future work includes the implementation of additional filtering techniques to further improve the performance of our AoA algorithm. Secondly, the embedded C code will be further optimized to reduce the memory footprint and the processing latency, at a minimal cost in accuracy, to support a wide range of applications. Finally, a detailed comparison will be conducted with existing available BLE-based AoA algorithms.

Discovering Vulnerabilities in Embedded Firmware with Fuzzing Techniques

D. Vizár, M. I. Ben Salah, M. Marty

Connected embedded devices are exposed to adversarial interactions, making exploitable firmware bugs a major concern for their security. CSEM developed an experimental embedded firmware test bench, combining fuzzing and hardware emulation, to identify and eliminate the maximum of the firmware bugs before the firmware is deployed.

The presence of programming errors (a.k.a. bugs) that constitute an exploitable vulnerability, such as the well-known buffer overflow vulnerabilities, are among the dominant attack vectors used by cybercriminals [1]. As applications of embedded devices evolve to incorporate various forms of untrusted input, such as inputs received over the user interface, firmware update packages and generally any received communication frames, the issue of exploitable bugs becomes a pressing one in this context as well. For example, an exploitable buffer overflow in the BLE communication stack would allow attackers in the vicinity of a device to attack it remotely, without the need of physical interaction. By exploiting such a vulnerability, an attacker might execute arbitrary code on the targeted device. The impact of such an attack can be devastating on constrained devices, as they typically lack features such as a full-fledged memory protection unit able to contain the vulnerability. Even though recent devices do feature technology such as ARM TrustZone, these only separate the most sensitive resources from the rest of the system and do not fully isolate processes, for example. To make things worse, exploitable vulnerabilities are frequently imported by 3rd party software modules.

Fuzzing is one of the techniques able to reduce the number of exploitable bugs in software. It consists in feeding a program under investigation with large amounts of varying inputs, until an input is found that forces the program to exhibit an unexpected, or faulty behavior. The software managing this process and choosing how to vary the test inputs is called a fuzzer. Modern fuzzers are designed to optimize the mutation of test inputs such that an error-provoking one is found faster with various techniques, either by observing the black box behavior of the program binary (black box fuzzing) or by working directly with the source code (white box fuzzing). Fuzzers are indeed effective tools for identification and elimination of bugs in software, however, because they need to fully control and manipulate the execution of software target, they are intractable on embedded systems, which do not have enough memory and computational power to run both the firmware and the fuzzer.

Recent academic research proposed new approaches and tools that enable the fuzzing of embedded firmware. One such tool called HAL-fuzz [2] uses an emulation-based approach (see Figure 1). The target firmware binary is executed on the host, in a CPU emulator, such that arbitrary symbols in the binary may be intercepted and their execution skipped, modified, or mocked. This allows drivers and peripherals to be efficiently mocked in a way that is consistent across several embedded platforms; when a driver function is called, the emulation is stopped, the effects of the driver function call evaluated in high-level language and the emulated system is modified accordingly, jumping over the driver call. The same approach also allows for the injection of fuzzing

inputs as well as assertions on the system state to be checked. Because the framework work with a binary but requires symbols to be intercepted, it represents a gray-box approach.

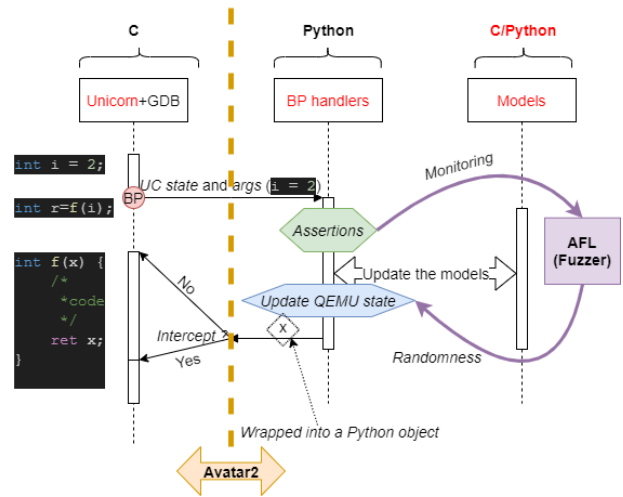


Figure 1: Embedded firmware fuzzing based on the HAL-fuzz framework, combining Unicorn CPU emulator, Avatar2 emulation control framework and AFL Fuzzer.

At CSEM, a proof of concept of an embedded fuzzing testbench has been implemented using the HAL-fuzz framework, with the ultimate goal of integrating an automated fuzzing step into the continuous development pipeline of critical firmware modules. In the proof of concept, the CSEM proprietary ultra-low power real-time operating system μ111 has been designated as target and a mock console utility has been implemented with a purposefully included buffer overflow bug. The HAL-fuzz framework has been deployed, emulating the execution on ARM Cortex M3. Handlers have been implemented to intercept all input/output driver calls of a UART console, which has been emulated in Python. The detection of buffer overflow has been implemented with help of canaries. In this configuration, the test bench was able to successfully identify the buffer overflow vulnerability, with a total runtime of ~30 min and 0,03 fuzzer executions per second.

This result confirms that complex embedded firmware, such as a real-time operating system, can be effectively fuzzed. The setup is also compatible with integration in a continuous development environment, where vulnerability testing of critical software modules (e.g., communication stack) could be run automatically. For that purpose, performance optimizations are expected, e.g., by executing only the targeted software module from a snapshot. It is also necessary to consider the fuzzing of third-party software modules as well as to design generic, target-code-independent assertions for detection of memory leaks.

[1] MITRE "2023 CWE top 25 most dangerous software weaknesses", https://cwe.mitre.org/top25/archive/2023/2023_top25_list.html

[2] A. A. Clements, E. Gustafson, T. Scharnowski, P. Grosen, D. Fritz, C. Kruegel, M. Payer, "HALucinator: firmware re-hosting through abstraction layer emulation", USENIX (2020).

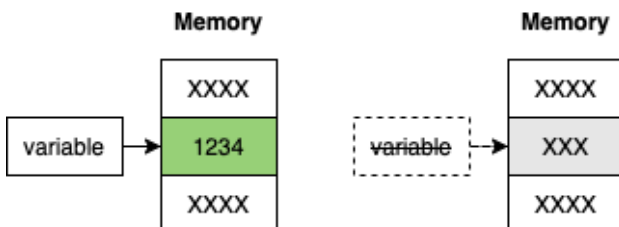
Enhancing Memory Safety by Integrating Rust in the μ111 Real-time Operating System

M. I. Ben Salah, P. Liechti, D. Keller

As embedded systems are growing in complexity, maintaining their firmware correctness (memory-leak free, out of bounds access) and application performance requires appropriate development tools. The CSEM ultra-low power RTOS now supports Rust, which natively provides runtime mechanisms for ensuring memory safety and compilation time checks, with a minimal impact on in terms of memory consumption and runtime execution.

The Rust^[1] language can be used for developing software components with stricter memory management in combination with μ111, benefiting from the properties of the Rust language in term of memory safety, while keeping the benefits of μ111 in terms of ultra-low power and development flexibility. It has been developed and evaluated on the NUCLEO-L4R5ZI based on the STM32L4R5 (Cortex-M4, 2 MB of Flash & 640 Kbytes of RAM).

Rust aims at preventing, at compile time, most data races and memory-related bugs by annotating the source code to statically prove that memory is not accessed after it is no longer valid. This is done by using the concepts of 1) memory ownership where the compiler manages the lifetime and the access scope of variables, indicating an error whenever the code tries to access an unreachable, freed, or expired variable; 2) references which are read-only by default, but whenever a mutable reference is created, are automatically invalidated, thus avoiding race conditions. Rust also provides the concept of safe/unsafe code: safe code uses high-level abstractions, i.e., references, where Rust guarantees can be verified, unsafe code is used for memory operations which validity cannot be checked by the compiler such as direct memory access with pointers, C/C++ libraries calls (using Foreign Function Interface) and accessing Memory-Mapped I/O.



```
fn safe_fill(array: &mut [i32]) {
    for i in 0..10 {
        array[i] = i;
    }
}

unsafe fn unsafe_fill(pointer: *mut i32) {
    for i in 0..10 {
        unsafe { *pointer.add(i) = i };
    }
}
```

Figure 2: Safe and unsafe version of accessing an array in Rust: safe uses a reference, where the unsafe version uses pointers.

To compile Rust source code as easily as existing C code in μ111, we created a Rust interface, which maps all the kernel calls in C, with the tooling needed to generate the correct compilation flags and integrate into existing makefiles.

The interfacing library exposes every μ111 kernel function and the appropriate macros to Rust, which enable native multi-processing execution of Rust code, benefitting from both the kernel and the ecosystem of Rust packages. Rust also comes with many programming facilities such as pattern matching, iterators, etc. The Rust mechanisms introduce an overhead in terms of performance and memory consumption, which was evaluated using a reimplementation of a benchmark tool on μ111, with fill array operation, X/Y projections and histogram computations. Figure 3 shows the impact in terms of runtime execution (max. 300% increase) and code size (max. 485% increase) caused by the additional runtime checks performed to ensure correct execution (memory ownership, out-of-bounds array access). However, unsafe Rust closely matches the original C performance. In addition, the optimized safe Rust implementation of the fill array operation is even faster than the original C code.

	Fill the array		X projection		Y projection		Histogram	
	μs	bytes	μs	bytes	μs	bytes	μs	Bytes
C	135	54	216	64	161	68	239	66
Safe Rust	100 - 539	316	212	288	165	208	301	158
Unsafe Rust	130	52	211	150	152	72	238	100

Figure 3: C/Rust comparison of μ111 bench tool.

One of the foreseen use cases of Rust on embedded platforms is the implementation of cryptography algorithms, where correctness is an absolute necessity and correct usage of the memory (avoiding buffer overflows) can be facilitated by Rust. This use case was chosen as a validation vector. Running the ASCON (Lightweight Authenticated Encryption & Hashing algorithms) implementations in C and Rust on standard test vectors resulted in an overhead of execution time of 10%, with a slightly smaller code footprint (C: 4.81 KB, Rust: 3.05 KB).

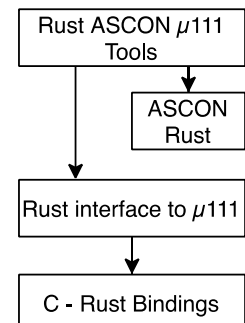


Figure 4: μ111 Rust structure with ASCON tool.

The native Rust support provided by CSEM covers the complete μ111 kernel API, which allows for its straightforward integration inside the μ111 compilation workflow, as shown by the 32 μ111 sample applications ported from C to Rust, reinforced by an in-depth tutorial for Rust usage in embedded systems and μ111. It also enables the use of external Rust libraries. Rust shows a great potential in embedded systems by providing significant robustness improvements with acceptable levels of overheads. With the support of Rust, the development of memory-checked secure IP, such as a Virtual Secure Element isolated in a Trusted Execution Environment, is greatly facilitated.

[1] <https://www.rust-lang.org>

Enabling VGA Graphic Applications with μ111 OS on Cortex-M7 integrated GPU

A. Dherse, M. I. Ben Salah

As embedded systems becomes more powerful, new opportunities arise to enhance user experience in home appliance/wearables with accelerated graphics engine integrated inside system-on-chips (SoCs). The CSEM μ111 ultra low-power RTOS now supports the NXP i.MX RT1060 SoC, which includes a display controller and a HW accelerator for graphical operations for graphical user interfaces while still maintaining low power consumption.

The first objective of this project is to port μ111 on the i.MX RT1060 SoC to address the needs of applications involving local interaction with the end-user. The i.MX RT1060 is based on a Cortex-M7 core going up to 600 MHz and includes multiple peripherals dedicated to multimedia processing, such as Quad-SPI memory controller (FlexSPI), a display controller (LCDIF) and a GPU called Pixel Processing Pipeline (PXP). For this purpose, all the development has been done on the MIMXRT1060-EVKB (32 MB SRAM & 8 MB of external flash) with a 480x272 LCD panel using RGB565 format.

As the SoC does not include internal flash, the executable image must be stored on an external flash. The code can then be executed in place from the NOR flash (XIP) or loaded in the internal RAM (OCRAM). This processor includes 1 MB of OCRAM with 512 KB of tightly coupled memory that can be optimized for instructions or data (ITCM, DTCM). Executing code stored in ITCM will improve performance by up to 6 times compared to XIP, removing the need to fetch data from external memory. Two variants of the μ111 port have been created, allowing to choose between optimal performance by ITCM code execution or additional internal storage by using XIP.

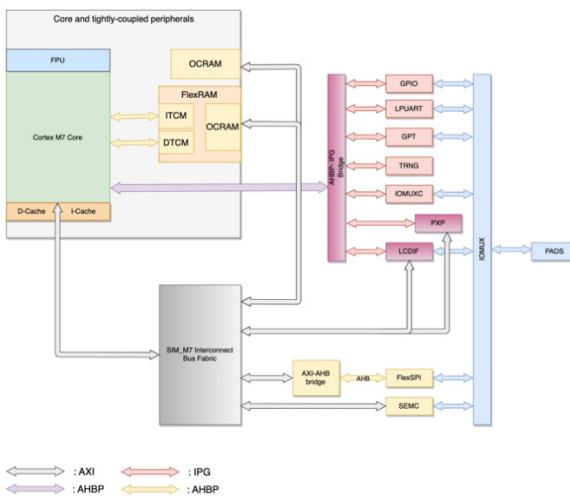


Figure 1: IMXRT1060 block diagram.

The second goal of the project was to evaluate the PXP features and capabilities, in terms of image processing and output of image buffers to be displayed by the LCDIF. The PXP provides two main advantages: faster computation speed for supported 2D operations and reduction of memory space needed to display images. The following operations are supported:

- Flipping, scaling, and rotating sprites.
- Conversion between multiple color space including YCbCr, YUV, and RGB.

[1] NXP "i.MX RT1060 processor reference manual", <https://www.nxp.com/document/guide/get-started-with-the-mimxrt1060-evk:GS-MIMXRT1060-EVK>

- Alpha blending two surfaces.

The LCDIF and PXP can also be synchronized, working together to display the image as it is computed. With this method only a partial frame buffer is needed, being continuously updated by the PXP and read by the LCDIF, greatly reducing the memory amount needed to display an image.

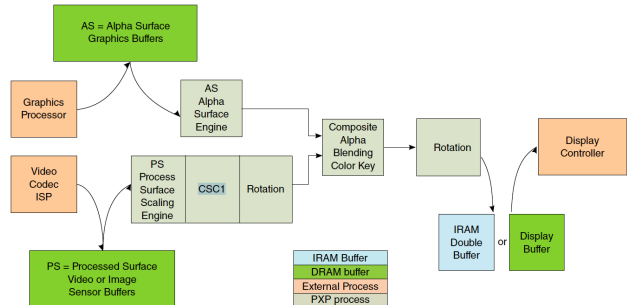


Figure 2: PXP pipeline [1].

The PXP performance was then evaluated against a software graphical library capable of 2D operations, Olive.c [2]. It is a single header library that is lightweight, easily portable and renders images in a ABGR8888 format (which are then converted in RGB565 by LCDIF). Figure 3 provides a comparison between the PXP in its 2 operation modes (full & partial buffer) and the software solution when gradually distorting on both X/Y axis a 112x112 pixels image.

Resizing an image using	PXP, full buffer	PXP, partial frame buffer	Olive.c
Image buffer size	512KB + sprite size	15KB + sprite size	1MB + sprite size
Mean current consumption [mA]	26	28	32
Computing time [ms]	1	N/A	80 - 100

Figure 3: Comparison of PXP and software resizing (measures at 3.3 V).

When using the PXP, we observe that every frame was generated in less than 16 ms, allowing animations at a constant 60 FPS. Using the partial frame buffer mode saves a lot of memory (97% decrease.) at the cost of an increased power consumption (7% increase). On the other side Olive.c only managed less than 15 FPS for the same test, leading to choppy and inconsistent animations because of inefficient software resizing of the sprites. With this porting, μ111 now fully supports an additional SoC for high-end application such as computer vision and monitoring systems requiring a graphical user interfaces.

[2] <https://tsoding.github.io/olive.c/>

Threshold Signatures for Embedded Platforms

D. Gallay *, A. Duc *, D. Vizár

Embedded devices deployed in the so-called Internet of Things applications often face a tension between their generally weak security posture and a heightened exposure due to their connectivity (remote software exploits) and physical exposure (side channel attacks). The possibility of an ensuing leakage of a remote device's long-term keys may decrease trust in the application to an unacceptable level. This may be alleviated with help of threshold signatures, where the signing key is split into shares. Here, the usability of threshold signatures is evaluated for embedded devices.

The Internet of Things (IoT) application architecture enables new business models and unlocks new value in the existing markets thanks to a massive number of low-cost connected devices, which may be attached to objects (a.k.a. Things) to collect data, track assets, actuate and so on. However, the same features that act as enablers also create a tension in terms of security. The low cost means the IoT devices often use embedded HW platforms with medium to low security and are exposed to attacks such as remote software exploits (making use of the connectivity) and physical attack ranging from connected debugger, through PCB tampering, to side channel attacks (making use of the physical access available to the attacker). It is thus hard to prevent a motivated attacker from extracting key material from a device, including long-term keys. An attacker may impersonate the compromised device and push malicious data upstream.

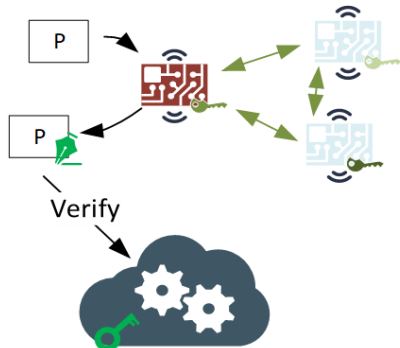


Figure 1: A distributed signature protocol with threshold $t=3$. The signing device (red) produces a signature with help of two companion devices, each of them possessing a private signing key share.

The risk related to these scenarios can be managed using threshold cryptography, where secret keys are cryptographically split into shares, and conventional cryptographic primitives, such as secret-key authenticated encryption or digital signatures are transformed into interactive protocols, such that each encryption, resp. signing requires a certain number of devices possessing the key shares to interact. In such a setup, whenever a device needs to sign a payload, it will run an interactive protocol with peer devices, such that their total number needs to be equal to a threshold t . The threshold t is configurable and allows for a trade-off between security and overhead; the higher t , the more devices must be compromised in a successful attack, but also more devices must participate in a distributed signature. The

procedure is illustrated in Figure 1. CSEM has evaluated [1,2] and confirmed a practical use of distributed encryption to harden the firmware update over the air [3], for example. For other use cases, however, the symmetric-key nature of distributed encryption is not ideal. For example, when data originating from an IoT fleet must be authenticated by other parties than the fleet owner, digital signatures are much better suited, as the public verification may be freely disseminated, while the private signing shares are distributed among the devices.

To assess the usability of threshold signatures in embedded platforms, two constructions have been evaluated. The first is a threshold variant of the BLS signature scheme [4]. Internally, BLS uses the so-called bilinear pairing, a special algebraic structure over certain elliptic curve groups yielding a construction that is easily transformed into a threshold version, albeit with a complex signature verification, which is not a major setback for the envisaged use case. The embedded implementation is based on the blst library [5]. The other scheme is a dedicated threshold signature design FROST [6], implemented over the elliptic curve secp256k1. The embedded implementation is based on the secp256k1-frost library [7]. Both libraries were adapted for integration with CSEM's real-time operating system μ 111 and benchmarked on the Nordic nRF52840 devkit running at 64 MHz. The results are summarized in Figure 2.

	BLS	FROST
Pub. k./priv. k. /sig. [B]	48/96/32	33/64/32
Signing time [s]	$0.94 + 0.4 \cdot t$	$0.036 + 0.11 \cdot t$
Communication [B]	196	168
Comm. rounds	A broadcast by each device	2 (or 1 with pre-processing)

Figure 2: Performance of threshold signatures on nRF52840 @ 64 MHz.

CSEM benchmarked the proof-of-concept implementations of BLS and FROST threshold signatures and confirms that they are usable in embedded systems, although the computational and communication overhead requires optimizations.

* HEIG-VD, Switzerland

[1] D. Vizár, "Distributed encryption for robust data confidentiality and integrity for IoT", CSEM Scientific and Technical Report (2021) 48.

[2] R. Müller, "Robust IoT security with threshold cryptography", bachelor's thesis, HEIG-VD (2021).

[3] D. Vizár, M. I. Ben Salah, Q. Liang, "Securing embedded firmware update over the air with distributed encryption", CSEM Scientific and Technical Report (2023).

[4] D. Boneh, B. Lynn, H. Shacham, "Short signatures from the Weil pairing" ASIACRYPT (2001).

[5] <https://github.com/supranational/blst>

[6] C. Komlo, I. Goldberg, "FROST: flexible round-optimized Schnorr threshold signatures", SAC (2020)

[7] <https://github.com/bancaditalia/secp256k1-frost>

An Autonomous Stereo-imaging System for the Monitoring of Mountain Streams Discharge

N. Cantale, D. Ros, M. Dia

The TORRENTS computer vision system uses stereoscopic imaging for 3D reconstruction for remote stream gauging. The system was tested in various settings with high robustness and accuracy in estimating surface velocity and discharge of streams. The results show successful extraction of discharge and stage information from images, even in sub-optimal weather conditions.

Because of climate change, efficient water management and reliable prediction of water-related hazards have become critical. Still, current methods rely on expensive, invasive structures (e.g., installation of concrete weirs) and base their predictions on extrapolated models with high uncertainty (>20% error rate). Although research made substantial progress in alternate streamflow monitoring techniques, it has failed to achieve widespread adoption.

Recent advancements in computer vision have led experimental hydrology research to explore optical streamflow monitoring methods. They provide significant advantages to traditional methods, such as upfront and maintenance costs and ease of deployment in remote, hostile environments. However, their reliability still suffers from the variability of environmental conditions and their dependence on empirically measured data, which has slowed down their wider acceptance.



Figure 1: Setup used in the project. Two synchronized infrared cameras provide the data in all environmental conditions, with the help of a powerful infrared illuminator. An additional color camera complements the system, for easy monitoring, and everything is powered by solar panels and is connected via 4G.

CSEM collaborated with Precidata to expand the scope of current techniques and tackle the limitations found in state-of-the-art monocular methods. These limitations include challenges in GRPs calibration and the inability to react to changes in the geometry of the environment. The collaboration resulted in a comprehensive stereo vision system and an image processing pipeline for non-contact and non-invasive monitoring of streamflow in mountain streams. Thanks to an automated 3D

reconstruction of the installation site, the water level, water surface velocity, and discharge rate can be extracted with minimal prerequisite knowledge about the site.

An extensive review of the existing methods for surface velocity estimation using manual *in-situ* measurements allowed us to identify the OTV algorithm^[1] as the optimal solution, outperforming the other techniques in terms of mean absolute error (MAE) and robustness to setup and environmental variations.

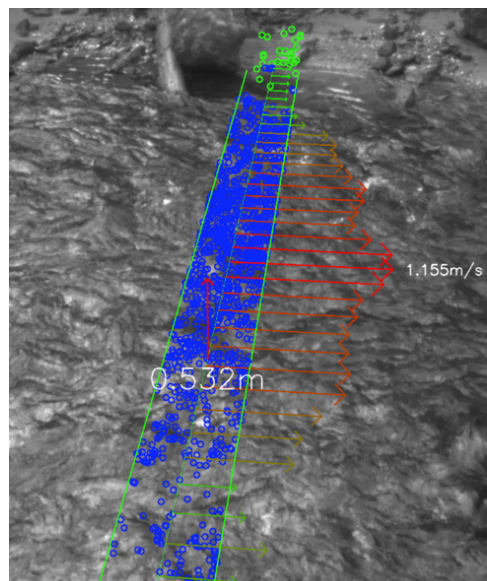


Figure 2: Discharge analysis example on la Dranse de Bagnes. The circles represent the keypoints detected (blue for the water keypoints and green for the ground), inside the region of interest (green lines). The velocity (in red) is measured along the river width.

The system has recently won a challenge from BlueArk^[2] and was selected for field testing in the municipality of Le Châble (VS), where most of the data has been acquired in challenging conditions (snow, rain, sun, etc.). The discharge computation was then validated against the measurements of an official monitoring station. The results have shown that the proposed system matches the reference values on average, within a 10% error margin, corresponding to a MAE of 0.061 m/s.

The demonstrated effectiveness of this work motivates further development to further improve its reliability in various environmental conditions. To this end, the elaborated setup (Figure 1) enables the collection of large amounts of data to capture environmental variability. A follow-up project has started, with the goal to overcome the remaining challenges towards a well-deserved modernization of our hydrological measurement network.

^[1] F. Tauro, et al., "Optical tracking velocimetry (otv): Leveraging optical flow and trajectory-based filtering for surface streamflow observations", *Remote Sensing* (2018) 10 (12) 2010

^[2] <https://www.blueark-challenge.ch>

Contactless Distance Measurement using Talbot-diffracted spaceCoder Technology

E. Grenet, C. Gimkiewicz, C. Kündig, N. Cantale, P. Stadelmann

An optical device allows accurate contactless distance measurement of a metallic piece thanks to a stereo implementation of the Talbot-diffracted spaceCoder technology. The system provides measurements at high speed with a resolution below 500 nm and can be used for profiling or quality control of mechanical pieces.

The CSEM spaceCoder technology has been recently improved with a patented Talbot-diffractive configuration [1] which provides improved metrological performances. Such a diffractive spaceCoder has been implemented in a stereo configuration to accurately extract the distance of a metallic piece without contact.

The system has been designed as follows (Figure 1): a point light source is focused on a device under test (DUT). The reflection of the collimated light on the DUT becomes the illumination source for the spaceCoder device, which is able to measure the distance to the DUT and extract its profile.

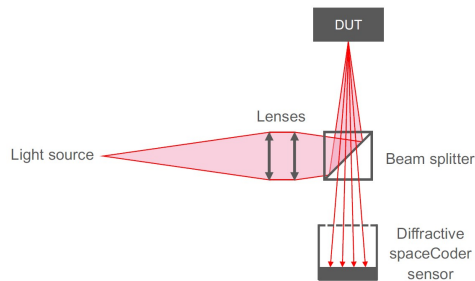


Figure 1: Setup for the DUT distance detection.

One of the major challenges of such a setup is the illumination on the DUT. The location of the illumination reflection point must be independent of the DUT shape (flat or curved). The use of a beam-splitter enables orthogonal illumination. However, this comes with a significant drawback, as it results in a 75% reduction in the intensity of the light source. Moreover, the amount of light reflected can be less than 10% of the initial power, depending on the material and surface characteristics of the DUT. Finally, the illumination point must be as focused as possible to guarantee a high spatial resolution. Different illumination technologies have been investigated. Laser sources were discarded because they produce speckles that degrade metrological performances. A high-power LED was preferred for its high temporal stability, despite a lower maximum power and the need for cooling to manage heat dissipation. To reduce the noise from the light source cooling, a fiber-coupled high-power LED was used.

The spaceCoder sensor is designed to have the ability to work with two different wavelengths in the UV range or in the NIR range, both wavelengths can also be activated simultaneously as they generate different patterns in a given plane of the Talbot diffraction carpet. For example, by placing a shadow mask of a given period ($75 \mu\text{m}$) at the Talbot distance (14 mm) for a NIR illumination (800 nm), the use of a halved wavelength UV illumination (400 nm) images the same pattern shifted by half a period: then both UV and NIR wavelengths can be analyzed simultaneously (Figure 2).

The distance of the DUT is computed via stereovision of two regions on the sensor, taking advantage from the high sensitivity

of the Talbot-diffracted spaceCoder signal. The CMOS imager selected for the setup was the Flash4K from Teledyne-E2V for its large baseline (24 mm) for triangulation and its high framerate (few kHz) for fast profile scanning. The system has a measurement range of $\pm 1 \text{ mm}$, defined by the focus range of the reflection point. Then the profiling of a DUT is done by a lateral scanning in the focus range, measuring small distance variations with a resolution below 500 nm.

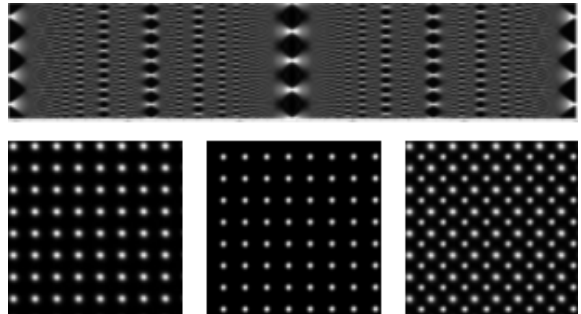


Figure 2: Top: Talbot diffraction carpet. Bottom: pattern imaging for NIR (left), UV (center), NIR and UV simultaneously (right).

Measurements have been performed by placing the DUT on an accurate reference stage to validate the distance estimations, as shown in Figure 3: the DUT is moved away from the sensor with $10 \mu\text{m}$ steps every 100 samples, showing contactless accurate distance measurements at $\sim 6.8 \text{ cm}$ distance.

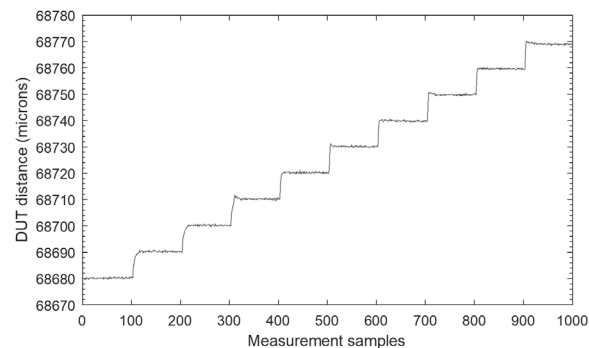


Figure 3: Measurement of $10 \mu\text{m}$ distance steps of a DUT.

This first concrete implementation of the Talbot-enhanced spaceCoder shows the measurement potential of the technology, providing contactless accurate distance measurement for the positioning or profile measurement of metallic parts (screws, etc.) as well as any reflective material (mirror, etc.). The same system can also be used for quality control of accurate tooling (shaft inspection, etc.) or for the analysis of surface condition (surface roughness, etc.).

Future investigations will explore potential extraction of additional characteristics of the DUT material with the simultaneous signal analysis of both different wavelengths in the UV and NIR ranges.

[1] EP3825659 & US20210148733: Position Encoder

Virtual Reality-based Eye Gaze Calibration for Early Diagnosis of Neurological Disorders

K. Sharma, E. Türetken, R. Gaulier, S. Saeedi, L. A. Dunbar

NeurOphthalmoscope (NEOS) is a virtual reality-based system aiming to provide fully automated eye examination to support early diagnosis and monitoring of neurological disorders, such as brain tumors and multiple sclerosis. CSEM has developed a specialized eye gaze calibration algorithm for accurate gaze tracking (< 2° accuracy), which holds utmost importance for ensuring reliable and effective diagnosis in clinical settings, especially in patients without perfect binocular vision.

In the context of eye gaze tracking applications, a personal calibration step is needed to achieve a reliable and accurate eye gaze estimation by effectively accommodating the inherent anatomical disparities observed in patients' eyes. This is done by calculating the offset between the optical axis, which passes through the corneal and pupil centers, and the visual axis, which is directed towards where the person is actually looking at. The foveal offset and other invisible personal variations such as size of the sclera, the curvature of the cornea and the position of pupil inside the eye make the personal calibration necessary for an accurate tracking. In the Innsuisse project NEOS, along with our partner machineMD, we aimed at applying this calibration technology to improve the diagnosis and monitoring of neurological disorders. The primary objective of the work was to develop a set of algorithms tailored to enhance the accuracy and reliability of the eye tracking information provided by a head-mounted display (HMD) device for extracting medical features.

The study started with a data collection campaign involving a total of 25 subjects. While 21 subjects had a visual acuity within ± 2 diopters of nominal sight, 4 subjects were out of this range, requiring a compensation with refractive correction lenses placed in the HMD. To develop and compare our method with the HMD's optional default calibration approach, we conducted two separate sessions: one without (any) calibration for capturing raw eye gaze data and the other with (only) HMD's default 5-point calibration. Both sessions involved viewing an 11x11 calibration grid in a 20° horizontal and vertical Field of View (FoV).

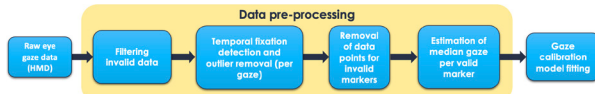


Figure 1: Eye gaze calibration algorithm pipeline.

To ensure high-quality input data for the gaze calibration algorithm, we performed various pre-processing steps as shown in Figure 1. Initially, we extracted stationary stimulus marker fixation data, discarding transitional and blink-related sections and filtering out invalid points flagged by the HMD. To remove outliers caused by saccadic eye movements, we developed a novel RANSAC-based algorithm that can robustly filter out user-or session-specific temporal saccadic data sections (patent filed). We also detect and remove the gaze data for markers that a patient fails to look at. These steps collectively enhanced the eye gaze calibration quality, addressing challenges linked to blink events, saccades and incorrect gazing. The preprocessed data is used to find the parameters of an eye gaze calibration model (polynomial or homography-based) that can estimate the ground-truth marker locations from the raw eye gaze coordinates provided by the HMD. Figure 2 shows that using the homography model, 9-point calibration performs equally well or better than the 13-point calibration in the central region (i.e., for the FoV of $\pm 5^\circ$, $\pm 10^\circ$, $\pm 15^\circ$). However, on the periphery of the FoV (i.e., $\pm 20^\circ$), 13-point calibration shows a marginal improvement over 9-point.

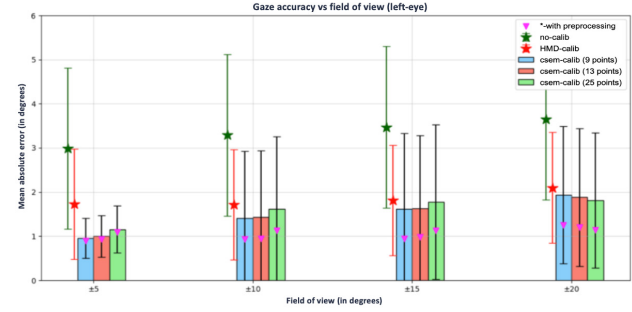


Figure 2: Comparison of eye gaze accuracy (mean absolute error) of homography-based gaze calibration model, trained on 9, 13, and 25 calibration points (blue, red, and green bars respectively), using different FoVs for validation markers.

The homography-based 13-point calibration method improved eye gaze accuracy by 52.4% compared to using raw eye gaze data and by 16.2% compared to using the default calibration of the HMD in the FoV of $\pm 20^\circ$. Similarly, the 13-point polynomial calibration method leads to a 51.5% improvement in the eye gaze accuracy compared to using raw eye gaze data and a 14.8% improvement compared to using the HMD's default calibration in the same FoV. As shown in Figure 3, our approach significantly reduces the angular error between the calibrated eye gaze and the ground-truth stimulus markers.

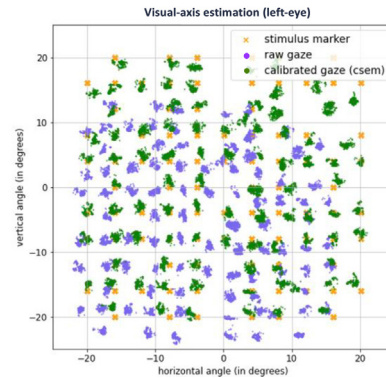


Figure 3: Calibration results for the left eye of a participant in the 2D angular space using the homography-based calibration model.

Based on this analysis, we opted for a 13-point calibration procedure using the homography-based model. On a single i9 processor core, while model fitting takes around 30 msec, inference on a raw gaze input takes less than 100 usec, enabling real-time performance on the HMD operating at 200 Hz. Our system significantly augments the eye gaze tracking capabilities of the commercial HMD device while aligning it with the specifications of a medical diagnostic instrument. This robust and highly efficient eye gaze calibration process can be seamlessly integrated across various applications in the VR and augmented reality landscape.

VIVALDI – Steel Billet Tracking with Advanced Computer Vision

P. Pad, S. Blanc, E. Türetken , N. Cantale, M. Dia, D. Honzátko, C. Kündig, L. A. Dunbar

Our groundbreaking computer vision system allows for the precise tracking of serial numbers on steel billets in challenging industrial settings. It combines cutting-edge hardware and machine learning, excelling in character recognition and localization while adapting to dynamic ambient lighting conditions. Moreover, it accurately measures crucial geometric parameters such as side sizes, bulging, and skewness. This multifaceted technology promises to elevate material tracking, quality assessment, and production optimization in the steel industry to unprecedented levels.

For many heavy industries, specifically steel production, the ability to monitor and trace materials throughout the production process is essential. In response to this need, CSEM has developed a cutting-edge computer vision system specifically designed to read and track the serial numbers engraved on steel billets. This system is optimized on both hardware and software domain to deliver the high accuracy and robustness required for a harsh industrial environment, including retraining for continuous optimization, assessment of geometric characteristics for better management of the production and smooth interaction through a user-friendly Web interface.

To achieve the level of accuracy and robustness necessary for industrial use, our computer vision system incorporates a multiple camera with active illumination. In addition, the optical layout is strategically positioned to capture the serial numbers engraved on steel billets from various angles and lighting conditions. This approach ensures that even in challenging environments with dust, debris, or low ambient lighting, the system can reliably capture the required information.

The associated software integrates data from all the cameras and illuminations, efficiently fusing and processing the information in real-time.

Due to high variability in the data specifically due to the quality of casting in this harsh environment and the need for high recognition accuracy (99.8%), at the heart of our software solution lies a neural network algorithm specifically designed to tackle the unique challenges posed by steel billet tracking. This neural network performs a dual role, simultaneously localizing and recognizing characters engraved on the billets. The uniqueness of the algorithm is its ability to leverage additional information about the structure of serial numbers. For example, it understands that the first two characters represent the year, the last character is always a letter, and so on. As in our method the localization and recognition happen jointly, this contextual awareness not only enhances character recognition but also improves the accuracy of character localization, making it an indispensable tool in a challenging industrial setting.

To cope with the dynamic nature of industrial processes, our system incorporates a retraining module. This feature allows for fine-tuning the neural network to adapt to the specific characteristics of their plant or production line. By providing a mechanism for constant optimization, our system ensures that it remains adaptable to changing conditions and requirements.

Beyond its novel serial number recognition capabilities, the proposed system accurately determines critical factors such as side sizes, bulging, skewness, and more, by measuring various geometric parameters of the steel billets, hence contributing to a deeper understanding of the billets' physical characteristics, enabling precise quality assessments and facilitating production optimization. This multifaceted functionality underscores our commitment to delivering a solution tailored to the specific complex demands of the steel industry.

To make our cutting-edge technology accessible and user-friendly, we also have developed a web-based interface. This interface serves as the gateway for users to interact with the underlying algorithm. It enhances the user experience in several ways:

1. Visualization of Inference Performance: Users can easily monitor and visualize the performance of the inference process in real-time. This transparency allows for quick identification of any issues and helps maintain optimal system performance.
2. Retraining and Fine-Tuning: Through the web interface, users can initiate the retraining process, fine-tuning the neural network to suit their specific needs. This flexibility ensures that the system continuously evolves to meet changing demands.
3. API Integration: The web interface seamlessly integrates with the underlying algorithm through APIs. This not only simplifies the interaction but also opens the door for further customization and integration into existing industrial systems.

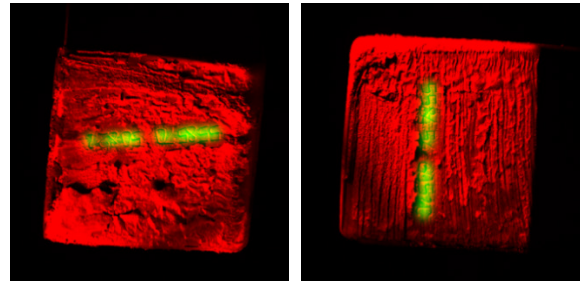


Figure 1: Illustrating the visible section of the steel billet (red), overlaid by the output of the character recognition (green).

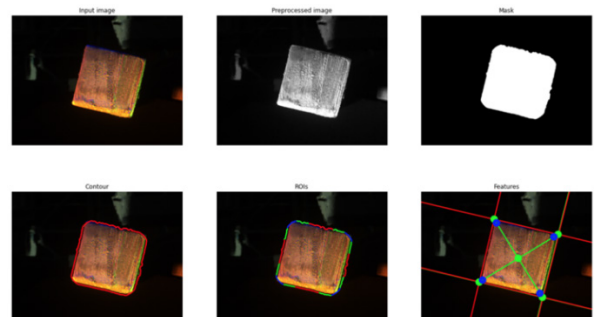


Figure 2: Segmenting the billet in the presence of background artifacts and measuring its geometrical characteristics.

Finally, since the system is flexible and modular, it can be customized for other inspection and quality control applications to have an end-to-end (from hardware to software and processing) optimized system for the application at hand. Automatization to reduce the need for human intervention for changes in the main building blocks of the system are expected to be implemented in the future versions.

RF Wireless Powering: Enabling Extended Autonomy in Wireless Devices

O. Vorobyov, M. Ghorbanpoor, A. Ahmadi Najafabadi, P. Nussbaum

Batteries in wireless devices contribute significantly to toxic waste generation and incur maintenance expenses. CSEM, ETHZ and EPFL collaborate on wirelessly transfer energy to small wireless systems (sensors, computer peripherals, wearables, disposable assays, etc.) for achieving battery-free systems. As a first step, future system specifications have been identified both for the transmitter module as well as for the receiver. Concepts for efficient RF rectifiers and Tx/Rx antennas are proposed.

Wireless power transmission consists of transmitting electrical energy from a power source to an electrical load, without interconnecting wires. Wireless Power Transfer (WPT) offers advantages that reach beyond cost savings and convenience. Some situations, settings, and uses are inherently incompatible with traditional wired electrical sources. This encompasses industrial scenarios demanding energy transmission spanning centimeters to meters and the deployment of small sensor networks in environments where wiring is impractical or impossible.

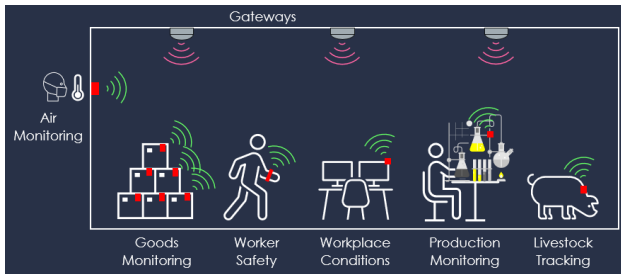


Figure 1: A vision of WPT for IoT system (purple: source of energy, green: receiver of energy).

Although solutions that harness energy from sources like ambient light, vibrations, or thermal gradients have been available for an extended period, their effectiveness is hampered by the sporadic nature of these sources, resulting in reliability issues. Wireless power transfer (WPT) has several unique features such as scalability, flexibility in device placement, adaptability, contactless operation, and ease of integration with potentially important and far-reaching benefits for clean energy and carbon emissions reductions. WPT system integration into a variety of devices, including IoT sensors, wearables, and medical implants, without the need for physical connectors or charging pads makes them potentially battery-free. This further radically reduces e-waste for these trillion-scale devices.

We aim at efficiently transmit RF wireless power transmission to small mobile IoT devices (remote sensing and actuation). The system is expected to meet various specifications, including accepting a wide power supply range, ensuring satisfactory transfer efficiency across a broad spectrum of harvested power and robustness regarding the wireless sensor's location. Millimetre-wave frequencies (e.g., 24 GHz or higher) are a promising band that allow the use of an intelligent transmitter with beamforming capabilities, allowing for smaller receiving antennas and less bulky receivers.

The basic principle of RF-WPT is to convert RF signals from either ambient or added power sources to DC electrical current. An important performance aspect of a dedicated RF-energy transfer is the ability to maintain RF-to-DC conversion efficiency over a wide range of operating conditions, including variations of input power and output load resistance. RF-WPT solutions efficiency are highly dependent on RF input power. Moreover, sustaining reliable operations within the regulatory constraints of possible radiation power limits is challenging.

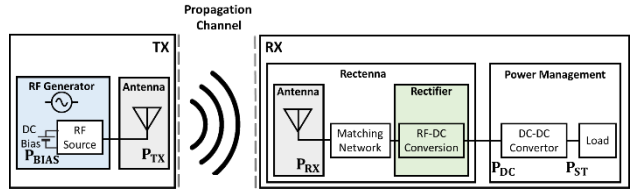


Figure 2: Typical RF-WPT block diagram.

The receiving chain includes a novel concurrent array structure, cross-coupled with harmonically terminated gates, to extract beneficial aspects of both synchronous and cross-coupled architectures. The key advantage of the proposed solution will be its flat efficiency curve over a wide input power range, as well as the superiority of existing designs in terms of adaptation to harsh radiation.

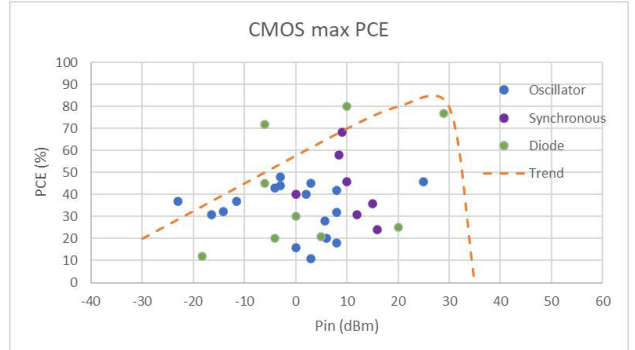


Figure 3: Power conversion efficiency comparison with respect to input level for different structures.

A 2-D beamforming network and antenna system will be implemented in TX, to allow for full coverage in indoor applications. The proposed antenna solution on the RX side is a relatively high-performance and wide-coverage antenna, which minimizes the importance of the device orientation.

In combination with the development of sustainable electronics, RF-WPT has the potential to achieve significant economic and societal impacts, including cost savings, environmental benefits, and improved convenience and safety. The disruption could be compared to the move from fixed-to-fixed points wireless links to fixed-to-mobile wireless links in telecommunication.

This project is still in its early phase. So far, a few novel rectifier subcircuit have been designed and successfully characterized (51.7% efficiency was attained, slightly below the theoretical estimate of 53%). These results will be used in advancing the development of a complete rectification chain. Additionally, a novel high-gain 3D-printed antenna concept has been designed and prototyped. The antenna characterization is ongoing.

Custom Antenna Design for Vehicles: Additive Manufacturing on Flexible Transparent Substrates

O. Vorobyov, S. Khan, D. Piguet

AerosolJet printing technology has emerged as a game-changer by becoming a rapid prototyping tool in antenna design, enabling the fabrication of antennas on flexible printed circuit boards (PCBs) with unparalleled precision and efficiency. CSEM explored the key advantages and applications of AerosolJet printed antennas on transparent flexible PCBs.

Unlike traditional prototyping techniques, aerosol jet printing is an additive manufacturing process that precisely deposits conductive materials, such as silver or copper inks, onto substrates.

The advantages of aerosol jet printing for antenna prototyping are manifold. It allows for the creation of intricate antenna designs with micrometer-level precision, ensuring optimal performance. Furthermore, the flexibility of this technology enables antennas to be printed on a variety of substrates, including flexible materials like polymers, enhancing their suitability for a wide range of applications.

Silver (Ag) nanoparticle-based ink is selected to print the desired Antenna design on a PET (polyethylene terephthalate) substrate. The wide nozzle feature of the AJP is adopted to print rapidly on larger areas (A4 size PET sheet). Pneumatic atomizer parameters were optimized to generate a stable aerosol jet that could last for at least two hours for continuous printing. The proposed design was simulated with the help of VMTool (Autocad) and pattern lines were adjusted such that to get uniformly covered structures at proper overlapping. Substrates were properly cleaned and treated with oxygen plasma to enhance the adhesion of Ag ink to the surface of the PET substrate. A thermal annealing step at 140°C was performed for four hours to remove all the additive from the dried ink and get highly conductive patterns.



Figure 1: Antenna prototyping using AerosolJet printing.

The advantages of using aerosol jet printing for window antennas are significant. It allows for the creation of high-performance antenna patterns that are nearly invisible, maintaining the aesthetics and transparency of the window. This is especially valuable in applications like automotive and building design, where aesthetics and functionality must coexist seamlessly.

The car window antenna serves as a viable alternative to the conventional external antennas commonly used for radio reception in vehicles. Unlike the traditional antennas mounted on the vehicle's exterior, the windshield antenna is specifically designed to be installed on the inside of the vehicle window. This internal placement not only ensures a clean and unobtrusive appearance from the outside but also provides a range of practical benefits, especially in projects where an efficient and protected antenna is essential.

In the context of forestry tractors and vehicles, where operating conditions can be challenging and unpredictable, the windshield antenna emerges as an advantageous solution for remote control. Forest settings present considerable challenges for external antennas, as they may come into contact with obstacles such as protruding branches and dense vegetation. Harm to external antennas can result in poorer radio signal quality, elevated upkeep expenses, and possible safety risks.

The window antenna design was carefully engineered to ensure omnidirectional coverage. This feature makes it suitable for wireless communication systems and IoT devices.

The antenna consists of four circular elements (CSEM logo). The distance between the circular element and the slots is optimized to achieve the best possible antenna matching in different installation scenarios and glass thickness (between 3 mm and 5 mm). The antenna was characterized in a controlled laboratory setting (see Figure 2) and in a forest environment using a spectrum analyzer (see Figure 3). Various parameters were measured and analyzed, including antenna gain, radiation, and impedance characteristics.

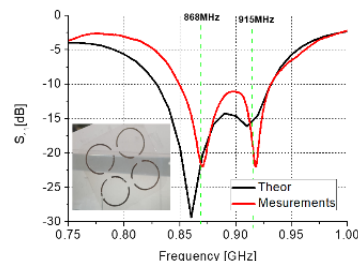


Figure 2: Measured antenna S-parameter (4 mm glass thickness).

In all cases, the antenna demonstrated good matching $S_{11} \leq -10$ dB for both ISM band frequencies 868 MHz and 915 MHz.

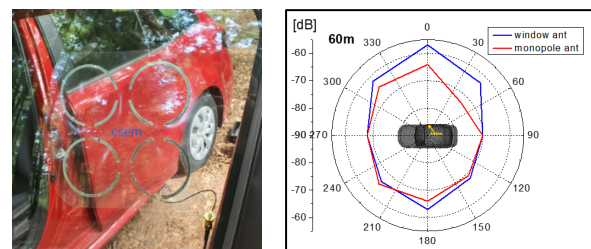


Figure 3: Antenna on the car window during the range test in the forest (left) and radiation performance window vs. roof monopole antennas.

Aerosol jet printing accelerates the prototyping process by enabling rapid design iterations and reducing material waste. This shortens development cycles and minimizes costs compared to traditional manufacturing methods. The prototyped antenna demonstrates good RF performance in terms of matching as well as radiation. In particular, it performs better as a monopole antenna at large distances in a forest environment.

Robust Aircraft Part Identification

M. Russi, T. Bendinelli, P. A. E. Schmid, M. Höchemer

Aircraft are complex systems with thousands of unique parts. Each part is labeled with an identification number (ID) that links to the associated drawing for correct assembly. As today, this ID is printed by hand during the component fabrication and workers have to manually match and check each part with its associated drawing. This process is both laborious and prone to misidentification. CSEM and Pilatus Aircraft Ltd, through an Innosuisse project, designed a camera-and-AI system to recognize plane parts quickly and accurately, reducing the need for human labor. The system will soon be optimized for full automation of the identification process and can be employed to support other procedures, aiming to enhance future profitability of Pilatus and preserve Swiss manufacturing.

Pilatus Aircraft Ltd, a renowned airplane manufacturer based in the heart of Switzerland, has a rich legacy of producing high-quality aircraft for global customers. Over one hundred airplanes are produced each year, which requires exceptional logistical and personnel efforts.

To ensure sustained profitability and efficiency, Pilatus is investing strongly in digital transformation, like streamlining and automating their manual processes. One pivotal process involves the precise part number printing on more than 10,000 diverse aircraft parts. The challenge lies in preventing errors, as these parts often share similar appearances, and thus reducing costly corrections at later stages.

An innovative solution was developed as part of the Innosuisse project. This advanced system utilizes a combination of one 3D and nine 2D cameras to capture images of aircraft components. At its core, a sophisticated AI algorithm processes multiple images in parallel and cross-references them with the part database.

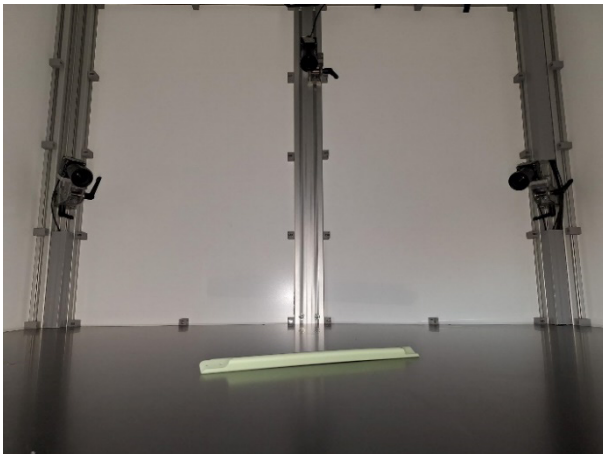


Figure 1: Aircraft part identification vision system at the CSEM Lab. Inside one 3D and nine 2D cameras combined with AI algorithms enable robust aircraft part identification.

The AI algorithm comprises of a convolutional neural network and Transformer decoder that can leverage multiple images from various angles to reliably infer the correct ID. The CNN serves as a feature extractor which generates embedded features for each. The Transformer combines these features for the final classification.

Getting high quality data to train AI algorithms is often tedious and costly. To work around this issue, all CAD models of the aircraft part were standardized by Pilatus and subsequently used to create photorealistic renderings. In total over 20 million images were rendered and used to train the AI algorithms. Special attentions were paid to robustness. To create a robust solution, thousands of different textures and colors were used in the rendering process for the background as well as for the aircraft parts. Furthermore, thousands of different poses per part were rendered to become pose independent.

The AI algorithms were trained with CSEM's AI high performance cluster. More than 4'000h computed hours over several months were used to create the final solution.



Figure 2: Rendered part from CAD model (top) vs real part (bottom).

In the next phase, Pilatus plans to seamlessly integrate the developed solution into their existing operations, marking a significant milestone in their pursuit of enhanced efficiency and quality control. With successful implementation, the adaptable solution holds the promise of enhancing and optimizing various other processes within Pilatus, further solidifying their strong position in the aviation industry.

The work has received funding from Innosuisse under grant agreement no. 56367.1 IP-ICT and support by the Cantons of Central Switzerland.

Expectant – Acoustic Localization of Rare Events

J. Montesinos, T. Bendinelli, A. Bürl, P. A. E. Schmid, I. Kastanis

Acoustic anomaly detection in machinery is a long-existing approach to identifying malfunctioning components in industrial devices. However, only experienced workers can distinguish such sounds, whereas localizing them is still a time-demanding task. CSEM proposes a new and autonomous method to identify, localize and classify abnormal sound sources coming from industrial machinery in a device agnostic manner. No prior knowledge of the machine configuration or its components is assumed. The system is calibrated using data from normal operations where the acoustic difference between normal and faulty operations is extracted and localized.

Acoustic Predictive Maintenance (APM) uses sound analysis of industrial devices and machine learning to identify potential faults before they occur, providing a non-invasive alternative to traditional sensor-based methods. It also facilitates monitoring in hard-to-reach locations and streamlines the deployment process by avoiding complex integrations with control systems and disruptions to machine operations. Expectant is a novel approach for APM focusing on identifying and localizing abnormal sounds in machinery without prior knowledge of the machine's specific configuration. Thus, it is a versatile and adaptive method for various industrial settings.

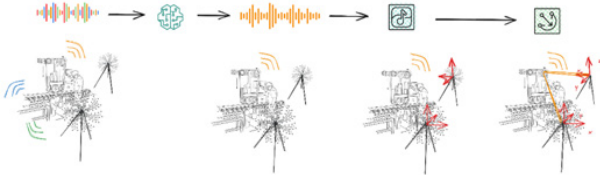


Figure 1: Pipeline for anomalous source separation and localization.

CSEM is developing a three-stage procedure to realize the Expectant project (Figure 1). First the anomalous sound is separated from the perceived mixture, second the anomalous waveform is used to estimate its direction of arrival (DoA) and finally the anomalous sound source is localized using triangulation. The source separation problem is approached by training a neural network with self-supervised learning to learn the distribution of normal soundscapes and then use this network to separate normal and abnormal sounds in a perceived mixture, as for example shown in Figure 2. This is made possible by the fact that acoustic scenarios can be realistically modeled as a sum of sounds. Therefore, if we can extract the normal soundscape from the mixture, we can isolate the anomaly by simple subtraction.

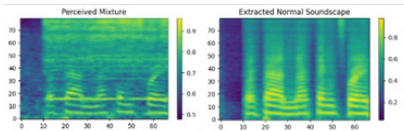


Figure 2: Separation of normal (middle) and anomalous (right) soundscape from a perceived mixture (left).

A major weakness of this approach lies in its need to generalize to out-of-distribution (OOD) data. But faults, or more generally, anomalies of any kind can be considered as OOD scenarios since there is no prior information about them. Where there exists research in this direction^{[1][2]}, it is a rather challenging setting. In

[1] Yang, Karren, et al., "Audio-visual speech codecs: Rethinking audio-visual speech enhancement by re-synthesis." Proceedings of the CVF 2022.

[2] Kong, Ping, et al., "DiffWave: A Versatile Diffusion Model for Audio Synthesis" Proceedings of the ICLR 2022.

a second step the DoA for the anomalous waveform (\hat{v}) is estimated for each array. Beamforming is a well-known and well-established technology that can be used for DoA estimation, provided an array of microphones. Ideally, each microphone will capture the same signal but with a delay of $\Delta t \propto d$. This delay depends on the direction θ of the incoming signal (Figure 3).

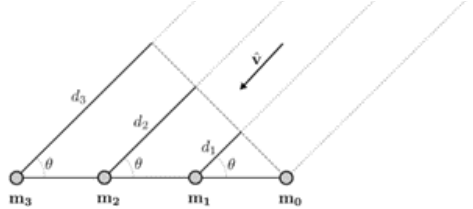


Figure 3: Theoretical model of a linear array.

By determining the appropriate delays between the microphones and adding the signals together, unwanted sources can be attenuated. This process can be repeated for all directions θ of interest, thereby dividing the space in a grid. This is known as SRP-PHAT algorithm^[3]. However, beamforming does have some major shortcomings such as assuming a planar waveform and spatial aliasing. To improve the DoA estimate, deep learning algorithms can be employed to, e.g., refine the SRP-PHAT map resolution and thus its accuracy. Finally, the anomalous sound can be localized in 3D by combining DoA estimates from multiple arrays. The simplest model to do so is triangulation, which requires angle measurements from two or more known locations (microphone arrays) to pinpoint the position of an object in space.

All pipeline components are currently developed and evaluated in simulated environments to facilitate fast prototype iterations. Using models as described in^[2] we can separate a perceived mixture such that the signal-to-noise (SNR) ratio is increased by a factor that depends on the initial SNR value. But separation is not yet good enough, because the DoA estimate is degraded significantly when combining the first and second stage of the pipeline. Furthermore, by employing hybrid beamforming with deep learning refinement, it is currently feasible to track a sound source within a simulated 10-meter room with an average error of 33 cm, given that it is the only source present.

Future work will be focused on combining source separation and localization as well as improving the separation performance in low SNR scenarios. A physical prototype will be built once the simulated results have reached a mature stage.

[3] Silverman, et al., "Performance of real-time source-location estimators for a large-aperture microphone array". IEEE Trans. Speech Audio Process 2005.

Smart Systems and Connectivity in the Mining Industry

J. F. Montesinos, I. Kastanis, P. A. E. Schmid

NetHelix (Intelligent digital toolbox towards more sustainable and safer extraction of mineral resources) is committed to introducing cutting-edge solutions for responsible mining by developing eco-friendly machinery, ensuring worker safety, and exploring new extraction schemes to minimize our industry's ecological footprint. CSEM is contributing by i) providing optimal control systems for ventilation on demand (VoD), ii) smart assistance for remote controlled vehicles, and iii) predictive analytics for the process plant. A key component to achieve this is data-driven predictive maintenance and asset health management.

The NetHelix^[1] project is a pioneering force in reshaping the mining sector, striving to optimize mineral extraction efficiency while reducing environmental impact. CSEM is involved in following aspects:

Ventilation on demand

Ventilation in mines is crucial for several reasons. Firstly, it ensures the safety of miners by removing harmful gases and dust from underground spaces. Secondly, it provides fresh air, essential for breathing and maintaining a suitable working environment. Lastly, proper ventilation helps regulate temperature and humidity, further ensuring miner comfort and safety. VoD is an advanced solution that actively adjusts ventilation based on real-time needs. Using IoT modules, VoD monitors air quality in mines reducing power consumption. CSEM is developing an optimal control system that can smartly and automatically adapt the ventilation taking the current mining plan into account. Technologies based on Reduced Order Modeling and Monte Carlo sampling are further developed to enable efficient and robust applications that are necessary in this harsh environment.

Smart assistance for remote controlled vehicles

Remote controlled vehicles in mining environments serve to significantly enhance worker safety and operational efficiency, particularly by enabling operations during post-blast periods when hazardous gas levels are too high for human exposure. CSEM is playing a pivotal role in this regard by developing smart assistance systems tailored for these vehicles.

Focusing on collision avoidance and vision systems, the smart assistance aims to mitigate challenges that operators often face, such as limited visibility due to poor lighting conditions underground and dust particles in the air. Advanced sensors and cameras are integrated into the vehicles to provide a more comprehensive field of vision. Real-time image and data processing techniques are employed to filter out noise and enhance image clarity, aiding operators in navigating through the challenging environment. Foundation models^[2] from state-of-the-art computer vision research are adapted by using application specific data. In this manner optimal performance can be achieved by applying the strength of big data in the specific needs of the mining environments.

Predictive analytics for the process plant

In line with NetHelix's commitment to responsible mining through the development of cutting-edge solutions, CSEM is actively engaged in the implementation of predictive maintenance, and anomaly detection systems for mining process plants. This

component is vital for enhancing efficiency, minimizing downtime, and ensuring the sustainability of mining operations.

Data collected in the process plant encompasses variables such as machine temperature, vibration levels, energy consumption, and throughput rates. Advanced machine learning algorithms analyze this data to identify patterns, optimize workflows, and predict potential inefficiencies or breakdowns before they occur.

Predictive maintenance, depicted in Figure 1, is a crucial feature that aims to preemptively address machine wear and tear, thus reducing costly unplanned downtimes. By utilizing sensor data and machine learning models, the system is capable of determining when machinery is likely to fail. This not only enhances operational efficiency but also extends the lifespan of the machinery, contributing to a reduced ecological footprint.

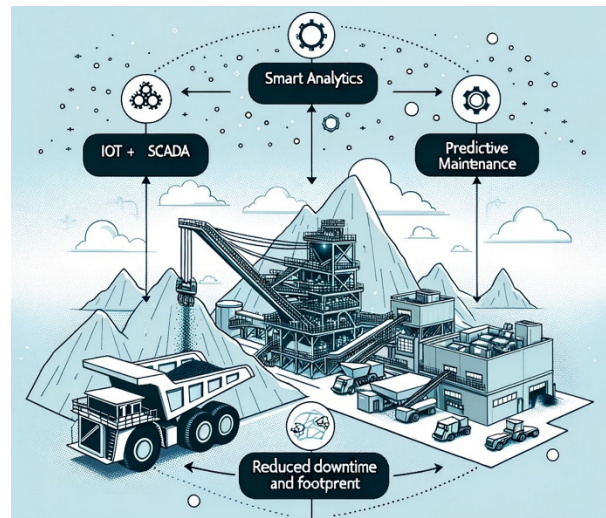


Figure 1: Predictive maintenance for mining operations.

Anomaly detection is another vital function served by this system. Never-before-seen events take place, and most models fail to perform in such cases. To alleviate this problem, anomaly detection focuses on handling out-of-distribution data by comparing to known situations. In real-time, the system can flag any irregularities in the plant's operation, such as unexpected spikes in energy consumption or anomalies in material quality. Immediate alerts are sent to operators and decision-makers, enabling rapid response to prevent accidents or inefficiencies.

By integrating smart analytics, predictive maintenance, and anomaly detection, CSEM's contribution aims to make mining process plants safer, more efficient, and more sustainable.

This work has received funding from the Swiss State Secretariat for Education, Research and Innovation (SERI).

[1] <https://nethelix.eu/>

[2] See for example, <https://arxiv.org/abs/2304.02643> and <https://arxiv.org/pdf/1506.02640v5.pdf>

Real-time Spore Measurement to Reduce Fungicide Usage in Vineyards

T. Bendinelli, S. Dietler, P. A. E. Schmid

Crop diseases caused by airborne spores are one of the main culprits driving the usage of fungicides in agriculture. Early detection of dissemination stages of plant pathogens, especially spores, is the key to optimize fungicide treatment strategies. Indeed, A higher precision of early detection would allow a better prevention of diseases and reduce the number of fungicide applications and/or enable alternative plant protection measures. However, the current state-of-the-art method of spore measurement requires manual identification under the microscope, which results in a delay of several days before the measurement results are available. CSEM, Swisens, AgroScope and Haute école spécialisée de Suisse occidentale, CHANGINS (HES-SO CHANGINS) have partnered together within the AGRARSENSE project for contributing to an early spores detection solution for precisions viticulture based on the air-flow cytometer SwisensPoleno Jupiter.

Food security is a global challenge and is impacted by rapidly compounding effects including climate change, supply chains, human labor shortages. This is the motivation behind AGRARSENSE, a 3-year Key Digital Technologies Joint Undertaking European consortium project aiming to develop microelectronics, photonics, electronic packaging for agricultural use and forestry.

One of the major objectives of AGRARSENSE is to reduce the use of fungicides while at the same time ensuring crop yield in vineyard by advancing precision viticulture.

Today, fungicides are often applied in quantities and frequencies that are not necessary to control plant diseases in vines. This is due to the lack of precise measurement of spore concentrations and thus inaccuracy of disease prediction models. In addition, when the disease outbreak is already visible, it is often too late to prevent the damage. Fungicides, have negative impacts on the environment and the health of humans and animals. Therefore, the applied quantity must be reduced, but plant protection must be ensured. If one could detect and predict the risk of spore infestation, fungicide treatment could be applied only when necessary.

This is the reason why CSEM, Swisens, AGROSCOPE and HES-SO CHANGINS have partnered together within AGRARSENSE to develop and validate a real time spore detection algorithm.



Figure 1: Two SwisensPoleno Jupiter on the roof of MeteoSwiss in Payerne.

[1] <https://www.swisens.ch/swisenspoleno-jupiter>

The detection is based on holographic imaging and fluorescence spectral measurements of single aerosol particles that go through by SwisensPoleno Jupiter flow-cytometer^[1], which is currently used for pollen recognition.

CSEM is building a neural network-enabled algorithm which will utilize two holographic images and fluorescence spectra as inputs to detect spores and identify their species. The algorithm, still under development, comprises a EfficientNet^[2] branch for the holographic images and a standard multi-layer perceptron for the spectral data which are then combined in the head of the network for the final prediction.

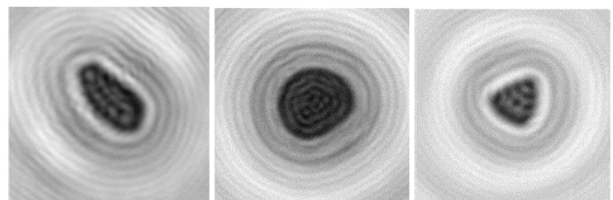


Figure 2: Example of reconstructed holographic images of an aerosol particle collected by the SwisensPoleno which are processed by the EfficientNet.

In the next two years the entire system will be validated extensively, particularly it will be installed in vineyards in Switzerland and Italy in collaboration with the Council for Agricultural Research and Economics (CREA) and compared against traditional spore traps.

Throughout the project AgroScope and HES-SO CHANGINS are leading the data collection and annotation efforts and are providing their expertise which will be used to further improve the algorithm performance.

If successful, the end solution will be integrated in modelling and forecast software for spore concentration and infection risk that can provide concrete recommendations to winegrowers.

The research has received funding from the Chips Joint Undertaking and the Swiss Confederation under grant agreement no. 101095835.

[2] Mingxing Tan, Q. V. (2019). EfficientNet: Rethinking Model Scaling for Convolutional Neural Networks. ICML

Gemtelligence – Accelerating Gemstone Classification with Deep Learning

T. Bendinelli, I. Kastanis, P. A. E. Schmid

A precious gemstone's origin and authenticity can mean an immense difference in its value, in some cases up to millions of dollars. Traditionally, stones are inspected manually by expert gemologist together with a set of advances analytical techniques. However, this is time-consuming and may offer inconsistent outcomes depending on the gemmologist experience. CSEM and Gübelin have partnered together and created Gemtelligence, a deep learning-based algorithm which can accurately and consistently identify gemstone origin and detect treatments in milliseconds, making analytical gemology more efficient, accurate and reliable.

Gübelin Gem Lab, with a tradition of almost one hundred years, is specialized in providing gemstone analyses and appraisals to buyers and sellers. The certificate that the company issues after the analysis, which includes most likely origin and treatments that the stone has undergone, influences dramatically the price of the stone as the price depends on rarity and the quality of the stone itself.

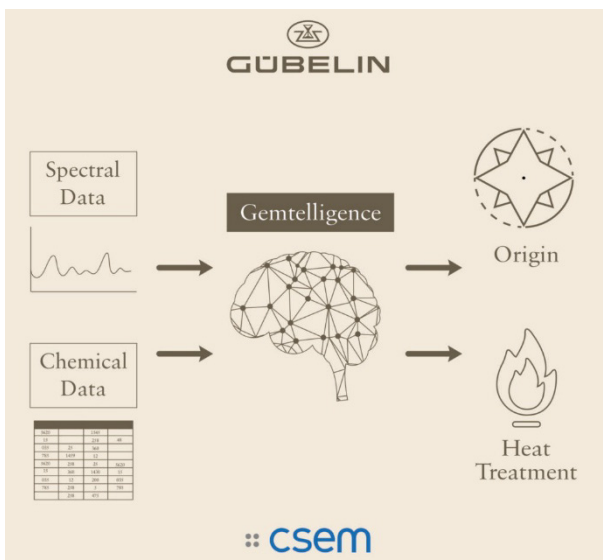


Figure 1: High-level schematic of input/output of the system. The system can work on Sapphire, Rubies and Emeralds and can work with only a subset of data sources at the time.

Currently the process of gemstone analysis and certification includes the inspection of the gem's physical characteristics by one or more gemologists and the use of various instruments to assess the chemical and physical properties of the material. The gathered information is later processed and discussed among gemologists to determine the gemstone's characteristics and possible treatments. The entire process takes one days or even weeks, depending on the complexity of the gemstone and it's ultimately subjective - as each gemologist may have their own interpretation and opinion about the gemstone.

To improve the assessment process, Gübelin Gem Lab partnered with CSEM in an Innosuisse to develop an AI system that can support the classification process. This project took two years of work and dedication resulting in the development of Gemtelligence.

Gemtelligence is a neural network designed to assess the quality and origin of gemstones through a range of spectroscopic methods, such as UV-Vis, FTIR, and ED-XRF. This advanced system leverages the latest deep learning architectures, particularly specialized encoder networks attention and convolution-based mechanism to embed each raw measurement. The resulting embeddings are then concatenated together and fed into a classifier network to generate the final predictions and confidence.

This confidence enables gemmologists to make an informed decision on whether to trust the automated prediction or to carry out further investigation, making the AI system a useful assistant that can help reduce the gemmologists' workload.

To train Gemtelligence, Gübelin Gem Lab provided thousands of gemstones records with high quality optical and spectroscopic data and corresponding expert assessment. The quality and size of this dataset was a fundamental cornerstone to make the model accurate and robust. As today this dataset is continuously extended, and in the network in the future will be re-trained to further improve its accuracy.

The system was put through an in-depth validation process comparing its predictions against Gübelin Gem Lab experts on unseen data. The results showed that it had classification performance on-par with the laborious laser-ablation ICP-MS and human inspection processes. This was a remarkable finding, as spectroscopic techniques are usually thought to have limited accuracy in the gemological realm for gemstone identification.

Currently, Gemtelligence is being rolled out to Gübelin Gem Lab offices across the world and is used to test sapphires, rubies, and emerald gemstones. The system is expected to revolutionize the gemological industry by allowing the gemstone analysis process to be standardized, significantly reducing the incidence of ambiguities, and increasing trust levels in the entire marketplace.

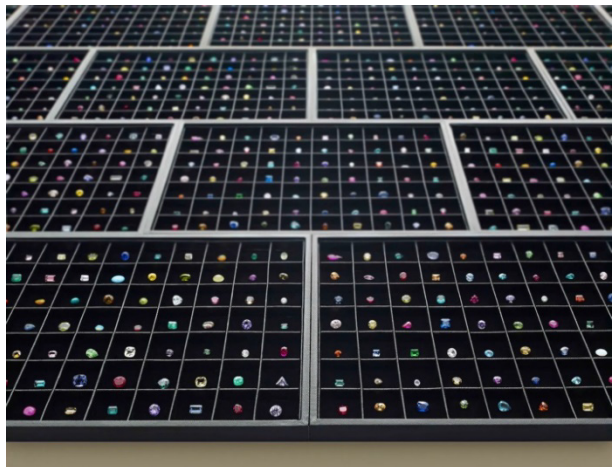


Figure 2: Gübelin's 28'000-stone reference collection, which contains scientific data on gemstones with provenance and more than 150'000 customer stones. This data has been compiled over the course of 100 years.

The work has received funding from Innosuisse under grant agreement no. 41844.1 IP-ICT and support by the Cantons of Central Switzerland.

Abnormal Rhythm Detection from Single-lead ECG

J. Van Zaen, G. Bonnier, J. Parak*, M. Salonen*, Y.-M. Proust, L. Marques**, A. Lemkaddem, C. Pellaton **, M. Lemay

Cardiac arrhythmias affect millions of individuals worldwide and can lead to severe complications such as stroke or heart failure. Due to their transient nature, they can be difficult to diagnose with ambulatory electrocardiogram monitors. A system for long-term arrhythmia monitoring is proposed. It measures single-lead electrocardiogram and tri-axis acceleration signals. This system is composed of a beat detector to extract interbeat intervals and a classifier to detect arrhythmias.

Millions of individuals suffer from cardiac arrhythmias (CAs). While most CAs are not directly life-threatening, they can lead to severe complications. Atrial fibrillation, the most common CA, affects between 2% and 4% of the adult population and is associated with substantial morbidity and mortality. In addition, ventricular arrhythmias are the cause of approximately 80% of sudden cardiac deaths. CAs may cause symptoms such as palpitations, shortness of breath, or fainting. However, symptoms are not necessarily present, and many patients are asymptomatic which prevent an early detection.

A 12-lead electrocardiogram (ECG) reviewed by a cardiologist is the gold standard to diagnose CAs. However, it is not applicable for long-term monitoring and thus might miss transient CAs. Consequently, long-term monitoring is usually performed with a Holter. A common drawback is the necessity to manually review Holter recordings of 24 hours or even several days, which is expensive and time-consuming. Usually, automatic systems are used to tag parts that most likely include CAs to be reviewed by a specialist. Such a system to detect CAs from a single-lead ECG and tri-axis acceleration signals recorded by a sensor that can be worn over long periods of time is proposed. It combines a detector to extract interbeat intervals (IBIs) and a recurrent neural network to classify CAs. This system performs CA detection with the following steps:

- Beat detection from ECG
- Extraction of IBI windows of 30 seconds
- Exclude IBI windows with motion based on acceleration
- IBI outlier detection
- Abnormal rhythm classification

Abnormal rhythm classification is performed with a recurrent neural network composed of two layers: a gated recurrent unit layer that takes sequences of IBIs as input and a sigmoid layer to output the probability of abnormal rhythm. The classification step yields a prediction for each IBI window from one of the following classes: abnormal, normal, tachycardia, or undecidable. The undecidable class is used to indicate that a reliable decision is not possible due to poor ECG signal quality.

The system was evaluated on two datasets collected with the Bodyguard 3 device (Firstbeat Technologies, Jyväskylä, Finland) shown in Figure 1. The first dataset was collected at Hôpital Poutalès, Neuchâtel, Switzerland, from patients with suspected CA during 24-hours monitoring. The second dataset was collected at KNF-Laboratori Oy, Helsinki, Finland from sleep apnea patients during overnight respiratory polygraphy. These two datasets include the following rhythms: atrial bigeminy, atrial

fibrillation, normal sinus rhythm, second degree heart block, sinoatrial block, sinus bradycardia, supraventricular tachyarrhythmia, ventricular bigeminy, and ventricular tachycardia.



Figure 1: Bodyguard 3 device by Firstbeat Technologies.

After excluding IBI windows with motion, multiple reference annotations, and undecidable predictions, 49,610 IBI windows of 30 seconds were used to compute performance metrics. The global accuracy was 96.7% and the metrics per class are reported in Table 1.

Table 1: Performance metrics for each class (TPR: true positive rate, TNR: true negative rate, PPV: positive predictive value, NPV: negative predictive value, F1 score: model accuracy).

Class	Abnormal	Normal	Tachycardia
Accuracy	98.8%	96.7%	97.9%
TPR	82.0%	97.3%	N/A
TNR	99.4%	82.0%	97.9%
PPV	85.4%	99.3%	0.0%
NPV	99.3%	54.5%	100.0%
F1 score	83.7%	98.3%	0.0%

The NPV for normal rhythm is quite low indicating too many false negatives for this class, and the TPR and PPV for abnormal rhythm are under 0.9 showing that there is still room for improvement. Nonetheless, the proposed system^[1] provides a robust solution to process daily life data, automatically rejecting low quality ECG, and detecting abnormal rhythm with a global accuracy above 95%. Performance can be further improved by combining successive IBI windows.

* Firstbeat Technologies, Jyväskylä, Finland
** Cardiology Unit, Réseau Hospitalier Neuchâtelois, Neuchâtel, Switzerland

[1] J. Van Zaen, et al., "Abnormal rhythm detection from a single-lead ECG via a recurrent neural network," Computing in Cardiology (2023).

Highly Accurate Step Detection from a Wrist-worn 3D Accelerometer

C. Moufawad el Achkar, R. Pilkar*, P. Renevey, D. Gerstel*, M. Biggs*, J. Nguyen*, M. Patterson*, A. Neishabouri*, C. Guo*, G. Dudnik, M. Lemay D. Ferrario

Step counting is the most used fitness and healthy mobility metric. Specific daily step recommendations have been provided by health organizations ever since the benefits of accumulating daily walks on overall health have been demonstrated. With smartwatches becoming ever so popular, many wrist-based algorithms have been developed to count and report steps. However, an objective validation of such algorithms is lacking. In this work, several algorithms were compared in different use-case scenarios for step counting, revealing the excellent accuracy of CSEM's approach.

Mobility is one of the main indicators of quality of life. As people moved to more sedentary lifestyles in recent centuries, it is crucial to remain active to retain the health benefits of movement and exercise. The WHO recommends that adults perform at least 10 000 steps per day, and this figure has been highlighted in scientific studies [1].

With the advent of MEMS, early pedometers were replaced by 3D accelerometers, whose signals vary with motion, enabling them to count steps. The body location at which these sensors are placed is important: for instance, the foot location has a clear advantage as steps inherently require foot motion, whereas the wrist is the location with most adoption, owing to the ubiquity of smartwatches. The main challenge at the wrist is to detect steps correctly while rejecting non-stepping movements, to reach a high accuracy and avoid over or under counting.

Different techniques have been used in the literature, including machine learning, peak detection, pattern matching, and frequency detection. CSEM's proprietary algorithm relies on a biomechanical model with a frequency calculation method that allows it to be robust to walking and running step detection [2].

This algorithm was put to the test in a study conducted by CSEM's partner, ActiGraph. A total of 17 healthy subjects performed 6 different tests, including 1-minute walking tests at slow, comfortable, and fast speeds, with two additional tests at comfortable speed: hand in pocket or holding a phone in the hand on which wrist sensor is worn. A 6-minute walking test was also performed. All users wore a GT9X and a CentrePoint Insight Watch (CPIW), two devices from ActiGraph each containing at least a 3D accelerometer. The collected data was run through 6 different algorithms:

- Lee, et al. [3]: peak detection with adaptive thresholding
- ADEPT [4]: pattern matching with predefined templates
- Femiano, et al. [5]: autocorrelation and peak detection
- CPIW v1: random forest with statistical signal features

[1] ActiGraph LLC, Pensacola, FL, USA

[2] Tudor-Locke C, et al., "How many steps/day are enough? For adults", Int J Behav Nutr Phys Act. 2011 Jul 28;8:79. doi: 10.1186/1479-5868-8-79. PMID: 21798015; PMCID: PMC3197470.

[3] R. Delgado-Gonzalo, et al., "Physical activity profiling: Activity-specific step counting and energy expenditure models using 3D wrist acceleration," 2015 37th Annual International Conference of the IEEE Engineering in Medicine and Biology Society (EMBC), Milan, Italy, 2015, pp. 8091-8094, doi: 10.1109/EMBC.2015.7320271.

- CPIW v2: improvement of v1 trained on larger age range and more activities
- CSEM: instantaneous motion frequency detection and biomechanical model

The results of the different algorithms are shown in Table 1.

Table 1: Step count results (SD: standard deviation, RMSE: root mean squared error).

Algorithm	Accuracy (%) \pm SD	RMSE (steps)
CSEM	96.7 \pm 6.4	11.4
CPIW v2	95.3 \pm 6.0	9.4
CPIW v1	95.1 \pm 7.5	10.6
ADEPT	90.1 \pm 10.3	17.9
Femiano, et al.	82.7 \pm 22.2	43.1
Lee, et al.	59.8 \pm 41.4	155.2

Compared to video reference, CSEM's algorithm had the highest accuracy (100-mean absolute percent error) at 96.66%, with CPIW v2 achieving lowest RMSE. The other algorithms exhibited lower accuracies: 90% for ADEPT down to 60% for Lee, et al. These results demonstrate that a motion frequency or a machine learning based approach is better suited to step detection than pattern matching or peak detection (which fared the worst). Besides, CSEM's algorithm works in a real-time fashion and is highly suitable for low-power, embedded applications.

The CSEM algorithm spans both general health and lifestyle monitoring, as well as step detection for clinical applications, and is easily adaptable to new applications since it does not need retraining. This study further demonstrates the accuracy and validity of CSEM's approach. Besides, this algorithm is part of an activity classification library that includes the analysis of walking, running, swimming, resting, and workouts, providing a complete solution for detailed activity monitoring and behavioral profiling.

[3] H. Lee, S. Choi, M. Lee, "Step Detection Robust against the Dynamics of Smartphones," Sensors, vol. 15, no. 10, pp. 27230-27250, Oct. 2015, doi: 10/gnh2s4.

[4] M. Karas, M. Strączkiewicz, W. Fadel, J. Harezlak, C. M. Crainiceanu, J. K. Urbanek, "Adaptive empirical pattern transformation (ADEPT) with application to walking stride segmentation," Biostatistics, vol. 22, no. 2, pp. 331-347, Apr. 2021, doi: 10.1093/biostatistics/kxz033.

[5] R. Femiano, C. Werner, M. Wilhelm, P. Eser, "Validation of open-source step-counting algorithms for wrist-worn tri-axial accelerometers in cardiovascular patients," Gait Posture, vol. 92, pp. 206-211, Feb. 2022, doi: 10/gpn5r9.

Hearing Instrument Fall Detection

C. Moufawad el Achkar, N. Ignasiak •, U. Lindemann •*, J. Van Zaen, R. Soltani, C. Verjus, H. Roeck •, C. Becker *, A. Lemkaddem

Remote, automatic fall detection based on wearables is an important challenge in digital health. While wrist wearables have witnessed incredible adoption in the last decade, the wrist is not an ideal location for fall detection. Hearing instruments, on the other hand, may offer better fall detection accuracy and are worn by persons who are at high risk of falling. This article describes the validation of using sensors embedded in hearing instruments to accurately detect falls in different activity contexts of older adult patients.

A third of adults above 65 years of age experience a fall on a yearly basis. A fall may lead to a devastating injury and, if unrecovered, may result in long lying times that eventually lead to institutionalization or even death^[1]. Persons who are prone to falls are often older adults or people with mobility problems (e.g., neurodegenerative diseases). A challenge arises when these people live alone: how to detect if they have fallen and send a message to emergency services or caregivers.

Wearables offer a solution to this challenge. In fact, almost all wearable devices include motion sensors, mainly 3D accelerometers, capable of detecting impacts, activity, posture, and orientation. However, for the specific case of fall detection, sensor location is extremely important. For example, placing sensors on the lower limbs may be irrelevant for this use case, as lower limbs are close to the ground and therefore little impact would be registered. The wrist is the location with the most user adoption, owing to the advent of smart bracelets and smartwatches^[2]. However, the wrist has such a level of freedom in daily life with possible high impacts that it may lead to many false positives (non-fall events that are detected as falls), which become a deterrent for the user.

Together with our partner Sonova, this project used hearing devices as wearables to investigate the benefits of positioning the sensor on the head for fall detection. The head is located far from the ground, has much less biomechanical freedom than the wrist, and a head impact after a fall may have drastic consequences so people try to avoid such impacts^[3]. Thus, at CSEM, a fall detection algorithm based on sensors embedded in a hearing device was developed and validated in a dedicated lab study.

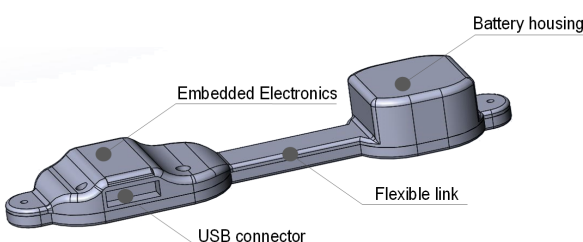


Figure 1: Device used for data collection.

The collection of raw sensor data was performed by the project partner Robert-Bosch-Hospital in Stuttgart. A device was

designed and built specifically for this purpose by CSEM, containing a 3D accelerometer with a high range of $\pm 16\text{g}$ and a barometer, and placed at the head near the ear (Figure 1). Data was collected in 3 different studies:

- Reenactment study to build the fall detection algorithm, consisting of 4 participants reenacting a total of 120 falls based on videos of real falls,
- In-lab study, with 42 older adults performing different activities of daily life to develop an activity classifier, and
- Inpatient study, with 14 older adult inpatients monitored over at least 1 day, to evaluate the fall detector's false positive rate.

The developed algorithm is based on biomechanical features and impact detection, which are analyzed in a machine learning model. Then, a recovery analysis is done using inputs from activity and posture context, to confirm a fall event (Figure 2).

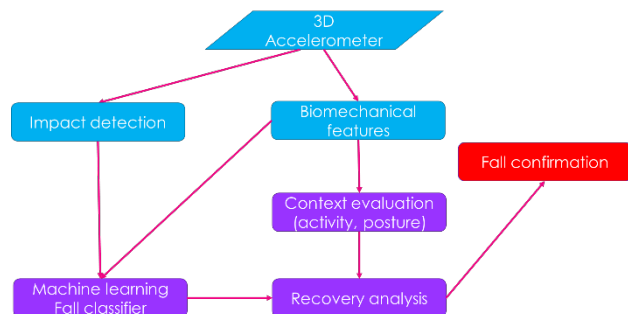


Figure 2: Fall detection algorithm flowchart.

The results of the activity classification algorithm showed excellent sensitivity/precision of 96%/96% for lying posture and 86%/95% for walking activity. The fall detection algorithm revealed a sensitivity/precision of 95% / 99%. Furthermore, the precision was confirmed in the inpatient study, with only 4 false positives in more than 400 hours of data collection.

In conclusion, the potential to detect falls with sensors at the head level is demonstrated. Furthermore, the evaluation of recovery is an important feature of this technology. For instance, an alarm could be raised when a fall is confirmed, and a verification could also be performed when a fall is recovered to check on the person. The low number of false positives reduces the deterrent effect of false alarms and increases the user acceptability of a wearable fall detection solution.

- Sonova AG, Zurich, Switzerland
- Department of Geriatrics, Robert-Bosch-Hospital, Auerbachstr. 110, 70376 Stuttgart, Germany
- * Unit Digitale Geriatrie, Universitätsklinikum Heidelberg, Heidelberg, Germany
- [1] Bagalà F., et al., (2012) "Evaluation of Accelerometer-Based Fall Detection Algorithms on Real-World Falls", PLOS ONE 7(5): e37062. <https://doi.org/10.1371/journal.pone.0037062>.

[2] C. Moufawad el Achkar, et al., "Real-time Fall Detection Using Smartwatches," EU Falls Festival (2018).

[3] Lindemann, U., Hock, A., Stuber, M., et al., "Evaluation of a fall detector based on accelerometers: A pilot study", Med. Biol. Eng. Comput. 43, 548–551 (2005), <https://doi.org/10.1007/BF02351026>.

Blood Pressure Monitoring in People with Spinal Cord Injury

M. Proen  a, J. Dedelley*, A. Gandhi**, F. Acquati*, N. Hankov**, G. Bonnier, P. Theurillat, M. Caban*, M. Lemay, D. Ferrario, L. Asboth**, R. Demesmaeker**, A. Rubio, V. Delattre*, P. Heck*, J. Bloch**, G. Courtine**

In a collaboration in the framework of the Eurostars IMPULSE project, CSEM, Onward Medical and -NeuroRestore are working on the development of a sensor for the closed-loop control of blood pressure for people with spinal cord injury. We present hereafter a preliminary analysis on the feasibility of the approach, by comparing CSEM's blood pressure monitoring technology with invasive measurements acquired in people with spinal cord injury.

Millions of people with spinal cord injury (SCI) suffer from hemodynamic instability, characterized by unstable blood pressure (BP), and usually treated with slow-acting drugs. However, these drugs cannot adequately address transient episodes. Both the absence of effective therapies and monitoring options to address these instability episodes make the condition difficult to manage and hamper recovery after SCI, reducing quality of life and increasing the risk of stroke and heart disease.

In the context of the Eurostars project IMPULSE, CSEM is collaborating with Onward Medical and -NeuroRestore to develop a solution to monitor hemodynamic instability in people with SCI. Prior to this collaboration, CSEM has developed a cuff-less BP monitoring technology based on photoplethysmography (PPG). EPFL has developed a therapeutic concept based on spinal cord stimulation to alleviate hemodynamic instability^[1]. Onward Medical has developed the cutting-edge clinical ARCTM platform, which enables the delivery of this therapeutic concept. The goal of the IMPULSE project is to develop a sensor integrated with the ARCTM system for long-term, user-friendly monitoring of hemodynamic biomarkers relevant to SCI. These developments will lead to the closed-loop "IMPULSE system" neuroprosthesis.

CSEM's BP monitoring technology has proven its capability to accurately track rapid BP changes induced by fast-acting drugs in operating rooms during induction of general anesthesia^[2], and circadian BP variations in patients undergoing 24-hour ambulatory BP monitoring^[3]. However, to date it was not tested in individuals with autonomic dysfunction, such as people with SCI. Thus, the first phase of the IMPULSE project is to evaluate the BP trending ability (i.e., the ability to track BP changes) of CSEM's BP technology in people with SCI. This report presents preliminary results of this investigation.

PPG signals were acquired in two individuals with SCI participating in the EPFL-sponsored HemON clinical study (ClinicalTrials.gov identifier: NCT05111093) during their stay in the post-operative, step-down unit of the Lausanne University Hospital (CHUV, Switzerland). Reference BP was measured invasively by means of a radial arterial line. The data were acquired in five recording sessions of 1h50min ±3 min. From the PPG signals – acquired at the upper arm – non-invasive BP was estimated using CSEM's BP technology and was compared for trending ability to the invasive reference. This was done by focusing on rapid BP changes, critical for detecting hemodynamic instability episodes such as events of orthostatic hypotension or autonomic dysreflexia in people with SCI. To that

end, systolic BP changes of at least 20 mmHg occurring over a time span no longer than 3 minutes were identified both in the invasive and non-invasive BP traces. Similarly, changes of at least 10 and 13.3 mmHg were identified in the diastolic and mean BP traces, respectively. The invasive and non-invasive BP changes were then compared through four-quadrant analysis^[4]. The concordance rate (CR), the percentage of BP changes showing a concordant direction of change between both methods, was assessed. The agreement on the estimated amplitude of the changes was also assessed. Finally, to evaluate the quality of the PPG signal – critical for a reliable PPG-based BP estimation – the number of cardiac harmonics distinguishable in the PPG spectrum was assessed. It is generally considered that a BP-related waveform is practically perfectly reconstructed using its 20 first harmonics^[5].

Four-quadrant analysis revealed a CR of 95% on systolic BP, and of 94% on both diastolic and mean BP. An average absolute difference of 11.9 mmHg, 5.1 mmHg, and 7.0 mmHg, respectively, was found between the amplitudes of the systolic, diastolic, and mean BP changes assessed by both methods. Finally, the number of harmonics averaged at 11.4.

This preliminary feasibility study reveals a good trending ability of the PPG-based BP estimation method, with an average CR of 94%. This suggests that a cuff-less PPG sensor placed on the upper arm can reliably detect the vast majority of potentially deleterious BP changes in individuals with SCI. The slight imprecision observed on the estimation of the amplitude of the changes is hypothesized to be due to the sub-optimal number of cardiac harmonics found in the PPG signals, linked with motion artefacts and occasional insufficient sensor tightening. There is therefore still room for improved BP precision, as PPG data quality was not optimized in the present data.

As part of the feasibility phase of the IMPULSE project, this preliminary analysis has shown promising results and confirms that rapid BP changes may indeed be reliably tracked using a PPG sensor at the upper arm in people with SCI. It has also revealed the importance of PPG signal quality on the precision of the estimated BP. Integration of the PPG-based BP estimation method in the IMPULSE sensor and confirmation of these findings in a larger sample size are next steps planned in the project. If confirmed, the IMPULSE sensor in conjunction with the use of closed-loop control of BP through an ARCTM spinal cord stimulation has the potential to drastically revolutionize the quality of life of people with SCI.

* Onward Medical, Lausanne, Switzerland

** -NeuroRestore, EPFL/CHUV/UNIL, Lausanne, Switzerland

^[1] J. W. Squair, et al., Nature, 590(7845):308-314, 2021.

^[2] Y. Ghamri, et al., Anesth Analg, 130(5):1222-1233, 2020.

^[3] M. Proen  a, et al., Sci Rep, 13:6149, 2023.

^[4] W. Verberk. In: J. Sol  a, R. Delgado-Gonzalo; The Handbook of Cuffless Blood Pressure Monitoring. Springer, Cham, 2019.

^[5] N. Westerhof, et al., Snapshots of hemodynamics: an aid for clinical research and graduate education. Springer, 2018.

ULTEEMNite – Ultra-long-term EEG Monitoring during Sleep

G. Yilmaz, J. A. Lahera Perez, M. Crettaz, L. Zhou, M. Frosio, A. Seiler*, O. Chételat, K. Schindler*

The ULTEEMNite device aims to provide physicians with objective sleep and seizure information collected over ultra-long-term time periods, i.e., weeks to months. Such information will help to significantly improve and personalize treatment of epilepsy. A successful implementation of the solution into the clinical workflow is expected to shorten the part of the patient journey, where patients need to try different drugs and dosages to find the most effective treatment for seizure control and sleep stabilization. In addition to the epilepsy use case, the ULTEEMNite device holds great potential for applications where tracking of the macro- and microstructure of sleep is required.

Electroencephalography (EEG) is accepted as the gold standard method for diagnosis, monitoring, and treatment follow-up of common neurological disorders, notably epilepsy and sleep disorders. In the context of epilepsy, the clinical practice to adjust epilepsy treatment strongly relies on patients' oral and written reports ("epilepsy diaries") during repetitive clinic visits including short EEG recordings. These two sources of information have known drawbacks: seizure counting by patients is generally inaccurate, particularly missing the nocturnal seizures during sleep and short EEG recordings on-site only give a snapshot of the patient's situation and fail to provide trends. Consequently, the physician has to make decisions based on incomplete or even false information. Objective seizure and sleep information recorded over ultra-long-term periods is therefore expected to help optimize and personalize epilepsy therapy. However, clinical grade EEG systems are bulky for ultra long-term use and consumer grade gadgets are not accurate enough for medical purposes. The ULTEEMNite project aims to address this unmet need by developing a medical-grade and user-friendly wearable device that can be worn during the night to collect EEG signals.

Conceptually and practically, ULTEEMNite functions as a complementary device to its day-use version, the ULTEEM eyeglasses^[1]. Two devices combined, 24-hour monitoring of generalized epileptic seizures becomes possible. When this around-the-clock approach is combined with ultra-long-term monitoring the clinicians will receive information, which they have never had the chance to obtain before with non-invasive devices. We anticipate an immediate improvement on personalized medication regime as a result of providing objective seizure counting, particularly nocturnal ones, as they mostly remain undocumented in the epilepsy diaries. The ULTEEMNite project builds upon a successful collaboration between CSEM and Schlaf-Wach-Epilepsie-Zentrum (SWEZ)/NeuroTec. In 2020, to address the unmet medical need of reliable ultra long-term EEG monitoring, a project (ULTEEM) funded by the European Space Agency (ESA) and CSEM had been launched. The pilot study using the device developed by CSEM had been performed by the team of Prof. Schindler and yielded highly promising results^[2].

The ULTEEMNite device consists of 3 electronic units: one central and two sensor units (Figure 1 top). Having a washable and even disposable headband combined with a disinfectable housing addresses the important practical need to be able to use the device on multiple patients. The largest part of the system, the central unit, is placed in the middle of the forehead to enable the patients to comfortably sleep on their back or on their sides

(Figure 1 bottom). Different head circumferences are addressed with an adjustable soft fixation system at the back of the head and different headband sizes. Importantly, the ULTEEMNite device is equipped with active dry electrodes and achieves high quality physiological signal acquisition thanks to CSEM's patented technology. The device has rechargeable batteries, an on-board memory allowing more than 16 hours of continuous data recording and a Bluetooth Low Energy module for live data streaming. A tablet or a smartphone is used to visualize the streamed data.



Figure 1: (top) ULTEEMNite device to monitor electric brain signals during sleep. (bottom) ULTEEMNite worn during sleep on the forehead.

ULTEEMNite measures 1-lead frontal EEG, which contains rich information including sleep spindles and K-complexes (Figure 2) that help to assess different sleep stages.

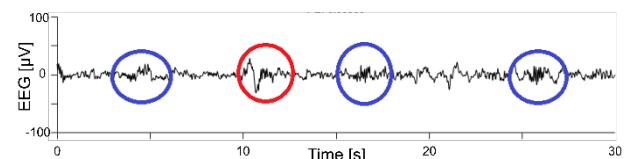


Figure 2: Sleep spindles (blue circles) and K-complex (red circle) recorded by ULTEEMNite and annotated by expert neurologists of the SWEZ, Inselspital.

A clinical study to evaluate the signal quality of ULTEEMNite has recently been completed at the Inselspital, Bern. Data analysis comparing ULTEEMNite data against reference EEG data is ongoing. This work was partially funded by the Canton of Bern. CSEM is thankful for their support.

* Schlaf-Wach-Epilepsie-Zentrum (SWEZ), University Clinic of Neurology, Inselspital, Bern.

^[1] <https://www.csem.ch/en/news/ulteem-ultra-long-term-eeg-monitoring>

^[2] K. Schindler, et al. "NeuroTec Sitem-Insel Bern: Closing the Last Mile in Neurology" Clin. Transl. Neurosci. 5 (2021) 13

Non-invasive Continuous Measurement of Intra-abdominal Pressure

J. Wacker, G. Yilmaz, E. Haenni, G. Bandet, P. Richard, J. Žumer*, S. Djordjević*, J. Jemec*, B. Plesnik**, B. Trolovšek**

Intra-abdominal hypertension (IAH) can lead to the failure of multiple organs. Currently, in patients susceptible to IAH, the intra-abdominal pressure (IAP) is assessed only sporadically with an urinary catheter. In a Swiss-Slovenian collaboration, a novel method was developed to monitor the IAP continuously and non-invasively by measuring the bioimpedance and the stiffness of the lower abdominal wall.

CSEM and the Slovenian company TMG-BMC Ltd. studied how the IAP can be monitored by measuring the bioimpedance (BioZ) and the mechanical stiffness of the lower abdominal wall. The partners developed and produced a demonstrator device, referred to as IAP-CMM, and tested it in a pilot clinical research project.

Figure 1 shows a 3D drawing of the IAP-CMM device. Its dimensions are $72 \times 42 \times 23 \text{ mm}^3$. BioZ is measured through four dry, glue-free stainless-steel electrodes which are integrated in the housing. These electrodes serve also to measure abdominal muscular activity (electromyography, EMG). Optionally, two more electrodes (e.g., gel electrodes with glue) can be connected to the device through two plugs on the side of the housing, to allow for longer inter-electrode distances for BioZ measurements. The tension of the abdominal wall is measured through a force sensor whose tip is in direct contact with the skin of the abdomen. The force sensor is conceptually a cantilever beam with a piezoresistive strain gauge at the fixed end. Importantly, the IAP-CMM device allows to synchronously record BioZ and tension of the abdominal wall non-invasively and continuously. A USB plug serves to recharge the internal battery of the device. The device is fixed on the lower abdomen with double-sided medical adhesive that is pre-cut to allow the electrodes and the tip of the force sensor to touch the skin, while covering the USB plug. The device streams the BioZ, EMG and force sensor data to a tablet through Bluetooth Low Energy (BLE). Additionally, at the end of a measurement all data can be downloaded via BLE.

To ensure safety, the development of the device was embedded in a risk management process according to ISO 14971, the relevant paragraphs of the IEC 60601 series were taken into account (e.g., limitation of leakage currents), and the device was rigorously tested against the requirements, partially by an external laboratory.

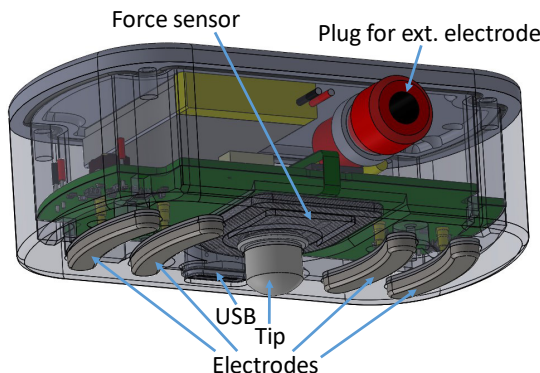


Figure 1: Drawing of the IAP-CMM demonstrator device.

- TMG-BMC Ltd., Ljubljana, Slovenia
- University Medical Centre Ljubljana, Slovenia

The principle of monitoring IAP changes through BioZ and force measurements was studied with the demonstrator device on 4 subjects who underwent medically indicated laparoscopic surgery at the University Medical Centre of Ljubljana. The study was reviewed by the Slovenian Ministry of Health (study number 0120-190/2021/6). The IAP of the patients was artificially modified during the intervention from 5 mmHg to 25 mmHg. Figure 2 shows how the BioZ and the tension of the abdominal wall increased with IAP. Confirming a previous study [1], we found a linear relationship between IAP and abdominal wall tension. We additionally found that the BioZ increases logarithmically with increases in IAP. At lower IAP, BioZ may therefore be more sensitive to pressure changes. Such behavior could be exploited to detect early onset of IAH, which is defined as IAP>12 mmHg. Note that the absolute, i.e., not normalized values of BioZ and tension are strongly different between subjects, e.g., due to the individual anatomy of the abdominal wall. Therefore, at the current stage, the approach seems mostly suitable for long-term intra-individual monitoring of the IAP.

In conclusion, the present study has shown in a small clinical research study with an experimental demonstrator that changes in the IAP can be monitored non-invasively and continuously by measuring the BioZ and the mechanical tension of the abdominal wall. These results shall be corroborated in already planned studies including more subjects, e.g., to reliably quantify the error with which the presented method estimates the IAP and to evaluate possible calibration procedures.

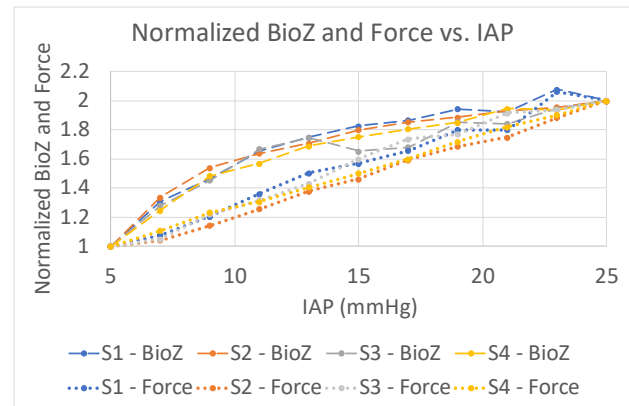


Figure 2: BioZ and force increase with IAP, as recorded on four subjects (S) during laparoscopic intervention.

This project has received funding from Eurostars-2 joint programme with co-funding from Innosuisse and the European Union Horizon 2020 research and innovation programme. CSEM thanks them for their support.

[1] M. Kušar, et al., "Preliminary study of reliability of transcutaneous sensors in measuring intra-abdominal pressure.", Sci Rep 12 (2022) 8268.

EXPERIENCE Physiological Integrated System: a Smart Wearable System for Mid-term 32-channel EEG, 1-lead ECG, and Motion Recording using Dry Electrodes

G. Dudnik, A. Falhi, J. Jorge, M. Crettaz, J.-A. Porchet, G. Yilmaz, M. Frosio, P. Pilloud, A. Moreira De Sousa, R. Rusconi

Hereafter a neurophysiology wearable monitoring prototype is presented, developed in the context of the EXPERIENCE EU project which, together with the devices developed by the other project partners, aims at creating a new generation of multimodal neuroimaging/electrophysiological biomarkers and methodological tools for the redefinition of psychiatric illnesses and disorders, unveiling for instance, new subtypes of anxiety and depression.

To achieve the project goal, CSEM contributes with the development of the EXPERIENCE physiological integrated system, composed of the EXPERIENCE Wearable System (EWS) and the related infrastructure: the EXPERIENCE Cloud and the linking communication means. The EWS records the physiological signals and uploads the recorded sessions to the cloud. The EXPERIENCE physiological integrated system has been completely developed, verified, and delivered on September 2023 to the partners for integration with their contribution. Once the paperwork is ready, the full system will be submitted for clinical trials at the University Hospital of Pisa in Italy.

EWS design and development

The EWS consists of a 32-dry electrode EEG cap, a digitalization module (EEG-AFE), an EEG, ECG, MOTION, and event recorder, a harness, a mobile app (eX App) (signal visualization, electrode positioning), a docking station (recorder battery recharge, recorded sessions upload to a secure cloud) and software drivers to decrypt and convert the downloaded sessions to BDF format. According to MDR 2017/745/EU, Annex VIII, the devices were classified as follows: EEG-AFE, Active Medical Device, Class IIa; recorder, Accessory of Active Medical Device Class IIa and the other parts, Class I.

Figure 1 shows the EWS parts finalized.



Figure 1: EXPERIENCE Wearable System (EWS) parts.

System verification – signal quality evaluation

The EWS successfully passed all the verification tests, including per-device and integrated functional tests, followed by Safety and EMC evaluations. Finally, to verify the quality of the signals the system acquires, an internal campaign with users was performed. A simple protocol was defined and executed on six candidates. Each participant underwent several recordings with the EWS, each one with a specific cognitive protocol, designed to elicit a particular brain activity and/or artifacts in a systematic manner. Each participant underwent three subsequent recordings as follows: sitting eyes-open still, standing (eyes open still, alternate eyes open and closed still, alternate eyes open and closed with head, eye, arm, jaw movements, then still) and walking (eyes open, alternate eyes open and closed).

The recordings were processed offline, where quality metrics were computed and compared across conditions and participants. The signal evaluation included metrics from both the temporal and frequency domain, some specific to the cognitive protocol and others more general, mainly RMS at specific frequencies and alpha peak amplitude.

Given the small group size, no statistical analyses were applied.

Results and discussion

Spectral properties: With users standing still, the RMS signals at 1–100 Hz range were about one order of magnitude stronger than that of the gold-standard, the disparity being caused by a stronger presence of broadband random noise and possibly motion artifacts at the lower frequencies. The RMS were strongest at 1–30 Hz and weaker at 65–85 Hz. **Alpha modulation:** when standing still, alpha peaks could be identified for each subject with the eyes-closed but were not identifiable with the eyes-open, becoming clearer in the ICA-derived data. When walking, the spectral background strongly masked the alpha peaks for both eye conditions. However, in the ICA-derived signals, the peaks could be identified once again, and they correctly demonstrated the amplification effect of closing the eyes, as shown in figure 2 for two of the participants.

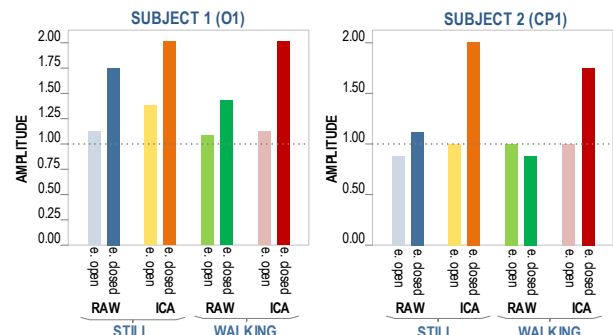


Figure 2: Alpha peak amplitude for two participants, for both raw EEG and ICA-derived signals selecting alpha components.

Conclusion

The tests demonstrate that the EWS can detect true meaningful aspects of brain activity (alpha waves). As expected, the signals are noisier than with gel electrodes. However, the use of multi-channel denoising techniques such as ICA may help with cleaning/separating part of these artifacts, allowing information to be extracted from periods of large motion.

The project partners are Universita Di Pisa (IT), Universitat Politècnica De Valencia (ES), Universita Degli Studi Di Roma Tor Vergata (IT), Commissariat à l'Energie Atomique et Aux Energies Alternatives (FR), Universita Degli Studi Di Padova (IT), Karolinska Institutet (SE), Quatechnion S.L. (ES). This project receives funding from the European Union's Horizon 2020 Research and Innovation program under grant agreement 101017727.

PRECISION MANUFACTURING

Michel Despont

The **Precision Manufacturing**'s priority research at CSEM is developing cutting-edge technologies tailored to bolster Swiss industry's competitiveness in a dynamic environment. Given Switzerland's status as a high-wage country, it's crucial that constant innovation underpin adaptations to the radical shifts in processes and business models ushered in by Industry 4.0. This drive for innovation finds practical expression in advanced microfabrication processes, which are pivotal in producing precise and functional components with meticulously controlled surfaces. Furthermore, the adoption of novel photonics technologies makes a fundamental contribution to the development of sophisticated instrumentation. This technology's versatility responds to demands ranging from those of aerospace to the intricate needs of life sciences. It showcases CSEM's commitment to pushing the boundaries of manufacturing.

This research priority aims to impact significantly the development of Swiss Microfabrication products, advanced photonics, and the overall quality and sustainability of the manufacturing sector. The program comprises two key aspects: technology-based and system-based areas, which are detailed in the following sections.

Technology-based areas

MEMS: This aspect provides a versatile technological platform for micro-fabrication to serve specialty applications and markets that require MEMS technologies and devices with demanding specifications. CSEM's broad and flexible technology portfolio, state-of-the-art infrastructure and equipment offer flexible opportunities for start-ups and SMEs to access technologies for customized devices in low and medium volumes. The entry barrier to access large commercial foundries or to internalize the technology is usually too high for SMEs in terms of investments, know-how, and time to market.

Additive Manufacturing (AM): CSEM's AM aspect endeavors to extend AM technologies beyond their current applications by focusing on high-precision manufacturing. The objective is to utilize high-performance materials, employ advanced design techniques such as topology optimization, integrate functional elements such as compliant structures, electrical wiring, damping mechanisms and printed sensors, and combine AM technologies with other manufacturing processes.

Functional Surfaces: This initiative develops know-how in surface structuring, modification, and interfacial engineering. The aim is to support partners in the manufacturing and scaling up of these developed processes. Surfaces and interfaces play a vital role in various chemical and physical processes, often key to fully harnessing the potential of new materials. From a cross-disciplinary perspective, the most important challenges faced by surface and interfacial engineering are the development of a deep understanding of atomic- and molecular-scale interfacial phenomena and its translation into the engineering of large-scale surface and interfacial properties, processes, and materials.

System-based areas

Photonics: This area specializes in innovative optical elements and systems utilizing micro- and nano-optics, integrated photonic

circuits (PICs), AI-enhanced image sensors, high-performance laser sources, and laser-based instruments. The primary focus is not only on developing miniaturized photonics components and systems to enhance performance, reduce power consumption, and lower costs, but also on extending the wavelength range for emerging applications, and leveraging AI to improve performance in sensing and imaging.

Tools for Life Sciences: This domain provides the necessary devices for handling and monitoring of body fluids, cells, and tissues. It encompasses the development of instruments, engineered biosystems, smart labware, sensors and other technologies employed in drug testing, diagnostics, and regenerative medicine. CSEM has established a significant presence in the pharmaceutical and diagnostics markets through its work on automating, standardizing, and parallelizing organoid-on-plate and cell-interacting microsystems. CSEM leverages its expertise in cell biosystems engineering to tackle the challenges of reproducibility, usability, and throughput in celomic research.

Scientific Instrumentation: This domain aims to meet emerging needs for advanced systems that have greater accuracy and novel functionalities in domains such as space, astrophysics, metrology, watchmaking, and industrial instrumentation. These developments involve higher precision, consistent motion patterns, fewer movable components using advanced manufacturing technologies, the elimination of friction and premature wear, as well as cost-effective production.

Ultra-sensitive Photonics-MEMS Accelerometers for Next-generation Seismic Sensor Networks

F. Ebrahimi, A. Manzoor, H. Sattari, D. Bayat, A. Hoogerwerf, Y. Pétremand, A. H. Ghadimi, M. Despont

Seismic sensors are powerful, highly versatile, and cost-efficient tools used in a wide range of applications with specific requirements in terms of frequency response and sensitivity. In this SNF funded project OPOSSUM, CSEM joins forces with the Swiss Seismic Institute at ETHZ, to develop and field test a new generation of opto-mechanical accelerometers and seismic sensors capable of reaching nano-g level sensitivity with ultra-high bandwidths.

MEMS-based accelerometers are ideal sensors for detecting ground motion, vibrations, micro-earthquakes, and for structural health monitoring. However, for many new applications covering a wide frequency band ranging from 1 Hz to 100 kHz, as well as for ultra-high sensitivity at the level of $<100 \text{ ng}/\sqrt{\text{Hz}}$, a low electronic noise floor is required in order to pick up the tiniest micro-seismic events at small dimensions. They also need to be robust enough to work for many years even in harsh environment such as high temperatures and high fluid pressures (such as on the seabed). These sensors need to be at the same time self-calibrated, reliable, and low-cost to allow installation in hundreds in the field, for instance in high resolution seismic imaging applications. The objective is to reach the following specifications: Ultra-low noise and thus ultra-sensitive [$<100 \text{ ng}/\sqrt{\text{Hz}}$], ultra-wide frequency range [1 Hz – 50 kHz], high dynamic range [$>140 \text{ dB} \equiv 24\text{bit digitizer}$] and 3D directionality with more than 20 dB reduction of off-axis signals.

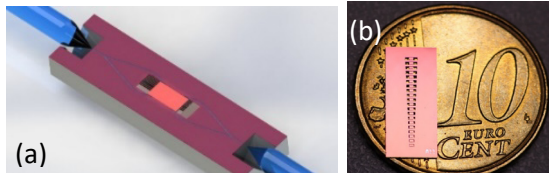


Figure 1: (a) Schematic 3D design of OPOSSUM sensor showing optical fiber and waveguides (blue) and test mass at the center (red). (b) Optical image showing an array of 20 fabricated test masses on a silicon chip illustrating a central silicon mass suspended with SiN tethers providing a high Q factor (image on top of 10 cent Euro coin for scale).

Several optimization cycles including sensor design, simulation, and fabrication loops have been performed to achieve the required target specifications and a robust fabrication process. For the mechanical test mass, three different resonators with frequencies of 1 kHz, 10 kHz, and 50 kHz, have been designed and simulated to meet the functional requirements in terms of bandwidth, noise, and directionality, while keeping the fabrication feasible. Each of these designs has a different bandwidth and a different noise floor of ~ 5 , 30 , and $100 \text{ ng}/\sqrt{\text{Hz}}$, respectively. The thermo-mechanical noise is dependent on the quality factor, resonance frequency, and test mass.

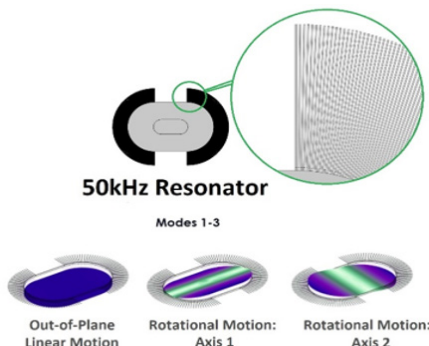


Figure 2: The comparatively scaled scheme of 3 resonators (from FEM simulation tool).

The ultra-high-quality factor is made possible using pre-stressed ($\sim 1 \text{ GPa}$) silicon nitride nano-beams, while a central silicon block provides a large enough mass to achieve the target sensitivity. Moreover, a series of compliant (spring-damper) elements constraining the motion of the resonator mass in other directions provides high directional sensitivity. Such a device of the first generation is shown in Figure 3.



Figure 3: First generation of OPOSSUM device.

The optical interaction with the test mass is done through evanescent coupling into SiN waveguides monolithically fabricated together with the test mass on the same wafer, providing efficient and strong opto-mechanical coupling. The light is coupled in and out of the chip using optical fibers that are connected to the optical interrogator on the other end.

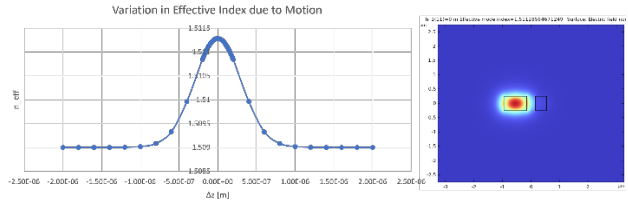


Figure 4: Optical simulation shows evanescent coupling of SiN waveguides in which effective index changes vs. displacement.

Since the sensors rely on high-quality factor of micro-mechanical resonators requiring low vacuum condition ($p < 10^{-3} \text{ mbar}$) for operation, a custom-made ultra-high vacuum (UHV) chamber was built with integrated vibration cancellation mechanism and a load lock for fast sample transfer. A laser interferometer provides the optical readout of ground truth and is mounted on the UHV setup. The mechanical displacement is measured through a homodyne Michelson interferometer which is capable of measuring displacements as small as $1 \text{ fm}/\sqrt{\text{Hz}}$.

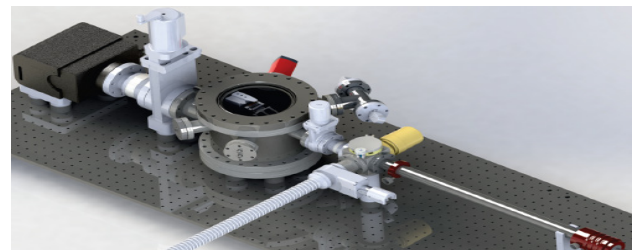


Figure 5: 3D rendering of the UHV chamber. The system was designed using SolidWorks.

Lifetime Evaluation and Reliability Assessment Methodology for NEM Switches

I. Marozau, O. Sereda, Qi Tang •, Dinesh Pamunuwa •, Piers Tremlett ••

Functionality and lifetime of a novel nanoelectromechanical (NEM) switch for computing and memory applications were evaluated. The NEM switch technology offers a number of unique attributes such as zero leakage in the off-state, capability to operate at very high and cryogenic temperatures as well as inherent radiation hardness. This makes the technology especially attractive for applications where operation at high temperatures with very high energy efficiency is required. The functionality of the switches for computing and memory applications was demonstrated. The designed memory switch exhibits non-volatile behavior with nearly zero leakage. The current switch designs can operate for up to few hundred switching cycles with work currently being conducted to improve the lifetime further.

Emerging applications such as the Internet-of-Things (IoT), all-electric vehicles and more electric aircraft (MEA) require electronics with integrated sensing, data processing and transmission capability that can operate at high temperatures with very high energy efficiency. The ZeroAmp EU project aims to develop a NEM switch technology that will serve these emerging requirements. This technology enables a NEM switch-based reprogrammable computing platform comprising logic and non-volatile memory (see Figure 1). This silicon-based NEM switch technology has significant advantages over other technologies for energy-efficient computation in extreme environment, due to the following unique attributes: (1) zero leakage in the off-state; (2) capability to operate at very high (up to 400°C) as well as cryogenic temperatures; (3) an inherent radiation hardness; and finally (4) ability to carry out large-scale integration using an innovative 3D stacking approach.

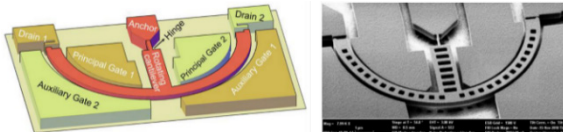


Figure 1: Sketch of bistable NEM switch that is used for non-volatile memory applications. The device's electrical state can be reversibly changed by the application of electrical bias at the respective pairs of gates. Figures are property of University of Bristol.

CSEM is involved in the development and execution of the test program that can be used for the lifetime evaluation and reliability assessment of the designed NEM switches as well as device based on them. The test program consists of two main parts:

- Functional and lifetime evaluation of the switches. The main aim is to assess the different switch design options and select the designs that enable best lifetime and stability performance.
- Reliability assessment of the switches and devices. The main aim is to study the robustness against deteriorative effects of various stress factors, such as thermal shocks, mechanical loads, radiation, etc...

In the first stage of the project, the functionality and lifetime evaluation methodology were developed and applied for testing early samples. Figure 2 (left) shows a typical IV characterization curve for a 3-terminal logic switch. The current between source and drain is measured during the gate voltage increase. At a certain gate voltage (known as V_{pull-in}) the attractive electrostatic force between gate and source (cantilever) overcomes the spring force of the cantilever resulting in a physical contact between the source (cantilever tip) and drain electrodes. This leads to a constant drain-source current. When the gate voltage is subsequently decreased below a certain voltage (V_{pull-out}), the contact is reversibly broken. V_{pull-out} is

less than V_{pull-in} due to the attractive van der Waals force between the cantilever tip and the drain electrode when they are in contact with each other.

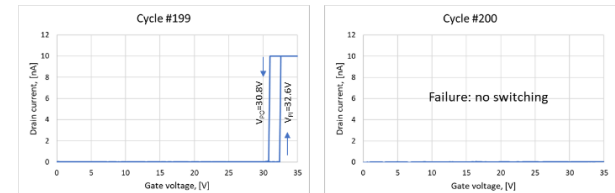


Figure 2: Switching cycles of a logic switch. (left) typical IV curve of a functional switch; (right) same switch failed after 200 cycles.

The 3-terminal switch can withstand a certain number of these pull-in / pull-out cycles, which is the main characteristic of their lifetime. The lifetime strongly depends on the sticking and friction properties of the cantilever tip. Therefore, the contact material applied at the cantilever tip plays a very important role. Our early experiments were carried out on switches with an Au coating. The lifetime of these switches can reach up to a few hundreds of switching cycles (see Figure 2). Other contact materials are being currently investigated with the aim to increase the lifetime to up to 10⁹ cycles.

Figure 3 shows a typical IV characterization curve for a 7-terminal switch for non-volatile memory (see Figure 1 for the switch design). The main difference to the 3-terminal version is that the van der Waals force can keep the cantilever tip in contact with the drain electrode, even with switched off gate bias. Thus, the switch state is preserved without any electrical biasing. In this state the leakage current is very close to zero, significantly smaller than for the competitor technologies. In order to reprogram the switch to another binary state, a gate bias shall be applied to the opposite gate electrodes (see Figure 1). It was demonstrated that using an Au coating on the tip enables the required non-volatile switch behavior. However, in order to improve the number of possible reprogramming cycles, other tip coating materials are currently being investigated as well.

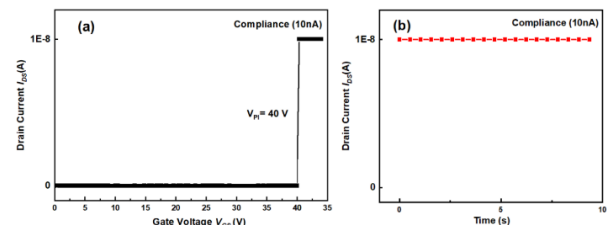


Figure 3: (a) Switching cycle of a non-volatile memory switch, (b) Non-volatile functionality after removing actuated gate voltage.

This project has received funding from the European Union's Horizon 2020 research and innovation program under grant agreement No 871740 (ZeroAMP).

• University of Bristol, UK

•• Microchip technology Inc, UK

In-cavity Marking for Plastic Part Traceability

J. Schildknecht, O. Dubochet, M.-A. Dubois

Many industries are under pressure to provide traceability for their products to comply with increasing demands of public and regulative forces. Today, producing parts and marking them are disjunct downstream processes. matriq has a radical innovation named DynamicMold®, that integrates marking directly into the forming process. This single-step solution for the marking of injection molded plastic parts dramatically reduces complexity and setup time, and has a twenty times lower energy consumption than laser marking, which is the state-of-the-art.

Plastics are key materials for the economy and can be found just about everywhere in our daily lives, from food packaging to healthcare products and luxury goods. They are lightweight and versatile, and as a result, their demand in the plastic injection market is booming. In turn, this is increasing pressure on plastic manufacturers to improve their quality control processes in order to ensure the end-to-end traceability and quality of their products to avoid recalls.

In the event of a recall, most plastic products have already been stamped with a unique identification code so manufacturers can quickly trace any defective parts. This marking happens post-production - once formed, the plastic material is either laser-engraved or stamped with a barcode. But both these procedures are complex and rely on additional bulky machinery. Now, thanks to a new technology developed by matriq AG, manufacturers can take advantage of a simple marking method that is directly integrated into their injection molding process.

Engineers at the Swiss company matriq have capitalized on the Industry 04 trend to develop DynamicMold®: a new technology that allows manufacturers to mark, number, identify and brand-protect their products. The new technology is installed directly into injection-molding machines, simplifying the marking procedure, cutting time and production costs, and saving precious floor space.

DynamicMold® inserts are directly mounted into the machinery's mold cavities, where they then imprint a unique data matrix code, which can be read directly on the surface of plastic parts. The whole marking procedure takes just a few milliseconds and doesn't delay or interfere with production runs. matriq's technology is the first digital marking system in the world that operates continuously in-mold and on the production line.



Figure 1: first generation insert (4x5 heaters).

The core component of the DynamicMold® inserts is a MEMS chip with a 2D matrix of heating pixels that can be individually activated (Figure 1). By switching the pixels on or off, the system can dynamically apply specific ID codes onto plastic while being molded. CSEM and matriq jointly develop this aspect of the technology to allow the industrial-scale application of this technology.

matriq collaborates with CSEM on the fabrication of the chip that generates the mark directly on the injected plastic part. After the validation of the first-generation device all the work is focused to transfer the process to the second generation that allows to generate a more complex marker. The heater matrix is increased from 4x5 to 14x14 points. The first goal is to stabilize the yield since the base substrate is not a silicon wafer but a highly complex ceramic substrate out of the standard dimension and properties normally used in cleanrooms.

Besides high accuracy lithography on non-standard substrates and layer patterning requiring a highly selective etching processes, the main challenge is the adhesion of the different layer materials involved to withstand temperature cycling and mechanical wear during the injection process to guarantee a long lifetime.

The process implementation will end with the validation of the test plan and the yield improvement to fulfill all industrial needs of the customer.

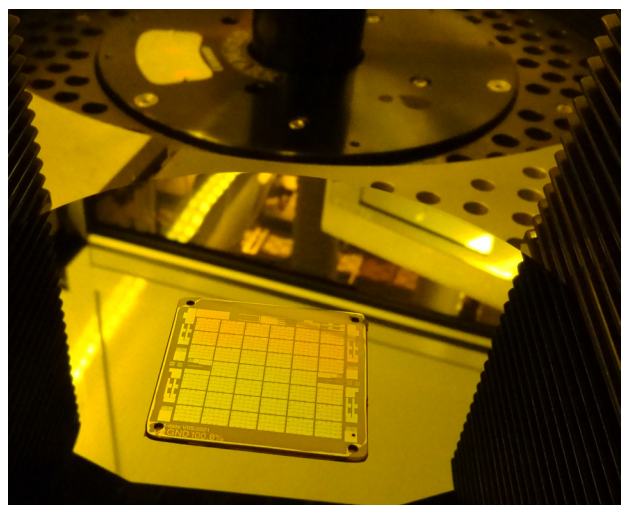


Figure 2: substrate on cleanroom equipment.

The industrial project partner is matriq AG.

A Precision Gradient Magnetometer

A. Hoogerwerf, D. Bayat, G. Spinola Durante, Y. Petremand, M. Despont, E. Gasparin, M. Tormen, G. Close

A gradient magnetometer has been developed with a resolution better than 50 nT/cm. The magnetometer is based on the capacitive sensing of a force exerted on a permanent magnet by a magnetic field gradient. A mass-balancing scheme has been used to reduce the effects of gravity and acceleration on the sensor.

The sensing of magnetic fields is used for a wide range of applications. Hall sensors measure fields in the mT range and are often used as proximity or position sensors in motor control. Sensors with sensitivities in the μT range are used in non-contact measurements of electrical currents and in navigation applications that measure the orientation with respect to the Earth's magnetic field of approximately 60 μT . For lower magnetic field measurements, magnetic field gradients are measured instead of magnetic fields since Earth's magnetic field that is present everywhere would overwhelm the magnetic field measurements. Field gradients in the order of nT/cm can be used for geophysical measurements, in the order of 100 pT/cm for magnetocardiography, and in the order of pT/cm for magneto encephalography.

A wide variety of techniques and devices are used to measure small magnetic fields [1], of which magneto-resistive techniques are the most common. However, techniques that directly measure magnetic field gradients and that are suited for miniaturization are rare.

A recent paper [2] presents a gradient magnetometer based on a MEMS accelerometer that is small in size. The authors of the paper mounted a magnet on top of an off-the-shelf MEMS accelerometer. The gradient magnetic field exerts a linear force on the mounted magnet that is detected by the capacitive readout of the accelerometer. The authors extrapolate from their measurements a resolution down to 100 pT/cm.

The approach of converting a magnetic field gradient to a force and using an accelerometer to measure this force has the merit of making a very small sensor that has a very good sensitivity to magnetic field gradients. However, there is a major drawback: by mounting a magnet on the accelerometer mass the authors have increased this mass more than hundred-fold. As a result, the device is also an accelerometer with a more than hundred-fold increase in sensitivity. The device therefore has a very high cross-sensitivity to vibrations and gravity. The effect of a 1g acceleration is equal to the effect of a 0.8 mT/cm magnetic field.

To overcome the drawback of the vibration sensitivity, CSEM has developed a gradient magnetometer based on the same principle, but with a mass balance compensation. The magnet is mounted on a mechanical guidance structure that allows for a linear movement as a result of forces due to either a magnetic field gradient or vibration. A second, non-magnetic mass that is approximately equal to the mass of the magnet is mounted on a similar mechanical guidance structure, allowing for the same linear movement. As a result, the magnetic mass and the non-

magnetic mass move by the same amount due to the force of acceleration, whereas only the magnetic mass moves due to the force of a magnetic field gradient. An interdigitated comb capacitor is placed between the guidance of the magnet and the guidance of the mass that only changes its capacitance when there is a relative movement of its guidance. Hence, the capacitor only changes its value due to a magnetic field gradient.

The gradient magnetometer hence designed has been implemented using Deep Reactive Ion Etching of Silicon-On-Insulator wafers. Structures with both two and three different silicon thickness values have been implemented. The device contains two mechanical guides, an interdigitated capacitor, a silicon mass and a cavity in which an off-the-shelf magnet [3] can be inserted. A front side view of one of the devices is presented in Figure 1.

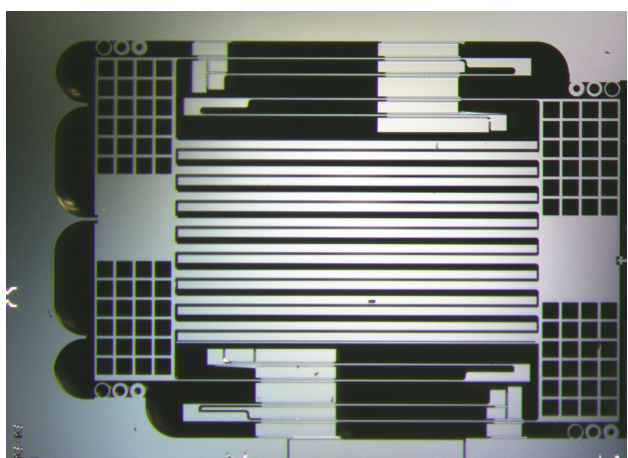


Figure 1: Picture of the front side of the gradient magnetometer. The guide beams are in the center on the top and bottom. The interdigitated sensing capacitor is in the center of the picture. The large squares on the left and right are the mass and the cavity holding the magnet respectively.

After the fabrication of the silicon structures, the wafer is separated into dies, the magnet is inserted and fixed with glue, the die is placed in non-magnetic package, wire-bonded, and protected from the environment with a glass lid.

The first packaged devices have been tested by the project partner on a tabletop without any further vibration damping. The first measurements demonstrate that field gradients down to 50 nT/cm/ $\sqrt{\text{Hz}}$ can be resolved using an AD7746 readout circuit.

The project has been supported by the Swiss Innovation Agency under InnoSuisse contract 101.507 IP-ENG.

[1] B. Brajon, E. Gasparin, G. Close, "A Benchmark of Integrated Magnetometers and Magnetic Gradiometers," IEEE Access, vol. 11, pp. 115635–115643, 2023.

[2] J. Javor, A. Stange, C. Pollock, N. Fuhr, D.J. Bishop, "100 pT/cm single-point MEMS magnetic gradiometer from a commercial accelerometer", Microsystems & Nanoengineering (2020) 6:71.

[3] <https://supermagnetman.com/collections/neo-cubes/products/c0005-10>

A MEMS Gas Chromatograph and its Fluidic Connections

A. Hoogerwerf, G. Spinola Durante

We present the MEMS components of a gas chromatograph with fluidic connections that can withstand operating temperatures of up to 300°C of the MEMS components. The components that have been developed are a pre-concentrator, different types of columns, and a Thermal Conductivity Detector. The developments will enable future hand-held gas chromatography systems.

Since the first published paper [1] on MEMS Gas Chromatography (GC) columns, much work has been done on making complete GC systems using MEMS technology. Much progress has been published on many aspects of MEMS GC systems. However, very little effort has been placed on making reliable fluidic connections to the MEMS system. Almost all MEMS GC components use a glass capillary that is inserted sideways into the silicon chip and that is held in place and sealed leak tight with epoxy around it. Such a simple sealing will have high leak rates of Helium which is generally used as a carrier gas in GC systems. Moreover, the seals cannot withstand operating temperatures much higher than 150°C due to the deterioration of the epoxy.

Making reliable and high-temperature resistant fluidic connections to MEMS components presents a major challenge. This is mainly due to the properties of silicon, which is the most widely used material in MEMS technologies. Silicon can be etched with very high precision using Deep Reactive Ion Etching techniques. However, the cross-section of the structures etched this way is rectangular. Moreover, silicon is a brittle material and rapidly forms a native oxide that is chemically quite inert.

In conventional GC systems, the most widely used fluidic connection element is a glass capillary that is coated with polyimide on the outside. Standardized metal fittings with carbon ferrules exist to connect the capillaries together or to other components.

CSEM has developed fluidic connections for MEMS components using a thermocompression bonding approach. First, the fluidic inlets and outlets are defined as holes in the silicon surface. The silicon surface is metallized with gold as its top layer. In parallel, a piece of Invar is machined with at least one polished side. Holes are machined in the Invar piece that corresponds to the hole pattern in the silicon. On one side the holes are threaded with threads for the standard GC fittings. The Invar piece is electroplated with gold, aligned to the silicon piece, and bonded by gold-gold thermocompression bonding. Standard GC fittings can now be used to the silicon GC component to glass capillaries.

The technique has been used on three components of a GC system: the pre-concentrator, the column, and the Thermal Conductivity Detector (TCD). Different sizes of columns that have been fabricated are shown in Figure 1, whereas Figure 2 shows a TCD with its connector.

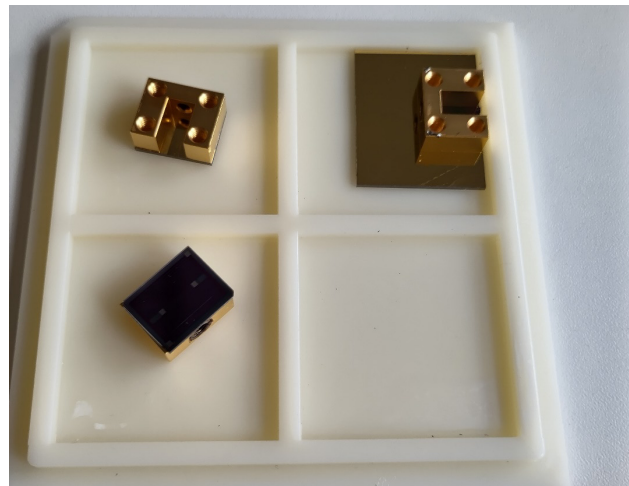


Figure 1: Columns with Invar connectors for standard GC fittings.

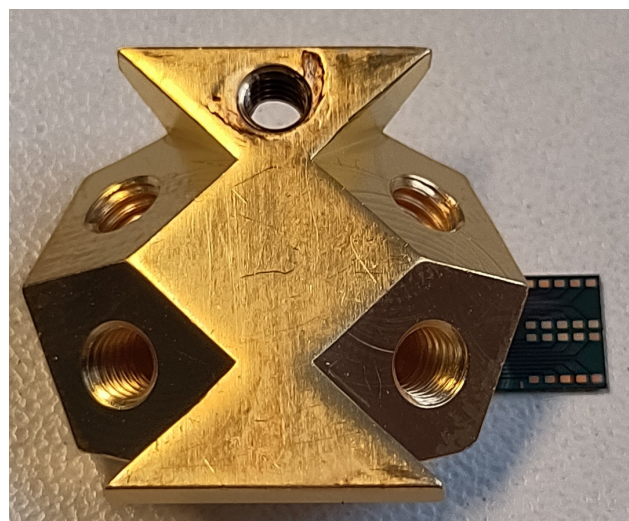


Figure 2: A TCD with an Invar connector for standard GC fittings.

The pre-concentrator will be connected using a similar Invar piece. However, the pre-concentrator must be capable of rapid heating and the Invar presents a large thermal mass. Therefore, the design and thermal simulation of the pre-concentrator require much more attention and have not yet been completely finished.

The first columns have been sent to the project partner for testing and the TCDs will follow once they have been connected to a flexible interconnect cable.

This work has been supported under ESA Contract No. 4000139571/22/NL/KML.

[1] S. C. Terry, J. H. Jerman, J. B. Angell, "A gas chromatographic air analyzer fabricated on a silicon wafer", IEEE Trans.Electron. Dev., vol. ED-26, no. 12, Dec. 1979.

Additive Manufacturing for Integrated Active Fluid Control in Life Science Applications

F. Boudoire, E. Aeby, M. Garzuel, C. Czekus, C. Fonta, D. Di Stadio, S. Heub, V. Pejchal, G. Weder, O. Sereda, T. Valentin

CSEM covers a broad spectrum of expertise, including biology, fluidic system development, and additive manufacturing (AM). Leveraging this knowledge, we've crafted a platform for high-resolution stereolithography (SLA) printing of biocompatible fluid-handling systems. We can now produce monolithic systems at the well-plate scale, complete with sub-millimetric embedded channels. This is especially valuable for developing well-plate smart lids to automate medium handling. We have expanded this technology by integrating actuation with membrane valves into these systems. This technology offers new possibilities for industrial partners in need of precision small liquid volume handling.

Organ-on-chip (OOC) devices have seen a growing presence in the Life Science research and industry. They enable building more complex and physiologically relevant in vitro models for diagnostics, drug development and tissue engineering. One key aspect of those micro-physiological systems is the necessity for active fluid control, either for the automation of routine maintenance steps (e.g., medium exchange) or the creation of a dynamic environment for maturation and testing mimicking physiological conditions, e.g., controlled medium perfusion and timely compound injection. The manufacturing state-of-the-art for such devices is plastic injection molding, hot embossing or milling, with the subsequent bonding of additional components like flexible membranes or valves. This approach limits design flexibility and drastically lengthens the time required between design iterations.

At CSEM, we have developed high-resolution additive manufacturing (AM) to push the boundaries of design possibilities and facilitate device development. To achieve this, we employ UV-stereolithography (SLA), a process with optimal balance between resolution and throughput for this application. With this technology, we produce parts at the scale of multi-well plates, meeting the demand for standard labware formats in Life Sciences. An achievement was the successful creation of integrated channels with diameters as small as 0.5 mm at this scale. In our ongoing efforts to advance this technology, we are now focusing on developing print-in-place membrane valves for pneumatic actuation.

The fabrication of print-in-place membrane valves using SLA has been explored by various research groups [1,2]. Nevertheless, these studies have not yielded valves with the desired footprint for our specific application, and they do not employ biocompatible materials. Furthermore, the overall device size reported in these scientific papers is considerably smaller, typically on a centimeter scale. To overcome these limitations, we developed devices with multiple membrane valves at a well-plate lid format (Figure 1).

Testing of these valves proved their ability to operate effectively for a minimum of 25,000 actuation cycles. Furthermore, we demonstrated that the sequential actuation of several valves arranged in series allowed for peristaltic pumping. To assess the volume transfer reproducibility of these peristaltic pumps, we conducted a benchmark test involving the parallel operation of 5 peristaltic pumps integrated into the same device. The transfer of liquid from one well to the next was successfully demonstrated, achieving a coefficient of variation of 10% for 40 µL across 5 channels (Figure 2).

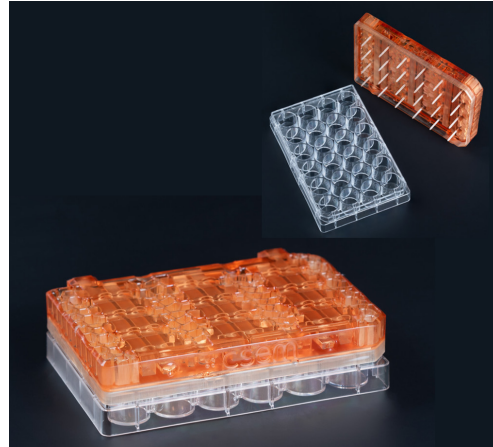


Figure 1: Smart Lid for 24-well plate with integrated peristaltic pumps.

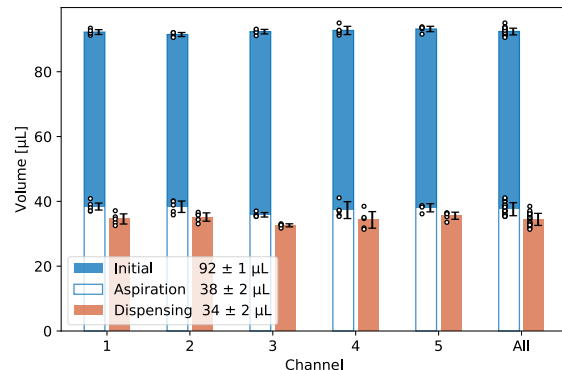


Figure 2: Volume transfer performance characterization.

As a proof-of-concept, a 24-well plate fluidic lid prototype was manufactured in one step, integrating 12 peristaltic pumps, pneumatic channels, pneumatic ports, fluidic channels and liquid collection and dispensing ports (Figure 1).

An adapted post-processing protocol was developed to ensure mechanical resistance of the membranes to sterilization procedures, including autoclaving, and biocompatibility. The material shows no acute toxicity, and long-term in vitro studies with exposure to various 2D and 3D biological models are ongoing and already showing promising results.

In conclusion, we have harnessed high-resolution additive manufacturing to develop print-in-place membrane valves, expanding the possibilities for OOC device design. Our testing demonstrated their robust performance, with the potential for peristaltic pumping in Smart Lid applications. Our ongoing work focuses on scaling up and ensuring biocompatibility for broader applications in this field.

[1] Au, et al., Lab Chip, 2015, 15, 1934

[2] Gong, et al., Lab Chip, 2016, 16, 2450

Development of Metal Ultra-thin Cold Plates by L-PBF Technology: Limits and Benefits

S. Unterhofer, M. Angeletti*, O. Sereda, P. Petagna*

Laser Powder Bed Fusion (L-PBF) Additive Manufacturing (AM) process is investigated as a promising technology to develop metal cold plates of the new generation detectors for subatomic particles accelerators on European AlDAInnova project. The investigation is conducted with Aluminum Silicon alloy and Kovar alloy, as the coefficient of thermal expansion and the thermal conductivity of these materials fits the scope of the project. This study includes the discovery of laser process parameters to achieve minimum wall thickness attainable for leak-tight single pipes and multi-microchannel devices, the minimum attainable ratio between inner diameter and pipe length to be able to remove the remaining powder, and the characterization of inner wall roughness, planarity, and dimensional accuracy for flat multi-microchannels.

New generation of subatomic particles detectors need more performing cooling systems. Despite the high performances that silicon microchannel coolers can provide (excellent thermal performance, low and uniform mass, no thermal expansion mismatch, radiation hard), the manufacturing costs is extremely elevated. AM opens the possibility to increase cold plates performance to costs ratio. Thin walls, small channels, structurization of the geometry device and new composites materials that AM provides enhance the cold plate performance while the manufacturing repeatability and the few assembly steps reduce the cold plate fabrication costs.

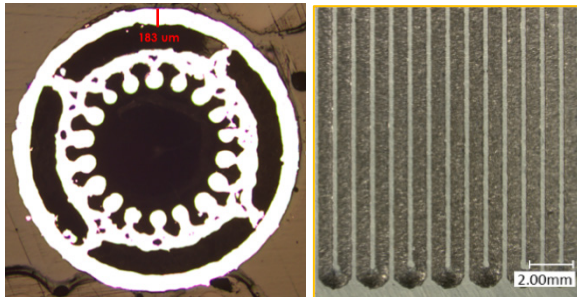


Figure 1: Examples of L-PBF applied to coolers. Structured pipe with porous inner wall and bulk outer wall (left) and multi-microchannel cold plate fabricated (right).

Process dependent factors that mainly impact the thermal performances are the wall thickness and the channel dimension (which depends on the surface roughness).

Figure 2 shows results obtained to determine the leak-tight minimal wall thickness and surface roughness on AISi12.

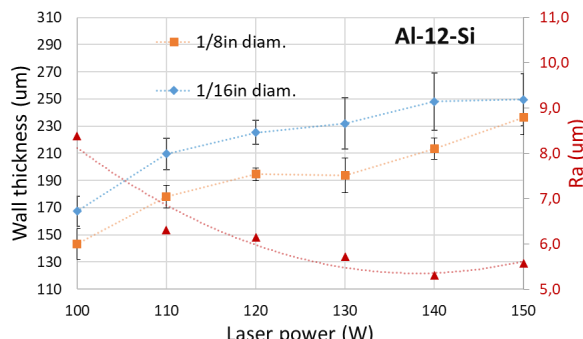


Figure 2: Measured wall thicknesses and surfaces roughness for different printing laser powers on AISi12.

Leak-tight (He leak rate of 10^{-10} mbar*l/min) threshold is found between 170 um and 180 um wall thickness. Fine tuning of the wall thickness proved the L-PBF process parameters limit of

leak-tightness for as-built Al-12-Si to be at 107 W. In fact, all samples produced at and above 107 W were tight, all samples produced at and below 104 W were not tight while samples produced at 105-106 W were occasionally tight.

This is confirmed by the wall thickness measurements in Figure 3, which show this transition zone where the wall thickness increases significantly.

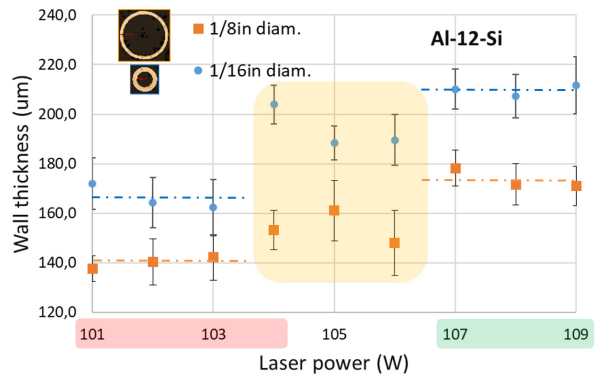


Figure 3: Fine tuning of wall thicknesses for different printing laser powers of AISi12.

An important observation to consider is that some untight walls are thicker than others which are tight. This is explained by the stabilization of the melt pool which moves from a situation of lack of fusion through a situation of regular fusion.

Another topic investigated is the minimum inner diameter to length ratio on AISi12 pipes, which provides a value of the minimal channel dimension feasible to fabricate in which the powder can be removed. A preliminary result shows the limit of powder removal to be at 0.44 mm inner diameter to 85 mm length, without using air pressure (see Figure 4).



Figure 4: Samples used to test the powder removal.

Further analysis will include the powder removal with high pressures on both straight and 180°bend single pipe as well as multi-microchannels. In conclusion, the achieved tight wall thickness meets specifications of cold plate thermal performance to be cost effective, showing the potential of LPBF process. This project has received funding from the EU Horizon 2020 Research and Innovation programme (Grant Agreement No 101004761).

* CERN, Switzerland

MANUELA – Additive Manufacturing using Metal Pilot Line Design Center

E. Onillon, G. Lang, D. Novo, V. Pejchal

In the frame of the H2020 research project MANUELA^[1], an open-access Metal Additive Manufacturing Pilot Line facility was deployed covering the whole production sequence, to show full potential of metal AM for industrial production. The Pilot Line was validated with the design and manufacturing of six use cases, covering a wide range of application fields. of the work with examples of applications and/or business opportunities. In the frame of the pilot line, CSEM is acting as design center. With the support of its partners, CSEM rethought and implemented an AM optimized development cycle, from design to manufacturing, including validation, illustrated in the following on an automotive use case.

Started in October 2018 and concluded early 2024, the H2020 research project MANUELA^[1] deployed, with the collaboration of 20 EU partners, an open access pilot line addressing key limitations of metal additive manufacturing (AM) process, namely limited speed, limited capability of right first-time production, limited number of qualified materials, limited of further data analytics. The potential of the pilot line, now managed by RISE in Sweden, was demonstrated via various use cases, one of them being the automotive industry, incredibly competitive. This degree of competition pushes manufacturers to streamline manufacturing processes. As such, small series often share common components to save on the cost of molds. This results in parts being oversized for most. As such, Renault Trucks investigates AM as an alternative to casting. Indeed, even for low volumes, AM allows to customize parts on clients' demand and thus rationalizes vehicles' weight, CO₂ emissions and resource consumptions. MANUELA's business use-case PARCO aims to design a series of customized truck's spring anchorage. The design shall not only be conducted for one specific truck, but for an entire range of vehicles. The actual line of trucks has four payload capacities and five structural interfaces (same size and position but different thickness of the chassis). Therefore, a total of twenty load cases shall be considered. The time allocated to this project does not allow us to design these parts separately. Hence, we developed this methodology to tackle this restriction.

CSEM proposed an alternative methodology aiming to decouple the development time from the number of designs relying on a product library^[2]. We focus on libraries where parts perform the same function, but where the load-cases vary or where each part fosters different performances. Even if we focus on structural applications in this paper, these foundations and concepts can be applied to other domains of engineering.

The novelty of this methodology does not lie in the tools used but comes from a selective reduction of complexity. We use the raw results of topology optimization to build a representative reduced model using shell and beam elements. Then a batch optimization is set up to model the optimal design parameters within the product family. Finally, traditional CAD software is used to reconstruct the parametrized part which includes all required manufacturing features.

Knowledge-Based Engineering (KBE) is a research topic which focusses on the structure of algorithms/processes to capture design intent and automatizes ill-structured processes using heuristic. These design rules are built on prior experience in solving a particular problem.

The proposed approach, inspired by KBE approach is composed on five main concepts: identification, interpretation, batch optimization, modeling, and reconstruction (see Figure 1).

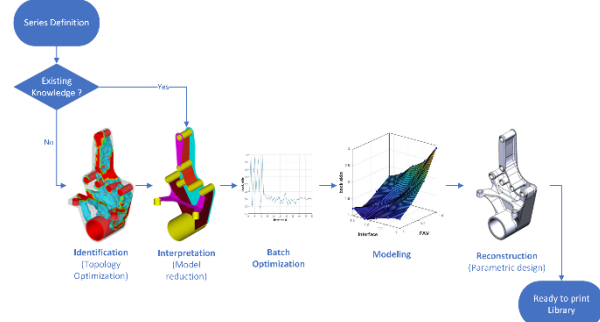


Figure 1: Proposed methodology.

Using the proposed methodology, the mass of the family of spring anchorage while keeping their stiffness and yield safety factor within admissible bounds was optimized. We were able to reduce the mass by approximately 40% for the whole family. As an example, the printed demonstrator shown in Figure 2, (optimized for a low front axial load and an intermediate interface thickness) weights 6.25 kg while its casted counterpart was above 10.5 kg.



Figure 2: Final CAD of PARCO (left) and printed part (right).

Furthermore, the design time was compared to a traditional AM design methodology used in MANUELA as baseline.

It is estimated that, for the development depicted above, a time saving by a factor up to 10 can be achieved for series production.

Table 1: Time saving for series production.

	Series size: 1	Series size: 5	Series size: 20
Traditional Design Process (estimation based on other use cases from MANUELA)			
Topology optimization	1.5d	7.5d	30d
Post treatment and validation	4 d	20d	80d
Total	5.5d	27.5d	110d
Proposed Design Process (based on PARCO experience)			
Identification (topology optimization)	1.5d	1.5d	1.5d
Interpretation	5d	5d	5d
Analysis	1d	2d	2d
Modeling	-	0.5d	0.5d
Reconstruction and validation	3.5d	5d	5.5d
Total	11d	14d	14.5d

[1] Grant agreement 820774

[2] <https://www.ri.se/en/am-center/our-offer/pilot-line-production-services-developed-by-the-manuela-project>

Chemical Treatment of Aluminum Current Collector in Li-Ion Batteries to Enhance Pitting Corrosion Resistance

J. Gay, L. Pires Da Veiga

Corrosion of the aluminum current collector on the cathode side of Li-ion batteries is a major concern. This phenomenon is even more present when using electrolytes containing imide-based salts (e.g., LiTFSI) above 4.1 V. In such cases, the native oxide layer of aluminum is firstly degraded, and anodic dissolution (i.e. pitting corrosion) occurs on aluminum underneath. We present herein various chemical treatments to prevent pitting corrosion on aluminum. Different self-assembled monolayer chemistries are investigated and show to mitigate corrosion but not totally suppress it. Thicker coatings (namely "Hybrid coating 1" and "Hybrid coating 2") fully stop corrosion.

Stable electrolytes are key to the development of "5 V" Li-ion batteries (LIB). While LiPF₆ remains the most used supporting salt, it presents several shortcomings such as low thermal stability and high reactivity towards moisture. Moreover, carbonate solvent combined with LiPF₆ can decompose above 4.2 V, limiting its application in high-voltage LIB.

Imide-based electrolytes (e.g., LiTFSI and LiFSI) present several advantages such as a lower toxicity, high ionic conductivity and high electrochemical stability. However, one drawback of using imide-based salts is the anodic dissolution process of the Al current collector (CC) occurring at high voltages, which is detrimental for battery performances. To prevent corrosion of the Al CC, various strategies have been investigated such as: electrolyte engineering (adapting salt concentration, change of solvent), the addition of inhibitors or the surface treatment of Al CC. Coatings on the Al CC need to: 1. prevent corrosion, 2. be electronically conductive and 3. form stable interfaces with other materials present in the battery.^[1]

CSEM developed a reproducible corrosion testing method (Figure 1), to investigate anti-corrosion properties of battery CCs coated with various materials. The corrosion test consists of performing 6 cyclic voltammetry cycles between 2.5 and 5 V in 1M LiFSI in EC:DMC 1:1 (vol.).

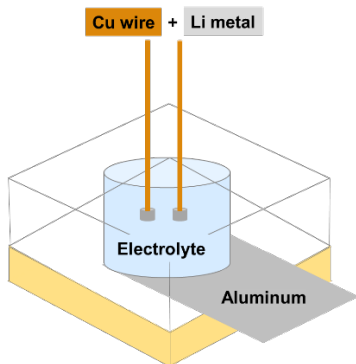


Figure 1: Scheme of the electrochemical set up used with Li-metal as counter and reference electrode.

After performing the CV test, Al samples are analyzed by optical microscopy (Figure 2), and the total corroded area is measured, as reported in Figure 3.

Self-assembled monolayers (SAM), which are only a few nanometers thick, show promising anti-corrosion properties in various applications such as the metallization of solar cells^[2]. In

this project, two SAM with different chemistries (SAM 1 & SAM 2) were used and deposited on Al via immersion. In parallel, two other coatings (Hybrid coating 1 & Hybrid coating 2) were also investigated with a thickness of more than 200nm.

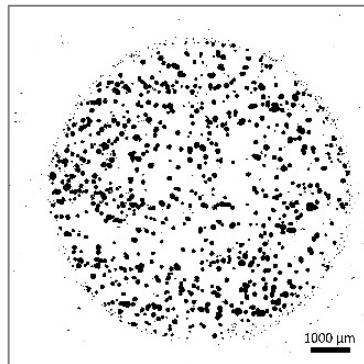


Figure 2: Optical microscopy image of a bare aluminum sample with pitting corrosion.

As shown in Figure 3, the median corroded area of bare Al is around 6%, while the median of the two SAM-coated samples is 2.5%. It shows that the SAM treatments mitigate corrosion but do not fully suppress it. Regarding "Hybrid coating 1" and "Hybrid coating 2", the median is close to 0%, demonstrating an efficient protection against corrosion.

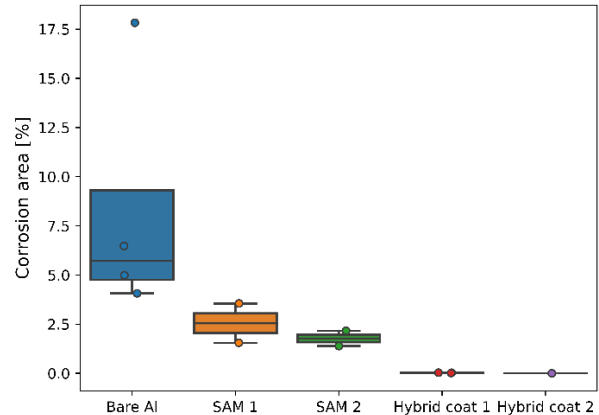


Figure 3: Corrosion area [%] for various coatings on aluminum.

Future works aim to investigate electron conductivity of the coatings using electrochemistry and fabricate batteries with Al-coated foils to improve long-term stability.

[1] Gabryelczyk, Agnieszka, et al., "Corrosion of aluminium current collector in lithium-ion batteries: A review." Journal of Energy Storage 43 (2021): 103226.

[2] Gay, Julien, et al., "Selective Copper Electroplating on Patterned Self-Assembled Monolayers for Photovoltaic Applications." ACS Applied Nano Materials 5.10 (2022): 15954-15961.

Carbon Nanotubes Field-effect Transistors for Biosensing Application

P. Clément, R. Pugin

Modern life has significantly impacted the availability and accessibility of food and exposition to light leading to changes in sleep patterns and sleep disorders. According to the Department of Health & Human Services, over a third of U.S adults report daytime sleepiness altering their efficiency at work, decision making and social functioning. Conventional approaches to quantify sleep hormones require collecting samples and sending them to a laboratory for analysis, which often takes several days before obtaining results. The field of diagnostics is trending away from traditional analysis equipment in hospitals and laboratories and increasingly towards clinics and medical offices for better accessibility and faster results. The objective of this exploratory study is to create an innovative biosensing method for rapid and non-invasive detection of cortisol, near to the patient. The Smart Biochip incorporates an array of nanosensors, utilizing single-stranded DNA as aptamer for hormone's molecular recognition, ensuring high affinity and specificity.

Cortisol is produced by the adrenal cortex and can serve as a measure of a healthy circadian rhythm. Current detection methods require the collection of saliva, urine or blood samples that have to be sent to the laboratory and the results are obtained a few days after. The field of diagnostics is trending away from hospitals and laboratories and increasingly towards clinics and medical offices for better accessibility and faster results. However, to allow this transition, the technology needs to mature towards user-friendly, portable and real-time detection systems with similar performances. In this regard, we have foreseen the development of a novel miniaturized Smart Biochip combining micro and nanotechnology, that requires a simple electrical read-out. DNA aptamers are a class of short single-stranded nucleic acids (20-100 bases) which can be used as an alternative to antibodies for biorecognition.

Field-effect-transistor (FET) based aptasensors enable label-free biosensing, extreme miniaturization and simple electrical read-out. They consist of a sensing channel (with an immobilized aptamer on it) between source and drain electrodes whose conductivity is regulated by a third gate electrode. One-dimensional (1D) nanomaterials such as semiconducting single-walled carbon nanotubes (SWCNTs) are particularly well suited for this configuration due to their hollow tubes shape with a diameter of around 1nm. They are very sensitive to small changes in their electrostatic surface potential, even by a single biomolecule since their sidewall are atomically thick (no bulk C-atoms). Their basic working principle involves structural rearrangements of the negatively charged aptamer phosphodiester backbone upon target capture. Aptamer conformational change drives surface charge rearrangement of the semiconducting channel, which enables the detection of even neutral small molecules.

Therefore, we have foreseen the development of a novel miniaturized SWCNTs aptasensors based Smart Biochip combining micro/nanotechnology, that requires a simple electrical read-out. We have designed an in-house electrical sensing platform allowing a plug-and-play configuration as described in Figure 1. SWCNTs were first immobilized onto the Si biochip between a pair of metal electrodes with nanoscale accuracy by dielectrophoresis (DEP) as shown in Figure 2. SWCNTs side walls are further covalently functionalized with the cortisol aptamer and sensing performances are evaluated in PBS (Figure 3). It resulted in the decrease of the current with the increase of cortisol concentration.

This proof-of-concept has the potential to be employed in detecting various small molecules and is adaptable for multiplexing. The ultimate goal is the development of a portable multisensing platform which could be used for establishing a fast diagnostic.

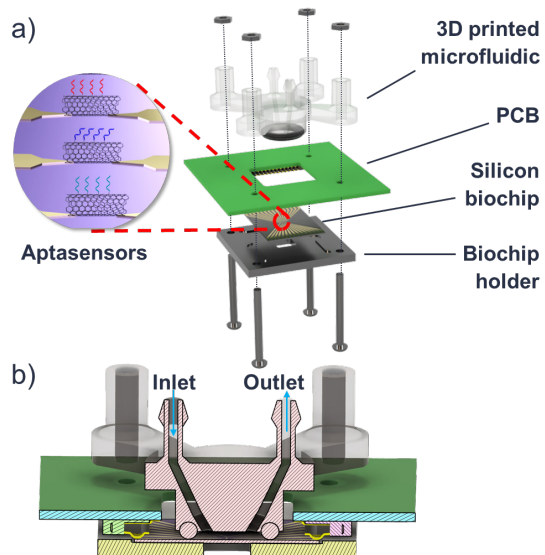


Figure 1: a) Magnified view of the different elements composing the electrical sensing platform and b) cross-section of the assembled elements.

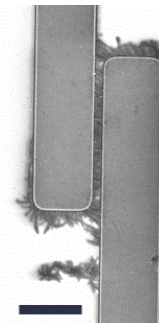


Figure 2: Selective immobilization of SWCNTs by DEP. Scale bar is 10 μm .

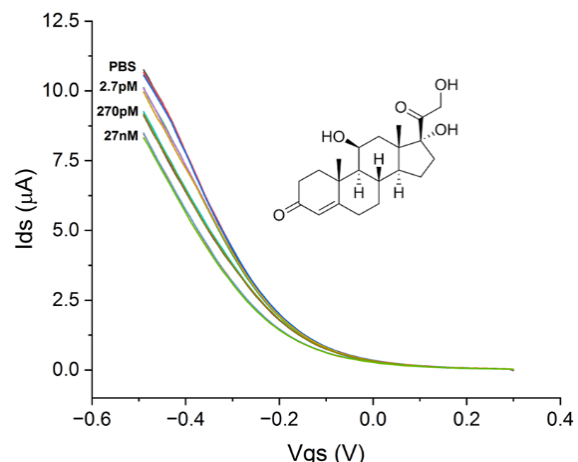


Figure 3: Cortisol detection in PBS buffer with SWCNTs based aptasensor.

Sol-gel Chemistry for Resistant Bactericidal Coatings

X. Bulliard, M. Crenna, A. Finelli, X. Lefèvre, J. Gay, R. Pugin, J. F Laithier*, C. Storrer*, T. Zwingelstein **, V. Humblot **, A. Figarol **, A. Marguier **, F. Chérioux **

Sol-gel chemistry was utilized to produce coatings with antibacterial properties. These coatings can be applied to a wide range of substrates. In this study, we focused on anodized aluminum components, potentially surgical tools. Various methods were explored to incorporate the antibacterial agent into the sol-gel coatings. The most promising method involved adding silver nitrate, which can induce an bactericidal effect through contact killing without being cytotoxic. The critical factors are the mechanisms and kinetics of silver release, which can be regulated through the curing of the sol-gel matrix, serving as a reservoir.

Sol-gel chemistry based on reaction of silane precursors represents a unique route for generating coatings with multifunctionalities. Metal alkoxide precursors reacts in solutions through hydrolysis and condensation to form a reticulated siloxane network, which is controlled by the amount of added water and catalyst. This leads to the formation of a "sol" state that will evolve to a "gel" as reaction proceeds, according to the scheme of Figure 1. Usually, before gelation, the sol can be deposited on the substrate as a coating that will solidify by curing during drying or heating to form a ceramic-like materials as the surface. Sol-gel chemistry also offers the possibility to incorporate new elements to the sol-gel formulation, such as particles or other specific molecules, to generate coatings with a wide range of different properties, in terms of optics, protection, or coloration. In this study, the sol-gel strategy was used to produce bactericidal coatings on anodized aluminum oxide components, for watch or Medtech components, such as surgical tools for instance.

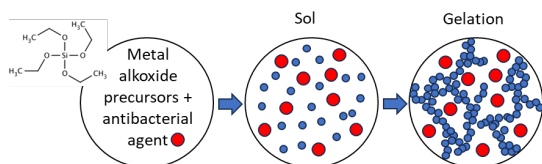


Figure 1: Sol-gel route scheme, in which anti-bacterial agents, such as particles or other silane precursors can be added, before deposition on a substrate.

In preliminary attempts to generate antibacterial properties, quaternary ammonium silanes (QAS) were used as they are known to have antibacterial effect by contact killing, causing conformational changes within the bacterial cell membrane. QAS were deposited at the surface of the sol-gel layer by dip-coating method, but the amount present at the surface were below the limit of bactericidal effect. Furthermore, the surface treatment can be damaged or removed during the successive sterilization process of MedTech components. The surface treatment approach was abandoned, and as alternative, the bulk approach was implemented. Four different routes were tested:

- Addition of QAS to the bulk sol-gel solution
- Addition of silver nitrate and reduction by dipping into solution of reducing agent to form Ag° colloids
- Addition of silver metal particles to the sol-gel solution
- Addition of silver salt, in the form of silver nitrate (AgNO_3)

For the first approach, the amount of the QAS that could be dissolved into the sol-gel solution without creating a phase separation was too low to induce a bactericidal effect. The corresponding level at the surface of the coating after curing was below the killing limit for Escherichia coli (*E. coli*) bacteria. The other three approaches all show bactericidal effects to some

extent and limit. For the direct addition of silver particles, bactericidal effect was observed only when large particles in the micron range were added to the coatings. Figure 2a shows the killing by contact of *E. coli* when the treated samples were exposed to bacteria inoculum. For the reduction of silver nitrate to form Ag° colloids, bactericidal effect was observed as well (Figure 2b) but the limit was the coloration of the coatings that turned dark grey due to the formation of Ag° colloids in high concentration uniformly dispersed in the bulk sol-gel. The addition of silver nitrate only was the most interesting approach, as its addition did not modify the original properties of the coatings, in terms of color and protection capacity. The principle is based on the slow and continuous release of silver ions at the surface. The sol-gel coating acts such as a reservoir. An extensive study was done to define the correct concentration windows to have an bactericidal effect, without affecting the viability of fibroblast cells. The results will soon be published in a peer-reviewed journal.

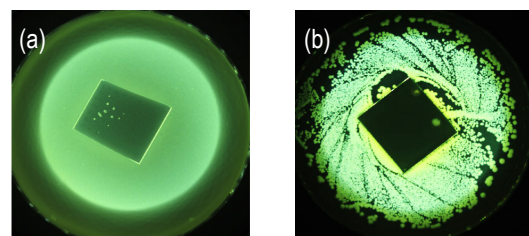


Figure 2: Contact killing of *E. coli* bacteria (a) through the addition of silver particles or (b) through the formation of in-situ Ag colloids in the sol-gel coatings.

In addition to bactericidal properties, the coating was designed to be resistant to corrosion in acidic and alkaline conditions, either at low pH (<2) or at high pH (>11). This added protection is essential to guarantee the integrity of components, at low pH for watch components and at high pH for medical tools, that should resist sterilization process at pH around 12. The sol-gel coating can cover this whole range of composition.

In summary, sol-gel chemistry represents a validated pathway for producing coatings with multifunctional properties. In this study, we employed this technique to create protective and bactericidal coatings through contact killing towards *E. coli* bacteria on anodized aluminum oxide components. The most effective approach involved the incorporation of silver nitrate into the sol-gel coating.

METEOR project is supported by the Interreg France-Suisse 2014-2020 program and has benefited from the European Regional Development Fund (FEDER), and on the Swiss side from federal and cantonal grants (Neuchâtel, Vaud). All authors thank them for their support.

* Coloral SA, Cressier, Switzerland

** FEMTO-ST, Besançon, France

Chemical Sensors for Water Quality Monitoring

A. Finelli, P. Clément, X. Lefèvre

Within the scope of the Agrarsense KDT-JU European project, we are actively engaged in the creation of sensing layers designed to track the presence of contaminants in both soil and treated water. The specific molecules we are focusing on are classified as compounds of emerging concerns (CECs), which include substances like pesticides and pharmaceutical residues. While these pollutants are typically found in very low quantities, it is crucial to monitor them in order to enhance the management of water resources and the judicious use of nutrients and pesticides in agricultural settings. To meet the required detection limits and address different classes of compounds, we have identified and chosen three distinct sensing layer technologies for the development of electrochemical sensors.

Water contamination monitoring is a pressing global concern, affecting individuals ranging from farmers to everyday consumers relying on tap water. Even treated water, despite its processing, can retain traces of human-induced substances, such as pesticides and pharmaceuticals. A well-known illustration of this issue is the presence of hormone residues from contraceptive medications in treated wastewater, posing significant public health and environmental challenges. Furthermore, improving water quality monitoring has the potential to enhance resource management, leading to reduced reliance on nutrients and pesticides in agriculture when the irrigation water already contains substantial levels of these substances. However, the current methods for monitoring compounds of emerging concern (CEC) in water, primarily relying on high-performance liquid chromatography coupled with mass spectrometry, demand substantial equipment and the expertise of skilled personnel. Therefore, there is a compelling need to advance novel sensing technologies for on-site water contamination monitoring.

To achieve this goal, we have engineered three distinct types of sensing layers designed for utilization in electrochemical sensors, enabling swift quantification of desired molecules using compact, deployable equipment suitable for on-site applications. The first type incorporates metal-organic frameworks (MOFs), combining organic and inorganic compounds. MOFs are characterized by their exceptional porosity and can be readily customized to target specific chemical functions of organic molecules, such as phosphate or nitro groups. Consequently, they present a compelling option for detecting compound families like organophosphorous pesticides or pyrethrins. Through the application of specialized deposition methods, we have managed to achieve detection capabilities within the range of parts per billion (ppb) using this technology (Figure 1).

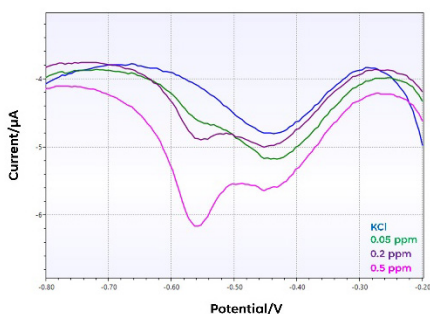


Figure 1: MOF-based electrochemical detection of organophosphorous pesticides.

The second sensing layer under investigation is rooted in the use of aptamers. Aptamers are single-stranded DNA sequences meticulously engineered to exhibit remarkable sensitivity and selectivity toward a specific target molecule. Additionally, they can be recycled following a straightforward cleaning procedure.

We have devised a method for immobilizing aptamers onto electrodes, enabling the detection of carbamazepine, an anti-epileptic drug, in the picomolar range (Figure 2).

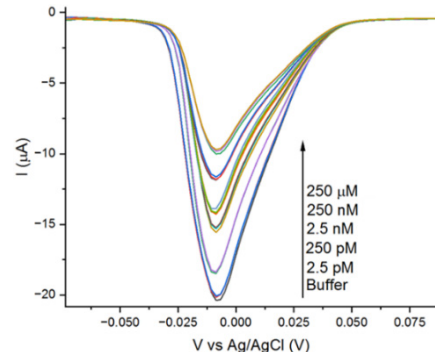


Figure 2: Carbamazepin electrochemical detection with aptamers.

In addition, we have created sensing layers based on molecularly imprinted polymers (MIPs). Our approach involves employing electrodeposition to form these polymers on electrode surfaces, and we have devised an electrochemical technique for sensor recovery after it has been exposed to the target molecule. MIPs are also porous materials known for their sensitivity and selectivity to the molecule used as a template during imprinting. In our project, we chose atrazine, an herbicide, as the target molecule due to its known presence in demonstration sites. We were able to detect atrazine at concentrations in the parts per billion (ppb) range (Figure 3).

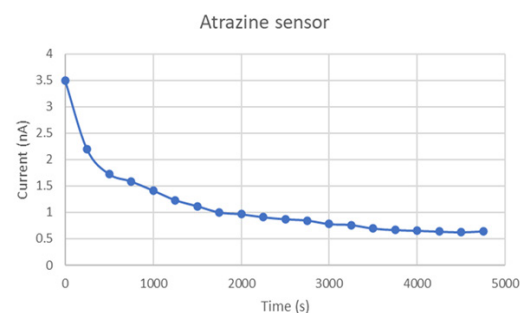


Figure 3: Rebinding of atrazine on a MIP-based electrochemical sensor. Detection is performed in 3.45 ppb solution.

These three methods offer highly effective and adaptable sensing layers capable of detecting minute quantities of CECs. We are presently in the process of fine-tuning these techniques and constructing calibration curves for each sensor. Our subsequent undertaking will involve the examination of actual samples obtained from the demonstration sites of the project to confirm the durability and reliability of these sensing layers.

This project is funded by Horizon-KDT-JU European project Agrarsense.

Integration of Sensors for Monitoring of Multiple Parameters for Newborns

S. Khan, A. Grivel, N. Bonzon, S. Dasen, X. Bulliard, R. Pugin

The European project Newlife aims at a better monitoring of vital parameters of premature newborns and pregnant women by integrating sensors into clothes. Within this frame, CSEM develops new sensing elements and components for a better integration into fabrics and textiles. This includes electrodes, conduction lines and novel sensing layers that can be prepared by using CSEM printing and deposition platform. These technologies will help for the integration of the different sensors of the partners for a common and parallel reading in a second stage. These sensors and components will help to record a wide range of parameters for better pregnancy care and newborn health diagnostics.

For a better monitoring of pregnant women and newborn babies, premature or not, it is crucial to record a wide range of vital parameters such as blood pressure, heart rate, temperature, pH, and oxygenation level of the mother and the baby. Currently, in most cases, independent sensors are developed for each of these vital signs, that not only increases discomfort of the patients, but can also lead to non-optimized data acquisition and analysis. Newlife aims at developing clothes such as caps, armbands or bodysuits, that can integrate these sensors into fabrics. Collective monitoring and data acquisition of these parameters would help the clinician for a better and faster diagnostic, as well as provide feedback and guidance to the patient. They also provide continuous medical monitoring while ensuring maximum data security. CSEM's teams are now working on ways to make these sensors smaller, lighter, washable, and even more secure.

In this first part of the project, CSEM is developing new sensing elements, such as electrodes and interconnection lines. These elements are important for improving the performance of the sensors themselves, for connecting the different systems, or for adapting the electrodes for the integration into fabrics and textiles. For that purpose, we used our deposition and printing platform, and more specifically Aerosol Jet Printing (AJP). AJP is based on the formation of aerosol that can be accurately printed on substrates. A key point is the versatility of the AJP technique in terms of shape and materials for both the substrates and the printed materials itself. Currently the focus is placed on the choice of electrodes materials, that include silver, carbon, and copper. These materials are printed on different substrates, such as plastics and fabrics directly. Illustrating examples are found in Figure 1, which shows a silver electrode on a plastic PET film (left) and a carbon coated electrodes on silver integrated into a fabrics.

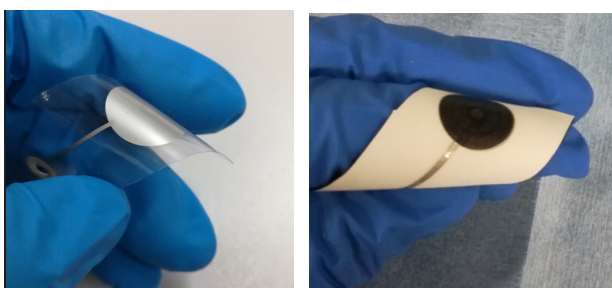


Figure 1: Printing by AerosolJet of silver electrodes on plastic and carbon-coated electrodes on special fabrics.

These electrodes and sensing probes can then be linked with interconnection lines that are printed by AJP as well. Figure 2 shows an additional picture of silver conduction line printed on PET plastic. Other materials such as copper can as well be processed. The technique is also adapted to direct printing of additional elements on PCB for instance.

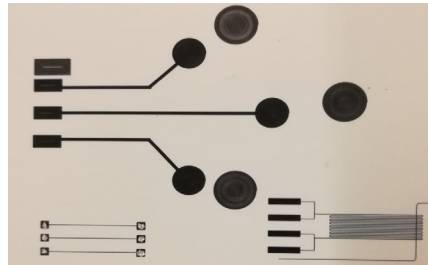


Figure 2: Printing on PET film of conduction lines that can be used for the connection of sensing elements to the respective reader system.

In addition to sensing elements, CSEM has a long experience in the development of oxygen optical sensors, using its unique technology based on mesoporous layers. This is used to develop new sensors and sensing layer patches. Figure 3 shows a patch layer that was printed by slot-die coating. The cut patch can then be put into contact with the skin for monitoring oxygenation of blood through skin (transcutaneous monitoring). An optical read-out system will be added to build a complete detection system.



Figure 3: Printing oxygen sensing layer that can be cut into patches for oxygen sensing.

In summary, the Newlife project aims at improving pregnancy care and newborn health by providing innovative sensing solutions that are user-friendly, cost-effective, and can be integrated into clothes. Multi-sensing is a key to have a complete and synchronized monitoring of multiple vital signs. In a wider perspective, the project will contribute to reducing maternal and infant mortality and morbidity rates, as well as enhancing the quality of life of mothers and babies.

This project has received funding from the KDT Joint Undertaking (JU) under Grant Agreement No. 101095792. This work has received funding from the Swiss State Secretariat for Education, Research and Innovation (SERI).

Molecular Imprinted Polymers-based Sensors for Nicotine Monitoring in Aerosol

A. Finelli, X. Lefèvre

Nicotine is the main active component of tobacco. Its quantification in aerosols and particularly the amount delivered in lungs is of great interest to track its impact on health. Current detection methods rely on the use of mass spectroscopy coupled with liquid chromatography. However, this requires highly qualified personnel and expensive equipment. In this context, we demonstrated that Molecular Imprinted Polymers (MIP) as sensing layer deposited on electrodes are very efficient to allow fast and cheaper quantification of nicotine in aerosols. Our current research focuses on the improvement of these sensing layers in terms of sensitivity, selectivity and ease of use.

Inhalation toxicological investigations and the development and pre-clinical testing of inhalable drugs require, in many instances, assessing the deposition kinetics of aerosol constituents on the epithelia of the respiratory tract or on in vitro models thereof. A commonly applied in vitro approach is the deposition of the test aerosol on a trapping surface under controlled conditions, followed by quantification of deposited individual targeted aerosol constituents. Particularly when working with complex aerosols such as smoke, this requires highly sensitive and selective analytical methodologies such as coupled chromatography - mass spectrometry. Such methodologies commonly require highly qualified personnel and expensive equipment and are not accessible in many instances. In this context, a promising technology for the quantification of aerosol deposition are chemically selective sensors and among them, molecularly imprinted polymers (MIP) showed very interesting abilities to selectively concentrate the target molecule for a better read-out. They could also be integrated in transducers to build a complete sensor that could be adapted to any detection measurement (from molecular spectroscopy like IR or NMR to optical detection or electrochemistry).

For this purpose, we developed formulations and methods to reproducibly deposit MIP layers on electrodes by electrochemistry. Compared to standard MIP bulk-synthesis, this approach required the use of new electropolymerizable monomers such as aniline, pyrrole or thiophene. Several parameters control the formation of the electro-grafted layer (Figure 1). For instance, the number of grafting cycles impacts the growth of the layer whereas the potential window used controls potential cross-linking of the layer.

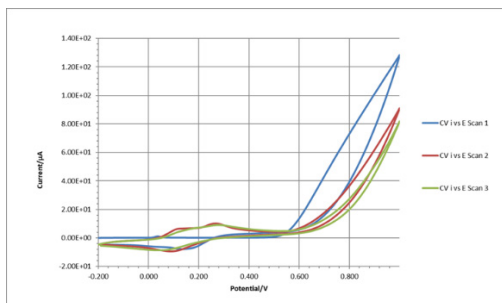


Figure 1: MIP electrodeposition by cyclic voltammetry. The decrease of current underlines the growth of the layer and the control on it with electrochemical parameters.

Formulations were then refined to increase the sensitivity and the selectivity by incorporating co-monomers such as acrylic acid or methyl acrylate. Those functional monomers promote more specific interactions with the target molecule nicotine which, in theory, enhances the selectivity. We were thus able to reach a very high sensitivity (in nanomolar/ppb range) while keeping short analysis times (typically 5 minutes) and high selectivity (Figure 2).

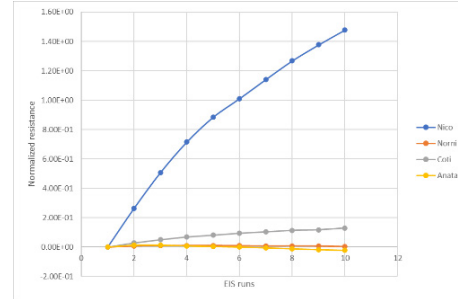


Figure 2: Nicotine MIP-based sensor showing selectivity towards nicotine analogues.

To further increase the sensitivity, we investigated the elaboration of hybrid layers comprising MIP and embedded gold nanoparticles. We synthesized MIP and gold nanoparticles which showed interesting performances. We also developed strategies to co-deposit MIP and gold nanoparticles by electrochemistry providing easy access to such hybrid sensing layers (Figure 3).

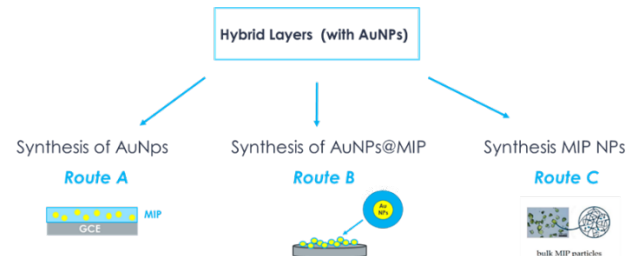


Figure 3: Schematics of hybrid layers fabrication.

Sensitivity of the MIP layers was significantly improved when adding gold nanoparticles. However, more work is needed to better control their incorporation as their growth induces perturbation of the MIP layer formation (Figure 4).

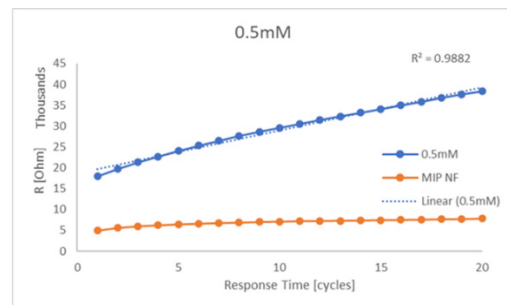


Figure 4: Effect of gold nanoparticles incorporation on the sensitivity.

Future work will target the refinement of hybrid layers as well as the integration of electrochemical probes to facilitate the measurements. The limit of the sensors will also be tested by scanning their ability to detect nicotine at the air-liquid interface.

Large Area UV Imprinting of Optical Microstructures

T. Offermans, E. Glushkov, C. Eggenspiller, G. Basset

Free-form micro-optical arrays (FMOAs) gain increasing interest because they can overcome some limitations of rotationally symmetric optical components, and thereby enable better performance and compactness of optical devices. Various technologies to fabricate free-form microstructures are available, such as diamond and laser micro-machining, two-photon absorption, maskless grey-scale lithography, and fs-laser-ablation. Since such maskless origination methods can be time consuming and therefore expensive, the area of the originated structure is often kept small, typically between 1-9 cm². Here we present two complementary methods to enlarge the small area of the originated structure to larger areas with high accuracy, fidelity and reproducibility.

UV imprint replication is a widely used technology for the low-cost and high throughput replication of complex 3D micro- and nanostructures with ultra-high precision. The recent development of large-area UV imprint processes has enabled the mass manufacturing of large-area micro/nano-structures thereby enabling new commercial applications.

Step & repeat UV imprinting – In analogy with optical lithography steppers, the so-called UV imprint step-and-repeat (S&R) technology enables the up-scaling of small masters to large-area tools for subsequent large-area replication thus keeping the origination effort limited to small areas and affordable cost. Large-area applications often demand for seamless working masters/tools where the adjacent FMOAs are precisely positioned in contact to one another, i.e., with negligible gaps or alternatively with well-controlled slight overlapping.

Since there is currently no commercial Step & Repeat machine on the market able to replicate free-form micro-structures on large area with the required precision, CSEM has developed a high precision S&R UV-replication platform designed specifically to this purpose, with a targeted position accuracy of 1-2 µm in X/Y/Z. The platform (Figure 1) can handle substrates with dimensions up to 35×60 cm. The maximum square area which is uniformly UV-illuminated is 80×80 mm.

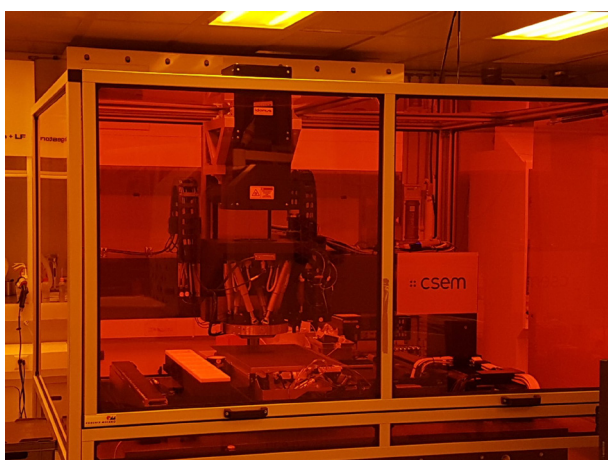


Figure 1: CSEM's Step & Repeat UV-imprinting platform, developed for high precision upscaling of micro-structures.

Once the master structure is upscaled to larger area using Step & Repeat, various process paths are possible, including a galvanic electroplating process which is used to transfer microstructured surface of the up-scaled master onto a robust (but flexible) replication tool for subsequent high-throughput and cost-effective UV imprint replication. In other cases, full wafer (8" or 12") UV imprinting tools can be made.

Roll-to-plate UV imprint replication technology (Figure 2) focuses on three fundamental aspects namely the technology scalability, cost effectiveness (large area & high volume) and compatibility with available production lines using large glass panels. Various processes for nanostructures and microstructures up to 500 µm height are proven, with shrinkage around 5% and industry-compatible manufacturing yields.

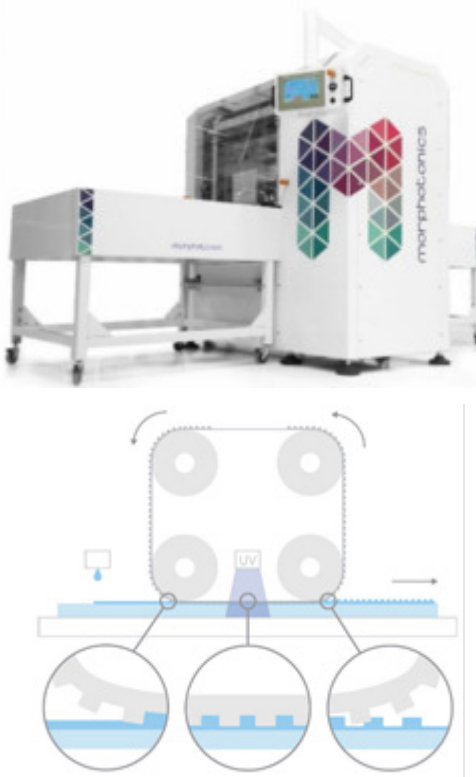


Figure 2: (top) CSEM's Portis NIL600 tool, (bottom) Schematic diagram of the roll-to-plate ultraviolet nanoimprint lithography (R2P NIL) process. Surfaces up to 600x1000 mm² can be processed in a few minutes.

Both Step & Repeat and Roll-to-Plate UV imprinting have been successfully demonstrated within the PHABULOUS Pilot Line for high precision upscaling of rigid small masters to flexible tools for the cost-effective production of large-area FFMOs.

This work has been carried out within the PHABULOUS project (<https://phabulous.eu>) and was published at the SPIE (<https://doi.org/10.1117/12.2675845>). The project has received funding from the European Union's Horizon 2020 research and innovation programme under grant agreement n° 871710 in a public-private partnership with Photonics21.

Mastering of Multi-sag Microlens Arrays at Wafer Scale

M. K. Lahmar, F. Zanella, J. Schildknecht, L. Ceric, G. Basset

CSEM offers to its customers an engineering and foundry service of microlens arrays (MLA), ranging from design, origination and prototyping up to small-series production on bare dies of few mm^2 , arrays of dies or wafers. The sag, the distance between the top microlens vertex to its base, provides the lens focal length when combined with the lens diameter and the material used. CSEM is improving its MLA wafer-scale origination process from mono-sag to multi-sag as reported here.

Microlens arrays (MLA) are extensively used in optical systems. They are present in cameras and other light sensors to enhance the light collection efficiency by focusing the light onto small photodetectors. They are also used in optical interconnects like fiber optics to improve light coupling and transmission. They can also be integrated in display technologies to improve image quality, brightness, viewing angles or producing 3D images. In addition, MLAs can be found in security documents such as banknotes, ID cards and passports.

At CSEM, MLAs are originated at wafer scale by a photolithography step to get photoresist pillars, followed by a thermal reflow process which melts those pillars into microlenses with spherical profiles. Then, the opposite MLA polarity (i.e., from convex to concave) is obtained by UV replication/imprint on a photomask, resulting in a so-called mold or stamp. Finally, the same UV-imprint process is used to replicate the MLA of the mold onto the final substrate. This process step is performed in a mask aligner to accurately align the MLA with the devices on the final substrate (e.g., photodiodes).

The question rises how to deal with multi-project wafers where multiple detectors or imagers, with different photodiode sizes and pitches are present on the same CMOS wafer. Indeed, the process described above can only yield a single common sag. With different photodiode pitches, i.e., microlens diameters, this translates to multiple radii of curvatures hence focal lengths. Therefore, with the current process limitation, either a trade-off must be made on the performance by identifying a suitable common sag, or different molds must be fabricated, one per sag^[1]. In the latter case, only the detector(s) corresponding to the selected mono-sag mold will be equipped with MLAs, meaning sacrificing the others of this substrate, which is detrimental in terms of costs. The best way to address this issue is to maintain a constant focal length among the different photodetectors present on the wafer with different pixel pitches and therefore, originate MLAs with multiple sags, as depicted in Figure 1.

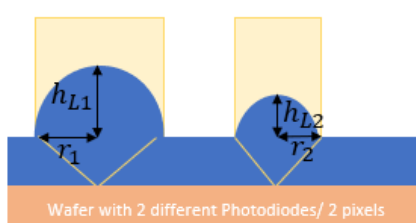


Figure 1: Two microlenses sharing the same focal length despite having different diameters thanks to their distinct sags.

[1] C. Bruschini, et al., "Challenges and prospects for multi-chip microlens imprints on front-side illuminated SPAD imagers", Opt. Express 31 (2023) 21935

The origination of dual-sag microlens arrays (DS-MLAs) is here demonstrated with two approaches yielding photoresist pillars with two different heights, both followed by a thermal reflow process. Both approaches can be extended to originate multi-sag MLAs. The first approach relies on a multi-layer photolithography technique with a negative photoresist^[2] and the second one on a multi-step/dose photolithography with a positive photoresist. The results are shown in Figures 2 and 3, respectively.

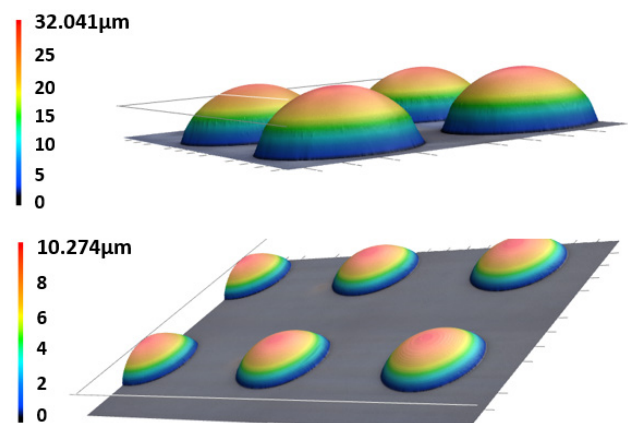


Figure 2: 3D images obtained by confocal laser microscopy showing two MLAs with different sags made on the same substrate from a negative photoresist. Top MLA: Sag = 32 μm & $\varnothing = 85 \mu\text{m}$. Bottom MLA: Sag = 10 μm & $\varnothing = 39 \mu\text{m}$.

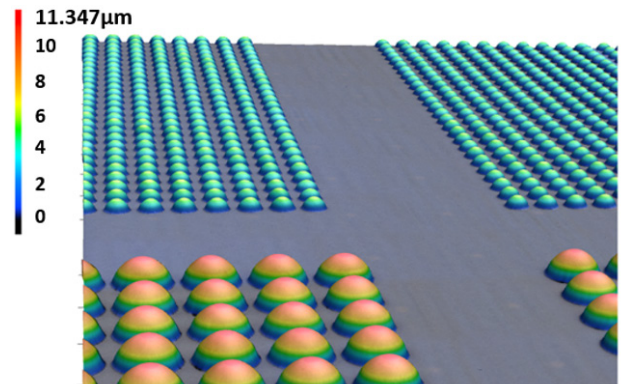


Figure 3: 3D image obtained by confocal laser microscopy showing DS-MLAs made of a positive photoresist. Front MLA: Sag = 11 μm & $\varnothing = 34 \mu\text{m}$. Back MLA: Sag = 6 μm & $\varnothing = 16 \mu\text{m}$.

[2] S.-I. Bae, et al., "Multifocal microlens arrays using multilayer photolithography", Opt. Express 28 (2020) 9082.

Phase-shifting Metasurfaces for Flexible and Foldable Displays

L. Ceric, B. Gallinet, G. Basset, D. Kazazis*, I. Giannopoulos*, D. Pires**, F. Federspiel**, R. Frantz**

Rising demand for thin, flexible and foldable displays has launched the quest for their enabling technologies. To enhance image contrast by reducing back reflection, polarizers and waveplates are currently employed. The metasurface technology is promising to achieve identical functionalities within much thinner layers, usually of less than one micrometer. Such metasurfaces are fabricated using nanoimprint lithography (NIL) to be scalable. Simulation results indicate they meet display industry standards. After creating a high-quality master and optimizing nanoimprints, the next step is integrating metasurfaces into a demonstrator device, potentially benefiting consumer electronics like foldable smartphones.

Increasing demand for foldable and rollable displays stimulated the search for new technologies that can significantly lower their present thickness. The reduction of back reflection from ambient light is crucial to maximize contrast, and it is currently handled with a polarizer and a waveplate. Metasurface based layers possess large potential to replace existing bulky waveplates as they can have the same functionality by achieving desired electromagnetic (EM) field phase retardation within a micrometer^[1,2] (Figure 1). The generation of the metasurface building blocks is performed with NIL using a stamp, itself created from a master that is fabricated by e-beam lithography (EBL) and reactive ion etching (RIE) in Si. After the NIL, the metasurface elements are transferred into the dielectric layer by RIE, both processes being scalable to the needs of the display industry. The simulations of phase retardation based on the design show very promising results (Figure 2) that meet the requirements of displays.

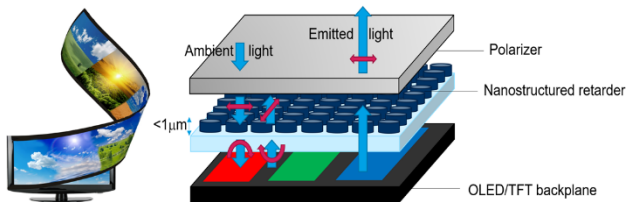


Figure 1: (left) Foldable screen illustration. (right) Phase retardation stack with metasurface layer. Unpolarized light passes through an x-linear polarizer, becomes anticlockwise circularly polarized after 1/4 waveplate. Reflection from LED backplane results in clockwise polarization, by 1/4 waveplate further transformed back to linear polarization but orthogonal to initial linear polarization, thus preventing any light emission.

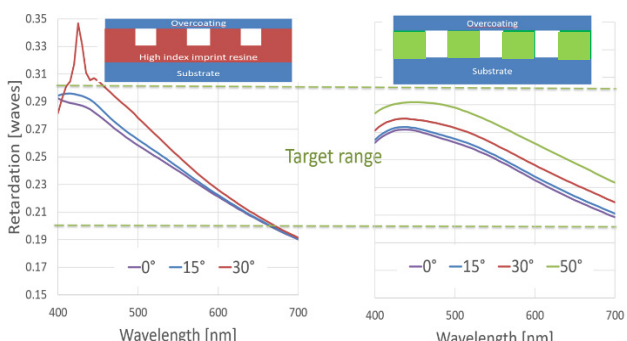


Figure 2: Simulation of EM phase retardation with wavelength/angle of incidence. (left) Case of UV NIL of high refractive index material. (right) Case of NIL + RIE transfer in dielectric (in green). Between the dashed green lines is the range of retardation that is targeted to obtain a high contrast. Low angle and wavelength dependences are targeted.

For the proof of concepts, the 1/4 waveplate grating was fabricated by EBL and RIE (Figures 3, 4, and 5). First preliminary characterizations of series of such gratings show promising

results of phase retardance ranging from 0.27 to 0.3 with a good angular stability. The transmission is very high, close to 85%.

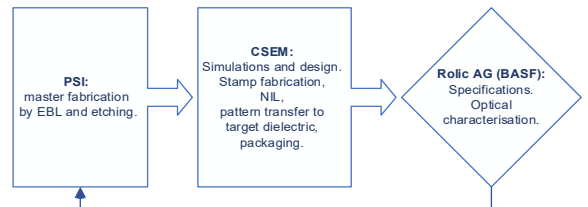


Figure 3: Technical fabrication collaboration scheme.

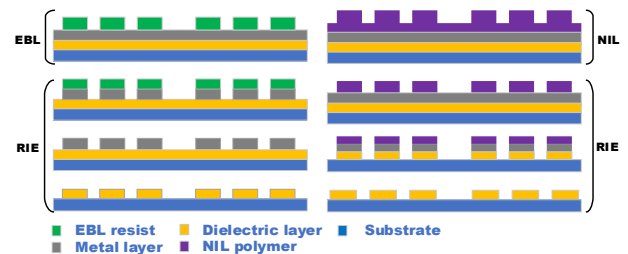


Figure 4: (left) Process flow of EBL (done ad hoc as a proof of concept) followed by RIE steps. (right) Thermal embossing NIL with RIE.

For the proof of scalability NIL approach is under development.

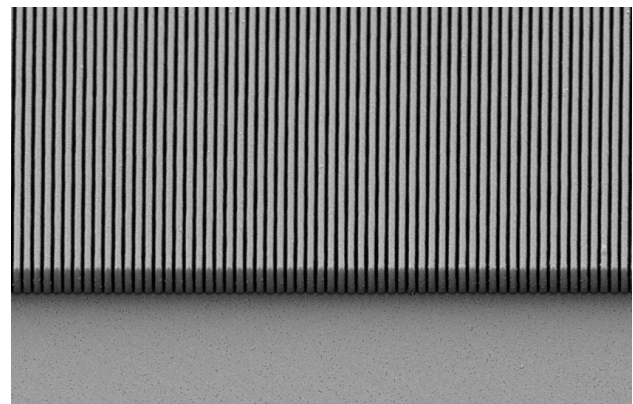


Figure 5: A scanning electron microscopy image of 1/4 waveplate made in dielectric nanostructures.

In the next phase, the metasurface will be integrated into a complete demonstrator device. The metasurface technology has the potential to be applied in other segments of the consumer electronics market, such as flat imaging in next-gen smartphones.

The project partners are Paul Scherrer Institut (PSI) and Rolic AG, a subsidiary of BASF. This work was partly funded by the Swiss Nanoscience Institute (SNI). CSEM thanks them for their support.

* Paul Scherrer Institut, Forschungstrasse 111, 5232 Villigen.
** ROLIC Technologies Ltd, Gewerbestrasse 18, 4123 Allschwil.

[1] A. Arbabi, et al., Nature Nanotechnology 10, 937- 943 (2015).

[2] F. Lütolf, et al., Optics Continuum 1, 1051- 1059 (2022).

Thin-film Lithium Niobate on Insulator Photonic Integrated Circuits (LNOI PICs) Platform

H. Sattari, I. Prieto, H. Zarebidaki, G. Cheng, J. Leo, Y. Petremand, M. Orvietani, F. Arefi, A. Della Torre, A. Ghadimi, D. Grassani, S. Lecomte, A. Voelker, M. Palmieri, O. Dubochet, M. Despont

Recent strides in electro-optics and nonlinear optics within Lithium Niobate on Insulator (LNOI) have yielded impressive results primarily within academic circles. However, translating these advancements to an industrial scale requires a reliable fabrication process. CSEM is pioneering an open PIC foundry using a process design kit (PDK), introducing a wafer-scale fabrication technique for various technology nodes. These breakthroughs promise transformative applications in telecom, LiDAR, sensing, and pivotal quantum endeavors. Our technology enables seamless integration of passive and active components, marking a significant leap in integrated photonics.

Photonic integrated circuits technology has been flourished tremendously in the last decade mainly driven by the telecommunication industry. This advancement has brought the opportunity to also investigate the potential of PICs in many other domains, such as LIDAR, environment monitoring, health diagnosis and quantum. Although the potential use cases of PICs are diverse, the manufacturing technology of PICs and the essential facility for this purpose are not accessible to every photonic designer. Therefore, various foundries are offering their manufacturing technologies to the PIC customers through a fabless scheme by implementing process design kits (PDK). The PDK is a library of well tested building blocks that comply with a set of design rules ensuring a reliable fabrication process. Among various PIC materials addressing the light generation, routing, manipulation and detection functionalities, lithium niobate in the form of thin film lithium niobate on insulator (LNOI) stands out, thanks to its unique combination of optical and piezoelectric properties. However, it is worth noting that its manufacturing technology has not yet reached a level of maturity to fully meet the demands of the PIC domain.

CSEM is set to establish the first open PIC foundry based on LNOI platform leveraging a well-tested PDK, introducing a wafer-scale fabrication technique for various technology nodes. We present our latest manufacturing advancements towards standardization of the LNOI PIC platform.

Figure 1 represents some of the key elements of our LNOI PIC platform manufacturing. Our fabrication technology is based on commercially available thin film LNOI 150 mm wafers which consist of a stack with 600 nm thick mono-crystal x-cut LiNbO₃ layer on top of a 4.7 μm buried thermal oxide (BOX) layer. The main technology layers include: three waveguide layers (device layer), two metal layer, a VIA, and a deep grid for the chip release.

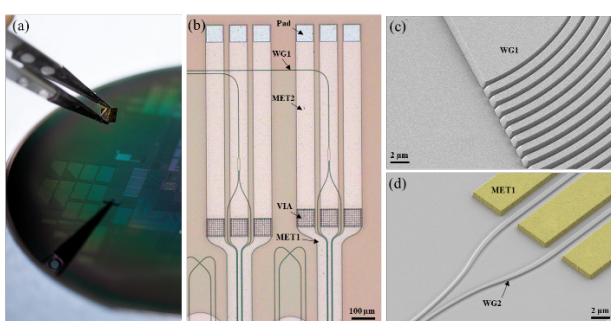


Figure 1: (a) 150 mm LNOI wafer with fabricated PICs, (b) Optical microscope image of the LNOI PIC, (c) SEM image of a grating coupler patterned in WG1 layer, and (d) SEM image of an electro optical modulator in WG2 and MET1 layers (MET1 layer false-colored).

Our LNOI PIC platform opens a broad range of opportunities for the PIC designers to devise novel solutions for many domains.

Internet of things (IOT), Frequency Modulated Continuous Wave LIDARs, integrated quantum computation, neuromorphic computing, various sensing schemes for health and environment monitoring, etc., can benefit from offerings of this platform. Particularly, fast electro-optical light manipulation, wavelength conversion, low loss waveguides, and compatibility with the heterogeneous and hybrid integration strategies, all in one PIC platform outstands the LNOI among other PIC platforms. As a cornerstone of this platform, we have demonstrated low loss waveguides with a propagation loss of < 0.2 dB/cm and Multimode Interferometer with insertion loss of < 0.15 dB. We continue improving the PDK by regular characterization of the building blocks and design optimization iterations.

To conclude, the unique combination of material properties and manufacturing developments in the LNOI PIC platform provides a technology which is elusive using other PIC material platforms. Our PDK development process from the design to testing steps pushes the technology to offer a wide range of reliable building blocks as schematically presented in Figure 2. Such a PDK empowers complex PICs with small footprint and low power consumption, promising for fast large-scale PIC solutions.

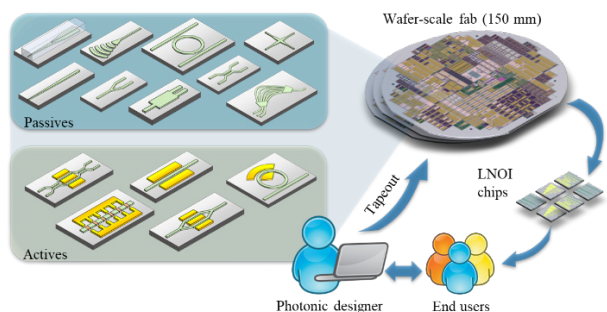


Figure 2. Envisioned LNOI PIC building blocks offered via a reliable PDK to the end users through a fabless scheme.

Our development aims to standardize the platform, ultimately granting the PIC domain convenient access to the foundry. The extensive portfolio of European and national projects, along with significant industrial interest from diverse application domains, confirms the platform's significance for the global PIC ecosystem. This development is supported by our flagship projects:

1. ELENA^[1] and PATTERN^[2]: these projects focus on the primary technology development concerning PDK and heterogeneous integration;
2. SPRINTER and LOLIPO: these projects target applications in Telecom and LiDAR;
3. uTP4Q and CLUSTEC: these projects concentrate on quantum applications.

[1] <https://www.project-elena.eu/>

[2] <https://pattern-project.eu/>

Statistical Measurements of LNOI PICs for Quality Assurance of the Process Design Kit

A. Della Torre, J. Leo, A. Monney, A. Mettraux, A. Ghadimi, H. Zarebidaki, M. Despont, H. Sattari

CSEM is pioneering the development of an LNOI PICs foundry to bridge the technological gap between LNOI and other PIC platforms. Statistical measurements play a crucial role in ensuring the performance and reliability of these PICs building blocks. Our automated setups enable to efficiently measure a large number of PIC components. We illustrate here such statistical measurements. These results set the ground for the use of LNOI PICs in several applications, such as telecommunications and quantum computing, being pursued by different European project in which CSEM is involved.

Photonic Integrated Circuits (PICs) have revolutionized the field of photonics, enabling compact and efficient optical devices for various applications, from telecommunications to quantum computing. One promising platform for PICs is Lithium Niobate on Insulator (LNOI), which offers remarkable optical and electro-optical (EO) properties and has witnessed significant advancements in recent years. However, the technological maturity of LNOI has not yet reached the level of other PICs platforms like silicon and silicon nitride. To bridge this gap, CSEM is pioneering the development of an LNOI foundry for high yield fabrication of LNOI PICs. A PIC foundry service must provide a reliable fabrication process as well as a library of optimized building blocks that are offered as a process design kit (PDK). To this end, statistical measurements of the performances of the building blocks are of paramount importance.

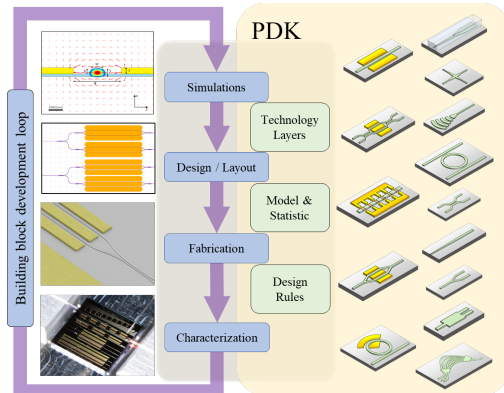


Figure 1: Schematics of the Process Design Kit (PDK) development iteration yielding to reliable building blocks. This tool kit assists the PIC designers in modeling complex PICs relying on guaranteed fabrication and performance metrics.

We have set semi-automated setups to measure a large number of PICs in an efficient approach. The metrology datasets is used to develop and maintain the PDK. A set of passive and active components have been successfully measured and the results are exported into the PDK, including waveguides, Multimode interferometers (MMIs) and EO modulators. These blocks are used by most PIC designers using our platform as the main building blocks for complex circuits. By measuring the resonances of a large number of resonators of different lengths at the C-band, we reported waveguide losses as low as 0.14 dB/cm (Figure 2)^[1]. For MMI power splitters we measured insertion loss of only 0.13 dB per beam splitter (see Figure 2, a slope of -3.13 dB means an excess of 0.13 dB as compared to the -3 dB expected in a lossless MMI)^[2]. These values are matching the requirements for most practical applications.

On the active components side, fast EO modulators with low driving voltage are essential for many of the applications for

which LNOI PICs are in great demand, such as switches for high-speed optical communication, quantum communication and computing, and optical neural networks. We measured folded electro-optical Mach-Zehnder modulators with a half-wave voltage as low as 1 V. This is the target voltage for integrated electro-optical modulators as it enables driving the modulators with fully integrated CMOS circuits without off-chip amplification. High-performances modulators are an essential element for different European projects involving CSEM, including uTP4Q and CLUSTEC, which are aiming to develop a PIC platform for quantum communication and quantum computing.

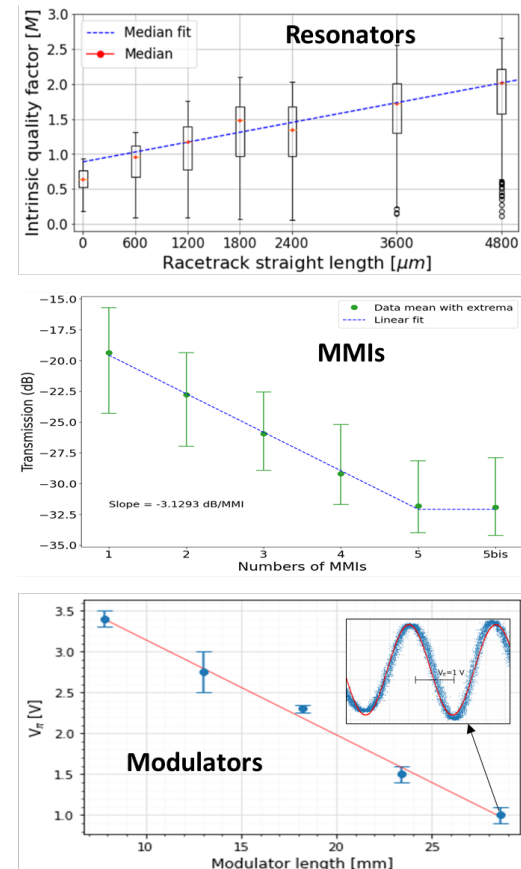


Figure 2: Examples of data acquired from the statistical measurements of the resonators to deduce the waveguide propagation loss, the MMI series to export their insertion loss, and the EO modulators.

In conclusion, LNOI PICs, with their unique characteristics are expected to continue transforming the world of photonics. CSEM is developing a foundry for high-yield fabrication of LNOI PICs, and statistical measurements of the key building blocks ensures the quality of the platform and of its PDK. LNOI PICs developed and produced by CSEM are at the core of many ongoing industrial and ambitious European projects.

[1] J. Leo, et al., "Wafer-scale fabrication of low-loss waveguides in lithium niobate on insulator (LNOI) integrated photonics platform," in ECOC, 2022.

[2] A. Monney, et al., "Statistical characterization of MMI beam splitters on thin film lithium niobate on insulator (LNOI) platform at telecom wavelength," in CLEO Europe, 2023.

Acoustofluidic Platform for Controlled Microtissue Manipulation

E. Vuille-dit-Bille, M. Dubois, D. Bayat, T. Overstolz, S. Heub, M. Despont, G. Weder

*Microtissues and organoids are both complex 3D *in vitro* models that serve as valuable tools in biomedical research for studying drug responses, tissue engineering, and personalized medicine. However, the manipulation and precise positioning of large biological entities such as microtissues has received little attention. At CSEM we are combining our expertise in piezoelectric MEMS and biology to develop a compact acoustofluidic platform to precisely handle and manipulate individual microtissues without physically touching them. This non-invasive approach will streamline the controlled positioning of complex 3D models in organ-on-chip systems.*

Complex 3D models are fundamentally reshaping the fields of disease modeling, drug testing, and organ replacement. Derived from stem cells, organoids are capable to autonomously arrange into three-dimensional structures to replicate the architecture and functionalities of real tissues, thereby forming mini organs. The multiplication of newly available biological models and microphysiological systems leads to a need for new tools to efficiently handle spheroids, microtissues and organoids. Non-invasive techniques for three-dimensional manipulation and positioning of these biological entities are of particular interest in the study of tissue-tissue interactions, multi-organoid assemblies, and high-throughput analysis [1].

CSEM is developing a MEMS-based acoustofluidic platform for precise spatial positioning of heterogeneous microtissue populations in water-based environment. Acoustic forces offer the advantage of biocompatible label-free and contactless manipulation. The technology is based on piezoelectric micromachined ultrasonic transducers (PMUT) and enables to simultaneously translate several biological entities through complex manipulation schemes, while allowing easy integration in lab-on-chip devices.

The acoustic platform is composed of a silicon chip containing an array of PMUTs and covered by an acoustofluidic chamber made of polydimethylsiloxane (PDMS) (Figure 1a, 1b). Each PMUT is activated by a highly piezoelectric Al0.7Sc0.3N layer. Dynamic manipulation and spatial patterning can be achieved by controlling each transducer's relative amplitude and phase.

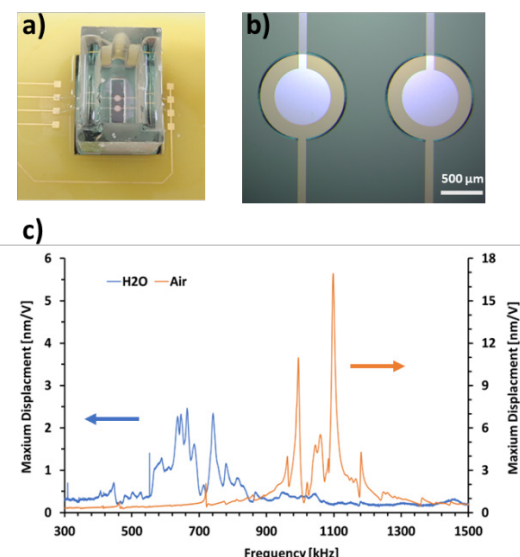


Figure 1: a) Prototype of the acoustic platform: silicon chip mounted on a PCB with a PDMS chamber; b) Micrograph of PMUTs; c) Maximum displacement of the PMUTs measured in water and air.

The performances of the microfabricated PMUTs were characterized using a laser Doppler vibrometer (Figure 1c). The resonance peaks were identified in air and water by looking at the maximum displacement of the transducers.

Numerical simulations were performed using COMSOL Multiphysics to study the repartition of particles inside the fluidic chamber. The potential associated to the acoustic force, the Gor'kov potential, was simulated for a device containing 2 PMUTs. The behavior of the particles is driven by the Gor'Kov potential and the acoustic contrast factor, which depends on the density and the compressibility of the particle and medium. The acoustic platform was initially tested with 30 μm diameter polystyrene (PS) beads and polydisperse PDMS particles, showing positioning on the Gor'kov potential according to the particle's acoustic contrast factor, as predicted by the numerical model (Figure 2).

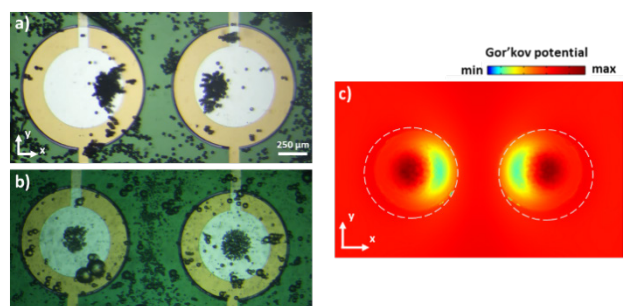


Figure 2: a) Polystyrene and b) polydimethylsiloxane beads patterned on top of the PMUTs in agreement with c) FEM simulation of the Gor'kov potential of the XY plane 20 μm above the surface, highlighting zones with low and high potential where polystyrene and polydimethylsiloxane particles collect, according to their positive and negative acoustic factors, respectively.

The manipulation of particles with PMUTs was demonstrated in two-dimensions. Ongoing developments focus on the development of the platform for the manipulation of microtissues, ranging from 100 to 500 μm , in three-dimensions.

Overall, acoustic microtissue manipulation offers a non-invasive approach that combines acoustic waves with microfluidic technology to create, manipulate, and study microtissues in a controlled and physiologically relevant environment. Importantly, it is non-contact and non-invasive, meaning it does not physically touch or damage the microtissues, thereby opening new opportunities to perform dynamic studies.

[1] E. Vuille-dit-Bille, et al., Lab Chip, 2022

Automated Multi-axis Bioreactor for Standardized Preclinical Assessment of ex vivo Tissues

D. Ledroit, F. Crivelli, R. Ischer, F. Auf der Maur, T. Bendinelli, S. Unterhofer, S. Heub, F. Boudoire, M. Alini*, S. Ferguson **, G. Weder

Low back pain is a worldwide social and economic burden reducing the ability to work and perform daily tasks, which is mostly associated with intervertebral disc (IVD) degeneration. Despite recent advances in potential therapeutics with restorative actions targeting IVDs, such developments are impeded by the lack of an *in vitro* model for drug assessment that can mimic typical motions occurring in the human body while maintaining IVD viability. CSEM, AORI and ETHZ have developed a unique automated and fully closed multi-axis bioreactor allowing the multi-axial loading of an *ex vivo* bovine IVD organ model in a controlled environment.

Musculo-skeletal disorders, including low back pain, appear in the top five causes of disability-adjusted life year worldwide [1]. Although not life-threatening, it is considered an important social burden with a high socioeconomic impact. Therefore, progress has been made towards developing new therapeutics to restore some of the impaired functions, especially in the IVD. However, the development of advanced *in vitro* systems mimicking the complex motions occurring in the human body is required to further characterize their performance and accelerate their access to the market.

A novel 6-degrees of freedom (DOF) automated bioreactor was developed for multi-axial actuation of IVDs in a controlled environment (Figure 1). This system efficiently transfers forces to the IVD, mimicking flexion, extension, lateral bending, torsion, tension, and compression in confined, physiological, and sterile environment. It consists of a biochamber containing the IVD specimen in physiological conditions; fluidic ports to enable automated medium exchange; a hexapod as actuation system with an integrated force sensor; a Visard-based software enabling the control of the entire platform; and a transparent environmental enclosure to control temperature, humidity, and gas (not shown).

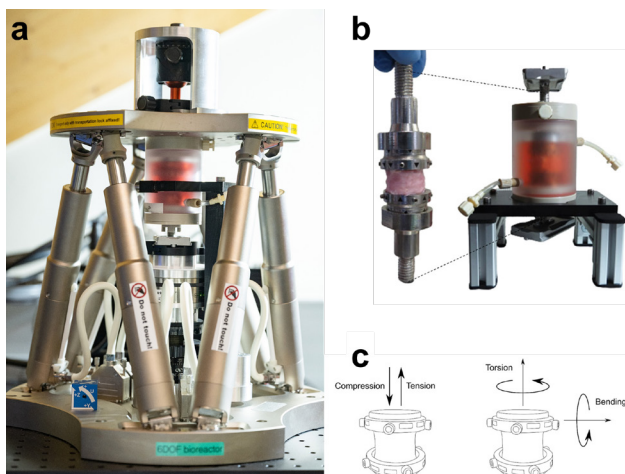


Figure 1: (a) 6-DOF bioreactor, (b) biochamber enclosing the IVD sample between holders, (c) to perform multi-axial loading on IVDs while preserving sample viability and sterility.

The mechanical coupling between the IVD specimen and the hexapod actuator is ensured by customized sample holders manufactured in stainless steel by 3D printing (Figure 2). Lateral and top screws are added during sample assembly for a robust

fixation. The sample holders were designed to optimize the delivery of oxygen and nutrients to the tissue.



Figure 2: 3D printed sample holders for intervertebral discs manufactured at CSEM.

This advanced bioreactor enables mechanical actuation from 1- to 6-DOFs without microbiological contamination after 9 days in operation. This newly established IVD organ model was shown to maintain cell viability to a similar level as in uniaxial bioreactors under physiological loading [2], while enabling degenerative protocols (Figure 3). After 3 days of loading, cell viability was assessed in 3 different regions of the IVD and showed a significant decrease under degenerative conditions. These results demonstrated the capacity of the system for long-term biological studies under different types of mechanical loading.

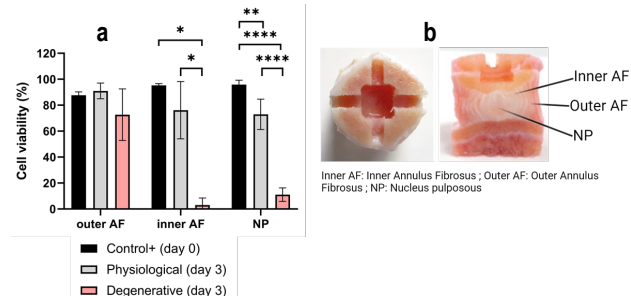


Figure 3: (a) Cell viability under physiological and degenerative loading in the multi-axis bioreactor, in 3 regions of the IVD, with day 0 the non-loaded positive control group; (b) IVD specimen prepared for fixation in the bioreactor.

Latest results show that the bioreactor replicates multi-axial loading, simulating everyday movements like bending and sports-related stress. A new finite element study determined these load-motion combinations [3], offering a unique platform for testing biomaterials, grafts, and therapies in realistic spinal conditions.

This project was co-funded by SNSF – Swiss National Science Foundation under Sinergia grant CRSII5_189915.

* AO Research Institute, Davos

** Laboratory for Orthopaedic Technology, ETH Zürich

[1] GBD 2019 Diseases and Injuries Collaborators, The Lancet, 2020.

[2] A. Šećerović, et al., ACS Biomaterials Science & Engineering, 2022.

[3] A. Ristaniemi, et al., Journal of the Mechanical Behavior of Biomedical Materials, 2023.

Automated Sorting of Microtissues using Deep Learning for Label-free Characterization

C. Sampaio da Silva, J. Goldowsky, N. Schmid, S. Boder-Pasche, C. Fonta, V. Revol, G. Weder, T. Valentin

Over the past decade, there has been a significant shift in the field of cell culture towards the use of complex *in vitro* models, such as spheroids, microtissues and organoids. These 3D culture systems more closely mimic the *in vivo* microenvironment compared to traditional 2D cell culture. However, their adoption in industry is hampered by the difficulty of scaling up their production while ensuring standardized microtissue populations. CSEM has developed automated, deep learning-based platforms for label-free characterization, individualization, and sorting of microtissues. These automated systems adapted for sterile conditions provide a flexible solution for the use of microtissues in large quantities in drug testing and tissue engineering.

Spheroids, microtissues and organoids are currently bridging the gap between *in vitro* models and *in vivo* physiology. Since cell 3D models have proven to better replicate structural and functional complexity of organs, their use has increased in drug screening and regenerative medicine. In both applications, large numbers of homogenous microtissues are required. However, conventional production and maturation methods often lead to high morphological variability. CSEM has developed two sorting platforms to increase homogeneity in large microtissue populations.

The EU-funded project ORGANTRANS (www.organtrans.eu) used 3D tissue printing combining spheroids and biomaterials to treat liver disease. Large quantities of liver spheroids of approximatively 150 µm diameter were produced in spheroid microwell plates (Figure 1a). CSEM developed an automated system integrating microtissue imaging, analysis, and sorting on a single platform. The ORGANTRANS platform (Figure 1b) is composed of a motorized XY-stage that enables movement of the plate with spheroids over a microscope with 4X magnification for imaging. A deep learning algorithm trained by experts is used to classify spheroids according to the required criteria for bioprinting. The use of a 300 µm-diameter capillary needle enables precise picking and removal of individual spheroids that do not match the characteristics. All high-quality spheroids remaining in the culture plate after sorting are harvested in bulk for further processing.

The ORGANTRANS' platform enables the sorting of one plate with 8'000 spheroids in less than 90 minutes when up to 2% of the unhealthy spheroids must be sorted out (typical ratio for the liver spheroids used in this application). The viability of spheroids after sorting was monitored for 3 days, showing no statistically significant differences compared to manual harvesting.

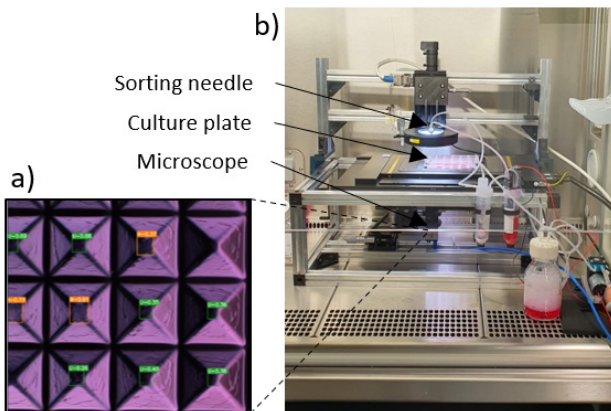


Figure 1: a) Microscopic view of the culture plate for high-throughput production with liver spheroids labeled as "low quality" (green) and "high-quality" (orange) for bioprinting using a trained deep learning algorithm. b) Spheroid sorter platform inside a laminar flow.

Organoid production techniques vary depending on tissue type and model complexity. Retinal organoids cultured in standard low

attachment flasks are non-spherical entities with a diameter ranging from 1.5 to 3 mm and are composed of different morphological structures. The OrganEYEzer sorting platform is the result of an Innosuisse collaboration with the Institute of Molecular and Clinical Ophthalmology in Basel (IOB) where retinal organoids are used for different drug screening studies. CSEM developed a new platform dedicated to large organoid handling, sorting and individualization into 24- and 96-well plates. In this case, the organoids are being picked with a pipet from a Petri dish and transferred into a 96-well plate. To minimize the movement of free-floating retinal organoids, the Petri dish containing the organoids is kept stationary, while the pipet and the microscope move between the dish and the plate, enabling live imaging during the whole sorting process.

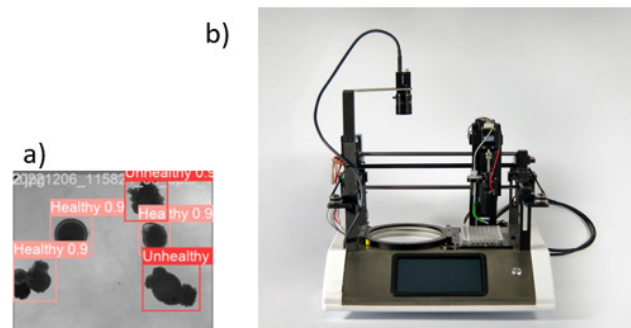


Figure 2: a) Microscopic view of retinal organoids in a standard Petri dish labeled as "healthy" (orange) and "unhealthy" (red) for drug screening applications using a trained deep learning algorithm. b) Global view of the OrganEYEzer platform sized to fit into a laminar flow.

The custom brightfield microscope enables imaging of photoreceptor structures, which are essential for microtissue characterization and sorting. Again, a deep learning network is trained by experts for localization and classification of retinal organoids.

The development of automated platforms for rapid sorting of microtissues helps to facilitate the use of models with increase biological relevance, whenever large quantities of standardized microtissues are needed. Automated platforms increase reproducibility and accuracy of the sorting process while reducing efforts and errors linked to manual handling. The use of deep learning on microscope images enables label-free analysis of microtissues while using expert knowledge.

The sorting consistency and throughput of these platforms broaden potential fields of application of microtissues from relatively low throughput research applications to regenerative medicine and industrial drug screening applications.

Automated Well Plate Sampling and Integrated Glucose Measurement

S. Graf, M. Garzuel, M. Dorrestijn, N. Schmid, J. Rohrer, S. Heub, A. Freitag •, L. Höltig •, O. Frey •, V. Revol

CSEM's Smart Lid platform aims at automating cell culture and cell assays using functions integrated in the lid such as media exchange, mixing or dilution. Newly, the platform has been extended to enable low volume sampling and sensing. A first solution has been tailored to the InSphero Akura™ Flow 384 plate and allows for sampling 6- μ l from 24 channels and sequentially transferring these samples to a glucose sensor. The system was validated by measuring the glucose response of liver tissues to glucagon. The results demonstrate that the Smart Sampling Lid can be used for automated low volume sampling and subsequent (glucose) sensing.

Well plates are widely used in laboratory automation for toxicity screening, disease modelling, diagnostics and much more. Most well plates follow the ANSI/SLAS standards (e.g., 96 and 384 well plates) but customized solutions for organ-on-chip cultivation have also been developed.

The common denominator between these different well plates is their lid that protect the cell culture from contaminations. In the past years, CSEM has developed the Smart Lid platform to integrate functions to such lids. In this report, the new sampling and sensing function is presented which has been bio-validated with InSphero's Akura™ Flow technology.

The Akura™ Flow 384 plate allows for loading up to 12 microtissues as mono or co-cultures such as for example liver and pancreatic islet tissues in each of the 24 parallel channels. Thanks to gravity-driven perfusion (provided by the All-In-One Tilter) these tissues can interact with each other to model complex diseases such as diabetes. Measuring glucose in the cell culture medium is done typically through fluorometric assays, which do not allow for continuous monitoring of the glucose over time. This is the gap that the Smart Sampling Lid allows to fill.

The customized Smart Sampling Lid uses a disposable lid with an injection molded strip (with 24 tips) which is clamped onto the reusable fluidics using the clamping bar (Figure 1).

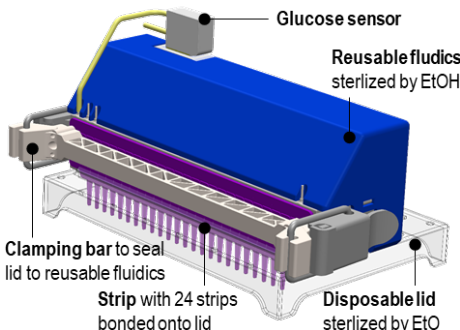


Figure 1: Smart Lid design with reusable fluidics and disposable lid.

In a common effort, CSEM and InSphero, successfully demonstrated the integration of the Smart Sampling Lid prototype with the Akura™ Flow 384 multi-organ plate. Figure 2 shows the setup inside the incubator and the control unit aside. Liver spheroids have been cultured in the Akura™ Flow 384 plate, while 6- μ l samples have been removed every 9 hours from each channel sequentially and measured using the glucose sensor. Figure 3 depicts the sensor signal over a period of 29 hours. Thanks to these measurements, the release of glucose from the liver spheroids into the medium could be observed in real time. As expected, liver tissue's glucose release could be stimulated

by glucagon (pancreatic hormone) resulting in higher values for these conditions compared to non-stimulated conditions (Figure 4). Figure 5 shows two exemplary graphs from two individual channels and the obtained glucose kinetics in the media. It underlines the potential of the system to better study and understand the molecular interaction of multiple organs in an in-vitro system.

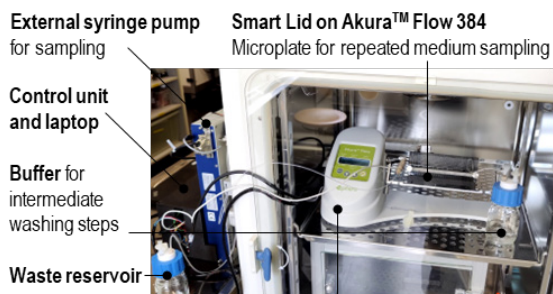


Figure 2: Test setup with the Smart Sampling Lid in the incubator.

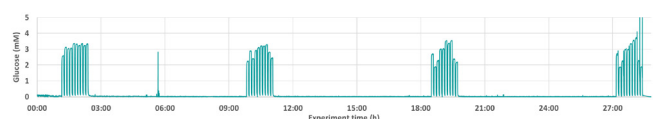


Figure 3: Recording of all measurements performed over the time of 29 hours in intervals of about 9 hours.

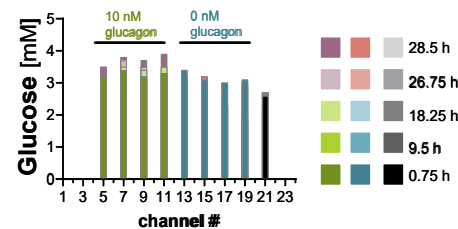


Figure 4: Summary of the glucose readings per channel showing an increase of glucose over time for the spheroids exposed to glucagon compared to the ones not exposed to glucagon.

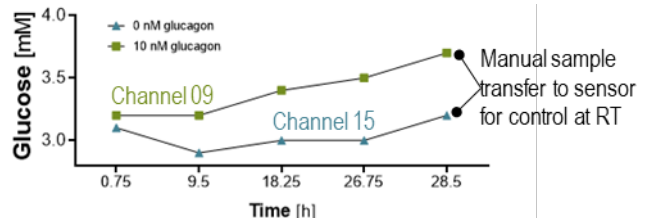


Figure 5: Glucose readings of channel 9 (increased glucose level due to glucagon presence) and 15 (constant glucose level due to absence of glucagon).

This work was (partly) funded by H2020-ECSEL-2019-IA-876190. CSEM thanks them for their support.

• InSphero AG

Droplet Microfluidics – Artificial Compartments for Applications in Life Sciences

P. Rottmann, J. Zhou, L. Chen, C. Bichsel, M. Blache, P. Odermatt, F. Kurth

Single cell analysis has emerged as an important tool for biological research, diagnostics, and for the development of drugs and biomarkers. Droplet microfluidics, by providing homogenous and miniaturized compartmentalization, is particularly suited for single cell manipulation and highly sensitive low-content measurements. Advantages include integrated and automated workflows, significant reduction in sample and reagent consumption, and lower costs. Currently, CSEM is developing translational droplet microfluidics technologies for industrial applications by addressing challenges such as scalable manufacturing of devices, robust bioassays, and workflow automation for biologists and clinical users packaged in user-friendly benchtop systems.

Droplet microfluidics refers to all processes involving droplet compartments made using two immiscible phases in micron-scale channels. Typically, these compartments are in the range of 20-200 μm in diameter and may be aqueous-in-oil, or oil-in-aqueous droplets, stabilized by surfactants. They are perfectly suited for biological applications, due to matching length scales with cells and the ability to use biocompatible reagents. A range of operations can be performed with droplets in microfluidic chips, all of which can be tailored to a specific application. Figure 1 depicts the most common operations in droplet microfluidics as individual building blocks that can be custom assembled to build an integrated system.

Droplet microfluidics building blocks

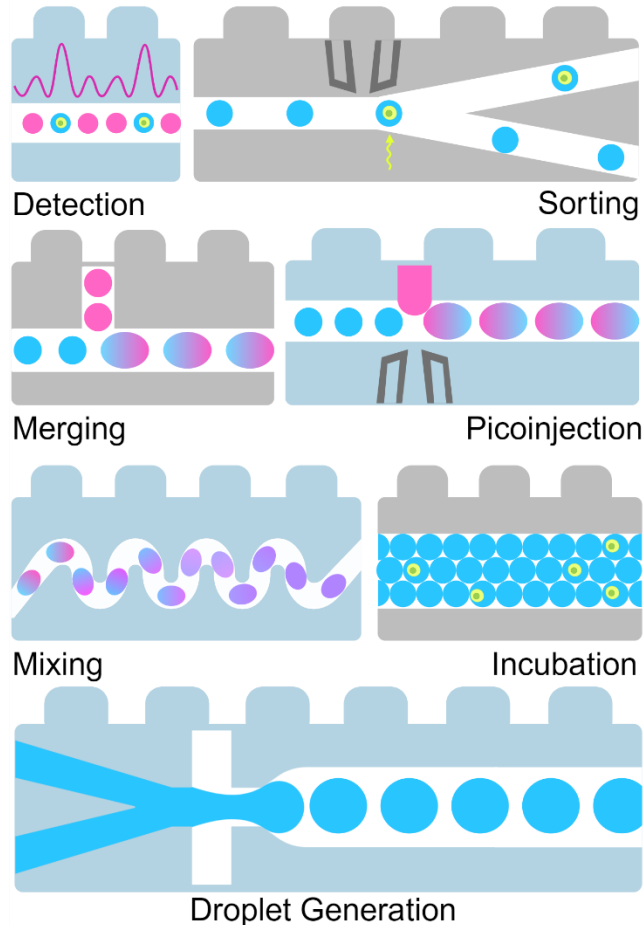


Figure 1: Schematic showing various droplet microfluidic unit operations, depicted as building blocks. The building blocks droplet generation, mixing, incubation, merging, picoinjection, detection and sorting can be assembled in different configurations to construct a customizable, integrated system for different biological workflows.

The foundation is the production of monodisperse, uniform droplets at high-throughputs (up to kHz-MHz). Using specific channel designs, these picolitre to nanoliter volume droplets can then be merged, their contents can be mixed, they can be incubated and imaged in fixed positions over time, or they can be

analyzed and sorted in flow. Using these versatile building blocks, compact, bench-top systems can be built for a variety of life-science applications.

Since its advent two decades ago, droplet microfluidics has found its way into a broad spectrum of fields at the interface of biology, biochemistry, and physics. In recent years, droplet microfluidics has revolutionized the field of genetic sequencing with the commercialization and growing popularity of single-cell RNA sequencing technology. Furthermore, screening campaigns of small molecules such as antibodies or enzymes can be conducted in pL scale droplets, increasing throughput, and reducing reagent volumes and costs by multiple orders of magnitude.

Droplet microfluidic tools are already widely used in several projects at CSEM. The internal project ORCA deals with the dissociation of organoids into single cells and their subsequent encapsulation in water-in-oil droplets containing a staining solution that gives information about their viability (Figure 2e). CSEM and Parithera, a start-up in Lausanne, received an Innosuisse grant (ExTrace) that addresses the isolation of rare cells from liquid biopsy and their co-encapsulation with DNA hydrogel beads into droplets to perform a single-cell RNA sequencing procedure (Figure 2a and b). CSEM has also developed scalable techniques important for commercial applications in droplet merging (Figure 2c), passive sorting (Figure 2f), and droplet quantification using AI-based image analysis, a key feature to guarantee optimal process control (Figure 2g).

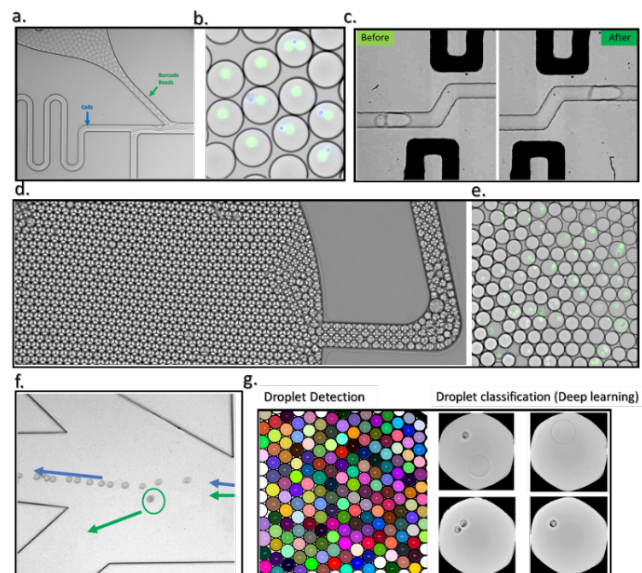


Figure 2: a) and b) Co-encapsulation of single cells and barcoded beads for next generation sequencing; c) Droplet merging; d) Re-injection; e) Single cell imaging and incubation; f) Passive sorting; and g) Droplet image analysis.

AML.AI – Deciphering Bone Marrow Remodelling in Acute Myeloid Leukaemia using Single-cell Omics

K. Zielinska, A. Pereira*, C. Nombela-Arrieta*

The AML.AI project aims to investigate bone marrow changes in the stromal compartment during acute myeloid leukemia (AML) in collaboration with the University Hospital Zürich (USZ) and the University of Zürich (UZH). Leukemic cells likely affect bone marrow stromal niche and induce major perturbations in the composition and function of the cells. We employ a mouse model of AML that mimics the natural course of disease and perform scRNA-seq to gain high resolution of these changes during disease course.

Acute myeloid leukemia (AML) is the most common type of acute and fatal leukemia in adults and its incidence increases with age. This disease usually has rapid onset of symptoms and is diagnosed based on the accumulation of immature progenitors (myeloblasts) in the bone marrow and blood. Additional tests are used to distinguish this type of leukemia from others and define the subtype. AML is a malignant disease characterized by abnormal growth and differentiation of haematopoietic stem cells (HSCs) and accumulation of immature precursors in the bone marrow and blood. This expansion of immature progenitors takes place at the expense of normal hematopoiesis.

During disease development, AML cells progressively occupy and likely alter the bone marrow niche where the normal hematopoietic stem cells reside. Research evidence suggests that AML likely induces changes in certain populations of cells in the bone marrow microenvironment, which ultimately support leukemia progression.

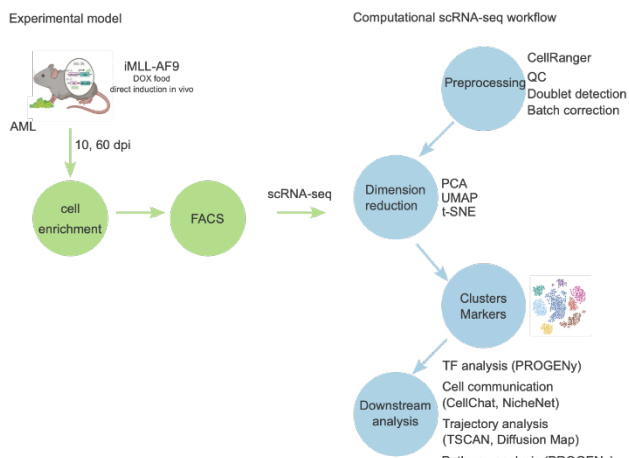


Figure 1: Experimental set-up to study bone marrow remodeling in AML.

In this project, we aim to characterize the morphologic, spatial, and functional changes in the bone marrow microenvironment during AML. To this end the team at the USZ uses transgenic iMLL-AF9 mice (generated by Prof. Schwaller, University of Basel) which develop leukemia upon direct induction. We follow disease progression and isolate both endothelial and mesenchymal stem cells at specific time points for single-cell RNA-seq as depicted in Figure 1. After data preprocessing, advanced tools such as trajectory and interactions analyses are

applied to uncover the effect of AML on the cell populations. Preliminary results reveal decrease in canonical niche markers in mesenchymal stem cells and decrease in permeability-related genes in endothelial cells during AML progression.

The data analysis workflow includes initial steps such as running CellRanger, performing quality control and batch correction. After subsequent data normalization, we perform dimension reduction, e.g., using PCA, tSNE and UMAP, to visualize data in a low dimensional space. Next steps include clustering of the data and marker detection (Figure 1). In the second part of the analysis, advanced tools including trajectory analysis and cell-cell communication analysis were used. Trajectory analysis was applied to uncover the changes in transcriptional profile in the mesenchymal stem cells along the disease course. For this type of analysis, the TSCAN algorithm was selected (Figure 2). Cell communication analysis will reveal the how AML affects the interactions between the two compartments (mesenchymal stem cells and endothelial cells).

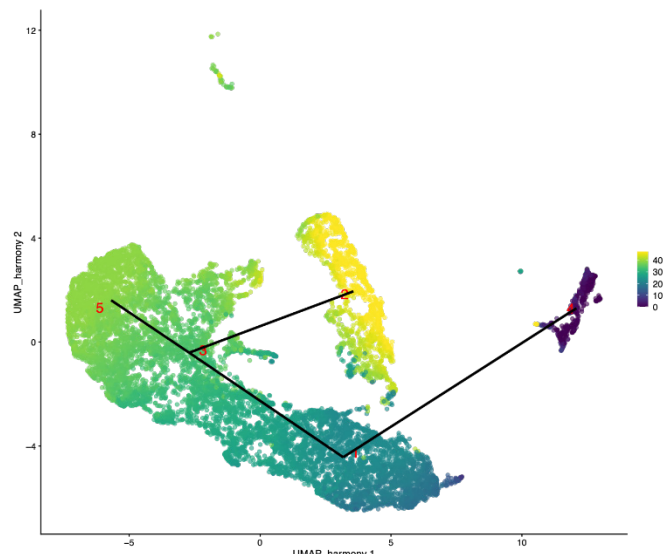


Figure 2: Trajectory analysis of mesenchymal stem cells compartment. Cells are colored according to pseudo time values.

The workflow developed for AML can be applied and customized for other single cell RNA-seq datasets for applications in biomarker identification and disease analysis.

* Affiliated at University Hospital Zürich and the University of Zürich

Self-standing Sensor System as in vivo Implant for Smart Bone Regeneration

J. Disser, C. Hennemann, N. Marjanovic, M. Kraus, L. Berganin, L. André, J. Beysens, P. Nussbaum, F. Kurth

This project introduces an innovative solution for bone defect management: a biocompatible, flexible, and wireless system of sensors embedded within a 3D-printed implant designed to monitor bone regeneration and implant acceptance in real-time. Through the integration of advanced sensor technology and 3D printing, the project brings forth a solution that not only addresses the limitations of current treatments but also envisions a future where real-time monitoring becomes a standard in bone regeneration.

Bone defects, especially large ones, have posed significant challenges to the medical community. The current clinical practice for treating large bone defects (where at least 3 cm of bone is missing) involves either the technique of bone transport (distraction osteogenesis) or the induced membrane technique (Masquelet technique).^[1] The evolving landscape of medical technology has been moving towards more efficient, minimally invasive solutions that leverage advancements in sensor technology and biocompatible materials. Recent technological advancements have opened doors to innovations that can bridge the gap between current treatments and the desired outcomes. Integrating sensors into bone implants represents one such frontier, offering real-time insights into bone reformation processes that were previously inaccessible.

The central challenge is the effective monitoring and management of bone defects, ensuring the optimal integration of implants and the successful regeneration of bone tissue. The traditional methods, while effective, are not without drawbacks, including the potential for complications, multiple surgical interventions, and an increased burden on the healthcare system. Furthermore, the lack of real-time monitoring capabilities in existing treatments poses challenges in determining the effectiveness of interventions, necessitating reliance on periodic check-ups which might not provide timely data. Together with a total of 10 project partners part of the EU project "Smart Bone Regeneration" (EU grant no. 874896), CSEM co-develops a novel strategy to solve those shortcomings to consequently allow for a real-time monitored bone defect treatment approach.

The project's solution is a 3D-printed, resorbable bone implant embedded with a suite of multi-sensing capabilities. These sensors, silicon-encapsulated for durability and biocompatibility, are designed to track vital parameters for bone regeneration: pH, temperature, strain, and transforming growth factor (TGF- β 1). The communication framework of the implant is based on Bluetooth technology, and ensures real-time data transmission, enabling timely medical interventions. The temperature and strain sensors are commercially available components assembled on a flexible printed circuit board. The TGF- β 1 sensors are fabricated by combining inkjet and screen-printing processes, whereby the sensing electrodes for the TGF- β 1 are printed with a particle-free platinum ink. The pH sensor is composed of an iridium oxide working electrode and a silver chloride pseudo reference electrode (see Figure 1). It is designed to cover the pH range 3-11 with an expected lifetime of more than a week under in vivo conditions. The TGF- β 1 sensor's capability to track cellular activities provides a window into the

microscopic events, enabling professionals to understand the pace and quality of bone regeneration. The biocompatible nature of the implant ensures that patients do not face complications arising from material rejection, and its flexibility enables the implant to adapt to various bone structures and defects.

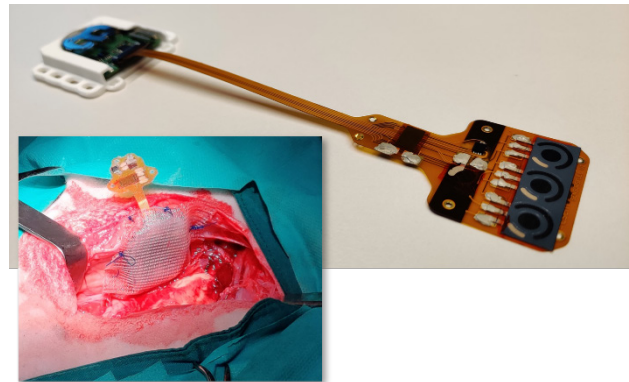


Figure 1: Non-encapsulated implant. Bluetooth and protection on the left, sensor head composed of Flex PCB with pH, strain gauge, temperature, and three TGF- β 1 sensors on the right. Insert: Sensor system during initial animal surgery.

Preliminary findings indicate the successful integration of the sensors within the 3D-printed implant, with temperature, strain, and pH sensors showing promising results in tracking the healing process evolution.^[2] The Bluetooth communication has been robust, ensuring real-time data transmission with minimal interruptions. The cytotoxicity tests according to ISO 10993-12:2021 and ISO 10993-5:2009 indicated that the materials used in the implant and sensors did not induce adverse reactions, ensuring patient safety. The sensor system is now ready for in vivo testing trials, which will be conducted by the project partner AO Davos.

The development of the implantable sensor system represents a significant advancement in bone defect treatment. Its potential not only lies in the real-time monitoring capabilities but also in paving the way for more personalized, efficient, and minimally invasive treatments. The confluence of sensor technology, biocompatible materials, and real-time communication in this project represents a holistic approach addressing a longstanding medical challenge. Despite the initial results, continuous iterations and improvements based on feedback from in vivo tests will be crucial to a thorough system validation and ultimately its widespread adoption. The potential applications of such technology extend beyond bone regeneration, possibly ushering in a new era of implantable monitoring devices for various medical applications.

[1] P. V. Giannoudis, O. Faour, T. Goff, N. Kanakaris, R. Dimitriou, "Masquelet technique for the treatment of bone defects: Tips-tricks and future directions", Injury-International Journal of the Care of the Injured, vol. 42, pp. 591-598, 2011.

[2] E. Guerrero San Vicente, C. Hennemann, J. Disser, R. Grinyte, N. Marjanovic, J. M. Cabot, "Implantable sensors and biosensors to monitor bone regeneration", IEEE Sensors 2023, accepted.

Portable Fluorescence Biosensing System for Low-cost, Quantitative, and Multiplexed Allergen Screening

Y. Shynkarenko, H. Chai-Gao, S. Demuru, N. Hermann, P. Boia, P. Cristofolini, B. Petkus, S. Generelli, S. Paoletti, L. Burr, S. Cattaneo

There is a pressing need for innovative portable multiplexing tools for point-of-care diagnostics. CSEM developed a miniaturized fluorescence multi-sensing system for the rapid identification of immune-mediated responses, enabling the simultaneous detection of multiple allergens in just one hour. The portable solution eliminates painful skin tests and time-consuming lab procedures towards efficient allergy diagnosis and timely treatment. CSEM's solution consists of a microfluidic chip and an automated processing system to identify allergy-specific IgEs in serum by using fluorescence-labeled antibodies. At the core of this advancement lies a user-friendly portable optical reader that can be easily integrated into a doctor's daily routine.

CSEM recently developed a microarray chip for allergen analysis ("IncaSlide"), as previously reported [1]. It consists of a meandering channel with an array of microstructures functionalized with allergen recombinant proteins, the latter immobilized using Optodex® chemistry. Once the patient's serum is flown on the functionalized chip, a subsequent reaction with fluorescence-labeled anti-IgE antibodies unveils the specific allergens by the fluorescence responses. So far, the assay has been read out with commercial microarray scanners. However, commercial readers' cost and size render them unsuitable for use in point-of-care settings.

To circumvent these limitations, an alternative portable reader was developed for fluorescence-based bio-detection (Figure 1). The reader employs fluorescence imaging instead of confocal scanning utilized by commercial slide scanners. This enables a reduction in size and cost and improves speed, at the cost of a slightly lower sensitivity. The reader comprises a camera, collection and beam-forming optics, a light source, emission and excitation filters, and a light trap. Based on the spectral properties of the selected dye (Alexa-647), a 642 nm fiber laser was selected as a light source. Light-forming optics consists of a fiber collimator, an excitation filter to remove unwanted emission from the laser, and an engineered top-hat diffusor to ensure uniform sample illumination. A combination of a color glass filter and an interferometric filter was used for spectral filtering. Fluorescence emission was then collected with a camera objective modified for macro performance. A monochromatic CMOS camera based on a Sony IMX265 sensor chip was employed, featuring manual control of integration time, gain, gamma, and 12-bit data output. Finally, a trigger from the camera is used to activate the laser during the measurement. Thanks to the use of a fiber-based laser, the system is easily adaptable to other fluorophores.



Figure 1: Photo of the compact fluorescence reader.

To assess the performance of the portable reader, a comparison was made with a commercial confocal microarray reader (InnoScan 710). IncaSlide with varying dye concentrations were analyzed using both readers. Considering three times the

standard deviation (3σ), the detection limit of the portable device was determined to be equivalent to ~ 500 dye molecules per μm^2 . Despite the lower sensitivity compared to the commercial reader, the performance of the portable reader is suitable for the detection of allergic reactions. Tested with control serum samples (167 and 274 IU/mL total IgE concentrations), equivalent to the minimum allergen-specific IgE produced in case of a reaction, the CSEM portable solution shows high sensitivity for the biosensing application and comparable performances as the commercial system (Figure 2).

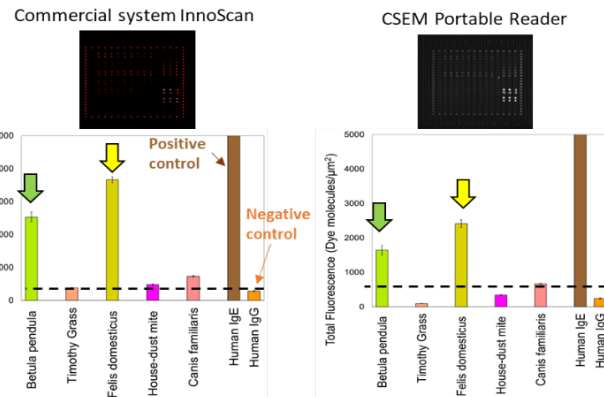


Figure 2: Comparison of the data acquired by InnoScan and CSEM's portable reader, using an IncaSlide with different recombinant allergens. Tested with control serum (274 IU/mL total IgE). Top: relative optical image.

The portable reader represents a viable option for point-of-care applications in allergy diagnostics but also in the broader landscape of biosensing. Its compact design and lower cost allow the widespread adoption of this technology. The unique features of the reader are:

- i. portable (size (20x smaller: 20×16×7 cm)
- ii. cost-effective (40x less expensive: 1.5 k€)
- iii. fast time to result: 60x faster (1-minute scan with InnoScan 710 vs 1 second with the portable reader).

The reader's software also developed at CSEM features fast image acquisition, automated image preprocessing, fluorescence marker grid detection, and computation of the result, significantly reducing operator involvement and potential result bias. Additionally, the web-based frontend interface ensures the system's usability on various platforms.

This work was funded by the European Commission, project HEDIMED, grant number 874864.

[1] S. Heub, "Disposable Glass Microfluidics for Nucleic Acids Bioassays", CSEM Scientific and Technical Report (2019), 56.

Mid-IR QCL-powered Modular Platform for Contactless, Real-time Metabolite Monitoring

C. Beyer, V. Zubkovs, I. Marozau, S. Zabihzadeh, S. Cattaneo

In the field of bioprocesses, noncontact, real-time metabolite monitoring is increasingly in demand, as it plays a key role in optimizing production processes, ensuring product quality, and improving the efficiency and reliability of biomanufacturing operations. Based on the recent advancement in the field of mid-IR vibrational spectroscopy, leveraging Quantum Cascade Lasers (QCLs) and nanophotonic structures, the concept of a novel modular sensing platform is presented which facilitates continuous, real-time metabolite quantification in cell culture media.

Mid-Infrared (Mid-IR) vibrational spectroscopy represents a pivotal analytical approach in contemporary bio-photonics, particularly due to its capacity to interrogate molecular vibrations that yield highly specific spectral signatures of functional groups within organic molecules in liquids^[1]. However, several challenges limit its application in industry. The most advanced instruments are FTIR spectrometers, which are large, stationary systems and not suitable for high-throughput online applications.

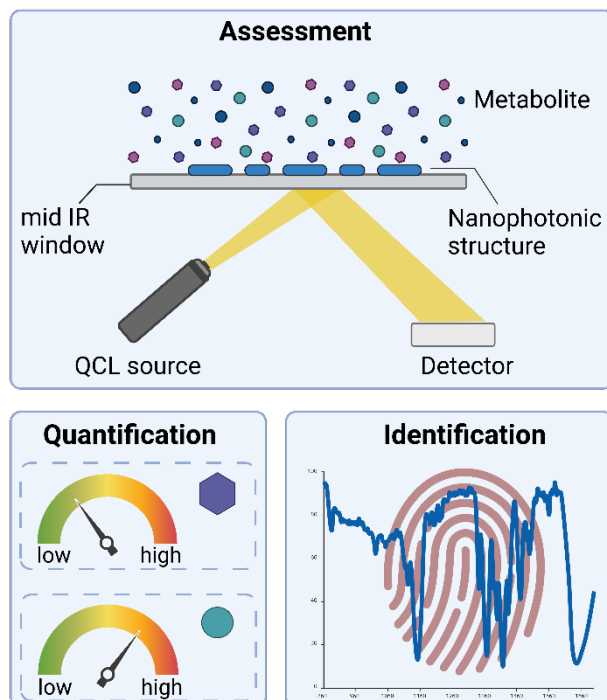


Figure 1: Overview of the implementation concepts.

The advent of QCLs in recent years has facilitated a resolution and sensitivity hitherto unachievable with traditional light sources. QCLs, with their narrow, tuneable emission bands and high output powers, combined with nanophotonic structures, such as plasmonic antennas and dielectric metasurfaces, enhance the signal-to-noise ratio (SNR) critical for the precise quantification of low-concentration metabolites like glucose. Plasmonic antennas, exploiting the phenomena of localised surface plasmon resonances, facilitate the concentration of electromagnetic fields in the vicinity of the analyte, thereby significantly amplifying the molecular absorption signal^[2]. The application of machine learning (ML) methods to IR spectroscopy was also recently shown to enhance chemical quantification in complex, multicomponent matrices^[2]. The integration of all these elements paves the way for the development of compact, sensitive, and selective sensing platforms for real-time metabolites monitoring in complex biological media.

Based on these advancements we explored in the framework of a feasibility study multiple concepts for the development of a contactless, label free sensing platform for real-time monitoring of glucose and lactate in cell culture medium. The platform consists of a disposable, low-cost flow cell with an integrated sterilisable, optical interface and an optical QCL-based reader (Figure 1). Advanced chemometrics approaches will be applied to assess multiple analytes simultaneously. Proof of principle have been shown by FTIR measurements of DMEM cell culture medium spiked with two concentrations of glucose in the range relevant to cell culturing (Figure 2). The multi-disciplinary project leverage CSEM's expertise ranging from optical system integration, liquid handling, advanced packaging.

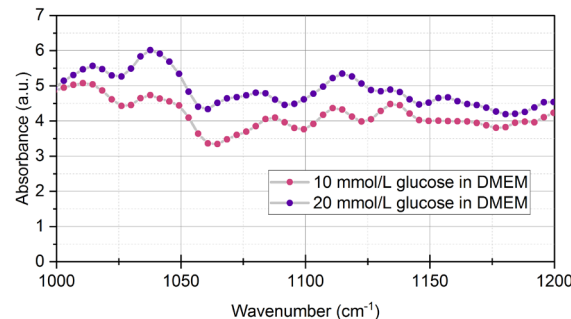


Figure 2: Mid-IR spectra of glucose in DMEM cell culture medium.

The modular configuration of the sensing platform allows for effortless customisation of the setup to encompass other spectral ranges, underlining its versatility. Additionally, the inherent low-drift characteristic of the QCL-based system reduces the frequency of recalibrations, assuring consistent and reliable measurements over extended periods. The sensing platform features a low sample volume (< 10 µl) with a potential for recirculating the sample, ensuring resource-efficient measurement processes. This feature, coupled with its non-invasive nature, permits continuous monitoring without necessitating discrete sampling stages, paving the way for seamless real-time data acquisition. The system's functionality extends to allow real-time analytical capabilities for durations of up to four weeks, proving invaluable in long-term studies.

This approach provides immense potential for the advancement of organ-on-chip (OOC) platforms and pharmaceutical bioreactor processes allowing for tighter process control and rapid response to deviations. The maturation of semiconductor technologies and the perspective of increased QCL production volumes herald a significant reduction in costs in the future. This economic shift holds the promise of making QCL-powered Mid-IR spectroscopy an accessible and standard tool for real-time, precise metabolite monitoring in microvolumes, unlocking new frontiers in cellular metabolism research and bioprocess monitoring.

^[1] Haas, et. al., "Advances in mid-infrared spectroscopy for chemical analysis." Annual Review of Analytical Chemistry 9 (2016): 45-68.

^[2] John Herpin, et al., "Metasurface – Enhanced Infrared Spectroscopy", Advanced Materials 35.34 (2023): 2110163.

CRISPR-Cas Systems

S. Del Giovane, D. Migliorelli, L. Burr, H. Altug •, A. Porchetta •*

Clustered Regularly Interspaced Short Palindromic Repeats (CRISPR)-based diagnostics have emerged as promising tool to revolutionize molecular diagnostics. Despite notable progress, challenges exist in utilizing CRISPR platforms for point-of-care (POC) applications, such as amplification steps and a focus on non-nucleic acids target detection. We propose an innovative approach, exploiting a DNA circuit, to detect antibodies with an amplification-free CRISPR-based assay.

The demand for clinical analyses in hospital is growing, and proteins and nucleic acids are the most relevant biomarker categories for diagnostics. The gold standard techniques for quantitative analysis of these biomarkers require expensive, bulky, and complicated instrumentation to use, making them inaccessible to the average end user at home.

At CSEM we are developing a novel POC platform that utilizes a CRISPR assay to detect monoclonal antibodies. The sensing method is based on a DNA circuit for the recognition of the antibody and the successive activation of the ribonucleoprotein (RNP) made of CRISPR RNA sequence and the CRISPR-associated protein (Cas) system.

The circuit used for recognition consists of four different single-stranded DNAs: 1) the translator, 2) two splits and 3) a reporter.

- 1) The translator is in a hairpin conformation. This conformation is achieved using the complementary sequence of the Protospacer Adjacent Motif (PAM) to prevent cleavage by RNP.
- 2) The splits are used to activate of the translator. They are made of the complementary sequences to the translator and are functionalized with peptide nucleic acid (PNA). The PNA is the recognition element that specifically binds the antibody of interest.
- 3) The reporter is a short single-strand DNA in a molecular beacon conformation, labelled with a fluorophore and a quencher.

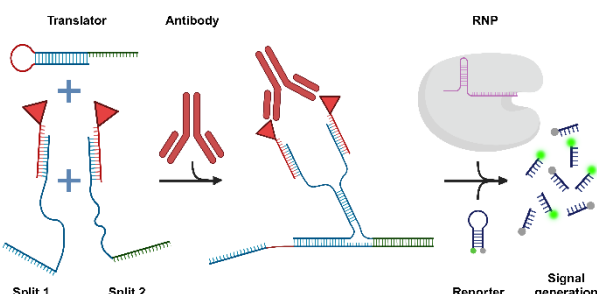


Figure 1: Assay sketch. The activation and the detection are occurring only in presence of the monoclonal antibody contained in the sample.

In our patent [1] we exploited the above-mentioned DNA circuit to activate the Cas in presence of a target antibody: when the antibody binds the recognition elements brought by the splits, it co-localizes them, starting the displacement of the translator and consequently activating it by the formation of a double-strand PAM sequence. The active translator can then recognized by the

ribonucleoprotein, initiating the cleavage of both the translator (cis-cleavage) and the reporter (trans-cleavage), and generating the fluorescent signal.

In the present work, we successfully demonstrated the concept of CRISPR-Cas system for the detection of a model monoclonal antibody: anti-hemagglutinin (α HA) from human influenza A virus. In addition, we proved that the usage of our detection system can be simplified and fastened thus indicating compatibility with its integration in future easy to use POC devices.

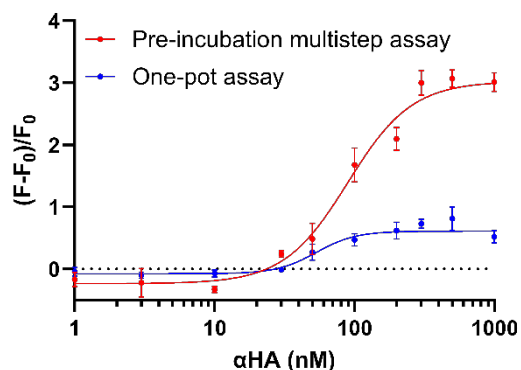


Figure 2. Calibration curves obtained from the multistep CRISPR-based assay for the quantification of the anti-hemagglutinin (α HA) monoclonal antibody. $N=3$.

Figure 2 shows calibration curves obtained for the detection of α HA. The red curve is the calibration curve obtained for a multistep assay where each component is pre-incubated and added sequentially as depicted in Figure 1. This complex process enables to obtain linear range from 27 ± 5 to 342 ± 84 nm within an assay time of 90 min. The simplified process results are depicted by the blue calibration curve. These results evidence that despite a lower sensitivity and a reduced detection range from 25 ± 6 to 136 ± 48 nM, similar detection limits could be achieved by adding all the different components: translator, splits, reporter, RNP and sample at once in a one-pot assay.

This major success paves the way for the usage of this CRISPR-Cas detection system in POC solutions. Currently ongoing work on this system relates to various topics: optimizing the assay conditions, extending the detection process to other analytes as well as translating the detection method to electrochemical process to enhance the method sensitivity, speed, and range as well as to develop a sensing method which can be produced on industrial scale and easily interfaced with electronic readout solutions.

* Bionanophotonic Systems Laboratory, EPFL, Lausanne, Switzerland.
• Department of Sciences and Chemical Technologies, University of Rome Tor Vergata, Rome, Italy

[1] "CRISPR-Cas based method for the detection of non-nucleic acid targets" P-530275-EP.

LiDAR and End-effector Technologies for In-orbit Servicing Demonstration Mission

A. Ummel, E. Bosch, S. Humbert, S. Oeschger, A. Fivaz, J. Rouvinet, L. Salamin, M. Gumy, S. Hayoz, J.-L. Helfer, G. Perruchoud, O. Rousseaux, Y. Ruffieux, C. Pache, E. Dominé

Traditionally, and with very few exceptions, space assets are placed into orbit to fulfil their purpose and decommissioned when they reach their end-of-life or when they fail. Similarly, until the first relaunch of a previously-flown Falcon 9 first stage by Space-X in 2017, launchers were single-use items. Launcher reusability transformed the space economy by making it more accessible. Applying the same concept to satellites opens new perspectives such as mega-constellation and in-orbit servicing (IOS). ESA's long-term plan regarding access to space is to change from space missions to space logistics^[1]. Space assets would be placed into the desired orbit by a series of vehicles and would become equipment to be maintained, recommissioned, and recycled. To reach that goal, many technologies are yet to be developed. In the frame of the European project EROSS^[2] (Grant agreement ID: 101082464), CSEM is two enabling technologies for IOS: a LiDAR for navigation and a GRIPPER for capture.

At CSEM, the EROSS IOD project covers two different technology developments, a LiDAR and a GRIPPER, each having its dedicated development team and partners. In Switzerland, the LiDAR is being developed in partnership with Thales Alenia Space Switzerland (TAS-CH), while the GRIPPER is being developed in partnership with ALMATECH.

LiDAR development

The flash LiDAR is based on the direct Time-of-Flight technology matured at CSEM^[3,4]. Illustrated in Figure 1, the system is composed of four MILA detectors^[5], receiver optics with a mechanical iris, pulsed laser, emitter optics, electronics, and housing.



Parameter	Value
Operational range	From 10 m to 50 m
Field of View	Square 10° x 10°
Resolution	128 x 128 pixels
Distance measurement accuracy	75 mm
Sampling frequency	Up to 10 Hz
Operating light wavelength	532 nm
Power consumption	Up to 50 W
Size	200 x 200 x 150 mm
Mass	< 5 kg
Power interface	26V to 50V
Communication interface	SpaceWire

Figure 2: EROSS LiDAR design and specifications.

The instrument is developed following a new-space approach: taking the necessary measures to ensure the item will function in space without implementing the complete space standards. Hence, the electronics design integrates high industrial quality components and a limited number of space-grade components (i.e., radiation hardened) to avoid failure propagation to the spacecraft. The targeted specifications of this LiDAR are provided in Figure 1.

GRIPPER development

The developed GRIPPER fulfils a critical function: capturing and holding the targeted spacecraft to berth it, dock it and maintain it. This gripper is designed to catch the target space by its Launch Adapter Ring (LAR). The design is compatible with various LARs and with a specific interface that will be mounted on the target spacecraft. It can accept an error in positioning of the LAR of 40 mm and 5° in all directions. The selection of technologies and materials was performed following the new-space approach and based on known heritage. The current design, illustrated in Figure 2, was optimized to avoid kinematic blocking points and reduce the loads in the transmission system.

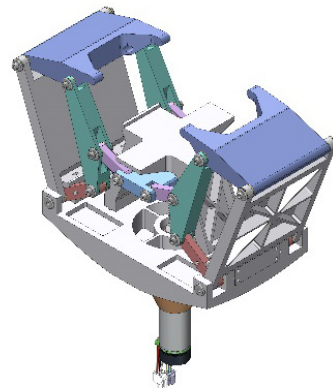


Figure 2: EROSS GRIPPER design.

- [1] Y. Tincelin, et al., 'Enabling a European In-Space Transportation ecosystem', presented at the Aerospace Europe Conference 2023 Joint 10th EUCASS – 9th CEAS Conference, Lausanne, July 2023
[2] D. Just, 'European Robotic Orbital Support Services ready for In-Orbit Demonstration', EROSS IOD. Accessed: Nov. 09, 2023. [Online]. Available: <https://www.eross-iod.com/>
[3] A. Pollini, N. Blanc, V. Mitev, 'Flash optical sensors for guidance, navigation and control systems', Advances in the Astronautical Sciences, vol. 144, pp. 503–517, Feb. 2012.

- [4] C. Pache, et al., 'Miniature Flash LiDAR for Bathymetry: An Experimental Proof-of-Concept', in 2021 International Geoscience and Remote Sensing Symposium (IGARSS), Brussels, BE, July 2021.
[5] M. Perenzoni, et al., "A 64x64-Pixels Digital Silicon Photomultiplier Direct TOF Sensor", in IEEE Journal of Solid-State Circuits, vol. 52, no. 1, pp. 151-160, Jan. 2017, doi: 10.1109/JSSC.2016.2623635.

fs-Laser System for the Repair of Defective Pixels and Defective Circuits in μLED Displays

C. Hofer, N. Torcheboeuf, C. Bonzon, S. Lecomte

The project objective was to create an ultrafast laser-based repair technology and repair machine for defective pixels and defective circuits of Micro-LED displays, a next-generation display that can be applied to AR, VR, future medical devices and consumer products. The key performance characteristics to achieve are at least 100 μJ pulse energy corresponding to 10 W of output power at a repetition rate of 100 kHz, an output beam quality M^2 under 1.4 and pulse duration below 200 fs. In this project CSEM successfully oversaw the laser system general architecture, developed an amplification stage and a nonlinear solid-state pulse compression stage and performed the characterization and testing of the system. Furthermore, CSEM realized the manufacturing, assembly, and integration of the breadboard system.

The next-generation display technology based on Micro-LED offers immense commercial potential with applications in AR, VR, future medical devices, and consumer products. So far commercial implementation has been hindered by the lack of a high-yield low-cost technology for display in-line repair. The goal of the REDULAS project is to develop a repair technology for defective pixels. The repair is performed by selective ablation and substitution of the defective component using a versatile ultrafast laser with energetic pulses having a duration below 200 fs and 100 μJ pulse energy in a good quality beam ($M^2 < 1.4$).

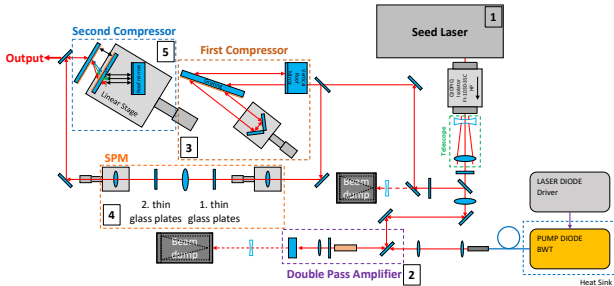


Figure 1: Shows the schematic of the laser system.

The laser system is based on a chirped pulse amplification architecture. The main components of the laser are the seed laser (1), the double pass amplification stage (2), the first pulse compression unit (3), the self-phase modulation (SPM) broadening stage (4) and the second pulse compressor (5).

In this design, SPM is employed to broaden the laser spectrum, allowing for a shortening of the pulse duration in the subsequent compressor^[1]. SPM being a consequence of Kerr non-linearity, the strength of refractive index change scales with the pulse intensity. The amplification stage and the first compressor's purpose is to produce short high energy pulses.

The seed laser beam features 5 W of average output power at 100 kHz and chirped pulses. In the amplification stage, the seed laser beam is amplified to 20 W of average power. An Ytterbium-Doped Yttria Ceramic (Yb:Y₂O₃) rod is used as gain medium. This sesquioxide was selected because of its high laser induced damage threshold and broad gain bandwidth. It is able to provide a high-power amplification, a good beam quality, and a low gain narrowing at high pump power. The amplifier is setup in a double pass configuration and is pumped with 103 W at 976 nm.

After the amplifier and the first compression stage the beam features 430 fs pulses of 183 μJ . This beam is used to feed the

two 0.6 mm glass plates of the broadening stage. In addition to the spectral broadening induced by the SPM, a strong Kerr lensing is generated; the optical design of the stage needs to account for it. The two plates are tilted at Brewster angle, such as to maximize transmission, they are positioned in a chevron configuration to cancel beam offset. The downside of using tilted plates is the introduction of an anisotropy on the far-field, see Figure 1.

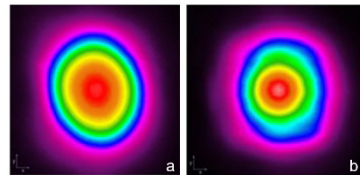


Figure 2: a) Beam profile after the amplification stage; b) Beam profile at system output.

Table 1: Summary of the measured parameters compared to the project targets.

Parameter	Target	Obtained
Output power [W]	10	16.8
Pulse repetition rate [kHz]	100	100
Pulse energy [μJ]	100	168
M^2 X-Axis []	1.4	1.36
M^2 Y-Axis []	1.4	1.30
Pulse width autocorrelation [fs]	200	193
Pulse width retrieved [fs]	200	208

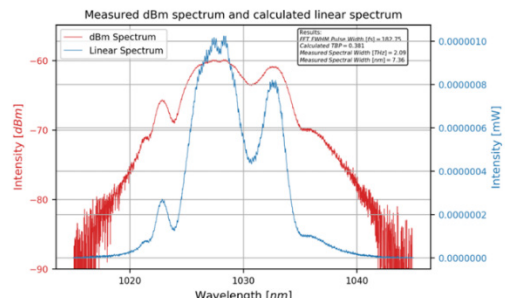


Figure 3: Laser output spectrum in linear (blue) and log (red) scales.

In conclusion, CSEM designed manufactured and delivered a laser system prototype fulfilling the requirements for Micro-LED display repair. It features an amplification stage from 5 W to 20 W average power with good M^2 and without gain narrowing and is equipped with an SPM broadening stage using a pair of glass plates to achieve sub-200 fs energetic pulses.

^[1] C. H. Lu, et al., Generation of intense supercontinuum in condensed media, Optica Vol. 1, No. 6, 2014.

Nonlinear Photonic Circuits on Lithium Niobate on Insulator for Laser Metrology and Atomic Sensors

O. Hefti, J.-E. Tremblay, A. Volpini, I. Prieto , R. Blum, H. Zarebidaki, S. Karlen, F. Droz , J. Haesler, M. Depont, H. Sattari, D. Grassani, S. Lecomte

Stable laser frequency references are of importance in many modern technologies including precise spectroscopy, LIDARs, optical clocks, metrology and telecommunications. Reducing Size, Weight and Power consumption (SWaP) will open even new opportunities both in space applications and in on-field deployment. CSEM is tackling this objective within the SNF Bridge project ENABLE, which leverages on CSEM Lithium Niobate on Insulator (LNOI) Photonic Integrated Circuit (PIC) platform and MEMS vapor cells to enable telecom laser stabilization through second harmonic generation on a two-photon rubidium transition.

Alkali atoms, like rubidium (Rb), offer narrow optical transitions and large absorption cross-sections at room temperature and can be employed as a reliable frequency reference to stabilize lasers in the near infrared. However, widely employed telecom lasers, which are important in application such as CO₂ monitoring, or frequency standard distribution over telecom fiber networks, cannot be directly referenced to such transitions. Indeed, stabilization of lasers in the telecom band usually relies on CO₂ or C₂H₂ lines [1] which show a limited absorption and require large cells or cavity, which limit their miniaturization.

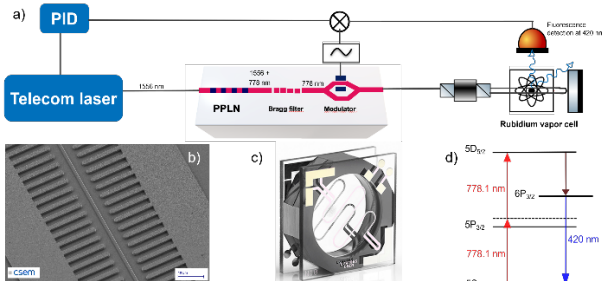


Figure 1: a) schematic of the laser stabilization set-up. b) SEM image of the LNOI waveguides with periodic electrodes for electric field poling. c) CSEM Rb MEMS cell. d) Energy diagram of the Rb two-photon transition.

In the SNF project ENABE, CSEM is developing a compact and power efficient module allowing to stabilize a telecom laser system to a Doppler-free two-photon transition of Rb exploiting two in-house technologies: atomic vapor MEMS cells [2] and LNOI PIC. The Rb MEMS cell developed by CSEM is fabricated at wafer level and has a volume of about 30 mm³. The LNOI PICs are developed at wafer level too and are offered by CSEM in Multi-Project-Wafer (MPW) runs [3]. The working principle of the system is illustrated in Figure 1. A telecom laser is frequency doubled thanks to a second harmonic generation (SHG) process within a LNOI waveguide and then locked to a Doppler-free two-photon transition in Rb. Also, the LNOI PIC can host additional element like filters and modulators. Usually, efficient SHG is prevented by phase-mismatch due to the large dispersion of Lithium Niobate crystals or waveguides. A common method to

[1] Numata, K., Chen, J. R., Wu, S. T., Abshire, J. B., Krainak, M. A., "Frequency stabilization of distributed-feedback laser diodes at 1572 nm for lidar measurements of atmospheric carbon dioxide", Appl. Opt. 50, 1047–1056 (2011).

overcome this issue is by Quasi-Phase-Matching (QPM), which consists in periodically reversing the direction of the nonlinear domains of the material. The efficiency of the process inversely depends on the area of the optical modes, and LNOI waveguides can in principle be hundreds of times more efficient than bulk crystals and tens of times more efficient than large mode area waveguides. However, periodic poling is still not commercially available neither well-established in the LNOI platform.

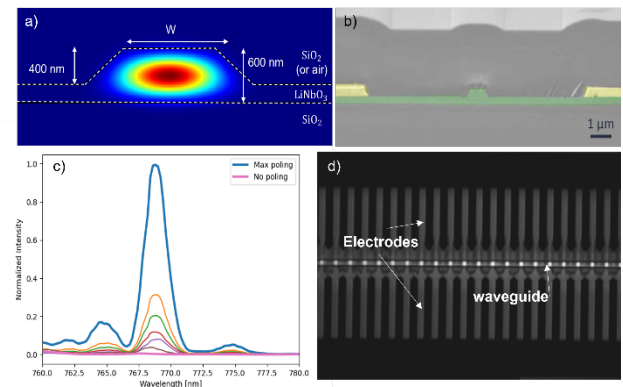


Figure 2: a) Simulated mode profile and b) SEM cross section of the LNOI waveguide c) second harmonic signal detected for different poling iterations. d) Two-photon microscope image of the poled waveguide. Dark regions indicate inversion of the domains due to electric field poling.

At CSEM we are developing periodic poling on LNOI waveguides by simulating their nonlinear response and QPM period, while poling is carried out identifying suitable strong electric pulses that are applied across the waveguides. So far, the achieved normalized SHG efficiency is about 1000% / Wcm² and, although this value is already well-above the data reported in commercial structures, further optimization is ongoing to improve the uniformity of the poling to get closer to the theoretical value and its repeatability.

The project partner is EPFL – Photonic System Laboratory. This work is funded by Swiss National Science Foundation (SNSF) (194693). CSEM thanks them for their support.

[2] S. Karlen, J. Gobet, T. Overstolz, J. Haesler, S. Lecomte, "Lifetime assessment of RbN₃-filled MEMS atomic vapor cells with Al₂O₃ coating", Optics express 25 (3), 2187-2194 (2017)

[3] J. Leo, et al., "Wafer-scale fabrication of low-loss waveguides in lithium niobate on insulator (LNOI) integrated photonics platform," in European Conference on Optical Communication (ECOC) 2022

Electro-optic Laser Frequency Comb for the NIRPS Spectrograph Calibration

E. Obrzud, L. Bischof, L. Beltran, S. Denis, N. Torcheboeuf, C. Hofer, C. Bonzon , S. Lecomte

Exoplanet detection by the measurement of stellar radial velocity is a method that sparked the interest of astronomers and eventually granted the Nobel prize to D. Queloz and M. Mayor. A signature of a planet orbiting its host star can be tracked with astronomical spectrographs by measuring minute shifts in stellar optical spectra over time. Therefore, astronomical spectrographs require precise (and in some cases absolute) wavelength calibration. CSEM's laser frequency comb (LFC) technology^[1] provides a broadband, extremely stable and accurate light source for astronomical spectrograph calibration. Such a laser frequency comb was setup in the La Silla observatory, Chile, on the 3.6 m telescope for calibration of the NIRPS^[2] spectrograph.

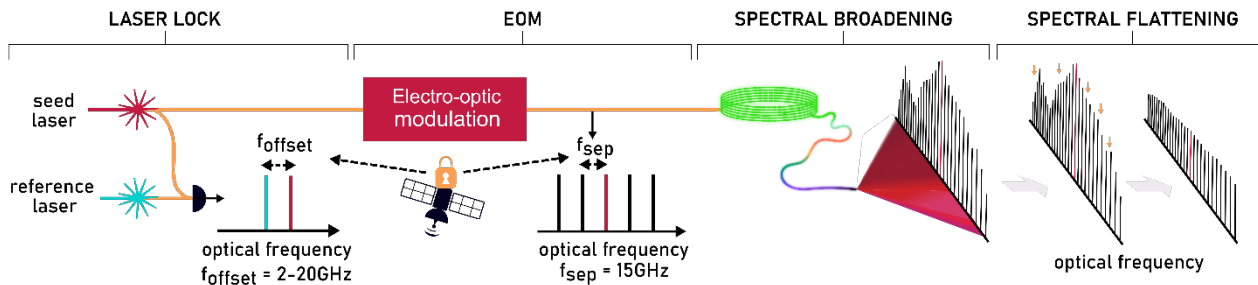


Figure 1: Schematic of the laser system, split in four main functional parts. EOM – electro-optic modulation.

Almost three decades after the first discoveries, the field of precision astronomical spectroscopy and radial velocities is thriving: there are more than 25 active spectrographs, which contributed to the discovery of over 5000 exoplanets as of 2022, and which continue examining exoplanet atmospheres and probing fundamental physics. LFCs, producing a dense grid of equidistant optical emission lines, are considered the best calibration sources for precision astronomical spectrographs. The Astronomy Department of the University of Geneva has contracted CSEM to develop and install an optical calibration source for the NIRPS spectrograph^[2].

In this project, CSEM designed and developed the laser system as sketched in Figure 1. The system is composed of four functional parts: laser lock, electro-optic modulation (EOM), spectral broadening and spectral flattening. The frequency stability of the system is ensured by a 1542 nm reference laser stabilized to an acetylene optical transition. The seed laser, offset-locked to the reference laser, can be tuned over the frequency range of 18 GHz (allowing for a tuning of the full LFC by 1.2 times the line separation frequency). Then, the seed laser feeds a cascade of 3 electro-optic modulators, operating at 15 GHz, producing an initial 6 nm-bandwidth comb. Both the optical reference as well as the RF electronics are disciplined by a 10 MHz reference GNSS signal. Next, the optical pulses are formed by a dispersion compensation module, amplified, and sent to a chain of carefully tailored optical fibres for further compression of the optical pulses and finally the spectral broadening. As a result, a frequency comb spectrum extending from 1060 nm to 1830 nm is produced (Figure 2). Due to a high dynamic range of the optical spectrum, the light undergoes spectral flattening to provide a constant intensity over the full wavelength range. The flattening device, designed and assembled in CSEM, consists of a free-space static flattening through optical filters as well as a dynamic flattening assembly based on a LCOS spatial light modulator (SLM). The latter is

achieved by inducing a phase shift as a function of wavelength on the SLM what results in redirecting a part of the beam with a desired intensity into the output fibre. The flattening unit achieves a uniform spectrum over the full wavelength range with a dynamic range of < 4 dB for 95% of the optical spectrum span (Figure 2).

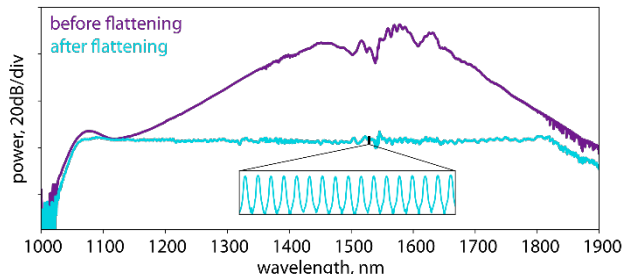


Figure 2: LFC spectrum before and after the spectral flattening (RBW = 0.5 nm). The inset shows a zoom-in to a part of the spectrum spanning 2 nm (RBW = 0.05 nm).

The whole system was assembled in a temperature controlled 2m high, 1m deep 19" rack. The system is fully automated; given the remote location of operation, all vital parameters of the system are continuously monitored. Error flags are implemented to assure a smooth operation and a rapid problem resolution and maintenance if needed. The user will be able to probe all spectrograph pixels by sweeping the offset frequency between the reference and the seed laser, shifting the whole LFC spectrum over a range exceeding the separation frequency. The LFC is characterised by a temporal spectral stability within $\pm 10\%$ at any wavelength over 24h and the fractional frequency accuracy under 2×10^{-10} over the full spectral range. The system achieves a fractional frequency stability of less than 10^{-13} after 10s.

The installation of the system is on-going and will be accomplished by the end of 2023.

^[1] E. Obrzud, et al., “Broadband near-infrared astronomical spectrometer calibration and on-sky validation with an electro-optic laser frequency comb”, Optics Express Vol. 26, Issue 26, pp. 34830-34841 (2018).

^[2] F. Bouchy, et al., Near-InfraRed Planet Searcher to Join HARPS on the ESO 3.6-metre Telescope, The Messenger (2017).

Test and Characterization of Photodiodes for the Earth Observation TRUTHS Mission

A. Ummel, L. Karlen, L. Bishof, S. Denis, S. Lecomte

In the context of global warming, getting accurate and calibrated measurements of the Earth's climate is paramount to understand and possibly predict extreme weather events. Toward that goal, ESA is leading the TRUTHS mission: "The Traceable Radiometry Underpinning Terrestrial- and Helio-Studies, as a 'laboratory in space', setting the 'gold standard' reference for climate measurements.". As part of the preliminary studies led by the mission Prime contractor, AIRBUS UK, CSEM has assessed the performance and resilience of various photodiodes as potential calibrated radiometric measurement sensors.

To assess the compatibility of the photodiodes to the TRUTHS mission, CSEM tested 5 different types of photodiodes against various representative environmental conditions. The performance of each photodiode was measured and compared before and after such environmental tests. Figure 1 gives the overall test campaign workflow. In this figure, the blue numbers provide the quantity of photodiode tested for each of the 5 types.

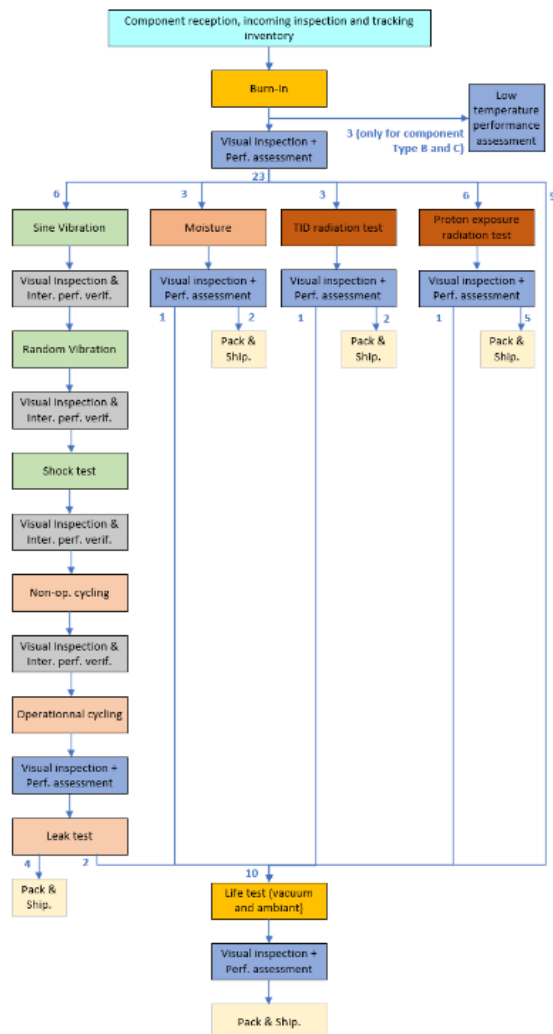


Figure 1: Test campaign workflow.

The complexity of this test campaign lies within two constraints:

- The great number of components tested: about 150 photodiodes. This required methodical and automated test procedures and data processing to mitigate the risk of human error.
- The stringent requirement for performance measurement accuracy and stability onto photodiodes of two different technologies (InGaAs & Silicium): This led to the conception of two performance test benches (Figure 2 and Figure 3), which were thoroughly characterized before the actual test campaign.

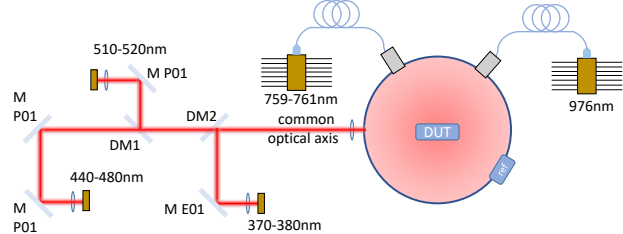


Figure 2: Performance measurement setup for Si Photodiode.

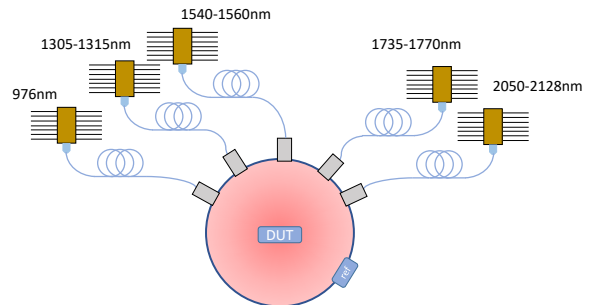


Figure 3: Performance measurement setup for InGaAs Photodiode.

Such a test campaign was successfully carried out. Most components survived the complete test sequence. The radiative environments seemed to have the largest effect on the components performance as revealed by the Total Ionizing Dose (TID) and Total Non-Ionizing Dose (TNID) tests.

Regarding the TID test, the following observations were made: all Si photodiodes show degradation in the responsivity for different wavelengths. The responsivity of InGaAs photodiodes is less impacted. The linearity and stability of photodiodes are not impacted by radiation. An increase in dark current is observed in the bias measurement for two out of three types of Si photodiodes.

Regarding the TNID test, the following observations were made: all Si photodiodes show a degradation in the responsivity and linearity and, in most cases, an increase in the dark current is observed. InGaAs photodiodes prove to resist way better but still show an increase in the dark current of the components.

Some performance recovery was also observed on irradiated components that underwent lifetime test: a response recovery was seen on Si photodiodes after TID test and a small linearity recovery can also be observed on Si photodiodes after TNID test.

WAVEGUIDE – Custom Voice Coil Actuator for Flexure-based Electromechanical RF Switch

D. Grivon, M. Gumi, E. Onillon

Radio-frequency (RF) switches are commonly used in telecommunication satellites to route high frequency signals through different transmission paths. In electromechanical switches, the rotor is moved between stable angular positions using a direct current (DC) motor. The rotating parts are sustained using ball bearings which may suffer from reliability in space. To overcome the well-known drawbacks of ball bearings while avoiding the use of special bearings, ALMATECH proposed to replace them with bistable compliant mechanisms. Nevertheless, conventional motors have high radial reluctant forces which prevent their use as actuators for compliant mechanisms. Consequently, CSEM has designed an actuator to minimize the impact of radial forces and adapt to the bistable flex mechanism.

The usually preferred actuating solution for flexures-based mechanisms are Voice Coil Actuators (VCA) because their actuating principle, which relies on the Lorentz' force, minimizes the parasitic forces, i.e., the forces arising in any direction other than the motion direction. This is particularly important because compliant mechanisms suffer from low transversal rigidity, especially close to the end of their motion stroke. Commercially available VCA have usually a topology with a large transversal (orthogonal to the rotation axis) footprint, to maximize the output torque and are rarely compliant with space requirements. For these reasons, a custom design has been developed by CSEM (in the frame of an ESA activity) to build a slender VCA (having a footprint $\leq 38 \times 38$ mm) able to provide up to 54 mNm of output torque when supplied with 500 mA, with an angular stroke of $\pm 45^\circ$ and for an operating temperature range of -35° to +75°C. Figure 1 shows a cut view of the actuator CAD model and Figure 2 displays the assembled EM of the VCA prior to be integrated in the RF switch.

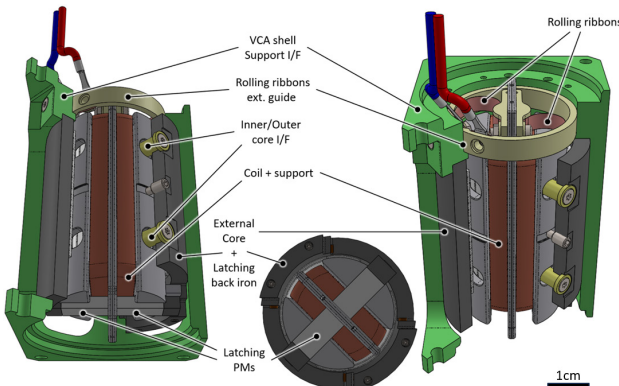


Figure 1: Cut view of the CAD model with main constitutive elements.

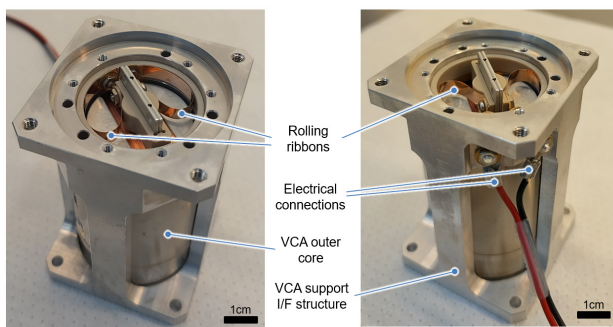


Figure 2: Assembled EM model of the VCA.

As introduced, the designed actuator must interface with a bistable compliant mechanism with a radial rigidity of ≈ 10 N/mm for which the maximum allowed lateral shift is in the order of ≤ 15 μm . This means that in the worst-case scenario, the maximum radial force would be ≤ 0.15 N. A particular disposition of the magnets on the two sides of the actuator airgap has been used to maximize the radial distribution of the magnetic flux and

minimize its tangential contribution. Figure 3 shows the expected distribution of the radial forces and the associated radial displacement: the maximum simulated parasitic force is < 80 mN with corresponding lateral displacement < 8 μm .

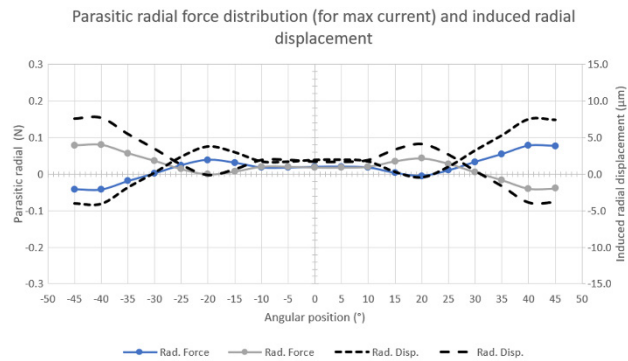


Figure 3: Parasitic radial forces and induced lateral shifts on the pivots.

To validate the design of the VCA the output torque has been measured (Figure 4), with a maximum relative error w.r.t. the simulation results below 7%.

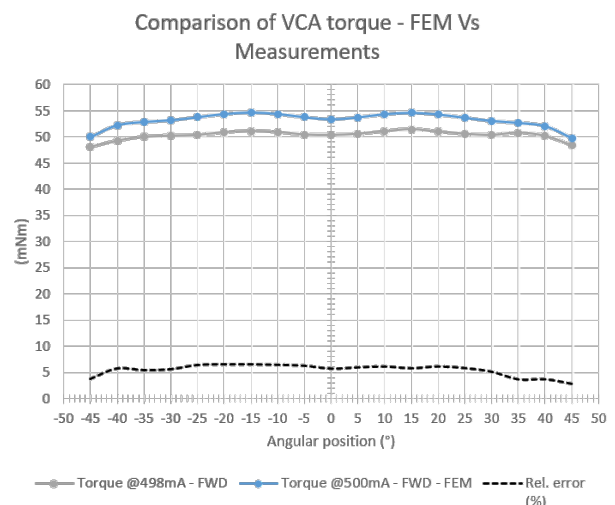


Figure 4: Measured torque Vs FE simulation results.

Two engineering models were manufactured and assembled and are currently at ALMATECH premises for the final integration. Random, shock, thermal and lifecycles tests are planned for the beginning of 2024.

SUSTAINABLE ENERGY

Christophe Ballif

The **Sustainable Energy**'s priority research at CSEM is the urgent issues of increasing usage of clean energy and reducing CO₂ emissions. This program consists of two key initiatives: renewable photovoltaic energy development and energy storage and digital management.

This research priority leads the way in promoting a clean-tech society. It strives to have a substantial impact on the development of Swiss solar energy products, autonomous (self-reliant) energy and storage solutions, and the overall efficiency and sustainability of the energy sector.

Renewable photovoltaic energy development

Through advanced photovoltaic (PV) technologies, this initiative harnesses sun power. It conducts extensive research and development on solar cells and modules, integrated and lightweight PV systems, and new materials and technologies that enhance the efficiency, integration, and lifetime of solar components. It innovates in advanced large-scale solar modules for the mainstream market, in architectural applications and in smaller, flexible formats for wearables and IoT devices.

Solar Cells & Modules: This area focuses on developing crystalline silicon and next-generation perovskite/silicon cells and modules. The goals are to improve reliability and reduce the cost, as well as optimize the use of expensive raw materials. The team also strives to maintain high efficiency and stability in tandem devices with perovskite under field conditions. Automated life-cycle analysis tools allow us to quickly evaluate the environmental impacts of these technologies.

Integrated and Lightweight PV: This area develops glass-based and lightweight, glass-free solar modules for various applications, such as transport and telecommunication. The emphasis is on using advanced materials to enhance durability and aesthetics and integrating them into different structures to both increase local electricity generation and lower CO₂ emissions. A full palette of PV solutions, with all levels of weight, color, and/or mechanical properties can be adapted to customer needs.

Energy storage and digital management

This undertaking explores the vital aspects of storing and managing energy produced from renewable sources. It aims to develop and/or support battery technologies, digital energy solutions, and intelligent management systems. It encompasses efforts to improve battery performance and lifespan, the integration of digital technologies to optimize energy distribution, and the development of smart systems that ensure efficient and sustainable energy usage.

Digital Energy: This area transforms energy conversion and distribution through connectivity, data, analytics, and artificial intelligence, it improves system resilience and efficiency by using graph machine learning for data processing and forecasting, learning-based control for energy optimization (conversion and distribution), and secure delivery for privacy and cybersecurity. These efforts are crucial for handling the complexity of distributed energy resources or sinks like PV and wind turbines or batteries.

Batteries: This area focuses on electrochemical storage. The research covers the whole battery value chain, with a focus on high-energy-density anodes, solid-polymer-electrolytes, advanced battery models, and intelligent management systems. The goal is to enhance battery safety, lifespan, and efficiency, with less environmental impact, to support the growing needs for grid management and electric mobility.

Adding a Perovskite Thin Film on Silicon for the Next Generation of High-efficiency Photovoltaic Modules

F. Sahli, X.Y. Chin, A. Paracchino, D. Jacobs, F. Saenz, R.A. Zanotto Razera, M. Dussouillez, J. Walter, M. De Bastiani, L. Champault, A. Theytaz, J.-D. Decoppet, Q Jeangros

Perovskite/silicon tandem solar cells have been identified as the most promising technology to increase the efficiency of photovoltaics beyond the performance limit of the silicon modules currently produced industrially at the TW-scale. As the only type of device structure currently available exhibiting both high power conversion efficiency and (potentially) competitive manufacturing costs, perovskite/silicon tandem solar cells are now included in the roadmaps of many industrial actors active in the field of photovoltaics. Through public and industrial projects, CSEM is focusing on the development of materials and manufacturing processes to demonstrate high-efficiency perovskite/Si tandem solar cells and (mini) modules exhibiting long operational stability to bring this new technology closer to commercialization.

The addition of a perovskite thin-film solar cell on the front side of a commercial silicon solar cell promises power conversion efficiencies beyond the theoretical efficiency limit of silicon photovoltaics, which sits at around 29.5%. Advantageously, the cost of adding this perovskite solar cell to form a tandem device should be diluted at the system level by balance-of-system components, making the approach attractive from a commercial perspective. The technology is predicted to enter the market in the coming years. However, critical challenges still need to be solved to make this technology an industrial success. First, perovskite deposition methods compatible with high throughput production should be developed to ensure low manufacturing costs and, second, the operational stability of the perovskite top-cell should be significantly improved to match current standards in the field of photovoltaics (>25 years).

CSEM activities on the topic are focusing on the development of materials and thin-film deposition methods to manufacture high-efficiency 2-terminal perovskite/Si tandem solar cells. More precisely, CSEM is focusing on two classes of deposition methods to deposit the perovskite absorber: i) 1-step solution-based coating methods and ii) hybrid 2-step processes, where a thermally evaporated template layer featuring the inorganic precursors is converted to a perovskite phase after the solution-based coating of the organic precursors and a subsequent annealing step. Activities are focusing on the optimization of the ink chemistry, deposition conditions and on the introduction of passivation interlayers to increase the performance of the solar cells. The open circuit voltage (V_{oc}) of the perovskite top cell now reaches values above 1.25 V thanks to the development of passivation interlayers, translating to 1-cm² tandems with a $V_{oc} > 1.95$ V and efficiencies on the order of 32%. The perovskite and some of its neighboring layers are produced by spin coating in these small devices, a method enabling a fast screening of the experimental space but that is not compatible with the manufacturing throughput requirements of the photovoltaic industry. CSEM is now developing scalable thin-film deposition techniques to produce the same stack of materials, but this time using a process flow compatible with the requirements of the photovoltaic industry. Figure 1 (right picture) shows a full-area perovskite/Si tandem produced solely using industrially applicable deposition methods.

CSEM is also developing electrode layers compatible with industrial production requirements. Notably, CSEM developed a Ag paste screen-printing process compatible with the low thermal budget of the perovskite top cell to replace the thermally evaporated grid of small-scale record prototypes. This Ag screen-printing process enables scaling up the active area of the devices with minimal series resistance losses. This industrial process is used in 4-cm² devices, where the efficiency now

reaches >30% at CSEM (Figure 1, left), and also full-size tandems (Figure 1, right). Smaller devices reported in literature usually employ a metal grid thermally evaporated through a shadow mask, a process inapplicable to industry due to higher costs.

CSEM is also investigating the module integration of perovskite/Si tandem solar cells. Research efforts are now focusing on the development of interconnection and encapsulation processes compatible with the low thermal budget of the perovskite film. Interconnection and lamination materials and processes have been validated with small-scale tandem prototypes. The next steps now involve replicating these results with devices of industrially relevant dimensions.

CSEM is also actively investigating the reliability of perovskite/silicon tandem solar cells through various stability testing procedures, including damp heat, thermal cycling, light soaking and other accelerated aging conditions set up to reveal the failure modes of perovskite solar cells. The tandems of CSEM pass the IEC 61215 damp heat and thermal cycling test criteria (<5%rel loss in efficiency after 1000 hours at 85°C in 85% relative humidity and <5%rel loss in efficiency after 200 thermal cycles from -40 to 85°C, respectively). Efforts are now focusing on improving the light soaking stability of perovskite/silicon tandem solar cells at elevated temperatures, the key challenge to solve for commercially viability.

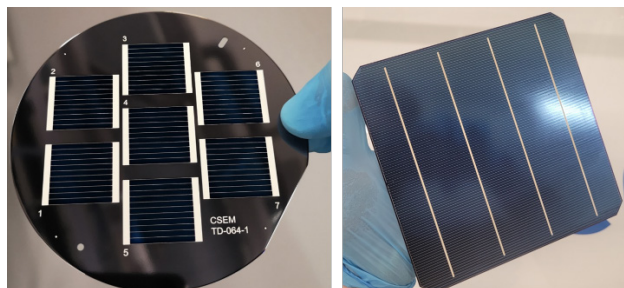


Figure 1: Tandem prototypes developed at CSEM project: (left) 4-cm² perovskite/Si tandems co-processed on a 4-inch silicon wafer, and (right) full-size M6 perovskite/silicon tandem solar cell.

Acknowledgements: this work is notably supported by the Swiss National Science Foundation grant 200021_197006 (PAPET); the European Union's Horizon 2020 research and innovation program under Grant Agreement No. 861985 (PerocUBE); the Swiss State Secretariat for Education, Research and Innovation (SERI) under contract numbers 22.00413 (PEPPERONI), 22.00369 (VALHALLA), 22.00319 (TRIUMPH).

PILATUS Project – Highly Reliable Silicon Heterojunction Tunnel Interdigitated Back Contact Solar Cells and Modules

J. Champliaud, L. Marthey, L. Baume, M. Despeisse, J. Zhao, B. Paviet-Salomon, G. Nogay*, D. Lachenal*

The PILATUS EU project focuses on industrializing silicon heterojunction tunnel interdigitated back contact (HJT-IBC) modules, and within this framework CSEM has successfully achieved the development of highly reliable PV module with Smartwire technology. The developed bill of materials (BoM) demonstrates an outstanding reliability by passing more than 8 times the IEC standards in several accelerated ageing testing and sequential testing. These results are promising for the next generation of Meyer Burger (MB) commercial product.

The tunnel HJT-IBC, an innovative patented solar cell technology developed through a collaboration between CSEM and EPFL and then industrialized by Meyer Burger (MB), represents the next generation in PV energy. With remarkable efficiency certified at more than 25.4%, HJT-IBC can outperform prior generation of HJT. Notably, this cutting-edge technology streamlines the manufacturing process, requiring fewer steps than other IBC technologies. This simplified approach is a major production advantage. Besides it allows for maximum device voltage, and hence improved temperature coefficient and low illumination behavior.

The ultimate objective of the PILATUS European project is to establish production lines for HJT-IBC cells and modules including smartwire connection technology. CSEM PV module team is dedicated to developing the BoM of the module. The aim is to enhance the module (Figure 1) reliability, simultaneously reduce costs, and incorporate European materials.

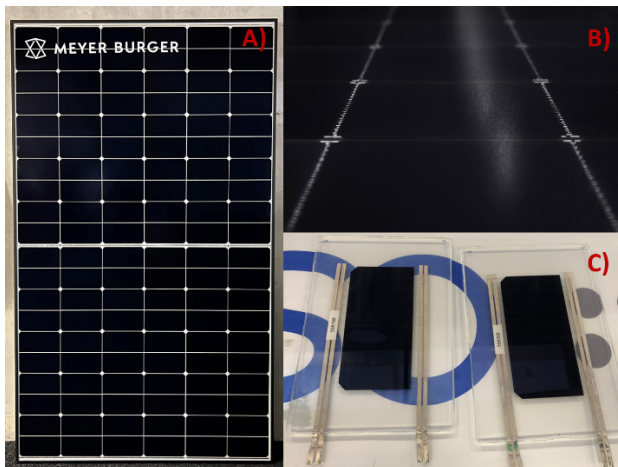


Figure 1: HJT-IBC modules. A: module with 120 1/2 cells; B: full cells module with Smartwire interconnection; C: examples of one 1/2 cell modules for BoM development.

HJT-IBC modules BoM development is based on the manufacture of one cell modules (Figure 1C) and their reliability testing. Modules are subjected to IEC standards accelerated testing. They go through damp heat (DH), thermal cycling (TC), humidity freeze (HF) and UV exposure (UV). After degradation a module must show an efficiency loss lower than 5%.

Our strategy involves the analysis of materials and investigation of degradation mechanisms. It is also characterized by continuous exchanges between MB and CSEM, emphasizing the impact of the cell structure on the module reliability.

* Meyer Burger, Switzerland

The SIRIUS project funded by Innosuisse previously resulted in stable BoMs. Their reliability was then challenged in PILATUS by extended testing to verify if any sudden non-acceptable failure modes were occurring (Figure 2). Glass/Backsheet (GB) and Glass/Glass (GG) modules were investigated.

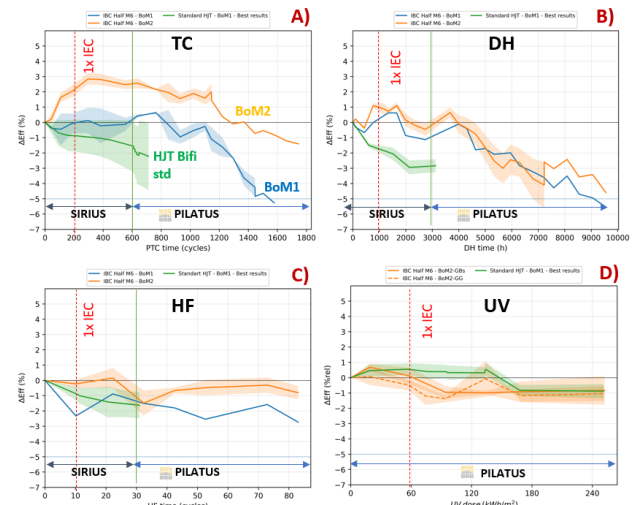


Figure 2: Modules performance loss in extended reliability testing on HJT-IBC technology. A: in TC; B: in DH; C: in HF, D: under UV.

Thanks to a close collaboration between MB and CSEM, HJT-IBC modules achieved an astonishing ultimate reliability, passing all tests performed so far without degradation to the following levels as of today aging tests status:

- More than 9 times IEC in TC
- 9 times IEC in DH
- 8 times in HF
- 4 times in UV

Moreover, these results show an improved reliability compared to standard HJT modules and to any modules ever evaluated over the past decade in CSEM.

Additionally, a variety of degradation tests were sequentially applied to a single module. This sequential testing aims to identify potential failure modes that may occur when modules are exposed to diverse environmental conditions. For instance, the module efficiency remains stable when exposed to HF after DH and when exposed to DH after TC.

Recent Developments of the Plastics Compounding Platform

H.-Y. Li, M. Roten, J. Escarré, M. Despeisse

The compounding platform at CSEM has been expanding its capacity in the recent years for the development of customized polymeric material formulations deployed in PV modules. A number of the materials developed with the platform are used for specialty PV applications or have been transferred to the industrial partners and are under commercialization process. The materials synthesized from the platform also contribute to the root cause analysis of the degradation of the PV modules with novel cell/interconnection technologies. The growing expertise at the compounding platform reassures the position of the CSEM as a unique R&D partner in the field of PV module technology.

A PV module mainly consists of a front cover, stringed cells and a back cover, bonded with two layers of polymeric adhesive film, commonly referred as the encapsulant. In 2022, about 40% of the modules are equipped with a multi-layered polymeric backsheets. Meanwhile, EVA accounts for 42% of the market, while POE together with EPE takes about 35% of the market share. In very recent years, the module industry has outspread its R&D activities from the longstanding needs of trimming down the leveled cost of PV electricity by cost reduction and lifetime prolongation to improving the adaptability of PV modules into diverse application scenarios, e.g., BIPV (building integrated PV), VIPV (Vehicle integrated PV), PIPV (Product integrated PV), etc. To cater with this growing demand, the plastics compounding platform at CSEM focuses on the development of polymeric materials for PV modules, including encapsulants, backsheets, frontsheets and other functional polymeric layers.



Figure 1: Main equipment available at compounding platform. a) lab compounding line; b) lab cast film line; c) pilot compounding line; d) pilot cast film line.

Recently, thanks to the success of technology transfers, CSEM has expanded the infrastructure available in the plastics compounding platform. At the moment, the platform includes mainly the following facilities (see Figure 1):

- Dr.COLLIN TEACH-LINE twin-screw compounder ZK 25 x 24 L/D equipped with a single strand pelletizer (max. throughput: 4.0 kg/h).
- Dr.COLLIN Single-Screw cast film extrusion line 25mm Φ x 25 D Type E 25E, capable of producing foils with width up to 18 cm wide (max. throughput: 10.0 kg/h).
- Pilot twin-screw compounding line equipped with underwater pelletizer (max. throughput: 20.0 kg/h).
- Pilot cast film extrusion line equipped with two extruders (50/35, 45/35), capable of producing foils up to 3 layers with usable width up to 50 cm (max. throughput: 40.0 kg/h).

- Material analysis facility (DMDR, TGA-DSC, FTIR, Raman, UV-Vis-Nir, Karl-Fischer Titration, Melt index meter, platen vulcanizer, high-speed mixer). In 2023, we also expanded to LC-/GC-MS through partnership.
- Accelerating lifetime testing facilities: climate chambers for damp heat, thermal cycling, humidity freeze, UV+ damp heat; UV chamber; Ovens; highly accelerated damp heat testing setup (high-pressure cooker test).

In addition, the platform has also built the infrastructure to develop wet coating formulations in the lab scale and has external partners for upscaling trials.

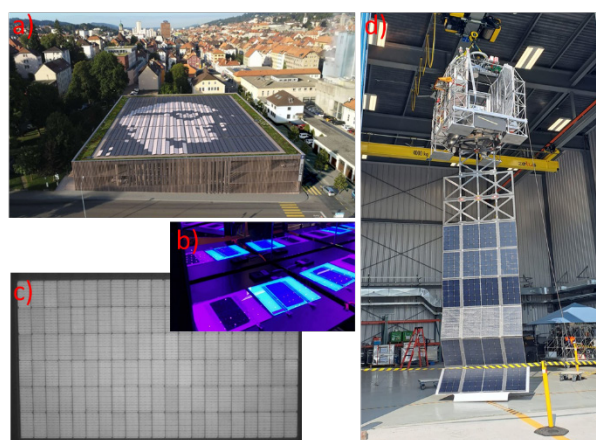


Figure 2: Examples of ongoing R&D and prototype production topics on the plastics compounding platform at CSEM.

Examples of ongoing R&D topics in 2023 are listed below:

- The coloured encapsulant technology (Figure 2a) transferred to SOLAXESS SA, which aims at transforming standard PV modules into coloured modules, is being upgraded into new generation with improved processability in modules with different configurations manufactured in (semi-) automated line.
- Encapsulant formulations with wavelength-converting capabilities (Figure 2b) are being developed for boosting the power output of standard modules and for agrivoltaics.
- In addition to industrialization of the developed formulation for conventional PV modules, new formulation are being developed which aims at coping with emerging cell and metallization technologies (Figure 2c).
- Specialty adhesive formulation (Figure 2d) has been developed and applied for various types of PV-integrated devices traveling in stratosphere.

Progress of Copper Metallization at CSEM

A. Lachowicz, N. Badel, A. Barrou, J. Zhao, B. Paviet-Salomon, C. Ballif

Replacement of silver for metallization of solar cells is essential for the deployment of PV and for facilitating the transition to 100% renewable energies. CSEM has developed a reliable, simple, and cost competitive process for copper electrodeposited metallization for heterojunction cells, which has attracted attention of several world's largest solar cell manufacturers. For TOPCon cells - the second future mainstream cell technology beside heterojunction - a novel copper plating process, advantageously enabling the application of very thin passivating layers is currently being developed.

Due to the tremendous quantity of solar cells required for the energy transition, the availability of materials, especially silver, poses a significant challenge [1]. The annual production volume is projected to exceed 1 terawatt in the coming year. With a power of 10 Watt per cell, this translates to 100 billion cells per year. Even a small silver consumption of only few mg per watt amounts to a cumulative demand of thousands of tons, surpassing more than half of the overall global silver supply.

The current technology for solar cell metallization involves screen printing of a silver particle paste. A direct substitution of silver with copper paste is not feasible due to high line resistance. However, printed copper lines reinforced with electrodeposited copper demonstrate excellent conductivity.

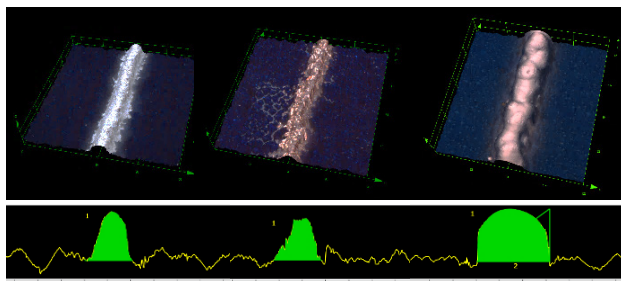


Figure 1: Seed-grid lines formed by PTP: silver-coated-copper paste (SCC), Cu-paste and Cu-paste with electrodeposited copper.

Table 1: Seed-grid line dimensions and resistance.

Line	Unit	SCC paste	Cu paste	Cu paste + plated Cu
Width	µm	18.9	21.5	25.0
Height	µm	10.3	9.3	17.6
CS area	µm ²	116	102	335
Resistance	Ω	1.5	5.1	0.2

The CSEM process (originally invented at EPFL) comprises only 3 steps: seed-grid printing, deposition of a dielectric layer, and plating. The addition of a dielectric (masking) layer enables a reduction in the thickness of ITO, resulting in decreased consumption of Indium, another scarce material. The process is self-aligning: the rough surface of the seed-grid leads to voids in the masking layer, while the layer tightly covers the ITO-area in between grid lines. Consequently, copper is selectively deposited only on grid positions. Good module stability has been confirmed for Smartwire® as well as for shingle interconnection, with excellent stability in thermocycling (>600 cycles) and good

resistance to damp-heat up to 2000 hours, even without edge sealing [2]. Pattern-transfer-printing (PTP) has enabled to realize narrow and high aspect ratio copper lines. The same efficiency level as with standard silver paste has been reached only with a pure copper seed-grid reinforced with electrodeposited copper, i.e., silver has been entirely eliminated while maintaining the cell performance. Following the interest of solar cell manufacturers, process samplings are currently in progress.

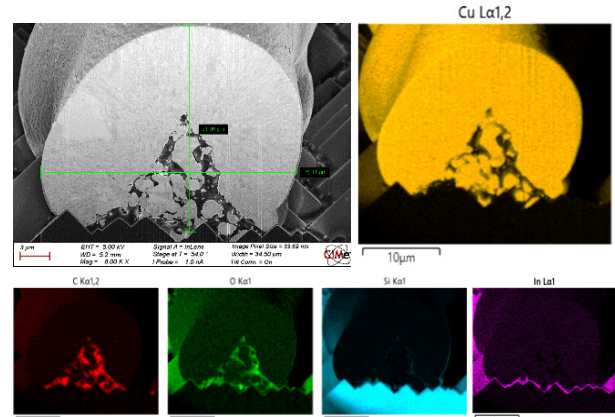


Figure 2: Ion beam cross section and EDX analysis of a line formed by pattern-transfer-printing and reinforced with electrodeposited copper. Line dimensions: width 26.1 µm, height 21.9 µm.

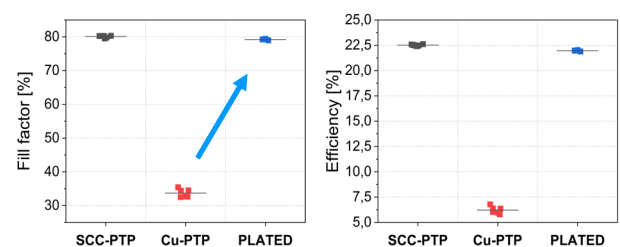


Figure 3: Fill factor and efficiency comparison of SCC-paste, Cu-paste and Cu-paste with plated Cu on M2 industrial heterojunction precursors.

For cells with poly-Si passivating contacts a novel plating process is being developed in collaboration with EPFL, JR, PCCL and Kalyon-PV within the project COMET, led by CSEM. Low contact resistance has been demonstrated on high quality poly-Si layer of only 20 nm thickness. Such a thin layer is advantageous for cell performance and enables to save process time and costs.

This work has received funding from the EU, project Resilex (GA 101058583) and from the SFOE, project COMET (SI/502483).

[1] P. Verlinden, Future challenges for photovoltaic manufacturing at the terawatt scale, *J. of Renewable and Sustainable Energy*, 2020

[2] A. Lachowicz, et al., Aging tests of mini-modules with copper-plated heterojunction solar cells and pattern-transfer-printing of copper paste, *EPJ-PV*, Special Issue EU PVSEC 2023

New In-house Tool for Rapid and Automated Life Cycle Assessment of Photovoltaic Systems

A. Barrou, S. Kandiyoti-Eskanazi, J. Levrat, C. Ballif, B. Paviet-Salomon

Life Cycle Assessment (LCA) methodology is relevant to evaluate the environmental footprint of energy production devices, such as Photovoltaic (PV) systems and helps to define eco-design strategies to lower their impacts, such as lifetime extension or material optimization. However, the LCA methodology is time consuming and needs a strong expertise to be used properly. To overcome this challenge, CSEM developed a user-friendly internal tool connected to its PV module database that automatizes LCA of PV systems and does not require any LCA expertise for the user. By including parameters variations, this fast-way LCA allows to rapidly evaluate the environmental footprint and develop strategies to reduce the impacts of PV products developed by CSEM in European and industrial projects.

The installed power capacity of solar photovoltaic (PV) systems is anticipated to surpass that of coal before 2027, on its route to become the major electricity source [1]. Life cycle assessment (LCA) methodology emerges as a crucial tool for evaluating the environmental impact of PV systems, where most of their impacts stem from the manufacturing phase, with minimal impact from end-of-life activities and virtually negligible emissions during its operational lifespan [2]. LCA does not only allow for a comprehensive evaluation of environmental footprints but also facilitates the formulation of eco-design strategies. These strategies aim at reducing impacts, emphasizing the extension of product lifetimes and material optimization. However, despite its advantages, the conventional application of LCA faces challenges such as being time-consuming and requiring specialized expertise.

In response to these challenges, the primary objective was to develop a user-friendly internal tool for LCA at CSEM. This tool, connected to the PV module database, aims to automate the LCA process for PV systems. The key focus is on creating a solution that is not only fast but also easily accessible, eliminating the need for specialized LCA expertise.

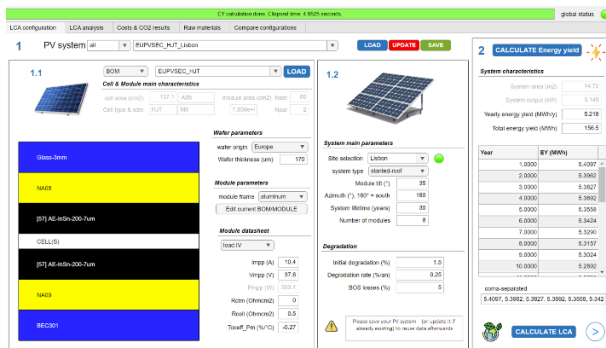


Figure 1: LCA tool software illustration.

The LCA tool follows a structured LCA methodology and can be used with a user-friendly interface (see Figure 1). In the initial step, the PV system is defined, encompassing the module and associated parameters linked to the CSEM's module database. The module Bill of Materials (BOM) and key system parameters, such as site selection, module orientation, and degradation rates are specified and, by using HETSIM software (developed at CSEM), the output power of the PV system is estimated. Finally, the LCA impact is calculated by utilizing previously detailed data. The automated processing, facilitated by an SQL code, produces within seconds tables and plots in the tool's interface, providing a detailed overview of the PV system's environmental footprint.

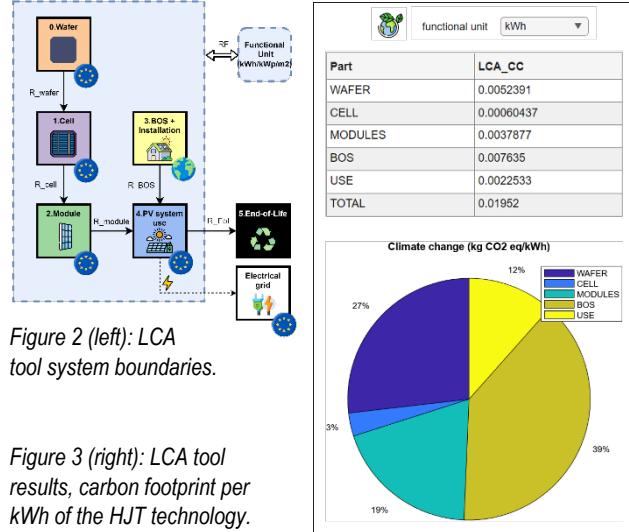


Figure 2 (left): LCA tool system boundaries.

Figure 3 (right): LCA tool results, carbon footprint per kWh of the HJT technology.

As an example, the environmental footprint of a 3.15 kWp HJT PV system installed in Lisbon for 30 years can be evaluated with the LCA tool. The results are obtained for this specific PV system configuration in various functional units such as kWh, kWp, and m² (see Figure 2) for diverse impact categories. Such PV system configuration has a carbon footprint of 19.5 gCO₂-eq/kWh, as illustrated by Figure 3, with BOS & Installation phase and wafer manufacturing (in Europe) representing 39%, respectively 27%, of the total carbon footprint. In addition to cleaning of the PV system, the replacement of BOS components (such as the inverter) is included in the use phase, leading to a no longer negligible impact (12%) due to the use of metal-intensive materials. Consequently, it is advisable to concentrate efforts on reducing the environmental impact of BOS and wafer production. Importantly, numerous parameters such as the PV system's lifetime, location, wafer thickness and PV module materials could be changed easily in the interface and results updated quickly, representing a net advantage to develop eco-designed PV systems.

In conclusion, the internal LCA tool is a critical advancement in CSEM's commitment to sustainable practices in the solar industry. It currently provides a simplified approach to assess the environmental footprint of PV products, enabling faster, more efficient decision-making in European and industrial projects, and its potential extension to batteries and electronics is testament to its versatility. Future developments on automatic report generation will enable the tool to improve transparency and efficiency, ultimately becoming an integral part of CSEM's sustainability strategies.

[1] <https://www.iea.org/energy-system/renewables/solar-pv> (2023)

[2] Muteri, et al., "Review on LCA of Solar Photovoltaic Panels" (2020).

Ultralight Weight Amorphous Silicon Solar Modules for Solar Power Satellites

G. Christmann, J.-W. Schüttauf, L. Pires da Veiga, F. Meyer, M. Krieger, A. Ingenito

CSEM has been developing ultralight weight solar modules based on amorphous silicon solar cells deposited on ultrathin polyimide substrates. These devices were fabricated in the framework of an ESA project aiming to explore the potential of the technology for solar power generation. While not aiming for ultrahigh power conversion efficiency like III-V space grade solar cells, these modules aim at reaching very high W/kg power conversion. These makes them suitable for applications where weight is a crucial factor for deployment and a lot of space is available.

Solar power satellites (SPS) propose to harvest the abundant and stable solar energy available 24 hours a day in geostationary orbit and transmit it to earth with a low power density microwave beam through the optical transparency window of the atmosphere. State of the art space solar power solutions are III-V compound semiconductor triple junction-based PV modules, which are 100 times too expensive and one order of magnitude too heavy to build a competitive SPS with terrestrial collection infrastructure. Despite its lower power conversion efficiency (PCE) than state-of-the-art multijunction solar cells, and even mainstream crystalline silicon (c-Si), amorphous silicon (a-Si) for solar is a thin-film technology requires minute amount of material and is adapted for low-cost large-area deposition, which is compatible with inexpensive/flexible substrates. Furthermore, a whole industrial platform has already been established for module fabrication. Fabricating a-Si solar module on ultrathin polymer substrates would therefore enable to reach very high W/Kg conversion values making this technology attractive for SPS.

CSEM merged two established technologies into one fully integrated novel PV array architecture combining space rated thin Polyimide foils from NEXOLVE Holding Company LLC USA (CP1) and thin film a-Si PV module technology. Very small ultralightweight demonstrator cells on polyimide have been demonstrated previously^[1], but the fabrication of a fully laser interconnected solar module was still lacking to demonstrate the scalability of the technology to large areas. CSEM therefore fabricated a medium area ($10 \times 10 \text{ cm}^2$) ultra-lightweight laser processed demonstrator module. This will allow to assess the potential of this technology for SPS, in terms of W/kg performances. The simplicity of the laser process (litho-free) will potentially enable cost < 1\$/W, which is impossible to reach with competing technologies (c-Si or III-V).

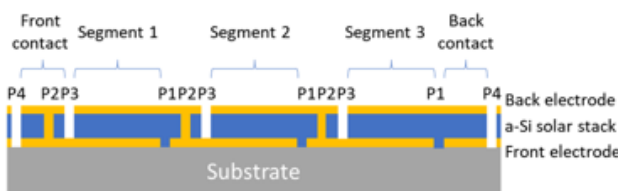


Figure 1: Schematic description of a solar module series interconnect.

A process flow to fabricate the fully interconnected module (Figure 1) on the thin CP1 has therefore been developed: first the CP1 is spun on a glass carrier substrate to the desired thickness, then the front transparent conductive electrode is sputtered, and laser patterned (P1, front electrode ablation). Then the a-Si p-i-n solar cell stack is deposited, and laser patterned (P2, selective

ablation of the solar cell layers). After that the back electrode is deposited and laser patterned (P3, selective ablation of the solar cell layers and back electrode, P4 ablation of all layers). Finally, the sample is released from the glass carrier substrate. CSEM managed to successfully fabricate such modules, the main challenge being the development of a laser process enabling P1 and P4 scribes without damaging the CP1 polymer substrate.

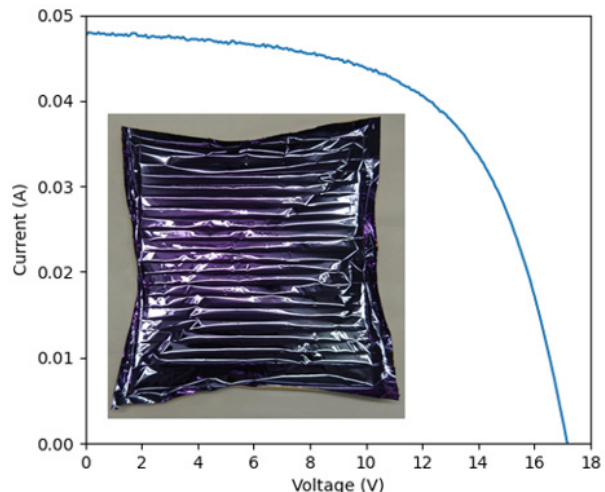


Figure 2: Current voltage measurement under AM1.5G illumination of a typical solar module. Inset: photograph of a solar module after release from the carrier glass substrate.

The modules were measured under AM1.5G (terrestrial) illumination as CSEM has this equipment but an estimation of the performances under AM0 (space) illumination was devised, based on concentration measurements and device spectral response measurements. Typical current voltage measurements are displayed in Figure 2 and summarized in the table below:

AM1.5G Eff. (%)	AM1.5G Pmax (W)	Weight (mg)	AM1.5G W/kg	AM0 W/kg
4.92	0.49	88	5591	6927

It can be seen that performance approaching 7000 W/kg can be achieved with the technology developed at CSEM. At system level however, the weight of the deployment system would have to be considered to get the full picture.

In summary, while the widespread availability of energy from SPS will require a lot more developments, these results demonstrated the possibility to produce thin film a-Si solar modules with very high W/kg performances offering a promising technology for SPS.

^[1] N. Wyrsch, et al., Proc. IEEE PV SC (2006), pp. 1785.

Perovskite Semiconductors for Light Emitting Diodes and Energy Harvesting

X. Y. Chin, D.A. Jacobs, Q. Jeangros

Taking advantage of the rapid development of metal halide perovskite optoelectronics, the EU H2020-funded project PeroCUBE (high-performance large area organic perovskite devices for lighting, energy and pervasive communication) aims to demonstrate high-efficiency perovskite single-junction solar cells, as well as red, green and blue perovskite LEDs by developing industrially relevant sheet-to-sheet and roll-to-roll deposition methods. The objective is then to combine these building blocks into smart devices featuring visual light communication capabilities, notably for the localization of assets in indoor conditions or localized information transfer. Led by CSEM, the 14-partners strong consortium is advancing metal halide perovskite technologies to create new opportunities for the lighting, energy harvesting and telecom industries in Europe.

Metal halide perovskite thin-film materials have the potential to advance energy harvesting, lighting and sensing technologies. Their high potential stems from their advantageous combination of properties ranging from high optical absorptance and color purity, bandgap tuneability, long charge carrier lifetimes, to their low temperature of processing. As laboratory tests have now successfully validated the performance of perovskite solar cells and light-emitting diode (LEDs) by demonstrating high-efficiency small-scale prototypes (with an active area of typically a few mm²), it is now imperative to shift research efforts towards i) developing industry-relevant techniques to manufacture large-area perovskite devices on both rigid and flexible substrates, ii) improving the operational stability of these technologies to maximize their commercial viability, and iii) extending the range of applications for these materials to create new markets.

In line with this context, this contribution will review the progress made by the EU H2020-funded project PeroCUBE (<https://perocube.eu/>), a project coordinated by CSEM. More specifically, PeroCUBE is focusing on the development of novel perovskite inks with optimized processability and high performance for sheet-to-sheet and roll-to-roll deposition on large areas. The final goals of the projects are to demonstrate large-area perovskite solar modules and light-emitting diodes (LEDs) on both rigid and flexible substrates, and eventually perovskite-based wearable devices combining energy harvesting and visual light communication capabilities to precisely track the position of goods (e.g., in a warehouse) or to transfer information at specific locations in space.

By screening – notably through computational methods – the wide compositional space of metal halide perovskites, inks suitable for upscaling activities were identified and experimentally tested. With this approach, CSEM could demonstrate, using first spin-coating to deposit the perovskite absorber/emitter, high-efficiency small-scale solar cells and red, green and blue LEDs with an area of 1 cm² (Figure 1a). Once the quality of materials validated with small-area prototypes, the project focused on the development of deposition methods to homogeneously coat large substrates, i.e., either 100-cm² rigid glass or m²-long flexible rolls. This was achieved by developing suitable sheet-to-sheet meniscus coating (i.e., blade coating) methods at CSEM, while other partners focused on the roll-to-roll printing of perovskite inks on flexible rolls (via meniscus and gravure printing). Associated ink drying/crystallization techniques were also optimized to achieve a high perovskite film quality and homogeneity.

Thanks to these materials and process developments, the consortium could demonstrate large-area LEDs and solar modules produced using industry-relevant methods (Figure 1b), with the photovoltaic modules reaching an efficiency >14% for an active area of close to 60 cm². A laser scribing process compatible with perovskite thin films was also developed to

interconnect in series solar cells into solar modules. The operational stability of these devices was also investigated and improved by developing suitable encapsulation processes tailored for both rigid and flexible devices.

Finally, the project has been focusing on the integration of perovskite solar cells in visual light communication systems to extend the range of possible applications of perovskite thin films. The project has been developing wearable devices, with some prototypes combining energy harvesting and precise indoor positioning using visual light communication for localized information transfer or goods tracking. This feat has been made possible by using the perovskite solar cells as both energy harvester and detector for visual light communication by developing a suitable laser scribing pattern at CSEM. These prototypes are being finalized and will be presented in the coming months.

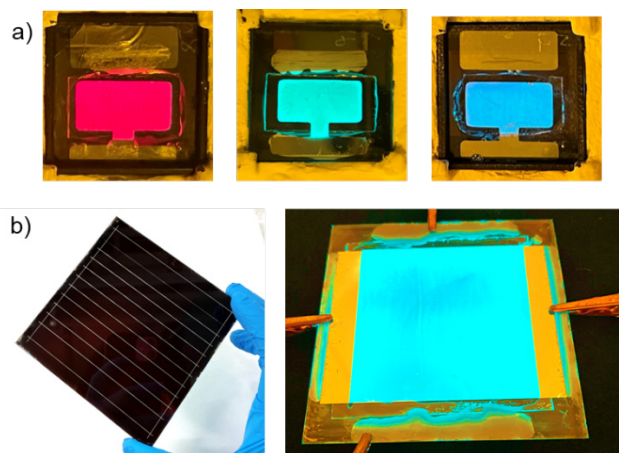


Figure 1: PeroCUBE prototypes made CSEM: a) red, green and blue perovskite LEDs featuring an active area of 1 cm²; b) large-area perovskite solar module and perovskite LED, with both devices deposited by blade coating.

PeroCUBE is a collaboration between CSEM, Alpes Lasers (CH), Optiva Media (ES), Aura Light (IT), Vodafone Innovus, University of Patras, Eulambia, Noesis (GR), CNRS (FR), TU Wien (AT), Fraunhofer FEP (DE), TNO (NL), VTT (FI), and University of Oxford (GB), placed under the coordination of CSEM. The PeroCUBE project has received funding from the European Union's Horizon 2020 research and innovation program under Grant Agreement No. 861985.

Lightweight PV Modules for Mobility Applications

P. Duvoisin, H. Li, A. Faes, X. Bulliard, C. Charrière, D. Petri, O. Arriaga Arruti, T. Auderset, N. Badel, L. Baume, G. Cattaneo, J. Champliaud, J. Escarré, J. Levrat, L. Marthey, P. Mermet, F. Mujovi, S. Pittet, M. Roten, B. Bonnet-Eymard, M. Despeisse, C. Ballif

Solar-powered mobility is bringing solutions to reduce emission of the transportation sector and is enabling new explorative missions. This is achieved by increasing the energy autonomy by using photovoltaic (PV) electricity produced directly on board. CSEM has taken up the challenge of developing solar modules meeting the requirements of this field of application with several partners.

Traditional PV modules rely on glass as a protective layer for the active solar cells against environmental conditions. The use of glass adds weight, increases the thickness of the overall structure, and enhances the rigidity of the module. These properties may not always align with the specific requirements for Vehicle Integrated PV (VIPV) applications. In this context, CSEM has developed innovative solutions along the entire chain of a PV module, ranging from material and cell developments as well as interconnection schemes. These new generations of glass-free PV module designs can demonstrate lightweight (LW), reduced thickness, flexibility and versatile designs while maintaining high performance and reliability.

In the CSEM module facilities in Hauterive and Marin (NE), different modules stacks were developed depending on the constraints of the vehicle. Three examples are given below.

Ultra-low weight and thin modules

In order to achieve utmost lightweight design while fitting the requirements of evolving in high altitude, CSEM developed on its polymer platform a new encapsulant foil layer based on silane grafted PO compound. Thin layers were extruded and Maxeon IBC solar cells sandwiched between only 2 layers of foils. The cells were connected using an ultra-thin connector developed at CSEM compatible for such thin polymer layers and for stratospheric conditions. These flexible modules achieved down to 700 g/m² with a thickness of only 400 µm and a power of over 210 W/m². Such ultra-low weight solar panels developed and produced at CSEM equip the wings of the two-seater Solarstratos plane, which is aiming at being the first manned solar plane penetrating the stratosphere.

Hail resistant LW modules

Hail resistance is a challenging feature for LW modules as they do not have a thick protective front sheet.

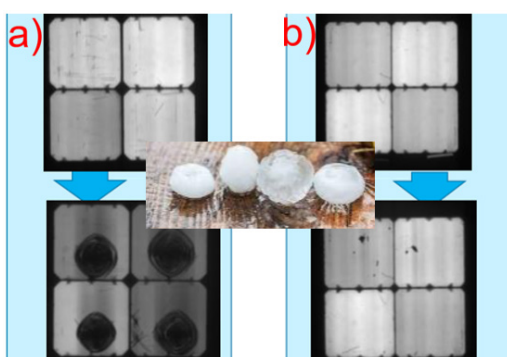


Figure 1: Electroluminescence pictures of mini-modules made of (a) an initial LW stack and (b) the optimized LW CSEM stack. The bottom images show the effect of hail on the cells embedded in the stack.

A distinct structure is necessary compared to previous ultra-lightweight designs in order to enhance the rigidity and the mechanical stability. CSEM tuned and optimized its silane grafted PO compound polymer, combined it with other

encapsulant types manufactured at CSEM and optimized the rear sheet. Modules with a weight down to 2 kg/m² are now achieving high hail resistance and passing the IEC hail tests, as illustrated in Figure 1.

Highly reliable LW modules in harsh environments

Further optimizations were made to enable the use of the modules in harsh environments such as in the stratosphere and on the seas. The rear side of the module was modified to obtain self-standing modules or to be applied to various holding structures. Figure 2 highlights selected projects with customers in which LW solar modules were developed.

Complementarily, to increase the power of the solar modules, advanced cells architectures and interconnection schemes were developed at CSEM with Meyer Burger: the tunnel IBC HJT SWCT cell which enables a laminate efficiency as high as 24.7% and high reliability in a module.



Figure 2: a) LW modules developed and produced at CSEM for Swiss Airtainer to equip their refrigerated pharma airfreight containers; b) Stratospheric, and c) meteorological balloons from CNES are equipped with measurement instruments and powered by ultralight solar panels from CSEM. d) The boats, ECO INSPIRATION for commercial usage, and e), the Swiss Solar Boat for racing, are also both equipped with light and resistant solar panels from CSEM.

To conclude, mastering the whole material and process chain enables unique combinations for successful PV deployment in emerging fields. Furthermore, exciting new results for LW solar panels for car integration can be found in "Glass-free PV module for automotive application" and "I-V Curve Simulation of Curved PV Modules for Vehicle Integration".

I-V Curve Simulation of Curved PV Modules for Vehicle Integration

F. Mujovi, J. Levrat, A. Faes, G. Cattaneo, S. Prabhudesai, K. Nicolet, J. Gerber, L. Jaques, M. Despeisse, B. Bonnet-Eymard, C. Ballif, G Arnoux*, R. Ambigapathy*

As part of an industrial collaboration, CSEM has added curved module electrical simulation functionalities to the portfolio of PV modules simulating tools. The tool can precisely simulate the electrical behavior of a curved module in indoor conditions found in typical sun simulators (PASAN tunnel flashers). CSEM conducted a validation campaign to confirm the capabilities of the tool.

Interest in Vehicle Integrated Photovoltaics (VIPV) is growing within the field of photovoltaic technologies, with efforts being made to incorporate curved modules into Electric Vehicles (EVs). Curved modules can more conveniently fit the complex aesthetics of EVs and enhance their effective autonomy. However, due to the novelty of these implementations, there is currently a lack of well-established tools for predicting performance or measuring their effectiveness. This gap in knowledge is particularly crucial because curved modules, by their design, will consistently face inhomogeneous levels of irradiance. We show here the results and levels of precision of our simulation tool by comparing the tool's simulated results with the measured ones obtained with a validation campaign.

The process flow of this simulations tool consists of taking the electrical characteristics of one single solar cell to simulate and predict the behavior of any module-scale device. This tool namely accounts for:

- the CTM (cell-to-module) losses
- the varying IAM (Internal Angle Modifier) applied to the projected light onto the curved surface
- the type of interconnection of each string (serial or parallel connections)
- the impact of the bypass diodes with the mismatched current between each cell.

To simulate the electrical behavior of a curved module, the 3D curved surface is generated by either inputting the spatial coordinates of each cell or by supplying the tool with the radii of curvature along each direction. The irradiance is then computed by projecting rays from a catalogue of modelled light sources. Figure 1 shows how the irradiance for a PASAN light source is projected onto a curved module.

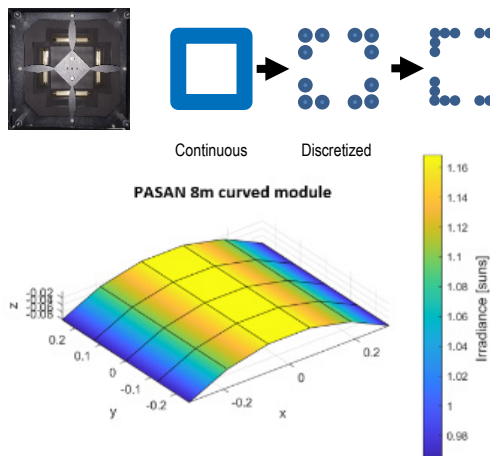


Figure 1: Discretized Pasan sun simulator light source with the projected irradiance on a curved module with a 0.6 m radius of curvature.

The cells are modelled by a 2-diode model, and by accounting for the projected irradiance of each cell, the module I-V (current-voltage) curve can be generated.

To validate this model, a validation campaign was conducted by designing and manufacturing a flexible module (see Figure 2b). The module allowed us to measure the I-V curves at different radii of curvature. With the help of specially made supports, we managed to measure the module when it was curved at: 1.8, 0.9, and 0.6 m of curvature. The module was flashed in indoor conditions in a PASAN 8 m tunnel flasher. Figure 2

Figure 2 shows the module itself with the three different bending configurations.

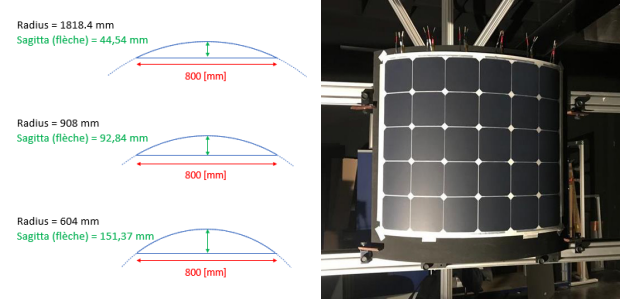


Figure 2: (a) Three levels of curvature were used in this project. (b) The module is fixated on the 0.6 m radius support.

The typical I-V curve shows step-like effects when bypass diodes are used because of the mismatched current between the bypassed strings. The simulation tool is able to reproduce the measured data within a 1% error for the maximum power point as shown in Figure 3.

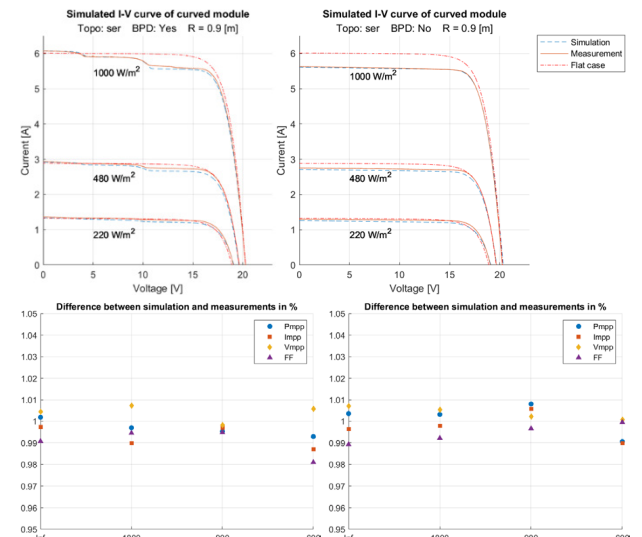


Figure 3: Typical simulated and measured I-V curves of the module at the 0.9 m of curvature (top) and a summary of all results at different curvatures (bottom). The left side shows results with bypass diode and the right side without bypass diodes.

Glass-free PV Module for Automotive Application

A. Faes, G. Cattaneo, F. Mujovi, S. Prabhudesai, K. Nicolet, J. Gerber, L. Jaques, J. Levrat, M. Despeisse, B. Bonnet-Eymard, J. Robin *, J. Silva **

CSEM has developed, in collaboration with Simoldes and CEiiA, an unique light-weight module with a thick polymeric front sheet for vehicle-integrated applications. CSEM has demonstrated the high reliability of integrating solar cells in a glass-free impact-proof laminate by reaching more than 2000 thermocycles without degradation. The final prototype was integrated and tested in a car produced in series.

The swift rise in Electric Vehicles (EVs) usage and the drop in Photovoltaic (PV) costs combined with the recent increase in energy costs in Europe, has revitalized innovation in Vehicle Integrated Photovoltaics (VIPV). PV modules integrated in vehicle roofs must be designed to match the requirements of the vehicle industry, such as superior aesthetics for a curved roof, crash resistance, compliance with automotive assembly lines, but the most important criteria being weight, to ensure the highest energy efficiency by minimizing the vehicle weight¹.

The thermo-cycling stability is one key limiting factor for the integration of glass-free PV modules in vehicles. Due to large coefficient of thermal expansion (CTE) difference (the ratio of polymer front-sheet CTE and silicon CTE is around 25), the crystalline silicon cells distance varies with temperature which induces stresses on the cell's interconnection based on copper. With the initial PV module design, the electrical performance of PV module dropped to zero after 30 to 40 thermo-cycles between -40°C and +85°C which is far from the 200 cycles with less than 5% relative degradation required by the IEC 61215 standard. By optimizing the materials thermo-mechanical properties, the material stack and the interconnection design, the stability was improved drastically to reach 2270 thermo-cycles without measurable degradation, which represents more than 11 times the reference test from IEC and about 17 months of testing in climatic chamber. Figure 1 shows the electroluminescence (EL) images and the electrical performance of the glass-free PV module along the 2270 cycles.

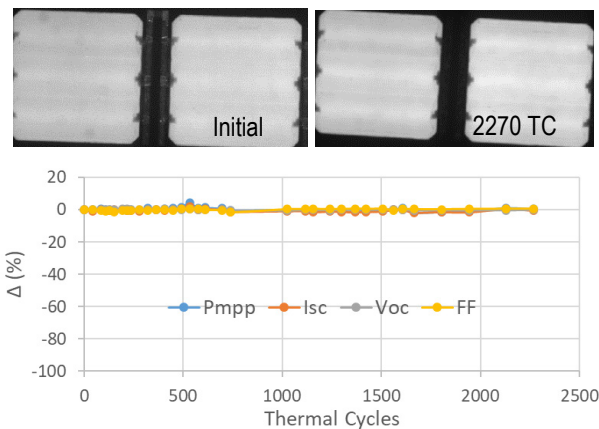


Figure 1: (top) electroluminescence images and (bottom) electrical performance of the developed glass-free PV module for automotive application during thermo-cycles (TC).

Small PV modules and final roof prototypes have been tested accordingly to IEC 61215 for product design qualification (namely

damp-heat, humidity freeze, mechanical load, UV-dose, hail, hot-spot, outdoor and combined tests) and more extensive testing required by electronics for automotive applications.

A full VIPV prototype design including polymer-based front-sheet, high performance solar cells laminated with optimized bill-of-materials and a modified base car roof is shown in Figure 2.

Based on CSEM energy yield model, the 140 W VIPV integrated roof will increase the daily average driving range by 5 km (7.5 km) or the summer daily driving range by nearly 8.6 km (11.3 km) in Paris (Sevilla) in optimal conditions. In the coming months, the series car modified with glass-free impact-proof solar roof will be tested on the open road to validate the range extension from the vehicle integrated PV roof.

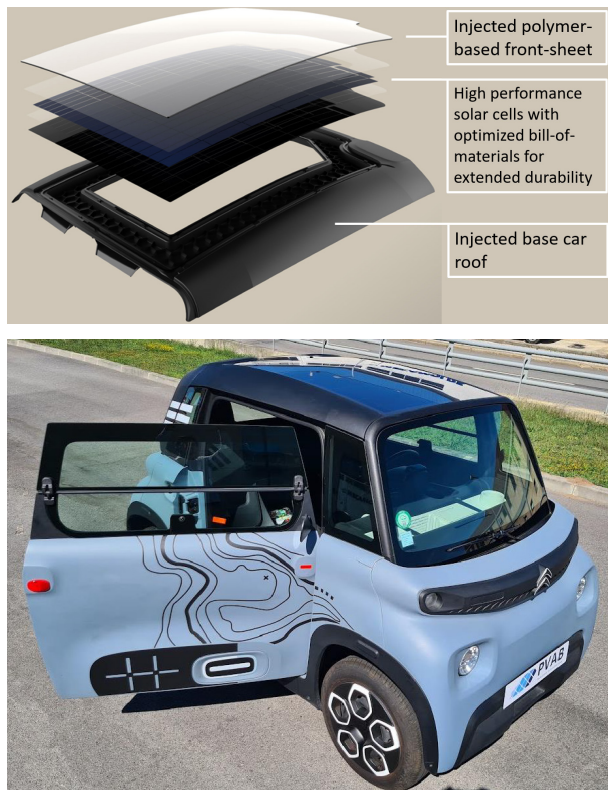


Figure 2: (top) Exploded view of the full vehicle integrated PV (VIPV) prototype design, and (bottom) picture of the final integration of the VIPV prototype in a car produced in series.

This work has been partially funded by the Swiss Federal Office of Energy (SFOE) under the Solarbody project (#IS/512317-01).

• Simoldes, Portugal
• CEiiA, Portugal

[1] A. Faes, et al. "La mobilité solaire : un rêve ou une réalité?", Bulletin Electrosuisse 6 (2023) 21-24 ([link](#)).

Microservices for Robust Estimation and Activation of Demand-side Flexibility

D. Achi, B. Schubnel, P. Scharnhorst, R. Langou

The increased electrification of mobility and heating technologies, coupled with the high variability of renewable energy sources, increases the strain on electricity grids, creating a need for reinforcement. To mitigate infrastructure investments, CSEM has developed a unique data-driven solution that exploits the demand-side flexibility of different types of electrical assets while preserving their functionality and end-users' comfort. The solution accounts for and manages the uncertainty of the system, ensuring a robust estimation and activation of demand-side flexibility.

The growing electrification of mobility and heating, combined with the fluctuating nature of renewable energy production, generates a need for grid reinforcement. This need can be mitigated by exploiting flexible assets. Demand-side management aims at adjusting electrical energy consumption to production while maintaining asset functionality and ensuring end-users' comfort. The potential of demand-side flexibility is projected to be around 200 TWh for residential electric heating and 125 TWh for e-mobility in the EU by 2030 [1]. However, major challenges arise from the uncertainty in both production and generation, due to stochastic weather variations, stochastic consumer behavior, or a wrong or partial system description. To deal with these challenges, CSEM has developed a unique data-driven solution that quantifies the demand-side flexibility of different types of assets and activates them based on the needs.

This solution can deal with different objectives: maximization of self-consumption, minimization of electricity costs or CO₂ emissions, tracking of power requests, and peak reduction. It supports battery equipped assets (stationary batteries, electric vehicles) and electrically powered thermal assets (thermal tanks coupled with a heat pump, building thermal envelopes). Both classes are modelled with virtual battery models where the state of charge is estimated using a probabilistic or robust method to ensure request fulfilment. The approach has two microservices as seen in Figure 1.

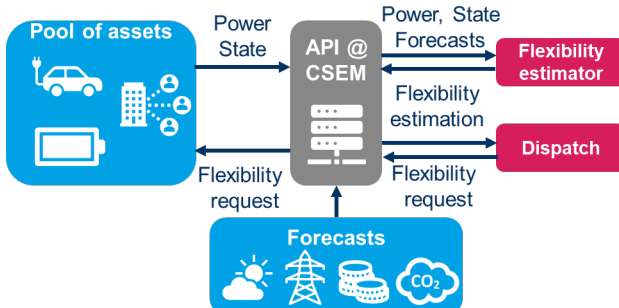


Figure 1: Overview of the developed solution.

In the **flexibility estimator**, the state and the power consumption curves of the assets are modelled as virtual batteries based on sample-efficient, data-driven models. Flexibility maps [2] are then derived from these models and consider comfort and technical constraints. They quantify the power consumption flexibility of the described assets, i.e., the power deviation that can be requested from an asset at any given time over the next 24 hours.

[1] smartEN, "Demand-side flexibility: quantification of the benefits in the EU". Sept. 2022.

[2] P. Scharnhorst, B. Schubnel, R. E. Carrillo, P.-J. Alet, C. N. Jones, "Uncertainty-aware Flexibility Envelope Prediction in Buildings with Controller-agnostic Battery Models," in 2023 American Control Conference (ACC), 2023, pp. 583–590.

Doi: 10.23919/ACC55779.2023.10156041.

The **dispatch algorithm** implements a mixed-integer linear programming (MILP) scheduling whose objective function depends on the operational scenario and whose constraints are derived from the assets' flexibility maps.

The method proposed is unique given its features:

- **Uncertainty management:** thanks to the quantification of the asset behavior in the virtual battery models, the acceptable risk level can be parameterised, which gives control over the solution's robustness.
- **Data-driven approach:** the modelling of assets with data-driven methods simplifies the onboarding of assets and ensures an effective representation of many types of control strategies that may pre-exist at asset level.
- **Scalable:** The service supports large pools of assets. It has been tested with up to 2000 assets in simulations.

The deployment of the microservices was validated on the Industrial Park in Las Cabezas, Spain, which is equipped with a stationary battery, within the scope of the NEON project [3]. The different features were validated in simulation, using the open-source library Energym [4] for building control simulation.

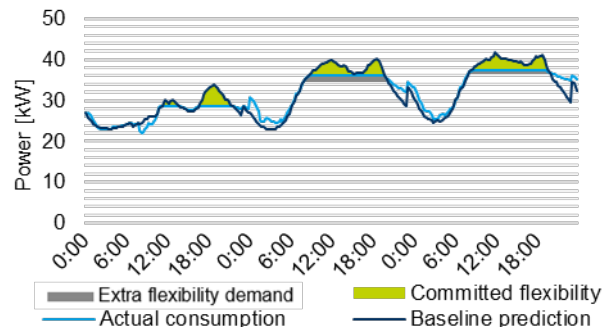


Figure 2: Peak reduction application in a pool of ten buildings.

An example of peak reduction in a pool of ten buildings during a period of three days is shown in Figure 2. CSEM's solution accurately predicts the baseline and activates the forecasted flexibility of the assets, providing a decrease of around 10% of the total peak power of the pool across the time horizon.

The NEON project has received funding from the European Union's Horizon 2020 research and innovation programme under grant agreement No 101033700.

[3] <https://neonproject.eu/>

[4] P. Scharnhorst, et al., "Energym: A Building Model Library for Controller Benchmarking," Applied Sciences, vol. 11, no. 8, p. 3518, Apr. 2021, doi: 10.3390/app11083518.

Probabilistic Forecasting of Irradiance and PV Power Production on a Variable Set of Locations with Graph Machine Learning

R. Carrillo, B. Schubnel, R. Langou, P.-J. Alet

CSEM has already demonstrated that graph neural networks (GNN) can outperform the state of the art in forecasting photovoltaic (PV) power production, while relying only on power measurements. At the time the same set of PV systems were present throughout training and evaluation. However, in a commercial application, nodes (i.e., PV systems) would be frequently added or removed. To address this constraint, CSEM has developed the DIGERATI solution for intraday forecasting (horizon up to six hours) that extends previous approaches by using dynamic GNN. In addition, it fuses information from heterogeneous data sources (PV power, irradiance, wind speed and temperature) measured at different locations and produces probabilistic forecasts.

Renewable energy sources (RES), such as wind power production or photovoltaic (PV) power production, play a key role in reaching a fully decarbonized electricity production. However, operating power systems with large amounts of RES raises many challenges for grid operators due to the variability of their power production. To ensure an adequate operation of the power grid, e.g., to anticipate and alleviate grid congestion, forecasting of power generation with fine temporal and spatial resolution is required.

State-of-the-art approaches for PV forecasting combine numerical weather predictions (NWP), satellite images and ground measurements with physical or machine learning models of the systems. The main limitation of current approaches is that they can only achieve precise spatial and temporal resolution at the expense of high computational, storage and instrumentation costs. An alternative approach is to use past measurements from a network of ground sensors (e.g., PV systems or meteorological stations) distributed in some region of interest and exploit their spatiotemporal relations to improve the forecast accuracy and resolution. Graph neural networks (GNN) have the capability to infer information from complex data defined in irregular domains (such as networks) by modelling their interdependence. This capability makes them suitable to exploit the spatiotemporal correlations of ground sensors. GNNs have indeed demonstrated excellent performance in forecasting tasks on such data^[1]. However, published forecasting approaches that use GNNs assume that their input data come from a fixed network of sensors (nodes). This assumption is a severe limitation for practical applications since nodes include renewable power plants, rooftop PV systems and weather stations, which can all be added or removed as new customers sign up or physical assets change.

To overcome this drawback, CSEM has developed the DIGERATI solution to provide probabilistic forecasts of solar sources (irradiance or PV power). DIGERATI extends our previous work by adding: (i) probabilistic forecasts capabilities by producing forecasts of the 5%, 50% and 95% quantiles for each forecast point in time, (ii) fusion of heterogeneous data sources (meteorological stations and rooftop PV systems) as inputs, and, (iii) use of dynamic graph machine learning to address the problem of changing (sensor) network, where nodes and edges can be added or removed dynamically. The solution can produce

forecasts for new “unseen” nodes, e.g., recently added PV stations or irradiance forecasts in sites where input data is not available.

DIGERATI was benchmarked against a commercial forecast solution, based on cloud motion tracking that uses satellite images and numerical weather models, achieving a reduction of the forecasting error of 25%^[2]. To evaluate the quality of the probabilistic forecasts (confidence intervals), the continuous rank probability score (CRPS) was computed over one year of historical data. Figure 1 shows the CRPS as a function of the forecasting horizon. The CRPS are reported as percentage of the peak value for each node. Overall, the normalized CRPS shows that the forecasting system manages to reproduce the 5%, 50%, and 95% quantiles of the empirical distribution of the data for the evaluation year.

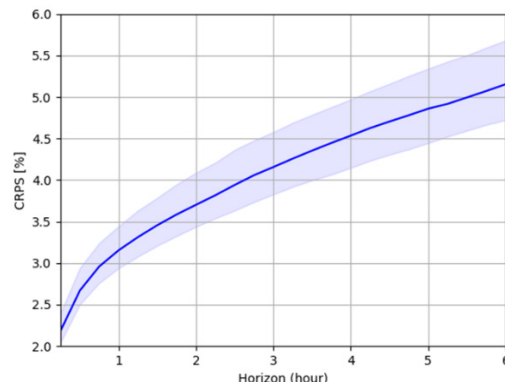


Figure 1. CRPS as a function of the forecasting horizon.

A live demonstrator was developed to showcase the solution^[3]. The demonstrator uses data from 192 nodes, 64 PV stations and 128 meteorological stations, as inputs to the forecasting system. The system generates a forecast every 15 minutes for the six hours ahead horizon, with a resolution of 15 minutes, of the irradiance in the locations of the 128 meteorological stations. Based on these forecasts, the system can forecast the irradiance at any location in Switzerland. The spatial resolution of the system will be improved as more nodes (PV systems or meteorological stations) are added.

This research was co-financed by Innosuisse, the Swiss innovation agency, project 57765.1 IP-EE: DIGERATI.

^[1] Simeunović, B. Schubnel, P. -J. Alet, R. E. Carrillo, "Spatio-Temporal Graph Neural Networks for Multi-Site PV Power Forecasting," in IEEE Transactions on Sustainable Energy, vol. 13, no. 2, pp. 1210-1220, April 2022.

^[2] R. E. Carrillo, B. Schubnel, R. Langou, P.-J. Alet, "Dynamic Graph Machine Learning for Mult-site Solar Forecasting," 40th EUPVSEC, September 2023.

^[3] <https://digerati.portal.csem.ch/>

A Dataspace for Secure and Collaborative Data Exchange in the PV Industry

R. Langou, B. Schubnel, P.-J. Alet

Many projects feature collaborations across companies, research institutes and universities. Data exchange in this context is delicate because of data sovereignty concerns, strict access policies, and interoperability needs. Unlike central storage solutions that require partners to relinquish control of their data to a central entity, the dataspace architecture from IDSA [1] fosters decentralized implementations that facilitate trust, seamless integration and interoperability among diverse data sources. Within the European project PILATUS, CSEM has set up a first dataspace for the European PV industry following the IDSA standard architecture.

Companies currently exchange data in various ways: via FTP (file transfer protocol), emails, central cloud storage solutions, APIs (application programming interfaces), web portals, or via VPN (virtual private network) access. All these protocols have inherent limitations that make them unsuitable for multi-partner data sharing initiatives. These shortcomings range from security concerns (lack of encryption or flawed access controls) to a lack of standardization (absence of a uniform interface) and issues with scalability (challenges in replication or scaling). Additionally, the centralized data storage approach of most methods compromises data sovereignty and requires ad-hoc bilateral agreements.

Exchange scenarios: The digital activities in the Horizon Europe project PILATUS aim at improving yield and product quality using data gathered over the entire module life cycle, from cell and module manufacturing lines to field performance tests made in research facilities in Switzerland, Germany, and the Czech Republic. Figure 1 shows that typically three entities participate and exchange data: the manufacturers, a research institute conducting detailed reliability tests, and another research institute or service provider offering analysis to determine possible causes of product degradation or malfunction post-deployment. The IDSA architecture enables this kind of exchange in a decentralized fashion, based on two main technical components: the connectors and the identity service provider.

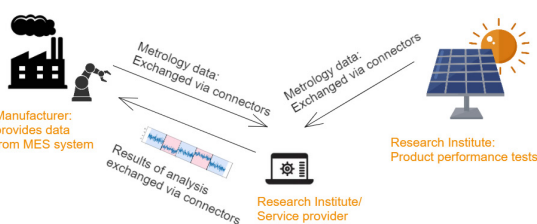


Figure 1: Multi-party data exchange scenario in the PV industry.

Connectors: The connectors act as gateways for data exchange. They implement the rules and policies set by data providers and ensure that data sovereignty is maintained. They also ensure the end-to-end encryption of data and allow dynamic and real-time data exchanges while providing dataset-specific access controls. Several open-source implementations of connectors are available and listed by IDSA [2]. Connectors are deployed with docker as a data consumer and/or data provider on each partner's infrastructure in a decentralized fashion. For security, partners can deploy connectors in their DMZ ("demilitarized zone"), a subnetwork presenting external-facing services online

[1] IDSRAM V4.2.0'. [Online]. Available: https://github.com/International-Data-Spaces-Association/IDSRAM_4_0/

which acts as a buffer against external cyber threats to their internal network; see Figure 2.

DAPS: The DAPS (Dynamic Attribute Provisioning Service) is a centralized service to provide identification. It ensures the central authentication of each data space participant. In the PILATUS project, the DAPS runs on a Linux server at CSEM and ensures that the certificates provided by connected partners are correct and allow connectors transactions. To ensure top-level security, data provider connectors have put in place further IP security restrictions on the connection of data consumer connectors.

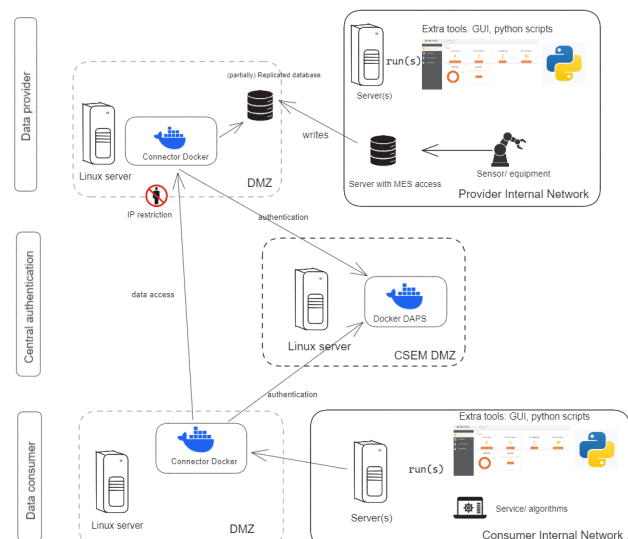


Figure 2: Implemented architecture in the PILATUS project.

Testing and further development: Simple exchange scenarios have been successfully tested with CSEM partners in the PILATUS project and the dataspace is up and running. Further tests involving APIs for real time access to databases are planned. In the PILATUS project, the dataspace will be crucial for applying causal machine learning to discern cause-and-effect links between pilot-line process parameters and field performance measurement, a scenario illustrated on Figure 1.

The PILATUS project is funded by the European Union under grant number 101084046. Views and opinions expressed are however those of the authors only and do not necessarily reflect those of the European Union. Neither the European Union nor the granting authority can be held responsible for them.

This work has received funding from the Swiss State Secretariat for Education, Research and Innovation (SERI).

[2] IDSA, 'Data Connector Report', Feb. 2023. [Online]. Available: https://internationaldataspaces.org/wp-content/uploads/dlm_uploads/IDSA-Data-Connector-Report-February-2023-1.pdf

Predicting Advection-Diffusion Phenomena with Physics-informed Graph Machine Learning

J. Simeunović, R. Carrillo, B. Schubnel, P.-J. Alet

Cloud formation and movement directly influence irradiance, the main driver of solar photovoltaic (PV) power generation. Since they are guided by advection-diffusion processes, predicting such processes is essential for accurate forecasting of PV power. While pure data-driven methods are attractive for forecasts, their ability to reliably generalize is limited. This is why CSEM has developed and evaluated PING, a physics-informed machine-learning method which predicts particle concentration in advection-diffusion processes. This method provides high-accuracy forecasts on cloud coverage, PV power and sea-surface temperature, even with irregular sensor networks.

Advection-diffusion processes play a crucial role in describing cloud formation, cloud movement and other natural atmospheric phenomena, such as sea surface temperature. Numerical solvers, which are traditionally used to solve the physical equations that describe the advection-diffusion processes, are computationally expensive. For forecasting purposes, data-driven methods are attractive since they accelerate inference by a factor 40 to 80 [1]. To improve physical consistency, physics-informed neural networks (PINNs) are trained with a loss function that incorporates known physical equations. However, most PINN models solve the tasks on regular grids, while forecasting data from sensor networks represents a problem that inherently lies on an irregular grid.

To address this challenge, CSEM introduced a physics-informed graph neural network (PING) model that estimates the particle velocities of the historical input data, in an unsupervised fashion, and forecasts the future particle concentration values of the advection-diffusion processes. PING introduces an Euler-based discretization scheme for irregular domains and exploits graph neural networks to estimate the underlying dynamics.

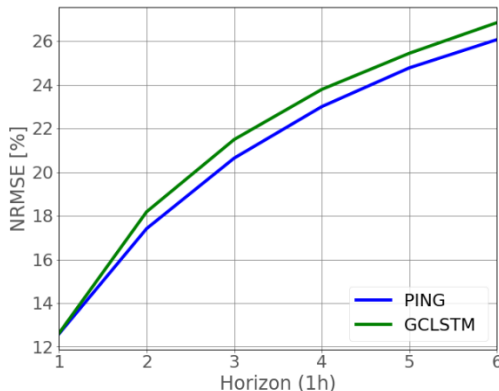


Figure 1: NRMSE evolution for six-step-ahead prediction on the cloud index dataset. Temporal resolution of one hour.

The performance of PING was compared to an encoder-decoder graph convolutional long-short-term memory network (GCLSTM) model [2] on two datasets: cloud concentration index, which is highly advective, and sea surface temperature (SST) [3], which is highly diffusive. For the cloud index dataset, both models were trained on three years and evaluated on one year. For the SST dataset the models were trained on twelve years and evaluated on four. On both datasets the models worked with an irregular grid of 150 nodes.

[1] D. Kochkov, J. A. Smith, A. Alieva, Q. Wang, M. P. Brenner, S. Hoyer, "Machine learning-accelerated computational fluid dynamics", Proceedings of the National Academy of Sciences, 118(21), 2021.

The resulting values of normalized root mean square error (NRMSE) are shown on Figure 1 and Figure 2. The NRMSE is comparable for the two models on the two datasets. However, on the highly advective cloud index dataset, PING slightly outperforms GCLSTM over the entire prediction horizon. An example of a cloud concentration index forecast for six hours ahead is shown on Figure 3. This instance is chosen since it exemplifies moments of significant dynamic changes in the cloud coverage, which are a particularly challenging situation for forecasting models. In this situation, PING benefits from the estimation of cloud dynamics and shows a prediction closer to the ground truth than GCLSTM.

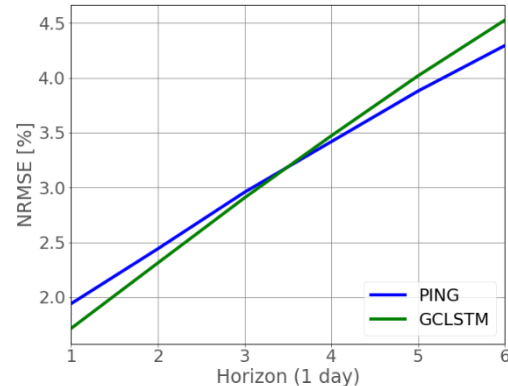


Figure 2: NRMSE evolution for six-step-ahead prediction on the SST dataset. Temporal resolution of one day.

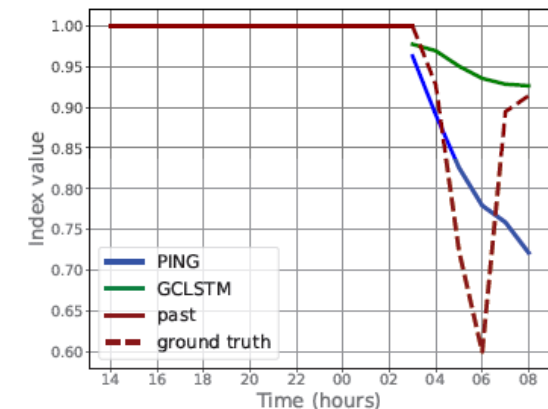


Figure 3: Example of six hours ahead prediction for cloud concentration index, for GCLSTM and PING.

[2] J. Simeunović, B. Schubnel, P. -J. Alet, R. E. Carrillo, "Spatio-Temporal Graph Neural Networks for Multi-Site PV Power Forecasting," in IEEE Transactions on Sustainable Energy, vol. 13, no. 2, pp. 1210-1220, April 2022

[3] <https://cds.climate.copernicus.eu/>

Optimizing Battery Storage Systems through Behavioral Models in Predictive Energy Management

T. Gorecki, A. Sutter, S. Bhoir

A novel method was developed to integrate a complex empirical degradation model of a lithium-ion battery into the optimization of an energy management system (EMS). The model uses relaxed nonlinear equations of a multi-factor degradation model and allows the degradation model to be included in an optimization framework. Based on this, better operation strategies can be computed in real time, explicitly considering the hidden degradation cost incurred by the cycling of batteries. This was confirmed in simulation with a large increase in the expected benefits for a battery managed by an EMS exploiting the developed model

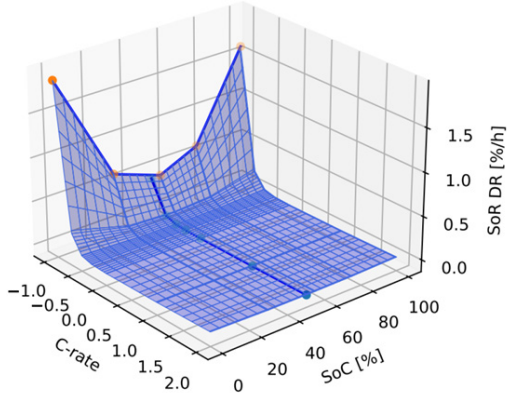


Figure 1: approximation of state-of-health degradation rate as a function of C-rate and operating SoC.

Battery models are used in various applications, from design to operations. Different levels of complexity and accuracy are required depending on the application. Battery degradation, a critical factor, is often inadequately considered in operation scenarios. The challenge is to have a model that is sufficiently simple to be used in numerical optimization but accurate enough to account for various influencing factors such as charging rates (c-rate), state of charge (SoC) or temperature. CSEM has developed an optimization-compatible battery degradation model which bridges the gap between existing simulation models and practical optimization contexts.

This work builds on SoXery^[1], an open-source battery degradation simulation model previously developed at CSEM. A method has been devised to simplify the SoXery model into a model that is compatible with mixed-integer linear optimization. It relies on assumptions to simplify the model structure and exploits a mathematical modelling technique called piecewise (PW) McCormick relaxation^[2]. This approach approximately represents bilinear relationships in the original model with approximate equations that involve only linear inequalities and discrete variables. Crucially, this approach allows to control the level of accuracy of the approximation at the expense of higher complexity of the resulting model (in terms of number of discrete variables introduced).

To study the benefit of explicitly considering degradation in battery management, we have considered three alternative battery models in a simulation study:

- A0: ignoring the degradation and limiting the charging rate to 0.5C and the SoC to between 10% and 90%
- A1: simple state-of-health (SoH) model, with only c-rate-dependent cycle ageing
- A2: complex SoH model, including SoC and depth of discharge

Table 1: Performance comparison of battery models for arbitrage.

Arbitrage	SoH loss [%/y]	Lifetime [y]	Accuracy of model	Complexity [s]	Total benefit [CHF/MWh/y]
A0: no deg	4.2	5	NA	0.1	-1200
A1 Simple SoH	1.7	12	1.20%	0.2	6250
A2 Complex SoH	1.7	12	<0.1%	5	10000

The operation scenario in the experiments was to perform arbitrage on electricity prices. In Table 1, “accuracy” denotes the approximation error with respect to the full SoXery model; “complexity” is reported as the time required to solve one optimization run; and “total benefit” is the gross profit generated by the arbitrage-performing battery, when considering the hidden cost of battery degradation that assumes a battery end of life when the battery reaches a SoH of 80%.

This gross profit is negative in option A0 (if degradation is only limited with hard constraints), which means that the degradation cost exceeds the benefit from using a battery for arbitrage. The simple SoH model of option A1 is quite accurate (1.2% difference with exact degradation equations); it allows to significantly reduce the SoH losses per year and extend the battery life to 12 years. As a result, the gross profit has a positive value of 6'250 €/MWh/year, making arbitrage beneficial over the battery lifetime. The complex SoH proposed in A2 allows to reduce further the degradation cost and yields a higher profit of up to 10'000 €/MWh/year.

These results have been published and presented at a conference^[3], and an open-source implementation of the model is publicly available on GitHub^[4].

This work was funded by the Swiss Federal Office of Energy (SFOE). CSEM thanks them for their support.

[1] CSEM and Swiss Federal Office of Energy (SFOE), "SoXery", Available online at <https://portal.csem.ch:9260/>

[2] Our formulation adapted from D. S. Wicaksono, I. A. Karimi, Piecewise MILP under- and overestimators for global optimization of bilinear programs, AIChE Journal, April 2008

[3] A. Sutter, Tomasz T. Gorecki, S. Bhoir, Method to Embed Behavioral Battery Model in Predictive Energy Management Systems, ISGT 2023, Grenoble

[4] <https://github.com/csem/batmaestro>

DRT-based State of Charge Estimation for Commercial Li-Ion Battery Pack

P. Iurilli, C. Brivio, N. Koch, RE Carrillo, Y. Stauffer, A. Hutter

Within the SPET project, CSEM benchmarked its Bestimator™ State of Charge (SoC) estimator for Li-ion batteries. The algorithm, which is constructed on a physics-based Equivalent Circuit Model (ECM) derived from EIS measurements, is applied to a commercial NMC battery module (20s1p) and compared with state-of-the art SoC estimator based on Coulomb Counting (CC). The case-study show that Bestimator™ SoC estimation can reduce the SoC estimation error of one order of magnitude per cycle, especially in scenarios where the CC cannot be re-calibrated.

The State of Charge (SoC) is the main indicator computed by the Battery Management Systems (BMSs) during battery operation, providing the current amount of energy available in the battery cell. The fine tracking of SoC can improve the safety and performances of battery packs. When having to develop precise SoC estimators, the technical challenge lies in fully understanding the electrochemistry behind all processes occurring during battery cell operations. This usually comes with more complex model formulations, which should often require to be simplified to be effectively used in embedded BMSs.

The SPET project, funded by SFOE (Swiss Federal Office of Energy) under project number SI/501727-01, tackled this challenge. It built upon CSEM's battery modeling know-how exploiting the Bestimator™ algorithm framework, which is a CSEM's proprietary SoC estimator that combines: a physics-based a-priori assumptions-free Equivalent Circuit Model (ECM) together with an Extended Kalman Filter (EKF) that corrects the SoC estimation based on real measurements [1]. The ECM is based on OCV (Open Circuit Voltage) and EIS (Electrochemical Impedance Spectroscopy) measurements, which are post-processed via DRT (Distribution of Relaxation Times) technique [2]. The Bestimator™ (referred to ECM-DRT in Table 1) has been compared against standard SoC estimation i.e., Coulomb Counting (CC) without OCV-based re-initialization (referred to CC in Table 1). The SoC estimation error is computed by comparing the estimated SoC with respect to defined evaluation points where the true-SoC is computed from the OCV measured at the very end of resting periods between charging/discharging cycles.

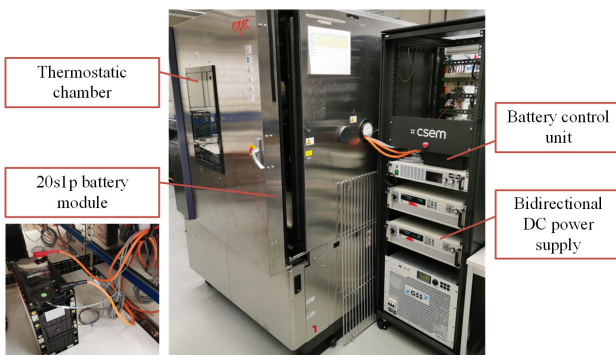


Figure 1: Experimental setup in the battery laboratory of CSEM Battery Innovation Hub, Battery module and conditioning units.

The experimental validation has been performed on a commercial battery pack made of 20 NMC cells, arranged in 20s1p configuration (Figure 1), for a nominal voltage of 73 V and

a measured capacity of ~60Ah, so roughly 4.5 kWh. The two SoC estimation methods are tested against two different current measurements: LAB current (accurate measurement based on laboratory equipment) and BMS current (real measurement from the commercial battery pack). By coupling the two current measurement setups with the three models, a total of 4 scenarios have been compared.

Validation results show that the Bestimator™ DRT-based ECM brings clear advantages in cases for which the standard CC approach cannot benefit from a precise current measurement or an OCV-based reinitialization, e.g., stationary Battery Energy Storage Systems (BESS) for grid applications (e.g., frequency regulation) or non-standard Electric Vehicle (EV) applications (e.g., Vehicle to Grid). The advantages from the proposed ECM-DRT estimator can be quantified in an error reduction of one order of magnitude per cycle, from around 1%/cycle down to 0.05%/cycle error accumulation on average (Table 1 and Figure 2).

Table 1: SoC estimation error results – CC reference vs. the Bestimator™ (DRT-based ECM).

SoC Error [%]	LAB current (superior current sensor)		PACK-BMS current (standard current sensor)	
	CC (Ref.)	ECM/DRT (Bestimator)	CC (Ref.)	ECM/DRT (Bestimator)
Avg error over cycles	0.89	0.35	6.89	0.61
Avg error increase per cycle	0.02	0.06	1.07	0.05

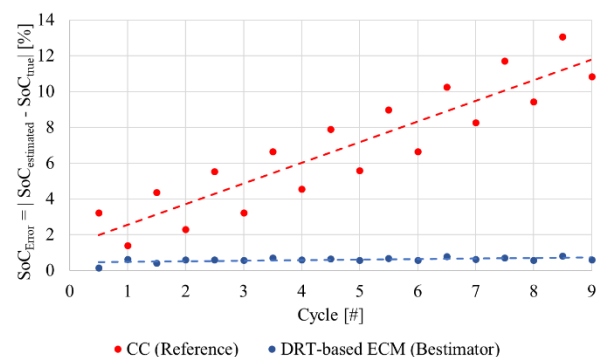


Figure 2: SoC error accumulation over cycles, model comparison.

Regardless from the specific application, the Bestimator™ brings further advantages: (i) it provides a robust solution for all those chemistries where the OCV recalibration is known to be difficult, such as the LFP; (ii) it brings direct quantification of degradation phenomena which can be used to update the SoC estimation while the cell is ageing (i.e., State of Health estimation).

[1] C. Brivio, R. E. Carrillo, P.-J. Alet, A. Hutter, "Bestimator: a novel model-based algorithm for robust estimation of battery SoC", in SPEEDAM symposium, Sorrento, Italy, pp. 184–188, 2020.

[2] P. Iurilli, C. Brivio, R. E. Carrillo, V. Wood, "Eis2mod: A drt-based modeling framework for li-ion cells," IEEE Transactions on Industry Applications, vol. 58, no. 2, pp. 1429–1439, 2022.

HYSTIMATOR – EIS-based Method to Physically Model Hysteresis of LFP Battery

G. Thenaisie, C. Brivio, A. Hutter

Withing the HYSTIMATOR project, CSEM addressed the hysteresis phenomenon in lithium iron phosphate (LFP) battery cells by using low-frequency Electrochemical Impedance Spectroscopy (EIS) and Distribution of Relaxation Times (DRT) analysis. It integrates hysteresis characteristics into a physics-based Equivalent Circuit Model and significantly reduces Root Mean Square Error (RMSE) during real-world laboratory testing. This approach holds promise for enhancing State of Charge (SoC) estimation in LFP battery cells, especially in embedded Battery Management Systems (BMS).

In recent years, due to the shift towards cleaner energy policies, a cumulative annual growth rate of 15-20% has been observed for the adoption of battery electric vehicles (BEVs) and Battery Energy Storage Systems (BESSs)^[1]. Lithium iron phosphate batteries (LFP), which are both cost-effective and inherently safer compared to other NMC or NCA-based battery technologies, have become increasingly popular. Major players in the industry, such as Tesla and BYD, are placing their bets on LFP batteries for the foreseeable future.

Estimating the State of Charge (SoC) in LFP batteries is still a challenge due to two main factors: (i) LFP batteries have a flat OCV (Open Circuit Voltage) relationship, making it difficult to gauge SoC based on voltage alone; (ii) LFP chemistry exhibits strong hysteresis between charging and discharging conditions, further complicating accurate SoC calculations.

The HYSTIMATOR project, funded by SFOE (Swiss Federal Office of Energy) under project number SI502441-0^[2], tackled this challenge. It built upon CSEM's battery modeling and state estimation expertise, extending it to the realm of LFP chemistry.

Previous studies in non-equilibrium thermodynamics have shown that within LFP batteries, the process of ions intercalation is governed by three distinct dynamics: lattice reconfiguration, ion diffusion, and bulk diffusion. Consequently, this research proposes that hysteresis in LFP batteries is not an inherent characteristic but rather a slower relaxation process when compared to other battery chemistries.

We used EIS at very low frequency deconvoluted by Distribution of Relaxation Times (DRT), which magnifies the information provided by EIS by highlighting the main dynamic phenomena^[3], to measure the hysteresis phenomenon and model it.

The testing campaign has been performed at the CSEM BIH, on several 90 Ah LFP cells, both fresh and aged, under controlled condition. Specifically, EIS were measured from 1 kHz down to 10 µHz by using potentiostats/galvanostats.

In addition to the typical DRT peaks associated with interfacial dynamics and charge transfer processes at high/medium frequencies, we identified three more peaks at specific relaxation times, confirming the three-stage intercalation process described in literature. Leveraging these EIS/DRT insights, we propose a physics-based Equivalent Circuit Model (ECM) that represents the seven key phenomena with seven RC elements (see Figure 1), coupled with an OCV derived via a standard symmetric GITT protocol.

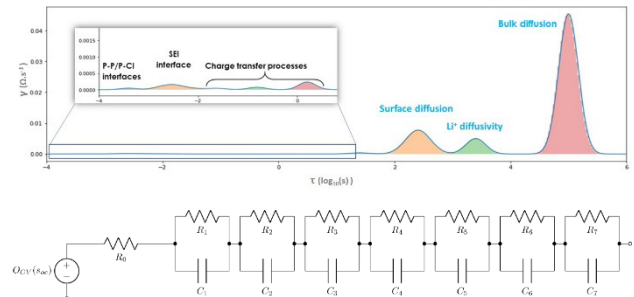


Figure 1: DRT of the studied 90Ah LFP cell and associated ECM model.

The proposed ECM has been validated against an existing model from literature, without hysteresis compensation. Two different power profiles have been employed: (i) a dynamic profile (DYN) to assess behavior with fast and replicating square current profiles (5-minute steps, see Figure 2), and (ii) a GITT discharge/charge profile to assess during full charge-discharge cycle with intermittent currents. The assessment of the model's accuracy involved the use of the Root Mean Square Error (RMSE) indicator, which measures the consistency between the estimated terminal voltage and the actual terminal voltage.

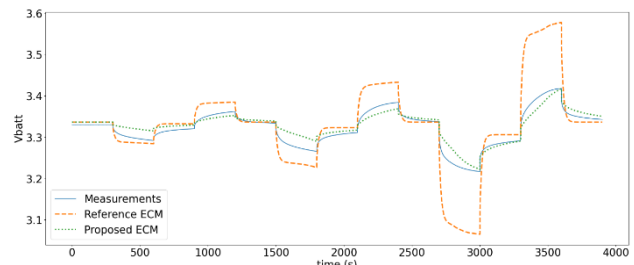


Figure 2: Models' performance comparison at SoC=50% for DYN test.

The results for fresh cells confirm that the proposed ECM outperforms the reference model by a factor of two to four, depending on the simulated profile. As the cells age, both models experience increased errors, but the rate of error increase is approximately two times lower in the proposed model compared to the reference model. This resilience in performance with aged cells validates the potential of the proposed ECM for use in a Kalman filter or other filtering framework to enhance state estimation accuracy for LFP cells.

This research contributes to the advancement of battery modeling techniques and lays the foundation for more precise State of Charge (SoC) estimation methods in LFP-based battery applications.

^[1] Future Market Insights (2021), "Battery Management System Market - Europe Industry Analysis 2016 – 2020 and Opportunity Assessment 2021– 2031.

^[2] <https://www.aramis.admin.ch/Texte/?ProjectID=50922>

^[3] P. Iurilli, C. Brivio, R. E. Carrillo, V. Wood, "Eis2mod: A drt-based modeling framework for li-ion cells," IEEE Transactions on Industry Applications, vol. 58, no. 2, pp. 1429–1439, 2022.

Internal Temperature Estimation of a Li-Ion Battery Cell by using EIS

S. Bhoir, G. Thenaisie, C. Brivio, A. Hutter

Within the flagship project CircuBAT, CSEM is addressing the biggest safety concern in the field of Lithium-ion batteries: Thermal Runaway (TR). CSEM is developing a methodology to use Electrochemical Impedance Spectroscopy (EIS) signals to estimate the inside temperature of battery cells. The frequency at which the phase of the impedance of the cell should be calculated is defined by using the Distribution of Relaxation Times (DRT) technique. The methodology has been validated on cells of different form factors (cylindrical and pouch) and for cells under load.

During their usage, batteries can undergo various types of abuses such as mechanical, electrical, and thermal abuses. These abuses can result in cells catching fire, also called Thermal Runaway (TR). For instance, a recent battery explosion was reported in Germany where a 30-kWh battery exploded in a household, leaving the residence uninhabitable. These events can be mitigated if a continuous, accurate measurement of the cell's temperature is performed. The simplest method is to deploy temperature sensors. But this may be economically infeasible due to the hundreds of cells in a standard battery pack. Among other sensing options, Electrochemical Impedance Spectroscopy (EIS) can be used to estimate the internal temperature of the cell. EIS is performed by injecting the battery cell with an alternating current at various frequencies and measuring the voltage response. The phase of the resulting cell's impedance has been shown to be appropriate for internal temperature estimation^[1].

Thanks to its established know-how on the use of EIS measurements, CSEM, within the flagship project CircuBAT, has been working to determine which EIS frequency is the most appropriate to be used for cell's internal temperature estimation. The Distribution of Relaxation Times (DRT), a post processing technique, is used for this purpose. The DRT magnifies EIS carried information and returns peaks at different time constants, (as shown in Figure 1), each of which can be attributed to a specific electrochemical process. It has been shown that the transportation of Lithium ions through the Solid Electrolyte Interface (SEI) layer is the most appropriate process, which is temperature dependent while being State of Charge (SoC) independent^[2]

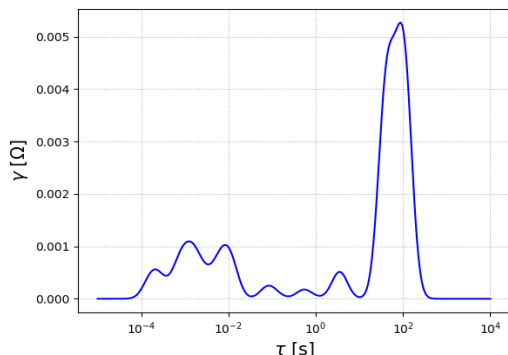


Figure 1: Result from DRT analysis of EIS.

Experiments are performed on fresh cylindrical (3.5 Ah) and pouch (12 Ah) cells to validate the accuracy in the temperature estimation. EIS measurements are performed on the cells at different SoCs and temperatures. The frequency to correlate the cell's temperature to the phase of its impedance is given by performing a DRT analysis on the EIS at 20°C and 50% SoC.

^[1] Srinivasan, Rengaswamy, et al., "Instantaneous measurement of the internal temperature in lithium-ion rechargeable cells." *Electrochimica Acta* 56.17 (2011): 6198-6204.

The frequency thus obtained is in the order of hundreds of Hertz. The characterization results performed at the selected frequency (Figure 2) show that the model can be used to estimate the internal temperature of a cell regardless of the cell form factor.

The methodology is validated by inserting a temperature sensor inside the cell and comparing the temperature recorded from it to the one on the cell's surface and the model's estimation. The results (Figure 3) show that the estimation follows the internal temperature more faithfully as compared to the surface temperature sensor. The Root-Mean-Square-Error (RMSE) obtained for the estimated temperature is approximately 0.8°C while that of the surface temperature is around 3°C.

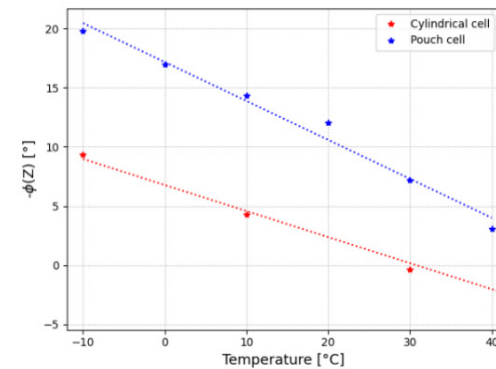


Figure 2: Model to implement internal temperature estimation.

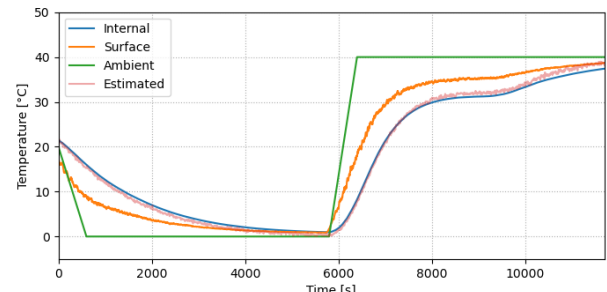


Figure 3: Comparison of estimated and surface temperature to internal temperature of cell, for an imposed temperature cycle.

Currently, this work focuses on two directions: (i) extending the validation for aged cells, and (ii) extending the characterization to TR process (up to 120°C). Once validated, the final step will be to embed the algorithm in the zBMS platform, CSEM's Battery Management System (BMS) which is re-defining the standard battery sensing options by adding more intelligence at cell level, including EIS. The final objective is to realize a BMS prototype which can increase battery safety by predicting when a thermal runaway is likely to happen.

^[2] P. Suresh, A. Shukla, N. Munichandraiah, "Temperature dependence studies of ac impedance of lithium-ion cells," *Journal of applied electrochemistry*, vol. 32, no. 3, pp. 267-273, 2002.

High-energy Density Li-Metal Anode by Physical Vapor Deposition

M. Srout, C. Fu, N. Rospars, L. Pires Da Veiga, A. Ingenito

CSEM aims at developing alternative high-quality and cost-effective methods for the fabrication of lithium metal (LiM) anodes to improve performances and safety of LiM batteries. Two are the main technologies under development: (i) Thin LiM deposition via thermal evaporation process, which possess better properties (e.g., roughness, homogeneity, thickness, cycle life, etc.) compared to the commercial extruded lithium, and (ii) Thin film coating solutions. Cycling data show an increase in cycle life of batteries with coated LiM anode by a factor 2x when compared to the ones with uncoated LiM.

LiM offers one of the highest theoretical gravimetric capacities (3860 mAh/g) and the lowest electrochemical potential (-3.04 V vs standard hydrogen electrode [1]). Nonetheless, the widespread adoption of LiM batteries has been hindered by the high reactivity of Li versus electrolytes which results in low coulombic efficiency, increased cell impedance, and reduced cyclability. Moreover, Li dendrites, which growth during cycling, poses severe safety concerns as it can cause cell short-circuiting and consequent thermal runaways [2]. Excess Li in the form of LiM, can compensate for the continuous loss of Li inventory but its thickness must be lower than 25 μm (~ 5 mAh/cm 2) to reach a competitive energy density. LiM is conventionally produced by the extrusion of a Li ingot through a die where the extruded foil is then calendered on a Cu current collector. This method has three major drawbacks: (i) the very high cost to produce thin Li-metal, (ii) the high roughness of the LiM surface, and (iii) the contamination of the Li surface due to the use of inorganic oils to prevent sticking of the LiM to the rolls. Recently, alternative processes to produce high purity and cost-effective LiM anodes have been investigated [1]. Physical vapor deposition (PVD) is one of the most promising as it is an industrially proven deposition method. At CSEM, we aim to demonstrate LiM anodes fabricated via PVD with improved electrochemical behavior with respect to state-of-the-art extruded LiM.

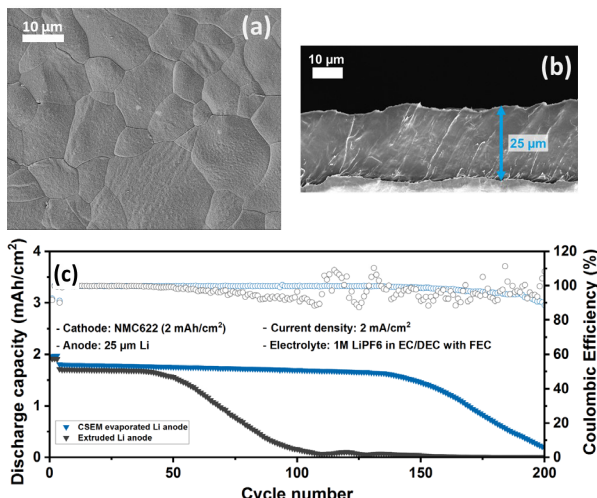


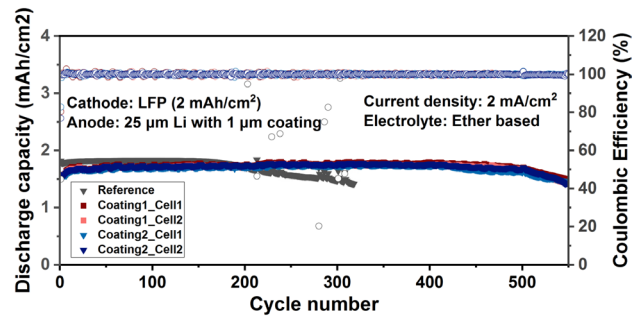
Figure 1: Morphology and performance of evaporated Lithium: (a) Top view SEM image; (b) Cross section image; (c) cycling performance of NMC622/Li (evaporated vs. extruded Li) cells.

The evaporation process (PVD) of LiM at CSEM has been validated and compared with commercially available extruded LiM anode. SEM analysis confirmed a good uniformity of both lithium morphology and its thickness (Figure 1a & 1b). Moreover, the electrochemical testing of the prepared lithium in both

[1] B. Acebedo, M. C. Morant-Miñana, E. Gonzalo, I. Ruiz de Larramendi, A. Villaverde, J. Rikarte, L. Fallarino, *Adv Energy Mater* 2023, 13, DOI 10.1002/aenm.202203744.

symmetric and full cells (coin cell format) versus NMC622 cathode demonstrated enhanced performance, a factor 2x in cycle life compared to extruded (Figure 1c).

To further improve the electrochemical performances of LiM and reduce its reactivity in air and ease its handling and cell integration, CSEM is developing PVD thin film coating. The processing routes for the fabrication of interfacial coating layers on the lithium metal anode are limited because of the tighter restrictions compared to other anode or cathode materials. Mostly, the application of wet-coating techniques is hindered by the high reactivity of most solvents with metallic lithium. Alternatively, CSEM is proposing the use of vacuum coating techniques (PVD techniques) such as thermal evaporation or sputtering for the fabrication of artificial solid electrolyte interphases that can improve the performance and stability of LiM anode. The approach consists in depositing the film in-situ directly on the LiM without breaking the vacuum. This has the advantages of preventing the formation of an unwanted passivation layer on the LiM surface as well as improving the electrochemical performance and reducing the reactivity of lithium, allowing easier handling in dry room environment. Figure 2 shows two examples of coating solutions developed at CSEM and which have improved the cycle life of LFP//Li cells by a factor 2x.



CSEM has demonstrated that superior LiM anode can be obtained by optimizing the deposition conditions for the evaporation process. Cycling data show an increase of a factor 2x in favor of PVD if compared to extruded LiM. Having that achieved, ongoing developments on coatings to enhance the stability and safety of the LiM anode, when used with both liquid and solid polymer electrolytes, also shows first promising results. An improvement of the cycle life of LiM batteries (Li//LFP cells) using ether-based liquid electrolyte by a factor 2x has been already achieved when coated PVD-LiM is used compared to uncoated PVD-Li anode.

[2] Q. Wang, B. Liu, Y. Shen, J. Wu, Z. Zhao, C. Zhong, W. Hu, *Advanced Science* 2021, 8, DOI 10.1002/advs.202101111.

SOLiD Project – Dual-layer Polymer Batteries with Vacuum Deposited Li-Metal Anode

L. Pires Da Veiga, A. Ingenito

In this work we investigate novel solid polymer electrolytes for solid-state Li-metal battery, based on random acrylic copolymers with cyclic carbonates as side-chains. The aim is to demonstrate the synthesis and the scaling up of this material in the framework of the EU project SOLiD, where double-layer polymer batteries will be validated in pouch cells. The polymer shows excellent oxidative stability and a good combination of mechanical integrity and ionic conductivity. Current work is focusing on increasing the mobility of the carbonate group to improve ionic conductivity at room temperature.

The SOLiD project will create a cost-efficient pilot scale manufacturing process for a high energy density, safe and easily recyclable solid-state Li-metal battery. The aim is to use existing roll-to-roll (RtR) tools, such as slot die coating, to manufacture a polymer-cathode composite to be paired with a Li-metal anode. Within the project, CSEM is in charge of developing solid polymer electrolytes (SPE) to replace the cathode binder and the separator, as shown in Figure 1.

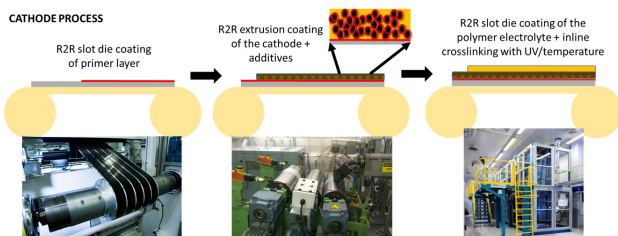


Figure 1: Diagram elucidating the concept for the production of polymer-cathode composite by RtR extrusion and slot die coating.

To achieve this, novel SPEs need to be designed to fit the production requirements. A polymer electrolyte is synthesized to replace the binder in the composite cathode. Glycerol carbonate acrylate (GCA) and butyl acrylate (BA) are polymerized by free radical polymerization to form P(GCA-BA) with varying molar ratios, see Figure 2. GCA is a polar group needed to dissociate the lithium salt, but if used alone the resulting SPE is too stiff. Therefore, BA is added to soften the polymer matrix. The butyl group is flexible; hence it increases the mobility of the polymer chains. Indee it is observed that the glass transition temperature (T_g) decreases with increasing content of BA. No melting peak is observed in the differential scanning calorimetry curves, indicating that the polymer is amorphous, which is ideal for ionic conductors.

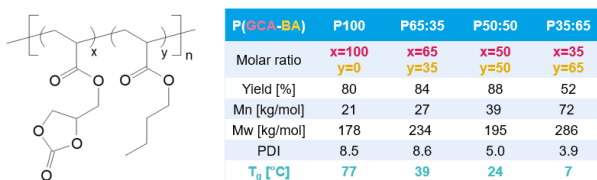


Figure 2: Molecular structure of P(GCA-BA) and the physical properties of the copolymers with their sample ID.

SPE films are made by mixing the polymers with a lithium salt and then casting it on an Aluminum foil. These films are then used to measure the ionic conductivity of the SPE. The best conductivity is demonstrated by P35:65 at 60°C, reaching 10-7 S/cm, for comparison, the conductivity of polypropylene carbonate (PPC), with LiTFSI is 10-6 S/cm at 60°C [1]. PPC is a commonly used SPE that has demonstrated good cycling

performance at 60°C in combination with high voltage cathode such as NMC811. The ionic conductivity of the SPE increases with an increasing ratio of BA, in Figure 3, which correlates to the decrease of T_g and the increase in segmental motion of the polymer chains. Such behavior is well-known and motivated our approach to copolymerize glycerol carbonate with butyl acrylate.

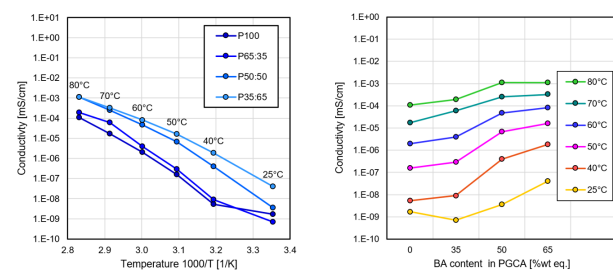


Figure 3: Comparison of the ionic conductivity of SPE made with P(GCA-BA) and LiTFSI.

To replace the polymer binder in the cathode composite, it is crucial that the SPE has high oxidative stability. This is evaluated by cyclic voltammetry, where an increase in current at higher voltage indicates a degradation of the polymer. In Figure 4 we compare the anodic stability of PGCA (P100) to P(GCA-BA) (P35:65), to see if the addition of BA has an impact on the stability. Both the SPEs display anodic currents below 1 $\mu\text{A}/\text{cm}^2$, which is comparable with previous literature on PPC [1], meaning it has excellent oxidative stability.

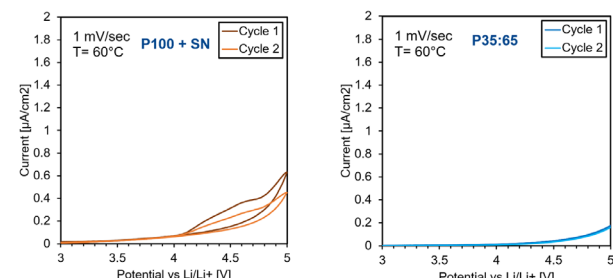


Figure 4: Comparison of the oxidative stability of SPEs made with P(GCA-BA) and LiTFSI.

CSEM's work demonstrated that: (i) random copolymers with cyclocarbonate side-groups and butyl acrylate units have low T_g , below room temperature, (ii) the ionic conductivity is comparable to commonly used SPE, (iii) voltammetry investigations suggest promising oxidative stability. Current work focuses on increasing the carbonate group's mobility to improve ionic conductivity at room temperature. Further work will integrate these polymers in a dry extrusion of cathode composites and their performance will be evaluated in batteries.

[1] Arrese-Igor, M.; et al., ACS Energy Lett. 2022, 7, 1473–1480.

ANNEXES

Publications

- [1] Aeberhard, Jasmin L.; Radan, Anda-Petronela; Delgado-Gonzalo, Ricard; Strahm, Karin Maya; Sigurthorsdottir, Halla Bjorg; Schneider, Sophie; Surbek, Daniel, "Artificial intelligence and machine learning in cardiotocography: A scoping review", European Journal of Obstetrics & Gynecology and Reproductive Biology, vol. 281, pp. 54-62, doi:10.1016/j.ejogrb.2022.12.008
- [2] Aguet, Clémentine; Jorge, João; Zaen, Jérôme Van; Proença, Martin; Bonnier, Guillaume; Frossard, Pascal; Lemay, Mathieu, "Blood pressure monitoring during anesthesia induction using PPG morphology features and machine learning", PLOS ONE, vol. 18 (2), pp. e0279419, doi:10.1371/journal.pone.0279419
- [3] Bruschini, Claudio; Antolovic, Ivan Michel; Zanella, Frédéric; Ulku, Arin C.; Lindner, Scott; Kalyanov, Alexander; Milanese, Tommaso; Bernasconi, Ermanno; Pešić, Vladimir; Charbon, Edoardo, "Challenges and prospects for multi-chip microlens imprints on front-side illuminated SPAD imagers", Optics Express 31 (13), 21935-21953, doi:10.1364/OE.488177
- [4] Chin, Sanghoon; Van Zaen, Jérôme; Denis, Séverine; Muntané, Enric; Schröder, Stephan; Martin, Hans; Balet, Laurent; Lecomte, Steve, "An Artificial Neural Network to Eliminate the Detrimental Spectral Shift on Mid-Infrared Gas Spectroscopy", Sensors, vol. 23 (19), pp. 8232, doi:10.3390/s23198232
- [5] Chin, Xin Yu; Turkay, Deniz; Steele, Julian A; Tabean, Saba; Eswara, Santhana; Mensi, Mounir; Fiala; Wolff, Christian; Paracchino, Adriana; Artuk, Kerem; Jacobs, Daniel; Guesnay, Quentin; Sahli, Florent; Andreatta, Gaëlle; Boccard, Matthieu; Jeangros, Quentin; Ballif, Christophe, "Interface passivation for 31.25%-efficient perovskite/silicon tandem solar cells", Science, 381, 59
- [6] Cimmino, Wanda; Migliorelli, Davide, "Design of a printed electrochemical strip towards miRNA-21 detection in urine samples: optimization of the experimental procedures for real sample application", Anal Bioanal Chem (2023), doi:10.1007/s00216-023-04659-x
- [7] Frerichs, Inez; Paradiso, Rita; Kilintzis, Vassilis; Rocha, Bruno M; Braun, Fabian; Rapin, Michael; Caldani, Laura; Beredimas, Nikolaos; Trechlis, Romanos; Suursalu, Sander; Strodthoff, Claas; Pessoa, Diogo; Chételat, Olivier; Paiva, Rui Pedro; de Carvalho, Paulo; Maglaveras, Nikolaos; Weiler, Norbert; Wacker, Josias, "Wearable pulmonary monitoring system with integrated functional lung imaging and chest sound recording: a clinical investigation in healthy subjects", Physiological Measurement, vol. 44 (4), pp. 045002, doi:10.1088/1361-6579/acc82a
- [8] Gsell, Monika; Bulliard, Xavier; Schorderet Weber, Sandra; Xiang, Yang; Constant, Samuel; Steiner, Sandro; Biselli, Silvia; Pugin, Raphaël; Palmieri, Michele; Hogg, Andreas; Peitsch, Manuel C.; Hoeng, Julia; Stan, Adrian, "Inactivation of SARS-CoV-2 on salt-coated surfaces: an in vitro study", Archives of Microbiology, 205, 272
- [9] Ingenito, A.; Allebé, C.; Libraro, S.; Ballif, C.; Paviet-Salomon, B.; Nicolay, S.; Diaz Leon, J. J., "22.8% full-area bifacial n-PERT solar cells with rear side sputtered poly-si(n) passivating contact", Solar Energy Materials and Solar Cells, 249, doi:doi:10.1016/j.solmat.2022.112043
- [10] Laithier, Jean-François; Storrer, Cédric; Bulliard, Xavier; Crenna, Maude; Gay, Julien; Pugin, Raphaël, "Des solutions de protection de l'aluminium pour les industries horlogère et médicale", Oberflächen Polysurfaces, 2023, Juillet-Aout, 4, p18-21
- [11] Lavielle, Nicolas; Mongruel, Anne; Bourouina, Tarik; Royon, Laurent; Beysens, Daniel, "Plastic foil micro-grooved by embossing enhances dew collection without aging effects", Plastic foil micro-grooved by embossing enhances dew collection without aging effects, doi:10.1016/j.mtsust.2023.100566
- [12] Libraro, S.; Lehmann, M.; Leon, J. J. D; Allebé, C.; Descoeuilles, A.; Ingenito, A; Haug, F. -J., "Interactions between aluminium and fired passivating contacts during fire-through metallization", Solar Energy Materials and Solar Cells, 249, doi:10.1016/j.solmat.2022.112051
- [13] Migliorelli, Davide; Ramos-Garcia, Victoria, "Fact-based nutrition for infants and lactating mothers—The NUTRISHIELD study", Front. Pediatr, Volume 11 - 2023, doi:10.3389/fped.2023.1130179

- [14] Motta, Margherita; Groves, Emily; Schneider, Andrea; Paolletti, Samantha; Henchoz, Nicolas; Ribes Lemay, Delphine, "Designing self-tracking experiences: A qualitative study of the perceptions of barriers and facilitators to adopting digital health technology for automatic urine analysis at home", PLOS Digital Health, 2023 Sep; 2(9): e0000319
- [15] Navaee, Fatemeh; Khornian, Niloofar; Longet, David; Heub, Sarah; Boder-Pasche, Stéphanie; Weder, Gilles; Kleger, Alexander; Renaud, Philippe; Braschler, Thomas, "A Three-Dimensional Engineered Cardiac In Vitro Model: Controlled Alignment of Cardiomyocytes in 3D Microphysiological Systems", Cells 2023, 12, 576, doi:10.3390/cells12040576
- [16] Navaee, Fatemeh; Renaud, Philippe; Piacentini, Niccolo; Durand, Mathilde; Bayat, Dara Zaman; Ledroit, Diane; Boder-Pasche, Stéphanie; Kleger, Alexander; Braschler, Thomas; Weder, Gilles, "Toward a Physiologically Relevant 3D Helicoidal-Oriented Cardiac Model: Simultaneous Application of Mechanical Stimulation and Surface Topography", Bioengineering 2023, 10, 266, doi:10.3390/bioengineering10020266
- [17] Proença, Martin; Ambühl, Jeremias; Bonnier, Guillaume; Meister, Théo A.; Valentin, Jérémie; Soria, Rodrigo; Ferrario, Damien; Lemay, Mathieu; Rexhaj, Emrush, "Method-comparison study between a watch-like sensor and a cuff-based device for 24-h ambulatory blood pressure monitoring", Scientific Reports, vol. 13 (1), pp. 6149, doi:10.1038/s41598-023-33205-z
- [18] Ristaniemi, Aapo; Secerovic, Amra; Dischl, Vincent; Crivelli, Francesco; Heub, Sarah; Ledroit, Diane; Weder, Gilles; Grad, Sibylle; Ferguson, Stephen J., "Physiological and degenerative loading of bovine intervertebral disc in a bioreactor: A finite element study of complex motions", Journal of the Mechanical Behavior of Biomedical Materials, Volume 143, 2023, 105900, doi:10.1016/j.jmbbm.2023.105900
- [19] Sainz Martinez, Cristina; Bach Cuadra, Meritxell; Jorge, João, "BigBrain-MR: a new digital phantom with anatomically-realistic magnetic resonance properties at 100-µm resolution for magnetic resonance methods development", NeuroImage, vol. 273, pp. 120074, doi:10.1016/j.neuroimage.2023.120074
- [20] Senaud, Laurie-Lou; Antognini, Luca; Christmann, Gabriel; Boccard, Mathieu; Despeisse, Matthieu; Ballif, Christophe; Paviet-Salomon, Bertrand, "Transfer-Length Method Measurements Under Variable Illumination to Investigate Hole-Selective Passivating Contacts on c-Si (p) and c-Si (n) Wafers", IEEE Journal of Photovoltaics 13(3) pp. 422-431, doi:10.1109/JPHOTOV.2023.3242131
- [21] Zein, Yamane El; Lemay, Mathieu; Huguenin, Kévin, "PrivaTree: Collaborative Privacy-Preserving Training of Decision Trees on Biomedical Data", IEEE/ACM Transactions on Computational Biology and Bioinformatics, pp. 1-14, doi:10.1109/TCBB.2023.3286274

Proceedings

- [1] Ayres-Ribeiro, Francisca; Wirsich, Jonathan; Abreu, Rodolfo; Jorge, João; Teixeira, Andreia Sofia; Francisco, Alexandre P.; Figueiredo, Patrícia, "Brain's Dynamic Functional Organization with Simultaneous EEG-fMRI Networks", Complex Networks XIV, A. Teixeira, F. Botta, J. Mendes, R. Menezes, G. Mangioni (Eds.), Aveiro (PT), pp. 1-13, doi:10.1007/978-3-031-28276-8_1
- [2] Bernard, Gaëtan; Pejchal, Vaclav; Larsson, Joel; Sereda, Olha; Logé, Roland, "Laser powder bed fusion of high stiffness titanium-based metal matrix composite for space applications", ECSSMET, European Conference on Spacecraft Structures Materials and Environmental Testing, Toulouse, France, 103-109
- [3] Bourely, James; Kim, Jaemin; Aeby, Xavier; Siqueira, Gilberto; Nyström, Gustav; Vorobyov, Oleksandr; Beyer, Christian; Schmid, David; Briand, Danick, "Ecoresorbable radio-frequency platform for humidity and temperature sensing", Eurosensors XXXIV MDPI Proceedings 2023
- [4] Carrillo, Rafael E; Schubnel, Baptiste; Langou, Renaud; Alet, Pierre-Jean, "Dynamic Graph Machine Learning for Multi-Site Solar Forecasting", EU PVSEC 2023, doi:10.4229/EUPVSEC2023/4CO.8.5

- [5] Chai-Gao, Hui; Shynkarenko, Yevhen; Demuru, Silvia; Hermann, Nicola; Boia, Patricia-Daiana; Cristofolini, Peter; Petkus, Bradley; Generelli, Silvia; Cattaneo, Stefano; Burr, Loïc, "Portable Fluorescence Biosensing System for Low-Cost, Quantitative, and Multiplexed Allergen Screening", *mdpi Proceedings* 2023, Conference Topic: Bio(medical) Sensors and Diagnostics, Presented at the Eurosensors XXXIV, Lecce, Italy, 10-13 September 2023
- [6] Chin, Sanghoon; Phelan, Richard; Carney, Kevin; Benoy, Thomas; Schröder, Stephan; Wastine, Benoit; Martin, Hans; Balet, Laurent; Lecomte, Steve, "Complete characterization of multipass gas cell using a high sensitive optical frequency-domain reflectometry", European Workshop on Optical Fibre Sensors (EWOFS 2023), M. Wuilpart, C. Caucheteur (Eds.), Mons (Belgium), pp. 21, doi:10.1117/12.2678102
- [7] Chin, Sanghoon; Van Zaen, Jérôme; Muntane, Enric; Denis, Séverine; Schröder, Stephan; Martin, Hans; Lecomte, Steve; Balet, Laurent, "Artificial Neural Network-assisted MIR gas spectroscopy to eliminate detrimental temperature-induced spectral shifts", *Optical Sensors* 2023, Munich (DE), pp. STu2D.5, doi:10.1364/SENSORS.2023.STu2D.5
- [8] Jang, Jaeoun; Chai-Gao, Hui; Summerfield, Artur; García-Nicolás, Obdulio; Bieri, Rudolf; Schweinar, Kevin; Limacher, Roger; Bayat, Dara; Schmid, David, "Initial attachment of saliva droplets containing SARS-CoV-2 to polymer surfaces", <http://dx.doi.org/10.13140/RG.2.2.14385.04966>, doi:10.13140/RG.2.2.14385.04966
- [9] Kiener, Lionel; Saudan, Hervé; Novo, David; Bernard, Gaétan; Miler, Mickaël, "Slipring made by Additive Manufacturing: from redesign to validation test results", ESMATS 2023, Warsaw (PL)
- [10] Klauser, Elias; Gupta, Vaibhav; Karimi, Alireza, "Data-Driven IQC-Based Robust Control Design for Hybrid Micro-Disturbance Isolation Platform", 62nd IEEE Conference on Decision and Control, Singapore (SG)
- [11] Klauser, Elias; Gupta, Vaibhav; Karimi, Alireza, "Data-driven IQC-Based Uncertainty Modelling for Robust Control Design", IFAC World Congress 2023, Yokohama (JP)
- [12] Lang, Guilain; Perruchoud, Gerald; Novo, David; Brun, Stephane, "Uncoupling Development Time From The Size Of A Library Of AM Parts Through Complexity Reduction And Modeling Of Topology Optimization Results", AMPA 2023, Luzern (CH), doi:10.1007/978-3-031-42983-5_9
- [13] Martinez, Cristina Sainz; Marques, José P.; Bonanno, Gabriele; Hilbert, Tom; Tuleasca, Constantin; Cuadra, Meritxell Bach; Jorge, João, "In-vivo imaging of the human thalamus: a comprehensive evaluation of structural imaging approaches for thalamic nuclei differentiation at 7T", ISMRM Annual Meeting, Toronto (CA)
- [14] Scharnhorst, Paul; Schubnel, Baptiste; Carrillo, Rafael E; Alet, Pierre-Jean; Jones, Colin N, "Uncertainty-aware Flexibility Envelope Prediction in Buildings with Controller-agnostic Battery Models", 2023 American Control Conference (ACC), doi:10.23919/ACC55779.2023.10156041
- [15] Sutter, Axel; Gorecki, Tomasz T.; Bhoir, Shubham S., "Method to Embed Behavioral Battery Model in Predictive Energy Management Systems", ISGT Europe 2023, Grenoble, France
- [16] Valenza, Gaetano; Alcaiz, Mariano; Alfeo, Antonio Luca; Bianchi, Matteo; Carli, Vladimir; Catrambone, Vincenzo; Cimino, Mario C. G. A.; Dudnik, Gabriela; Duggento, Andrea; Ferrante, Matteo; Gentili, Claudio; Guixeres, Jaime; Rossi, Simone; Toschi, Nicola; van Wassenhove, Virginie, "The EXPERIENCE Project: Unveiling Extended-Personal Reality through Automated VR Environments and Explainable Artificial Intelligence", 2023 IEEE International Conference on Metrology for eXtended Reality, Artificial Intelligence and Neural Engineering, Milano (IT)
- [17] Zanella, Frédéric; Fernandez, Oscar; Offermans, Ton; Aderneuer, Tamara; Chaves, Julio; Mohedano, Ruben; Basset, Guillaume, "Manufacturing acceleration of freeform micro-optical arrays (FMOAs) with CAD algorithms", SPIE OPTO, Advanced Fabrication Technologies for Micro/Nano Optics and Photonics XVI, 124330F, San Francisco, CA, USA, doi:10.1117/12.2647854
- [18] Zanella, Frédéric; Schneider, Christian; Ceric, Luka; Basset, Guillaume, "UV-replicated microlenses for quantum devices", SPIE OPTO, Quantum Sensing and Nano Electronics and Photonics XIX, 124300C, San Francisco, CA, USA, doi:10.1117/12.2648224

Conferences and Workshops

Alet, Pierre-Jean; Eftymiou, Venizelos; Adinolfi, Grazia; Arrowsmith, Greg; Barchi, Grazia; Chowdhury, Gofran; De Vito, Saverio; Garabetian, Thomas; Graditi, Giorgio; Leloux, Jonathan; Tsanakas, Ioannis, "Mapping the relevance of digitalisation for photovoltaics", European Photovoltaic Solar Energy Conference and Exhibition (EUPVSEC) 2023

Beysens, Jona; Sénéclauze, Martin; Dallermagne, Philippe; Bigdeli, Siavash, "Early Exiting with Compressible Activations for Efficient Neural Network Inference", IEEE, Smart Systems Integration, Bruges, Belgium

Boder-Pasche, Stéphanie; Heub, Sarah; Garzuel, Manon; Fonta, Charlotte; Atakan, H. Baris; Goldowsky, Jonas; Ischer, Réal; Ledroit, Diane; Valentin, Thomas; Schneeberger, Kerstin; Spee, Bart; Weder, Gilles, "Automated platform for the micro-perfusion of bioengineered tissues", MPS World Summit 2023, June 26 – June 30, 2023, JW Marriott Hotel Berlin, Berlin, Germany

Boder-Pasche, Stéphanie; Weder, Gilles, "ORGANTRANS project - bioprinted liver tissue engineering as new alternative to chronic liver patients", 3rd Regenerative Medicine Workshop, June 1st, 2023, Prague, Czech Republic

Boiko, Dmitri L., "Two faces of superradiance in tandem-cavity ridge waveguide heterostructures", NDSL 2023: Nonlinear Dynamics in Semiconductor Lasers, Berlin (DE)

Brohet, Marco; Valencia, Felipe; Regazzoni, Francesco, "Invited Paper: Instruction Set Extensions for Post-Quantum Cryptography", Brohet, M., Valencia, F., & Regazzoni, F. (in press). Invited Paper: Instruction Set Extensions for Post-Quantum Cryptography. In 2023 IEEE/ACM International Conference On Computer Aided Design (ICCAD) IEEE.

Cristofolini, Peter; Mühlbach, Lea; Markocic, Miha; Orawez, Georg; Shynkarenko, Yevhen; Martinez-Franzes, Elena; van Bavel, Bert; Cattaneo, Stefano, "Fluorescence-based sensor for continuous monitoring of microplastic in sea water", Precision Photonic Systems '23, FH OST in Buchs SG, 22nd-23rd October 2023

Del Giovane, Stefano; Migliorelli, Davide; Bagheri, Neda; Porchetta, Alessandro; Altug, Hatice; Burr, Loïc, "CRISPR-based one-pot assay for the detection of monoclonal antibodies", NanoBioTech-Montreux Conference 2023

Fahradin, Mujovi; Jacques, Levrat; Antonin, Faes; Pierrick, Duvoisin; Sukanya, Prabhudesai; Gianluca, Cattaneo; Lioui, Jaques; Matthieu, Despeisse; Christophe, Ballif; Gilles, Arnoux; Nicolas, Bassi; Rajesh, Ambigapathy, "I-V Curve Simulation of Curved PV Modules for VIPV under Various Irradiation Conditions", PVinMotion, 's-Hertogenbosch, Netherlands

Györvary, Erika, "State-of-the-art and future challenges for greener ECS manufacturing/PFAS", Chips JU Consultation Workshop „Sustainable and Greener Manufacturing of ECS“, webinar

Györvary, Erika, "How EU Gender Equality Strategy has pushed European RTO's and their sensor development to better gender balanced results", IEEE sensors conference, 30.10.2023, Vienna, Austria

Kastanis, Iason, "A bat on the production floor. Condition based monitoring with ultrasound", Kastanis, I., "Fledermaus in der Produktion - Condition Based Monitoring mit Ultraschall ", 8. F&E-Konferenz zu Industrie 4.0

Kurth, Felix, "Integrated sample preparation methods for portable point-of-care solutions", microTEC Südwest, Fachgruppe In-vitro-Diagnostik, 23. Fachgruppensitzung

Kurth, Felix; Glaser, Nicolas; Migliorelli, Davide; Gao, Hui; Wipf, Mathias; Paoletti, Samantha; Generelli, Silvia; Burr, Loïc, "On the integration of printed electronics in fluid cartridges and lateral flow devices for point-of-care", LOPEC 2023

Lachowicz, Agata, "Stability of minimodules with copper plated heterojunction solar cells", Metallization and Interconnection Workshop, 2023, Neuchâtel

Ledroit, Diane; Disser, Jérémie, "Smart Bone: from in vitro modelling of IVD damage to in vivo monitoring using implanted sensors", ORTHOMANUFACTURE, April 26 to 27, 2023, Beaulieu congress center Lausanne, Switzerland

Migliorelli, D.; Glaser, N.; Zinggeler, M.; Generelli, S.; Markocic, M.; Stergiou, I.; Orawez, G.; Gao, H.; Mühlbach, L.; Junuzovic, R.; Schmid, N.; Paoletti, S.; Abongomera, C; Paris, D.; Burr, L., "Smart Urine Analyser for the use in Low-Resource Environments", BioNanoMed 2023, Graz, Austria

Migliorelli, Davide, "Screen-printed DNA-based sensors for detection of the prostate cancer biomarker miR-21 – a feasibility study", EuroAnalysis 2023

Migliorelli, Davide; Julia, Kuligowski, "Advancing Urinary Health Monitoring: fact-based nutrition for infants and lactating mothers", 2023-10-25, 6th Swiss Symposium in POC Diagnostics

Offermans, Ton, "Phabulous – Fertigungstechnologien für die Freiform-Optik", Trends in Micro Nano - swiss mnt network

Offermans, Ton; Zanella, Frédéric; Basset, Guillaume, "Phabulous – Manufacturing of large surfaces with free-form micro optics", SPIE Digital Optical Technologies 2023

Preitner, Karen; Blanc, Sébastien; Honzatko, David; Kündig, Clément; Pad, Pedram; Saeedi, Sareh; Peña-Haro, Salvador; Lechevallier, Pierre; Rieckermann, Jörg; Dunbar, L. Andrea, "Intelligent multispectral vision system for non-contact water quality monitoring for wastewater", Proc. SPIE 12438-61, AI and Optical Data Sciences IV (2 February 2023)

Russi, Mario, "DeckCheck - One-Shot-Learning for Smart Lab Automation", 8. F&E-Konferenz zu Industrie 4.0, Industrie 2025

Schmid, David; Paoletti, Samantha; Grad, Sibylle; Hutter, Andreas; Schmid, Philipp. A. E.; Dennenwaldt, Teresa, "CSEM VIVA! 2023 Netzwerkanlass Präsentationen", CSEM VIVA!, 2023

Schmid, Philipp A. E., "Künstliche Intelligenz (KI) - Revolution im Maschinenbau?", 50 Jahre Jubiläum ATP Hydraulik

Schmid, Philipp A. E., "My Chemical Romance - Materialeigenschaften auswerten leicht gemacht", 8. F&E-Konferenz zu Industrie 4.0, Industrie 2025

Schmid, Philipp A. E., "Qualität dank (oder trotz) KI", CSEMVIVA! 2023

Schmid, Philipp A. E., "Predictive quality concept – utilising data sets to forecast product quality", Future Labs Live 2023

Schmid, Philipp A. E., "KI – Chancen in der Instandhaltung?", maintenance Schweiz

Schmid, Philipp A. E., "Künstliche Intelligenz - Revolution im Alltag", SATW TecNight Sarnen

Schmid, Philipp A. E., "Von der Produktionsmaschine zur Getriebeüberwachung - Maintenance mit wenig Sensoren", smart maintenance insights 2023

Schmid, Philipp A. E., "Wie ist Hochleistungsproduktion in der Schweiz noch möglich?", Swiss Automation 2023 «Efficiency in Automation»

Schmid, Philipp A. E., "Deep-Learning in der Industrie – was sind die Erfolgsfaktoren?", Swiss Medtech Fachgruppe Zuliefererindustrie, Biel

Schmid, Philipp A. E., "Die technologiewelle rollt - Komfortzone verlassen", CSEM technoVation, KKL Luzern

Schmid, Philipp A. E., "Das Potential künstlicher Intelligenz zur Vermeidung von Maschinenausfällen", Unternehmerraustausch Laufental / Künstliche Intelligenz und Re-shoring – Chancen für die regionale KMU-Wirtschaft

Schmid, Philipp A. E., "Industry 4.0 & Machine Learning", Workshop on Challenges and Novel Approaches for Industry 4.0 Joint Event by Innovation Booster Robotics and Databooster

Schmid, Philipp A. E., "Production Data for Predictive Quality", Workshop on Digital Twins and Data Usage

Schmid, Philipp A. E., "Keynote: Die Technologiewelle rollt – Komfortzone verlassen", World of Data

Schmid, Philipp A. E.; Kraus, Stephan, "Von der Vision zur Umsetzung: eine Digitalisierungsreise", CSEM next Landquart

Schmid, Philipp A. E.; Leiterer, Reik, "Daten sind Öl für KI - aber wie? Innovation Booster helfen!", Business Focus Day, Digital Days 23 in Aarau

Schmid, Philipp A. E.; Rüdlinger, Stephan; Linnenbach, Frank, "Industrieholz trifft Deep Learning", Schwyz Next Webinar

Schmid, Philipp A. E.; Steinecker, Alexander, "Die Technologiewelle rollt – Hochleistungsproduktion in der Schweiz dank Daten und KI", SwissICT INNOtalk

Šećerović, Amra; Ristaniemi, Aapo; Crivelli, Francesco; Heub, Sarah; Weder, Gilles; Ferguson, Stephen; Ledroit, Diane; Grad, Sibylle, "Advanced bioreactor studies of region-specific responses in the intervertebral disc to compression, flexion/extension and torsion", EORS 2023 31st Annual Meeting of the European Orthopaedic Research Society, 27-29 September 2023, Porto, Portugal

Shynkarenko, Yevhen; Chai-Gao, Hui; Demuru, Silvia; Hermann, Nicola; Boia, Patricia-Daiana; Cristofolini, Peter; Petkus, Bradley; Generelli, Silvia; Paoletti, Samantha; Burr, Loïc; Cattaneo, Stefano, "Miniaturized Fluorescence Biosensing Reader for Multiplexed Allergen Screening at the Point-Of-Care", Precision Photonic Systems '23, FH OST in Buchs SG, 22nd-23rd October 2023

Steinecker, Alexander, "Predictive maintenance, predictive quality - Get the best out of your machine data.", IVAM Hightech Summit, 3-4 May 2023, Bochum, Germany

Steinecker, Alexander; Schmid, Philipp A. E., "Breakoutsession an der AiCON: KI in der Industrie – und was passiert mit den Fachexperten?", AiCON 2023, Pfäffikon (SZ)

Widmer, Silvan, "eSorter - Schnelle und autonome Vereinzelung von Paketen aller Art", 8. F&E-Konferenz zu Industrie 4.0, Industrie 2025

Zanella, Frédéric; Schneider, Christian; Ceric, Luka; Basset, Guillaume, "Optimization of microlens arrays for photon detectors", SPIE Optics + Optoelectronics, Quantum Optics and Photon Counting 2023, PC1257005, Prague, Czech Republic 10.1117/12.2666068

Zubkovs, V.; Markocic, M.; Basoli, V.; Grad, S.; Sajjadi, S. H.; Boghossian, A. A.; Cattaneo, S., "Optical Readers for Monitoring Response of Fluorescent Sensors in SWIR Region", BioNanoMed 2023, Graz, Austria

Research Projects

Botnar Research Center for Child Health (BRC) COVENT – Improve ventilation safety by means of intra-tracheal pressure monitoring – a short-term and a long-term solution

Eurostars BEAT-IT – Breakthrough multi-purpose electrodes for activity tracking for interoperative patients and topsport athletes

Eurostars	COLIDE – Coherent LiDAR demonstration based on a novel swept laser engine in the beyond 2 µm wavelength range
Eurostars	DARE – Development of AI-supported remote patient monitoring solution
Eurostars	EMBODISENSE – Embodiment of sensors to improve real-life gait
Eurostars	FHE-CLOUD – Fully homomorphic encryption (FHE) based cloud service for healthcare
Eurostars	FITSILVER – Fitness and calorie tracking for the silver generation
Eurostars	IAP-CMM – Development and clinically test of a novel multimodal sensor system (hardware and algorithms) to continuously monitor in a noninvasive and straightforward way the intra-abdominal pressure (IAP) of intensive care patients (ICPs)
Eurostars	IMPULSE – Closed-loop control of blood pressure for people with spinal cord injury
Eurostars	LONGLIGHT – Long lifetime 1.5 um modelocked lasers via improved gain glasses
Eurostars	PROOFED – Piezoelectric motors for extreme conditions
Eurostars	SAFEUVC – Field-emission 210 nm light source for disinfection
Eurostars	SCREENBEAT – Screening and monitoring of cardiac arrhythmias and sleep apnea
Eurostars	RAMSES – Development of a GW peak power industrial laser
NTN Innovation Booster in Robotics	MASAFO – Improving sales forecast using machine learning and historic data for maxon motors
NTN Innovation Booster in Robotics	ROBOBRUSH – Proof of concept for automatic parquet floor brushing robot
NTN Innovation Booster – Microtech	FL-REF – Reference particles with defined sizes and fluorescence lifetimes
SNI – Nanoargovia	META-DISPLAYS – Design and fabrication of metasurfaces for rollable displays
SNI – Nanoargovia	QSBI – Quantum sensors for brain imaging
SNSF	BLUVES – Development of nanophotonics based structures to generate blue and UV frequency comb for the calibration of spectrographs used in exoplanet search
SNSF	ENHEART – Exploring full content of optical signals to enhance cardiac arrhythmia screening
SNSF	ENSQSENS – Novel, ensemble-based quantum sensors
SNSF	PAPET – Protective, passivating, and selective transport layers in perovskite/c-Si tandem solar cells
SNSF	PHASE-LOGIC – Phase logic networks for optimized computation
SNSF	RADICALS – Rationally designed thin contact layers enabling large-scale perovskite-on-silicon tandem photovoltaics
SNSF	SHAMAN – Shadow mask localization of thin films for back-contacted crystalline silicon solar cells and energy harvesters
SNSF	SQ-NET – Scalable high bandwidth quantum network
SNSF / Ambizione	PUZZLE – Bridging gaps in the neuroimaging puzzle: advanced techniques for comprehensive mapping of brain anatomy and multi-scale network activity
SNSF / BRIDGE	AOP-PLUGNPLAY – Implementation of adverse outcome pathway in a “plug & play” microfluidics system. Liver fibrosis as a proof of principle
SNSF / BRIDGE	EMIL – Emotion in the loop: a step towards a comprehensive closed-loop deep brain stimulation in Parkinson disease

SNSF / BRIDGE	ENABLE – Standardized integrated photonic nonlinear building blocks for lithium niobate on insulator
SNSF / BRIDGE	VIPS – Ultra-low power visual perception system
SNSF / BRIDGE Discovery	GREENSPACK – Green smart packaging for perishable goods
SNSF / BRIDGE Discovery	LINIOS – Gas spectrometer based on lithium niobate on insulator photonics integrated circuit
SNSF / BRIDGE Discovery	MICROAC2 – Acoustofluidic platform for 3D positioning of microtissues for efficient microhistology
SNSF / BRIDGE Discovery	OPOSSUM – Ultra-sensitive photonics accelerometers for next generation seismic sensor networks
SNSF / CHIST-ERA	TESLA – Transient, electronics for sustainable digital agriculture
SNSF / COST	PEDALO – Positive energy district algorithms for load forecasting and optimal dispatch
SNSF / ERA-NET QuantERA	UTP4Q – A versatile quantum photonic IC platform through micro-transfer printing
SNSF / Sinergia	BIOREACT – In vitro organ degeneration models for musculo-skeletal research
SNSF / Sinergia	RADICALS – Rationally designed thin contact layers enabling large-scale perovskite-on-silicon tandem photovoltaics
Swiss Federal Office of Energy (SFOE)	ENERGYCAD – Anergy grid in Bourg en Lavaux
Swiss Federal Office of Energy (SFOE)	ASSURED-PV – Assessing uncertainties and risks in photovoltaic plant performance and operation
Swiss Federal Office of Energy (SFOE)	BATMAESTRO – OFEN project for creation of optimization-compatible batteyr models
Swiss Federal Office of Energy (SFOE)	COMET – Developement of copper metallization processes for current p-type and future n-type solar cells and modules
Swiss Federal Office of Energy (SFOE)	DECIDER – Development of dry electrodes for solid state batteries
Swiss Federal Office of Energy (SFOE)	DELAPS – Demonstration of large-area passivating contact sputtering for high-efficiency solar cells
Swiss Federal Office of Energy (SFOE)	GIF – Greenhouse infrared filters
Swiss Federal Office of Energy (SFOE)	HYSTIMATOR – Automated online hysteresis estimation for improved state estimation for LFP batteries
Swiss Federal Office of Energy (SFOE)	IEA-TASK13-2022 – Performance, operation & reliability of photovoltaic systems – Swiss Consortium
Swiss Federal Office of Energy (SFOE)	IPRECISE – Industrial passivating contacts approaches for high efficiency c-Si Solar cells
Swiss Federal Office of Energy (SFOE)	LANTERN – Living Labs interface for the energy transition
Swiss Federal Office of Energy (SFOE)	OPEN-SESAME – Modelling of energy storages for simulation/optimization of energy systems – open source energy storage models
Swiss Federal Office of Energy (SFOE)	OPERA – Utilisation optimale de l'énergie renouvelable avec PAC pour les immeubles collectifs en rénovation
Swiss Federal Office of Energy (SFOE)	SINA – Smart interoperability architecture: the decentralized data space in the building industry
Swiss Federal Office of Energy (SFOE)	SIRIUS – Swiss pilot line for aesthetic and ultimate power PV modules

Swiss Federal Office of Energy (SFOE)	SOLARBODY-OFEN – Integration of photovoltaic element for automotive applications	
Swiss Federal Office of Energy (SFOE)	SPET – High performance versatile components for electrification of future solar-powered aeronautical power train	
Innosuisse – Swiss Innovation Agency		
47005.1 IP-ICT	ADAPTIVESTORM	An ultra-energy-efficient AI chip for next-gen ICT applications
52948.1 IP-EE	ADASTRA	A different approach for silicon-based tandem solar cells using perovskite on back-contacted devices with three-terminal wiring to go beyond 30% power conversion efficiency.
48036.1 IP-ICT	ADRIOS_LIDAR	Real-time autonomous navigation system for on-orbit servicing
65949.1 INNO-LS	AICLOTTABILITY-STUDY	Miniaturization and prototyping of lab-based diagnostic assays
107.610.1 IP-LS	AirLiWell	Microstructured membrane for organoid production and culture at air-liquid interface
56367.1 IP-ICT	AIRO-PRINT	Adaptive system for automatic identification and marking of complex parts
49735.1 IP-LS	AIRVIMO	Airborne virus monitoring
33572.1 IP-ENG	AMC	Process optimization for additive membrane care
106.920.1 IP-EE	AMICOOL2023	Artificial intelligence for maintenance and improved control of commercial refrigeration systems
51090.1 IP-ENG	ASPIRE	Next generation SiC power electronics for e-mobility
55307.1 IP-EE	ATLAS	Development of new generation agrivoltaic translucent module architecture based on silicon
104.300.1 IP-EE	BeePV	Building integrated lightweight PV
55450.1 IP-EE	BIO-NO2	Reducing agricultural emissions with a new manure treatment technology
65645.1 INNO-LS	CALFVIEW	Try and adapt cooperative sensors (ECG) and Icarus (Stethoscope) for calf monitoring around neck (collar) or thorax.
67695.1 INNO-LS	CARDIOFLEX-CHECK	Feasibility study for an implantable pulse generator for an electronic blood vessel
68886.1 INNO-EE	Carport-Solar	Testing of new design solution for lightweight PV module and mounting structure.
68273.1 INNO-LS	CELLSENSE	Biomonitoring in microfluidic chip
43533.1 IP-ENG	CERANO	Development of barrier coatings onto anodized aluminium part for watch and medtech applications
35221.1 IP-LS	CEREBRO	ASIC-enabled depth electrodes for neural recording and ablation
44317.1 IP-EE	CHAMELEON	Development of advanced interconnection, solar cells, stringing, as well as colouring technologies and data analytics for mass production in 3S SolarPlus manufacturing line.
57757.1 IP-ENG	CHAMLED	Development of high-power rod-type femtosecond laser for micro-LED display production
69369.1 INNO-ENG	Check-My-Screw	Quality control of small screws

FLAGSHIP PFFS-21-20	CIRCUBAT	Swiss circular economy model for automotive lithium batteries
102.375 IP-EE	COLORPOWER	New generation colored encapsulant foil solution for the manufacturing of next generation-colored photovoltaic modules for building integration, with focus on manufacturing costs, performance, aesthetics and reliability.
69572.1 INNO-EE	COLORSTILE	Development of new design of solar tile
70033.1 INNO-LS	CytoXpress	CytoExpress
37705.1 IP-ENG	DALIE	Dry auto-localizing integrated electrodes
51719.1 IP-ENG	DENTIN	Adaptive endodontic instrument made of shape memory alloy
57765.1 IP-EE	DIGERATI	Dynamic graph machine learning for high resolution forecasting
46776.1 IP-ICT	DRIVERCHECK2	Intelligent vision system for driver monitoring coupled with steering command control system for improved road safety
67037.1 INNO-ICT	DTRCA-STUDY	Diagnostic Truth – root cause analysis study, follow up of DeepDive project DTRCA
102.648.1 IP-LS	DURAPATCH	Implantable patch for dura sealing
105.699 IP-LS	EARONCHIP	Auditory hair cells and the blood-labyrinth barrier (BLB) are critical for normal hearing and crucial for maintaining homeostasis and cochlear protection against inflammation and disease. Here, a model for BLB-On-a-Chip was demonstrated and this model will be automatized for its subsequent utilisation for drug testing.
103.963 IP-ENG	Easy	Easy assessment of solubility with high efficiency second harmonic light scattering
51474.1 IP-ICT	EBRAIN	Smart robust wireless control and management of heavy machines
68582.1 INNO-LS	eLFA	At-home blood test optimization
68721.1 INNO-ENG	ELOISE	AM-based compliant gimbal for electrical thruster gimbal
40657.1 IP-ENG	ESORTER	Vollautomatisches Sortieren von Sendungen bis 30 kg stellt nach wie vor eine grosse Herausforderung dar.
103.713 IP-LS	EXTRACE	Enabling single cell resolution analysis of cancer cells extracted from blood
62984.1 INNO-EE	FALAFEL	Prototyping of new stack for translucent lightweight PV modules for AgriPV
104.350.1 IP-ENG	FEMTOALIGN	Investigation of ultrastable and ultraprecise optical bench alignment for high precision instruments
100.509 IP-ICT	Forklift	Industry 4.0 – teleoperations in a dynamic industrial environment
101.441 IP-EE	FREESTILE	Development of new generation of photovoltaic tiles demonstrating cost effective manufacturing and high reliability
101.599 IP-ENG	FUTURE_LC	Design, fabrication tolerancing and prototyping of future light carpets
65118.1 INNO-ENG	GENTIANALUTEA	Feasibility study of using RF-based angle-of-arrival and ranging equipment for an outdoor drone landing system in collaboration
106.492.1 IP-LS	Hedgehog	Non-invasive microneedle patch for glucose monitoring of interstitial fluid
65960.1 INNO-LS	HemAI	Digital pathology tools for swab samples (blood and pulmonary swab)

43410.1 IP-ENG	HIHOLO	High quality volume diffraction gratings for digital holography microscopy for enhanced resolution, acceptance angle and field of view
66944.1 INNO-LS	Horm-EC	Real-time wearable hormone level
100.379 IP-LS	HYGIE	Detection of respiratory infections in indoor spaces.
65900.1 INNO-ICT	ICLEAN	Pre-study to look at possibility to identify cutlery and plates for automatic returns after events
41363.1 IP-LS	IMPLANT	Development of innovative customer-tailored composite multilayers in orthopedic- and trauma surgery
56426.1 IP-ENG	IMPULSECOREPLATE	Development of a multiwell plate system for accurate 2D and 3D cell-based assays making use of groundbreaking, unique solutions that allow significant market opportunities to be seized.
58669.1 IP-LS	INSPIRING	Development of a device for in-mouth lactate monitoring for sports applications
65147.1 INNO-EE	IN-SYON	In-situ polymer electrolyte for Si-anode Lithium-ion batteries
103.882.1 IP-ENG	JETOPTICS	Fabrication of microwedges and semi-transparent coatings for pressure/temperature sensing on aircraft engines
48561.1 IP-ENG	LACER-Study	Hybrid physical-based and data-driven modelling for least-costly tuning in laser cutting
56816.1 IP-LS	LarvaeSorter	Development of a novel device capable of handling zebrafish larvae for high throughput
52368.1 IP-ICT	LCAT	Smart asset tracking is key for operational efficiency and minimization of capital expenses.
100.554 IP-EE	LEARN-CEM	Self-learning energy manager
43059.1 IP-ENG	LIFELUB	Development and implementation of a new lubrication technology
51734.1 INNO-LS	LOPLUS	Machine learning powered light obscuration technology for improved robustness and particle classification
50031.1 IP-ENG	LUPINE	High-resolution position sensor for space application
61801.1 IP-ENG	M-CUBE	Development of a high-resolution magnetic field gradiometer.
101.321.1 IP-ENG	MARIE	Automatized and electro mechanized syringe for animal health
64230.1 INNO-LS	METTLE	Mental stress evaluation with smartphone
69745.1 INNO-EE	MEZENC	Testing of new lightweight PV modules providers + combination with light mounting structures. Further develop expertise in light PV systems
102.837.1 IP-LS	MICE	Multispectral imaging for intra-operative cancer delineation
102.485.1 IP-ICT	MIEWA	Multispectral imaging for examination of works of art
107.611.1 IP-LS	MISO	Automation of mitochondria isolation process
64456.1 INNO-LS	MitoPrep	Concept study toward the automation of CellVie filtration process.
106.780.1 IP-ENG	MODEN	Moisture density sensor
52886.1 IP-LS	NEON	Neonate monitoring – SpO2, BP and oHRM features to OxyPRem NIRS medical system

107.108.1 IP-LS	Neophytes	Invasive plants (so-called ned must be monitored and restricted. Neophytes cophytes) are spreading along the SBB track network and their spreause specific problems (damage to infrastructure, health damage to humans & animals, threat to biodiversity). The management of neophytes needs automation.
55424.1 IP-LS	NEOS	The NeurOphthalmoscope – Early diagnosis of brain diseases
61069.1 INNO-ENG	NICE	Nonlinear interfeometer for f_CEO detection of 1550nm Menhir Photonics lasers
63681.1 INNO-LS	NIMP	Non-invasive microneedle patch for glucose monitoring
56034.1 IP-LS	NIOXIS	Nitric oxide optical sensors for inflammation monitoring
108.672 IP-LS	OPAFA	Redefining standard fatigue assessments with digital biomarkers
63050.1 INNO-EE	OPAL	Optimized PV panels for dichroic LCPV systems
57515.1 IP-LS	OrganEYEr	High-throughput sorting of large and small organoids powered by deep learning for drug discovery, tissue engineering, and disease modeling
105.335.1 IP-LS	OrganoCell	Standardized individualized organoid dissociation for single cell downstream analysis
60042.1 IP-LS	ORTHO	Closing the gap in digital orthopedics
105.402.1 IP-ICT	Panama	Customer specific, multi-modal solution for automatic characterization of thermoanalytical measurements
64278.1 INNO-ENG	PANDA	Industrial level packaging of PICs light sources for datacom applications
61071.1 IP-LS	Perform	Biomimetic 3D tumor microenvironment on-chip for preclinical testing of cancer immunotherapies
60157.1 INNO-EE	PIN7	Evaluation of lightweight pv modules for Agrivoltaics
106.177.1 IP-ENG	PLEASURE	Photoplethysmography simulator for blood pressure
103.067.1 IP-EE	PollutionKeeper2	Water flow and quality monitoring
68993.1 INNO-ICT	ProfileCheck-Study	ProfileCheck-Study
67673.1 INNO-ENG	QReam	Quality control and process automation for reaming parts
56972.1 IP-ENG	REACT	Development and implementation of a full pipeline for process optimization (offline, refinement & online) for generating gear grinding machines.
40504.1 IP-ENG	REDULAS	Development of advanced femtosecond laser based ultra-precision manufacturing system for smart micro-LED display
70175.1 INNO-ENG	SABRA	Feasibility study for an autonomous safety bracelet
61803.1 IP-ENG	SANPRO	Sanding professional
50339.1 IP-ENG	SAPHIR	Semi-transparent solar cells on watch saphir
102.006 IP-EE	SELMA	Development of Li-metal composite anodes for Li-metal batteries
65610.1 INNO-LS	SINIVALI	Feasibility study on monitoring and assessing risks of preeclampsia
57886.1 IP-ICT	SMARTLADLEGATE	Additive, real-time monitoring system to increase safety and efficiency for steel casting

100.583 IP-ICT	SMARTRAIL	Maintenance, asset management and health indicator of rolling stock materials.
43816.1 IP-ENG	SMARTSPRING	Intelligent spring that reduces machine downtime, prevents failures and helps to design the optimum spring
53212.1 IP-ICT	SmartWaste	Plug & Play smart waste management
58504.1 IP-ENG	SPADLENS	Reliable development and characterization of SPAD sensors enhanced with thin and gap-less microlenses
53012.1 IP-ICT	SPG-ROBOT	Development of a tool to automate floor processing tasks
50561.1 IP-LS	TESTMATE	A rapid self-test for sexually transmitted diseases that provides results in minutes, supported by digital health
101.260.1 IP-ENG	TID	Integrated tourbillon with detent for watch movement
43052.1 IP-ENG	TURBOPREDICTIONS	Steigerung der Effizienz, der Verfügbarkeit und der Lebensdauer von Turbokompressoren aufgrund einer erweiterten Datenerhebung und - Analytik
70138.1 INNO-ENG	VIBRATO	Industrial wireless vibration sensing
105.500.1 IP-ICT	Vital-Plus	Continuous non-invasive measurement of core vital signs on the hospital ward
46999.1 IP-ICT	VIVALDI	Quality control and high accuracy tracking system for steel mills
48014.1 IP-ENG	WATMON	Drinking water quality early indicator, base on refractive index change

European Commission Projects

HORIZON – KDT-JU 2022-1-IA	14AMI	Holistic metrology and quality control for 14 Angstroms module integration
HORIZON – KDT-JU 2021-1-IA	AGRARSENSE	Smart, digitalized components and systems for data-based Agriculture and Forestry
H2020 – ATTRACT	AHEAD	Advanced heat exchange device
H2020 – INFRAINNOV 2019-2020	AIDAINNOVA	Advancement and innovation for detectors at accelerators
H2020 – ECSEL 2019-2-RIA	ANDANTE	Ai for new devices and technologies at the edge
HORIZON – CL5 2022-D2-01	BATMAX	Battery management by multi-domain digital twins
HORIZON – CL5 2023-D2-01-04	BATTERY2LIFE	Battery management system and system design for stationary energy storage with 2nd LIFE batteries
H2020 – LC-SC3-RES-6 2018	BESMART	Innovative building envelope for sustainable, modular, aesthetic, reliable and efficient construction
H2020 – FETOPEN	CFLOW	Coherent ultra-fast long wave infrared communications
H2020 – ECSEL 2019-1-IA	CHARM	Challenging environments tolerant smart systems for IoT and AI
HORIZON – CL4 2021	CLUSTEC	Scalable continuous variable cluster state quantum technologies
HORIZON – CL4 2022- HUMAN-02	DAIEDGE	A network of technology enablers for the research and delivery of secure, efficient and scalable AI at the Edge & Deep Edge
H2020 – LC-SC3-EE-2019	DOMOS	Operating system for smart services in buildings
HORIZON – EIC-2021	ECLIPSE	ECL-based infectious pathogen (bio)sensor

HORIZON – KDT-JU 2022-2-RIA	EECONE	European ecosystem for green electronics
H2020 – ICT 2020	ELENA	European electro-optic and nonlinear PIC platform based on lithium niobate
H2020 – NMBP-23-2020	EMAPS	Electro-mechano-active polymer-based scaffolds for heart-on-chip
H2020 – ECSEL 2020-1-IA- two-stage	ENERGY ECS	Smart and secure energy solutions for future mobility
HORIZON – CL4 2022- SPACE-01-11	EROSS-IOD	European robotic orbital support services in-orbit demonstration
HORIZON – CL5 2022- D3-03	EVERPV	Highly efficient delamination technologies to recover and reuse metals, glass, polymers from end-of-life photovoltaic panels
H2020 – FETPROACT 2020-2	EXPERIENCE	The “Extended-Personal Reality”: augmented recording and transmission of virtual senses through artificial-intelligence
HORIZON – CL4 2021 TWIN-TRANSITION-01-02	FLASH-COMP	Flawless and sustainable production of composite parts through a human centred digital approach
HORIZON – CL5 2021	GENEX	New end-to-end digital framework for optimized manufacturing and maintenance of next generation aircraft composite structures
HORIZON – CL5 2022-D3-01	GLOCALFLEX	A global as well as local flexibility marketplace to demonstrate grid balancing mechanisms through cross-sectoral interconnected and integrated energy ecosystems enabling automatic flexibility trading
H2020 – SPACE 2018	HEATPACK	New generation of high thermal efficiency components packages for space
H2020 – SC1 2019 Single-Stage-RTD	HEDIMED	Linking immune-mediated diseases to early exposures for innovative solutions
HORIZON – KDT-JU 2021-1-IA	HICONNECTS	Heterogeneous Integration for connectivity and sustainability
H2020 – LC-BAT-14-2020	HIDDEN	Next generation lithium metal batteries with improved quality, reliability, and life (QRL)
H2020 – LC-SC3-RES-15 2019	HIGHLITE	High-performance low-cost modules with excellent environmental profiles for a competitive EU PV manufacturing industry
HORIZON – CL4 2023- DIGITAL-EMERGING-01-53	HIGHLIGHT	Highly integrated versatile laser source enabling two-photon excitation in digital diagnostics and biomedical research
H2020 – LC-SC3-RES-15 2019	HIPERION	Hybrid photovoltaics for efficiency record using integrated optical technology
HORIZON – CL4 2022- RESILIENCE-01	I-EDGE	Nanomechanical hardware platforms for edge computing
HORIZON – HLTH 2021- ENVHLTH-02	INCHILDHEALTH	Identifying determinants for indoor air quality and their health impact in environments for children: measures to improve indoor air quality and reduce disease burdens
HORIZON – CL5 2023-D3-01	INCREASE	Integrated PV solutions, effective advancements towards uptake of PV integrated in buildings & infrastructure
HORIZON – CL4 2022- DIGITAL-EMERGING-01	LIBRA	Light-based multisensing system for screening of pathogens and nutrients in bioreactors
HORIZON – KDT-JU-2022 2-RIA	LOLIPOP-IOT	Long life power IoT solutions for predictive maintenance

HORIZON – CL4 2021	LOLLIPOP	Lithium niobate empowered silicon nitride platform for fragmentation free operation in the visible and the NIR
HORIZON – CL4 2022-RESILIENCE-01	MADE-3D	Multi-material design using 3D printing
H2020 – NMBP-FOF 2018	MANUELA	Additive manufacturing using metal pilot line
H2020 – ICT 2019-2	MEDPHAB	Photonics solutions at pilot scale for accelerated medical device development
H2020 – ECSEL 2019-1-IA	MOORE4MEDICAL	Accelerating innovation in microfabricated medical devices
HORIZON – MSCA 2021 SE-01	NANOIMMUNOERA	Nanotechnology-enabled detection of clinically relevant antibodies for early cancer Diagnosis and immunotherapy monitoring
H2020 – BG 2020-1	NAUTILOS	New approach to underwater technologies for innovative, low-cost ocean observation
HORIZON – CL5 2022-D2-01	NEMO	Next-generation models for advanced battery electronics
H2020 – LC-SC3-EE-2020-2	NEON	Next-generation integrated energy services for citizen energy communities
HORIZON – CL4 2022-RESILIENCE-01	NETHELIX	Intelligent digital toolbox towards more sustainable and safer extraction of mineral resources
HORIZON – KDT-JU 2021-1- IA	NEWLIFE	New remote non-invasive monitoring solutions for ensuring the health of mothers and babies before and after birth
HORIZON – CL5 2022-D2-01	NEXTBAT	Next generation technologies for battery systems in transport electrification based on novel design approach to increase performance and reduce carbon footprint
H2020 – SFS 2018	NUTRISHIELD	Fact-based personalized nutrition for the young
H2020 – EIC-FTI 2018-2020	OFFSHOREMUSTER	An integrated emergency response decision support system for enhancing workers' safety in offshore oil & gas operations
H2020 – NMBP-FOF 2018	OLEDSOLAR	Innovative manufacturing processes and in-line monitoring techniques for the OLED and thin film and organic photovoltaic industries (CIGS and OPV)
H2020 – SC1 2019 Single-Stage-RTD	ORGANTRANS	Controlled organoids transplantation as enabler for regenerative medicine translation
HORIZON – CL4 2021	PATTERN	Next generation ultra-high-speed microwave photonic integrated circuits using advanced hybrid integration
HORIZON – CL5 2021	PEPPERONI	Pilot line for European production of perovskite-silicon tandem modules on industrial scale
H2020 – NMBP-TR-IND 2018-2020	PEROCUBE	High-performance large area organic perovskite devices for lighting, energy and pervasive communications
H2020 – ICT 2019-2	PHABULOUS	Pilot-line providing highly advanced & robust manufacturing technology for optical free-form micro-structures
HORIZON – CL5 2022-D2-01	PHOENIX	Building more reliable and performant batteries by embedding sensors and self-healing functionalities to detect degradation and repair damage via advanced battery management system
H2020 – FETFLAG 2018-2020	PHOG	Sub-poissonian photon gun by coherent diffusive photonics

HORIZON – CL4 2022-DIGITAL-EMERGING-01-03	PHOREVER	Photonic integrated OCT-enhanced flow cytometry for cancer and cardiovascular diagnostics enabled by extracellular vesicles discrimination
H2020 – DT 2020-1	PHOTONHUB	One-stop-shop open access to photonics innovation support for a Digital Europe
H2020 – EIC-FTI 2018-2020	PHOTONSENS	A plug-and-play photonics-based biosensing platform for salmon pathogen detection
HORIZON – CL5 2021-D3-03	PILATUS	Digitalised pilot lines for silicon heterojunction tunnel interdigitated back contact solar cells and modules
HORIZON – KDT-JU 2021-2-RIA	REBECCA	Reconfigurable heterogeneous highly parallel processing platform for safe and secure AI
HORIZON – CL5 2022-D2-01	RECIRCULATE	Reuse of batteries through characterization, smart logistics, automated pack and module dismantling and repackaging and a blockchain enabled marketplace
HORIZON – CL4 2021-RESILIENCE-01	RESILEX	Resilient enhancement for the silicon industry leveraging the European matrix.
HORIZON – KDT-JU 2022-2-RIA	RESILIENT-TRUST	Trusted SMEs for sustainable growth of Europeans economical backbone to strengthen the digital sovereignty
HORIZON – CL5 2022-D3-01	SEAMLESS-PV	Development of advanced manufacturing equipment and processes aimed at the seamless integration of multifunctional PV solutions, enabling the deployment of IPV sectors
HORIZON – CL5 2021	SIC4GRID	Next generation modular SiC-based advanced power electronics converters for enhanced renewables integration into the grid
H2020 – SC1 2019 Single-Stage-RTD	SIM4BDR	Smart bone regeneration
H2020 – CS2-CFP10 2019-01	SMARTWISE	Smart miniaturized and energy autonomous regional aircraft wireless sensor.
HORIZON – CL5 2021-D2-01	SOLID	Sustainable manufacturing and optimized materials and interfaces for lithium metal batteries with digital quality control
H2020 – LC-BAT 2020-3	SPARTACUS	Spatially resolved acoustic, mechanical, and ultrasonic sensing for smart batteries
HORIZON – CL5 2023-D3-01	SPHINX	Sustainable photovoltaics Integration in buildings and Infrastructure for multiple applications
HORIZON – CL4 2021	SPRINTER	Low-cost and energy-efficient hybrid photonic integrated circuits for fiber-optic, free-space optical and mm-wave communication systems supporting time critical networking in industrial environments
H2020 – ECSEL 2020-1-IA-two-stage	STORAGE	Embedded storage elements on next MCU generation ready for AI on the edge
H2020 – SPACE 2018-2020	SURPRISE	Super-resolved compressive instrument in the visible and medium infrared for Earth observation applications
HORIZON – KDT-JU 2022-2-RIA	SUSTRONICS	Sustainable electronics for circular economy and eco-design
H2020 – CS2-CFP10 2019-01	SWISSMODICS	Development of a sensor with wide spectrum sensitivity for monitoring of damage and defects in composite structures
HORIZON – CL5 2022-D6-02	TRACE	Integration and harmonization of logistics operations

H2020 – ICT 2020-2	TRIAGE	Development of a smart, compact and cost-effective optical air quality sensor network for the hyperspectral detection of all relevant atmospheric pollution gases
HORIZON – CL2 2022-HERITAGE-01	TRIQUETRA	Toolbox for assessing and mitigating climate change risks and natural hazards threatening cultural heritage
HORIZON – CL5-2021-D3-02	TRIUMPH	Triple junction solar modules based on perovskites and silicon for high performance, low-cost and small environmental footprint
HORIZON – CL5 2021-D3-03	VALHALLA	Perovskite solar cells with enhanced stability and applicability
H2020 – INFRAIA 2020-1	VIPERLAB	Fully connected virtual and physical perovskite photovoltaics lab
H2020 – ICT 2018-2	WELMO	Wearable electronics for effective lung monitoring
H2020 – ICT 2019-2	ZEROAMP	Nanomechanical switch-based logic and non-volatile memory for robust ultra-low power circuits

European Space Agency, Swiss Space Office, and Space Science Projects

Carnegie Institution for Science

MIRMOS-CSU	Configurable slit mask Unit for the MIRMOS instrument
------------	---

ESA Projects

AEOLUS_BSM	Beam steering mechanism
AMICA	Flexure pivot for SPICA SAFARI in additive manufacturing
ANGELE	Motion transformation compliant mechanism based on additive manufacturing
ATOM	Manufacturing of the complex feature demonstrator for space application made of meta matrix composite (MMC) having the specific modulus >30 GPa·cm ³ /g.
BATMAM	Battery packaging in additive manufacturing
BIDTS	Benchmarking of integrated digitalisation technologies for application to new space projects and future ESA missions
CCM-MTG	Development and manufacture of corner cube mechanisms for MTG satellite
COLA	In-orbit particle debris detection and monitoring: feasibility study and simulator development
COOLER	Compact opening louver
CRUSSADER	Capture system for servicing and debris removal.
ELISAMET	Laser metrology for the LISA mission
FIFREDO	Fibered frequency doubler at 1560 nm
GC-Connect	Development of fluidic connections and packaging for gas chromatography chips
GLOOM	Design methodology for compliant mechanisms
HEROIC	High-power fibre-coupled optical switch for space applications
IMPROVE	Microvibration simulation and analysis tools
INWAVE	Developement and validation of three breadboards of fully integrated passive feed chains (including Diplexers, OMTs, filters) at Q, V and W-band respectively
ISOL	Development of a high performance microvibration isolation system
LICORIS	Development of a compact LiDAR for futur new space mision
LINES	Lidar for infrastructure, natural risks, and environmental survey: space technology transfer programifac
LINGO	Flexible hinge design and analysis for the LISA optical assembly tracking mechanism development with OHB.
LISA-mvib	Actuator modelling and testing in micro-vibration (exported forces)

LPC	Low-power cathodes: development of field emitting cathodes arrays for space neutralisers
MACADAM	Magnetically levitated pump for space applications: requirements definition and commercial evaluation
MCC-X	Development of a miniaturized motor controller for space exploration
MDP-CHEF	Cost effective hermetically sealed chip fuse
MICOR	Microwave optical oscillator
OSIP-2PH	Light-shift reduction of two-photon rubidium atomic clock
OSIP-VIB	Adaptive regulation for micro-vibration active-passive isolation systems
OSRC	Digital stabilisation electronics for lasers
PHOTAC-DERISK	Future on-board atomic clock critical items de-risking
POWERSAIL	Disruptive PV power array technology to enable economic viability of SPS
RESHAPE	Reusable shape memory shock absorption elements for future landing systems using additive manufacturing (OSIP)
R-MTS	Development and fabrication of robust miniature timing source (R-mTS) engineering models (EMs). These R-mTS EMs are double-resonance miniature atomic clocks.
SLOTT	Straylight lidar OGSE verification tool
SMARTIES	Design, procurement and qualification testing of a slip ring assembly rotor based on additive manufacturing
STAMP	EGSE for laser detector elegant breadboard
TEM-BULB	Follow-up project for the finished AGAL project.
TRACTOR	Smart materials for space actuators
TRUMET-PDIODE	Characterization of photodiodes for the ESA's TRUTHS mission
WALLIE	Development new time-of-flight detector
WAVEGUIDE	Development of waveguide switches based on friction-free mechanisms

Industrial Property

Patent portfolio

In 2023, CSEM filed on its name 6 patent applications related to new inventions (first filings). All these filings were regular applications (no provisional filings).

The patent portfolio was further enhanced by the extension to different countries of 24 patent applications based on previously filed inventions (17 cases of "filing under priority" and 7 cases of "entries into national/regional phase" from international applications).

Three (3) additional patents were filed in the name of CSEM partners as a first filing for an invention developed in cooperation with CSEM inventors.

Collaboration with Research Institutes and Universities

University	Institute	Professor	Field of collaboration
Adolphe Merkle Institut	Soft Matter Physics and Polymer Chemistry	U. Steiner, C. Weder	Bioinspired nanomaterials
Agroscope	Animal Production Systems and Animal Health	C. Ollagnier	Vital sign monitoring in livestock (pigs)
AIT	Austrian Institute of Technology	L. Sajti	Magnetic inks
Alpen-Adria-Universität Klagenfurt, Austria	Digital Age Research Center	E. Oswald	Cryptography & security
AORI Davos	Regenerative Orthopaedics	M. Stoddart, S. Grad	Bioreactors
BFH	Mikro- und Medizintechnik	G. Gruener	BinPicking & robotics

University	Institute	Professor	Field of collaboration
Carolina Center for Neurostimulation	Department of Psychiatry, UNC School of Medicine, Chapel Hill, NC	F. Frohlich, A. Seiler	Effects of transcranial alternating current stimulation (tACS) on memory recall and sleep-EEG in healthy elderly participants
CHUV	Department of Nephrology and Hypertension	M. Pruijm	Continuous blood pressure monitoring in dialyzed patients
CHUV	Department of Cardiology	E. Pruvot	Classification of cardiac arrhythmias
CHUV	Department of Nephrology and Hypertension	G. Wuerzner	Long-term blood pressure monitoring in patients with chronic hypertension
CHUV	Head and Neck Surgery	S. Christian	Multispectral endoscopy for real time delineation in surger.
EMPA	Cellulose & Wood Materials	G. Nyström	Chipless compostable sensor tags
EMPA	Advanced Material Processing	P. Hoffmann	Solid-state lighting
EPF Lausanne	Telecommunications Circuits Laboratory	A. P. Burg	Ultra-low power design, bias control
EPF Lausanne	Microwave and Antenna Group (STI IEM SCI-STI-AS)	A. Skrivervic	Wireless power transfer
EPF Lausanne	Laboratoire de physique des hautes énergies OS (SB IPHYS LPHE-OS)	G. Haefeli	On-chip microlens arrays for photodetectors (SiPM)
EPF Lausanne	Engineering Mechanics of Soft Interfaces	J. M. Kolinski	Smart interfaces/coatings
EPF Lausanne	Mixed-Signal Integrated Circuits Lab	K. Choo	RF transceiver
EPF Lausanne	Distributed Electrical Systems Laboratory (DESL)	M. Paolone	Predictive maintenance for batteries
EPF Lausanne	Signal Processing Laboratory 4 (LTS4)	P. Frossard	Privacy preserving machine learning and hierachical computing
EPF Lausanne	Computer Vision Laboratory	P. Fua	Reduced labelling machine learning
EPF Lausanne	Processor Architecture Laboratory	P. lenne	Embedded systems
EPF Lausanne	School of Computer and Communication Sciences	S. Vaudenay	Security
EPF Lausanne	Laboratory for Functional Inorganic Materials	W. Lee Queen	Nanomaterials
EPF Lausanne	Laboratory of Nanobiotechnology	A. Boghossian	Biosensors
EPF Lausanne	Institute of Bioengineering	B. Deplancke	Sequencing
EPF Lausanne	Laboratory for Biomedical Microfluidics	C. Merten	Microfluidics
EPF Lausanne	Microengineering	D. Briand, V. Subramanian	Chipless compostable sensor tag
EPF Lausanne	School of Engineering, Institute of Bioengineering	D. Van De Ville	Cuffless blood pressure estimation using raw photoplethysmography signal; wearable heart rate measurement during daily life and sport

University	Institute	Professor	Field of collaboration
EPF Lausanne	Advanced Quantum Architecture Laboratory	E. Charbon	Micro-optics
EPF Lausanne	Laboratoire d'architecture quantique (STI IMT AQUA)	E. Charbon, C. Bruschini	Color filter arrays and on-chip microlens arrays for photodetectors (SPAD)
EPF Lausanne	Advanced NEMS Laboratory	G. Villanueva	Nanofabrication of devices made out lithium niobate on insulator
EPF Lausanne	Solar Energy and Building Physics Lab (LESO-PB)	J.-L. Scartezzini	Human centric lighting
EPF Lausanne	Laboratory of Integrated Performance in Design (LIPID)	M. Andersen	Human centric lighting
EPF Lausanne	Laboratory of Advanced Semiconductors for Photonics and Electronics	N. Grandjean	Solid state lighting
EPF Lausanne	EPFL-ECAL Lab	N. Henchoz	Digital experience – Meditation study in collaboration with Ming Shan (Bullet's Taoist center)
EPF Lausanne	High Energy Physics Laboratory	O. Schneider	Micro-optics
EPF Lausanne	Instant-Lab	S. Henein	Vibrations damping for compliant mechanisms
EPFL Lausanne	Institut de génie électrique et microtechnique	C. Ballif	New PV technologies
ETH Zurich	Biosystems Science and Engineering	A. Hierlemann	Organoid sorting
ETH Zurich	Computer Vision Laboratory	E. Konukoglu	Machine learning
ETH Zurich	Information Technology and Electrical Engineering	H. Wang	Wireless power transfer
ETH Zurich	Integrated Systems Laboratory	L. Benini	RISC-V ; Neural network
ETH Zurich	Computer Vision Laboratory	L. van Gool	Machine learning
ETH Zurich	Information Technology and Electrical Engineering	M. F. Yanik	Neuroinformatics
ETH Zurich	Product Development and Engineering Design	M. Meboldt	Automatic generation of compliant mechanism designs
ETH Zurich	Institute of Energy and Process Engineering	M. Tibbitt	Acoustofluidics
ETH Zurich	Optical Nanomaterial Group	R. Grange	Integrated photonics for gas spectroscopy
ETH Zurich	Computer Science	S. Capkun	System security group
ETH Zurich	Health Sciences and Technology	S. Sturla	Bio-sensing
ETH Zurich	Data Analytics Lab	T. Hofmann	Machine learning
ETH Zurich	Energy-Efficient Circuits and IoT Systems	T. Jang	Analog-to-digital converters

University	Institute	Professor	Field of collaboration
FHGR, University of Applied Sciences of the Grisons	Kompetenzzentrum für Datenanalyse, Visualisierung und Simulation	B. Studer, T. Leutenegger	Machine learning / Photonics
FHGR, University of Applied Sciences of the Grisons	Angewandte Zukunftstechnologien, Institut für Photonics und ICT IPI	U. Hauser-Ehninger	Solid state lighting
FHNW, University of Applied Sciences Northwestern Switzerland	Institute of Product and Production Engineering	B. Resan	Lasers
FHNW, University of Applied Sciences Northwestern Switzerland	Institute for Chemistry and Bioanalytics	L. Suter-Dick	Organoids
FHNW, University of Applied Sciences Northwestern Switzerland	Institut für Nanotechnische Kunststoffanwendungen	M. Kristiansen	Micro and nano structuring
Fondazione Bruno Kessler	Integrated Radiation and Image Sensors	L. Gasparini	Time-of-flight LiDAR detectors
HEIA-FR, Haute école d'ingénierie et d'architecture de Fribourg, Switzerland	Génie électrique	E. Fragnière	Expert projet de bachelor
HEIG-VD, Haute Ecole d'Ingénierie et de Gestion du Canton de Vaud	Institut de recherche appliquée et développement	E. Messerli	FPGA programming and embedded processing
HEIG-VD, Haute Ecole d'Ingénierie et de Gestion du Canton de Vaud	Information and Communication Technologies	A. Duc	Security
HE-Arc, University of Applied Sciences in the Jura Arc	Engineering – Medical Devices	A. Kaempfer-Homsy	Bio-sensing
HE-Arc, University of Applied Sciences in the Jura Arc	Institut d'ingénierie	N. Pasoz Escudero	Embedded & edge AI
HE-Arc, University of Applied Sciences in the Jura Arc	Computer Science	S. Monnerat	Embedded software
HSLU, Hochschule Luzern – Informatik	Informatik	R. Meier	Cooperation in Smart Card Forum
HSLU, Hochschule Luzern - Technik & Architektur	CC Electronics	E. Niederberger	Solid state lighting
HSLU, Hochschule Luzern - Technik & Architektur	Institute of Electrical Engineering	T. Prud'homme	Vision, polarization camera

University	Institute	Professor	Field of collaboration
HSLU, Hochschule Luzern – Technik & Architektur	Institut für Innovation und Technologiemanagement	C. Minonne	Machine learning
Idiap Research Institute	Speech and Audio Processing	M. Magimai Doss	Detection of QRS landmark in ECG signals
IFREMER	Centre Méditerranée	J. Opderbecke	Bathymetric LiDAR
Inselspital, University Hospital of Bern	Universitätsklinik für Frauenheilkunde	A. Radan, D. Surbek	AI-based decision support system for delivery & Fetal monitoring by transabdominal electrocardiogram recording
Inselspital, University Hospital of Bern	Universitätsklinik für Kardiologie	B. Schnegg	Pilot study on non-invasive blood pressure monitoring in patients with a left ventricular assist device
Inselspital, University Hospital of Bern	Universitätsklinik für Intensivmedizin	C. A. Pfortmüller	Non-invasive measurements of changes in pulmonary artery pressure in intensive care unit patients using electrical impedance tomography
Inselspital, University Hospital of Bern	Universitätsklinik für Pneumologie	C. Horvath	Detection of atrial fibrillation and other cardiac arrhythmic events during sleep polysomnography
Inselspital, University Hospital of Bern	Diabetes, Endocrinology, Nutritional Medicine and Clinical Nutrition (UDEM)	C. Stettler	Vocal biomarkers for the detection and prevention of hypoglycaemia (HypoVoice)
Inselspital, University Hospital of Bern	Diabetes, Endocrinology, Nutritional Medicine and Clinical Nutrition (UDEM)	C. Stettler, V. Lehmann	Noninvasive glucose measurement using impedance tomography (GLEAM)
Inselspital, University Hospital of Bern	Cardiology and Clinical Research	E. Rexhaj	Long-term blood pressure monitoring in patients with chronic hypertension
Inselspital, University Hospital of Bern	Cardiology and Clinical Research	E. Rexhaj, R. Bulgheroni Luigi	Post-partum blood pressure monitoring in pregnant preeclamptic patients
Inselspital, University Hospital of Bern	Lung Cancer Center	G. Kocher	Machine learning for efficient surgery
Inselspital, University Hospital of Bern	Universitätsklinik für Neurologie, Leitender Arzt, Geschäftsführender Direktor Schlaf-Wach-Epilepsie-Zentrum (SWEZ)	K. Schindler	Epilepsy detection and prediction
Inselspital, University Hospital of Bern	Universitätsklinik für Pneumologie	S. Guler	Electrical impedance tomography for the functional assessment of patients with interstitial lung disease and/or pulmonary hypertension
Inselspital, University Hospital of Bern	Universitätskliniken für Neurologie und Neurochirurgie	W. Z'Graggen	Blood pressure monitoring in patients with autonomic neuropathy
Inselspital, University Hospital of Bern	Chirurgie viscérale	Y. Borbély	Oesophageal reflux detection/monitoring

University	Institute	Professor	Field of collaboration
Institut für Kristallzüchtung, Berlin	Zentrum für Lasermaterialien	C. Kränkel	New laser crystals for high-power short pulse sources
IOB, Institute of Molecular and Clinical Ophthalmology Basel	Human Organoid Platform	M. Renner	Retina organoid sorting
Kantonsspital St. Gallen	Klinik für Pneumologie und Schlafmedizin	M. H. Brutsche	Unobtrusive long-term monitoring of sleep apnea using photoplethysmography
KNF-Laboratori Oy (Finland)	Sleep lab	J. Heiskala	Technical feasibility study on screening sleep related breathing disturbances and sleep apnoea with wearable sensors
Ł-IMiF Sieć Badawcza Łukasiewicz - Poland	Instytut Mikroelektroniki i Fotoniki	B. Synkiewicz-Musialksa	Sustainable electronics
National Research Council of Italy	Institute of Applied Physics (IFAC)	V. Raimondi	Compressive sensing for space applications
National Technical University of Athens (NTUA)	School of Mechanical Engineering	I. Paraskevas	Systems identification methods
ONERA, France	Optical measurement methods for Thermofluids research.	B. Fond	Pressure sensitive painting
ONERA, France	Modane-Avrieux Center	O. Guillerme, F. Paraz	Pressure sensitive painting
Politecnico Di Torino (POLITO)	Electronics and Telecommunications	E. Magli	Compressive sensing for space applications
Radboud University, Nijmegen, Netherlands	Institute for Computing and Information Sciences	B. Mennink	Security
Réseau Hospitalier Neuchâtelois (RHNe)	Department of Cardiology	C. Pellaton	Comparison of cardiac activity information contained in 1-lead ECG and multi-lead ECG signals (SCREENBEAT)
Réseau Hospitalier Neuchâtelois (RHNe)	Department of Anaesthesiology	Y. Degiorgis	VITAL+ – Continuous non-invasive measurement of core vital signs on the hospital ward
Robert-Bosch-Hospital	Clinical of Geriatric Rehabilitation	C. Becker	Fall prediction and detection
Sant'Anna School of Advanced Studies, Pisa	Institute of Communication, Information and Perception Technologies (TeCIP)	A. Bogoni	Photonics radar
Swedish University of Agricultural Sciences	Biosystems and Technology	A. Herlin	Vital sign monitoring in livestock (pigs) in the framework of IoF 2020
Swiss TPH	Department of Medicine	D. Paris	Diagnostics
TU Delft, Netherlands	Faculty of Electrical Engineering, Mathematics, and Computer Science	Q. Wang	Embedded & Edge AI
Tyndall National Institute	MicroNano Systems	O'Riordan	Sensors

University	Institute	Professor	Field of collaboration
Università della Svizzera Italiana	Istituto ricerche solari Aldo e Cele Daccò (IRSOL)	R. Ramelli, D. Gisler	Optical systems for CCD cameras
Université Bourgogne Franche-Comté	FEMTO ST and UTBM	F. Chérioux, V. Humblot, P. Briois	Smart coatings
University Hospital Basel	Research Center for Clinical Neuroimmunology and Neuroscience	J. Lorscheider	improving monitoring solutions for multiple sclerosis patients
University of Athens, Greece	Dept. of Informatics & Telecommunications	S. Hadjilefthymiades	Internet of Things, location-based services, mobile and vehicular applications
University of Basel	Psychiatry Hospital / Center for Chronobiology	C. Cajochen	Human centric lighting / Chronobiology
University of Basel	Chemistry	E. Constable, C. Housecroft	Photochemistry
University of Basel	Biomedicine	V. Petkovic	Inner EarResearch
University of Bern	Quantum Optics Lab	A. Stefanov	Entangled photons for microscopy
University of Bern – ARTORG	Organs-on-Chip Technologies	O. Guenat	Organ-on-chip, AI for multi-omics
University of Geneva	Astronomy Department	F. Bouchy	Laser frequency combs for calibration of spectrographs
University of Geneva	Sensors Group at Institut für Neuroinformatik,	S.-C. Liu	Neuroinformatics
University of Glasgow, UK	James Watt School of Engineering	J. Kettle	Sustainable electronics
University of Lausanne	Department of Information Systems	K. Huguenin	Privacy and security in healthcare IoT systems
University of Modena Reggio-Emilia, Italy	Dipartimento di Scienze Fisiche, Informatiche e Matematiche	P. Burgio	
University of Neuchâtel	Laboratoire Temps-Fréquence	G. Miletí	Atomic clocks
University of Sherbrooke	Neonatology	E. Fortin-Pelerin	Evaluation of PAP measurement accuracy in sheep and neonatal human patients
University of Tempere, Finland	Faculty of Information Technology and Communication Sciences	M. Mäntysalo	Sustainable electronics
University of Zurich	Institute of Neuroinformatics	T. Delbrück	On-chip convolutional neural network for visual scene processing
Vienna University	Department of Physical Chemistry	P. Lieberzeit	Chemical sensor
ZHAW, Zurich University of Applied Sciences	School of Life Sciences	M. Rimann	Organoids
ZHAW, Zurich University of Applied Sciences	High Performance Embedded Platforms	M. Rosenthal	Embedded & edge AI

Teaching

	<i>Title of lecture</i>	<i>Context</i>	<i>Location</i>
G. Basset	Applications of micro-nano structuring	ERASMUS mundus joint master degree photonics for security reliability and safety course	University of Saint Etienne
S. Blanc	Innovation management	Master management, technologie et entrepreneuriat	EPF Lausanne
O. Chételat	Sensors in medical instrumentation	EPFL Course EE-511	EPF Lausanne
A. Corbaz	Operating system	Bachelor course	HEIG-VD
A. Corbaz	Real-time computing	Bachelor course	HEIG-VD
M. Despont	Packaging and hybridization, the valorization of MEMS technologies	Micro- 534 Advanced MEMS 2023 (D. Briand)	EPF Lausanne
L. A. Dunbar	Digital transformation	EMBA	EPF Lausanne
L. A. Dunbar	Professor of practice	Professor at college of management	EPF Lausanne
R. Krähenbühl	Nanotechnology and industrialization at CSEM	Information lecture & excursion	University of Basel, SNI
M. Lemay, P. Renevey, J. Jorge, M. Proença, F. Braun, G. Bonnier, C. Moufawad El Achkar, and C. Aguet,	Applied biomedical signal processing	EPFL Course EE-512	EPF Lausanne
C. Loussert-Fonta	"More sugar and less ice". The Infinite power of cryo-immuno electron microscopy	Program CUSO: electron microscopy	University of Lausanne
S. Morisod, S. Blanc, B. Roustom	Tendances transformationnelles	CAS en management du changement	University of Lausanne
R. Pugin	Micro/Nano-structured functional surfaces & components	Highlights in microtechnology – Summer School	EPF Lausanne
V. Revol	The lab of the future	Lecture	FHNW, Hochschule für Life Sciences
D. Ruffieux	Radio frequency circuits design techniques	Master course	EPF Lausanne
G. Weder	Organ-on-chip and organoid technology for drug development	Swiss Foundation for Research in Microtechnology	FSRM Neuchâtel

Theses

PhD Degrees Awarded in 2023

Name	University	Title
Biggio, Luca	ETH Zurich	Machine learning based domain adaptation and interpretability for time-series
Cerida Rengifo, Sammy	EPF Lausanne	Ultra-low power short-range 60-GHz FMCW radar front-end
Dussouillez, Marion	EPF Lausanne	Identification and mitigation of degradation mechanisms induced by heat and light in NiOx-based perovskite solar cells
Ntavelis, Evangelos	ETH Zurich	Multimodal learning & generation: utilizing diverse inputs to generate & manipulate images

CSEM Employees carrying out a PhD

Name	Professor / University	Theme / CSEM Unit	Start year
Ahmadi Najafabadi, Amir Mohsen	A. Skrivervik / EPF Lausanne	Target-oriented mm-wave wireless power transfer for IoT applications / Integrated and Wireless Systems	2022
Bernard, Gaëtan	R. Logé / EPF Lausanne	Additive manufacturing of metal matrix composite / Micro & Nano Systems	2020
Bhoir, Shubham Sharad	M. Paolone / EPF Lausanne	Exploitation of electrochemical impedance spectroscopy for predictive maintenance for batteries / Sustainable Energy / Sustainable Energy	2021
Blache, Manon	K. Eyer / ETH Zurich	Highly selective continuous flow isolation of circulating rare cells from whole blood and retrieval for droplet microfluidic single cell analysis / Industry 4.0 and Life Sciences	2023
Blum Roman	G. Miletí / University of Neuchâtel	Long-term frequency stability improvement of a 2-photon Rubidium clock / Instrumentation	2021
Brero, Giorgio	P. Dittrich / ETH Zurich	Extracellular vesicle isolation from whole blood and labeling for flow cytometry / Industry 4.0 and Life Sciences	2023
Del Giovane, Stefano	H. Altug / EPF Lausanne	New generation point of care sensing / Industry 4.0 and Life Sciences	2022
Ebrahimi Argi, Farnaz	A. Eichler / ETH Zurich	Ultra-sensitive photonics accelerometers for next generation seismic sensor networks / Micro & Nano Systems	2023
El-Zein, Yamane	K. Huguenin / University of Lausanne	mHealth data privacy / Medtech	2019
Gaudilli��re, Pierre-Louis	D. Atienza / EPF Lausanne	Embedded machine learning for the controlling of PPG-based systems / Medtech	2021
Ghorbanpoor, Mohsen	H. Wang / ETH Zurich	Receiver SoC for long range mm-wave wireless power transfer with focus on IoT applications / Integrated and Wireless Systems	2022
Hefti, Olivia	C. Br��s / EPF Lausanne	Periodic poling of lithium niobate on insulator photonics waveguide and its application / Instrumentation	2022
Honz��tko, David	P. Fua / EPF Lausanne	Aggregating spatial and photometric context for photometric stereo / Integrated and Wireless Systems	2018
Jeanningsros, Lo��c	J.-P. Thiran / EPF Lausanne	Classification of cardiac arrhythmia based on PPG / Medtech	2020

Name	Professor / University	Theme / CSEM Unit	Start year
Klauser, Elias	A. Karimi / EPF Lausanne	Control for hybrid micro-disturbance isolation systems / Instrumentation	2020
Knuchel, Benoît	E. Oswald / AAU Klagenfurt	Embedded intrusion detection for the IoT / Integrated and Wireless Systems	2022
Lang, Guilain	M. Meboldt / ETH Zurich	Automatic generation of compliant mechanism designs / Instrumentation	2021
Luongo, Francesca	E. Konukoglu / ETH Zurich	Generative methods for organoid data augmentation and generation / Industry 4.0 and Life Sciences	2022
Miotello, Enrico	T. Jang / ETH Zurich	Advanced ADC design / Integrated and Wireless Systems	2022
Narduzzi, Simon	S-C. Liu / ETH Zurich	Ultra-low power resource algorithms for neuromorphic hardware / Integrated and Wireless Systems	2020
Sacchi, Nazareno	T. Jang / ETH Zurich	Compression-aware hardware architectures for edge AI / Integrated and Wireless Systems	2022
Sainz Martinez, Cristina	M. Bach Cuadra / CHUV	MRI and EEG processing applied to human brain structure and function / Medtech	2020
Sampaio Da Silva, Claudia	A. Hierlemann / ETH Zurich	Organoid sorting / Industry 4.0 and Life Sciences	2021
Scharnhorst, Paul	C. Jones / EPF Lausanne	Data-driven control approaches and applications in energy systems / Sustainable Energy	2019
Sepehri, Yamin	P. Frossard / EPF Lausanne	Smart edge for hierarchical vision systems / Integrated and Wireless Systems	2020
Sideris, Iason	M. Bambach / ETH Zurich	Data-driven modeling for metal additive manufacturing process optimization / Industry 4.0 and Life Sciences	2021
Simeunovic, Jelena	P. Frossard / EPF Lausanne	Network time series forecasting for solar resources / Sustainable Energy	2019
Vuille-dit-Bille, Emilie	S. Sakar / EPF Lausanne	Acoustic manipulation of organoids / Industry 4.0 and Life Sciences	2021

Commissions and Committees

P.-J. Alet	ETIP SNET (Smart Networks for the Energy Transition): Member of the Governing Board European Technology and Innovation Platform – Photovoltaics (ETIP-PV): Member of the Steering Committee, Leader of the Digital PV & Grid Working Group Top Jury, EM-Power Award Top Jury, Intersolar Award Topic Organiser, EUPVSEC
C. Beyer	Member of the board of Sensors.ch association
N. Blondiaux	Member of the scientific committee of the EUSPEN 21st international conference & exhibition
C. Brivio	BEPA – Batteries Europe integrated working group member to WG6 Stationary Applications and Integration
L. Burr	Expert for bachelor and master theses program at HE-ARC PhD Thesis Co-Director at EPFL
S. Cattaneo	Expert for MSE Master Theses at OST Eastern Switzerland University of Applied Sciences Expert for W.A. de Vigier Foundation Innovation Coach for INOS Innovationsnetzwerk Ostschweiz

H. Chai-Gao	ANR Expert External editor – MDPI - Biosensors
P. Dallemande	Secretary and Swiss representative of Technical Committee 5 "Information Technology Applications", International Federation for Information Processing (IFIP)
M. Despeisse	IPV workshop committee nPV workshop committee
M. Despont	Chairman of the Swiss-MNT network Co-Chair of the Swiss NanoConvention 2023 (SN C 2023), Neuchâtel, June 15-16, 2023 Swiss Representative of the iMNEs (international Micro and Nano Engineering society)
L. A. Dunbar	Academic co-Lead of Machine Learning Clinic in the Swiss Alliance for Data-Intensive Services Jury member of the BCN innovation prize Jury member of the Shapers Industry 4.0 prize TinyML Swiss Committee
S. Emery	Member of the Technical Committee of the IEEE SOI-3D-Subthreshold (S3S) Conference
F. Faes	PV in Motion committee
E. Györvary	Core group member & CSEM representative of EARTO Working Group on Emerging Technologies for Healthcare Member & CSEM representative of EPOSS Association; Chair of WG Green ECS Member of Finnish Chamber of Commerce in Switzerland Member of Organizing Committee and Session Chair of MPS World Summit 2023 Member of the Board of European Organ-on-Chip Society (EUROoC) Member of the Extended Board of the Heterogeneous Technology Alliance (alliance federating the Fraunhofer (microelectronics), VTT, CEA-Tech, and CSEM) & leading the Health & AgriFood Platform Member of the Scientific & Organizing Committee of "Next Gen Organ-on-Chip & Organoids" event Member of the Steering Board of Innovation Group Digitalization at Swiss Food Research
H. Heinzelmann	Expert, Austrian Research Promotion Agency FFG Expert, German Federal Ministry of Education and Research BMBF Member of the Board of the Heterogeneous Technology Alliance (HTA) Member of the Board, Advanced Manufacturing Technology Transfer Centers (AM-TTC) Member of the Executive Board, EARTO Member of the Foundation Board, Switzerland Innovation Member of the Strategic Advisory Board "Produktion der Zukunft", Austrian Federal Ministry for Climate Action, Environment, Energy, Mobility, Innovation and Technology (BMK) Membre du Conseil d'Administration de Centredoc Program Committee, MNE 2023 Berlin
M. Höchemer	SDS2022 Scientific Program Committee
A. Hutter	BEPA – Batteries Europe integrated working group member to WG5 Mobility Applications and Integration Federal Office of Transport (FOT), Energy Strategy for Public Transport 2050 (ESPT 2050) programme, expert Innosuisse expert President iBAT Association (www.ibat.swiss)
A. Ingenito	BEPA – Batteries Europe integrated working group member to WG3 Advanced Materials and WG4 Cell Design and Manufacturing
R. Jose James	Chairman Swiss Chapter IEEE Electronic Packaging Society
C. Julia-Schmutz	CSEM representative, BioAlps
H. F. Knapp	Board of Directors member for cluster initiative Toolpoint for Lab Science Jury member for the Innovationspreis of the Industrie- & Handelskammer Zentralschweiz Jury member for Zinno Ideenscheck Pre-jury member for Swiss Technology Award

J. Krauss	Board member of the Deep Tech Switzerland Foundation Member of Program Committee of the Swiss Medtech Day (SMD)
F. Kurth	Academic supervisor and external expert for PhD program at D-BSSE, ETH Zurich, Basel, and at D-CHAB, ETH Zürich, Zürich Coach BiolIncubate, ETH Zürich, Zürich Expert for bachelor and master theses program at FHNW Muttenz Member of the E&S committee, International Conference on Miniaturized Systems for Chemistry and Life Sciences (mTAS) Organizing committee member and executive program committee member Swiss e-Print 2024
M. Lemay	Board Member, Swiss Society for Biomedical Engineering
S. Paoletti	Chair of the Swiss Symposium in Point of care diagnostics Executive Board member of biotechnet, Switzerland and co-lead of the IVD platform Member of the Bridge proposal evaluation panel
A. Pauchard	Conseil d'administration de la CNCI Chambre Neuchâteloise du Commerce et de l'Industrie, Neuchâtel Comité aviseur section Microtechnique EPFL Commission Swiss Quantum Conseil d'administration de Silatech SA Full Member of the Swiss Academy of Engineering Sciences SATW Président du Conseil, Fondation de prévoyance du CSEM
D. Petri	Scientific committee for the AgriPV Conference
R. Pugin	Member of the Expert Committee of the Association Micronarc Member of the Expert Committee of the Association NTN Innovative Surfaces Member of the Omega Foundation Council
V. Revol	Chair of the Next Gen Organ-on-Chip & Organoids Symposium & Precision Liquid Handling Workshop Co-Founder and deputy head of the Digital Innovation Hub LifeHub.Swiss (www.lifehub.swiss) InnoSuisse expert
D. Ruffieux	Chair of the RF and mm-Wave Circuits Track of the International Technical Program Committee of the European Solid State Circuit Conference (ESSCIRC)
D. Schmid	Expert for bachelor and master theses program at HSLU Jury member for Tech Startup Award Südostschweiz Point of entry INOS Innovationsnetzwerk Ostschweiz President of the Board KinderLab Landquart, Switzerland
P. A. E. Schmid	Academic co-lead expert group ML-Clinic (ML in Industrial Practice) Swiss Alliance for Data-Intensive Services Accredited Coach for INOS Innovationsnetzwerk Ostschweiz CSEM Representative Swiss Mechatronics Cluster Founder and regional lead Digital Innovation Hub Robotics & Artificial Intelligence (www.raisehub.swiss) Industry 4.0 topic leader NTN Innovation Booster Databooster (www.databooster.ch) Member expert group Industry 4.0 SATW Steering committee PDA Robotics & Automation
P. Stadelmann	Jury member for the PhD thesis of Pooneh Mohaghegh "Indoor Real-time localization system design for Internet of Things applications" with Prof. Yves Perriard, EPFL-LAI
P. Steiert	Advisory Board Member for Institute für Chemistry and Biological Chemistry at the ZHAW Advisory Council for cluster initiative Toolpoint for Lab Science Member of the Executive Board for Verein Nachhaltigkeitsnetzwerk Zentralschweiz Member of the Executive Board for Verein Startup Pilatus Member of the Executive Board of the PHABULOUS Pilot Line Association

A. Steinecker	Cluster manager "Production & Systems" at Technologie Forum Zug Coach for RIS Zentralschweiz CSEM contact for Smart Card Forum (René Meier, HSLU) CSEM Representative EPoSS and Member of Working Group Robotics CSEM Representative IVAM
A. Voelker	Member of the Innovation Board Photonics Booster Photonics Focus Group Leader IVAM

Prizes and Awards

- January 2023 CSEM's team won the tinyML Challenge 2022, which was awarded in January 2023. This an international challenge aiming to build a smart weather station based on tiny Machine Learning without mechanical moving parts. With their novel acoustic solution, relying only on microphone data to infer wind and rain intensity.
- October 2023 Best Paper Award, 3rd place, 9th IEEE World Forum on the Internet of Things. "Optimizing IoT-based asset and utilization tracking: Efficient activity classification with MINIROCKET on resource-constrained devices", M. Giordano, S. Cortesi, M. Crabolu, L. Pedrollo, G. Bellusci, T. Bendinelli, E. Türetken, A. Dunbar, M. Magno.
- November 2023 Laurie-Lou Senaud was rewarded with the ASEA BROWN BOVERI LTD. (ABB) AWARD 2023 for her groundbreaking work and dedication to improving solar cell efficiencies, allowing the achievement of efficiencies over 25% with industry compatible processes.

ALLSCHWIL
Hegenheimermattweg 167A
CH-4123 Allschwil

ALPNACH
Untere Gründlistrasse 1
CH-6055 Alpnach

BERN
Weyermannstrasse 36
CH-3008 Bern

LANDQUART
Bahnhofstrasse 1
CH-7302 Landquart

NEUCHÂTEL
Jaquet-Droz 1
CH-2002 Neuchâtel

ZURICH
Technoparkstrasse 1
CH-8005 Zürich

www.csem.ch
info@csem.ch

